UNIVERSIDAD DE MÁLAGA

TESIS DOCTORAL

Para optar al Título de:

Doctor en Ingeniería Química con Mención Internacional

Programa de Doctorado: Química y Tecnologías Químicas. Materiales y Nanotecnología

ESTUDIO DE LA DESACTIVACIÓN DE CATALIZADORES DERIVADOS DE LA BIOMASA PARA LA PRODUCCIÓN DE DIMETILÉTER

Autor: Javier Torres Liñán

Directores: Dr. José Rodríguez Mirasol

Dr. Tomás Cordero Alcántara

Málaga, 2022

UNIVERSIDAD DE MÁLAGA

UNIVERSIDAD DE MÁLAGA

AUTOR: Javier Torres Liñán

https://orcid.org/0000-0002-6733-895X

EDITA: Publicaciones y Divulgación Científica. Universidad de Málaga

Esta obra está bajo una licencia de Creative Commons Reconocimiento-NoComercial-SinObraDerivada 4.0 Internacional:
http://creativecommons.org/licenses/by-nc-nd/4.0/legalcode
Cualquier parte de esta obra se puede reproducir sin autorización
pero con el reconocimiento y atribución de los autores.
No se puede hacer uso comercial de la obra y no se puede alterar, transformar o hacer obras derivadas.

Esta Tesis Doctoral está depositada en el Repositorio Institucional de la Universidad de Málaga (RIUMA): riuma.uma.es

UNIVERSIDAD DE MÁLAGA

DECLARACIÓN DE AUTORÍA Y ORIGINALIDAD DE LA TESIS PRESENTADA PARA OBTENER EL TÍTULO DE DOCTOR

D./Dña JAVIER TORRES LIÑÁN
Estudiante del programa de doctorado QUÍMICA Y TECNOLOGÍAS QUÍMICAS. MATERIALES Y NANOTECNOLOGÍA de la Universidad de Málaga, autor/a de la tesis, presentada para la obtención del título de doctor por la Universidad de Málaga, titulada: ESTUDIO DE LA DESACTIVACIÓN DE CATALIZADORES DERIVADOS DE LA BIOMASA PARA LA PRODUCCIÓN DE DIMETILETHER

Realizada bajo la tutorización de D. JOSÉ RODRÍGUEZ MIRASOL y dirección de D. JOSÉ RODRÍGUEZ MIRASOL Y D. TOMÁS CORDERO ALCÁNTARA (si tuviera varios directores deberá hacer constar el nombre de todos)

DECLARO QUE:

La tesis presentada es una obra original que no infringe los derechos de propiedad intelectual ni los derechos de propiedad industrial u otros, conforme al ordenamiento jurídico vigente (Real Decreto Legislativo 1/1996, de 12 de abril, por el que se aprueba el texto refundido de la Ley de Propiedad Intelectual, regularizando, aclarando y armonizando las disposiciones legales vigentes sobre la materia), modificado por la Ley 2/2019, de 1 de marzo.

Igualmente asumo, ante a la Universidad de Málaga y ante cualquier otra instancia, la responsabilidad que pudiera derivarse en caso de plagio de contenidos en la tesis presentada, conforme al ordenamiento jurídico vigente.

En Málaga, a 20 de ENERO de 2022

Fdo.: JAVIER TORRES LIÑÁN Doctorando/a	Fdo.: JOSÉ RODRÍGUEZ MIRASOL Tutor/a
Fdo.: JOSÉ RODRÍGUEZ MIRASOL Director/es de tesis	TOMÁS CORDERO ALCÁNTARA

UNIVERSIDAD
DE MÁLAGA

D. TOMÁS CORDERO ALCÁNTARA, Catedrático en Ingeniería Química de la Universidad de Málaga

D. JOSÉ RODRÍGUEZ MIRASOL, Catedrático en Ingeniería Química de la Universidad de Málaga

CERTIFICAN: Que el trabajo de investigación recogido en la presente Memoria ha sido realizado bajo su dirección en el Departamento de Ingeniería Química de la Universidad de Málaga por el Ingeniero D. JAVIER TORRES LIÑÁN, y reúne, a su juicio, contenido científico suficiente y las condiciones necesarias para ser presentado y defendido ante el Tribunal correspondiente para optar al Grado de Doctor con Mención Internacional.

Málaga, enero de 2022

Dr. Tomás Cordero Alcántara Dr. José Rodríguez Mirasol

UNIVERSIDAD DE MÁLAGA

Esta tesis doctoral ha sido realizada en el marco del proyecto de I+D+i del Programa Estatal de Investigación, Desarrollo e Innovación orientada a los Retos de la sociedad, del Ministerio de Economía y Competitividad, titulado: Catalizadores avanzados de base biomásica para la síntesis de dimetil éter en una etapa, con referencia: CTQ2015-68654-R, y del proyecto de I+D+i del Programa Estatal de Investigación, Desarrollo e Innovación de Retos de Investigación, del Ministerio de Ciencia, Innovación y Universidades, titulado: Combustibles a partir de gas de síntesis mediante catalizadores derivados de la biomasa (SynFuelBioCat), con referencia: RTI2018-097555-B-I00.

UNIVERSIDAD DE MÁLAGA

“He fallado una y otra vez a lo largo de mi vida.

Es por eso por lo que he tenido éxito”

Michael Jordan

UNIVERSIDAD DE MÁLAGA

UNIVERSIDAD
DE MÁLAGA

INDEX

UNIVERSIDAD DE MÁLAGA

UNIVERSIDAD DE MÁLAGA

UNIVERSIDAD DE MÁLAGA

UNIVERSIDAD
DE MÁLAGA

OVERVIEW

This thesis is developed within the framework of the efficient use of residual biomass resources in future biorefineries to substantially produce, not only fuels and chemicals, but also other bioproducts, such as catalysts, which involves a relevant strategy for boosting the bio-based circular economy. In particular, this thesis is focused on the study of lignocellulose waste derived catalysts for the production of dimethyl ether (DME), as in the Methanol-to-DME process (MTD). DME is a high valuable chemical that can be used as renewable alternative for conventional diesel or liquified petroleum gases (LPG), given that methanol can be obtained from syngas produced from biomass residues gasification. For this reason, the behavior of a Zr-loaded P-containing biomass-derived carbon catalyst has been studied under severe operation conditions (high temperature and long time on stream), in order to achieve high methanol conversions, similar to those that usually take place in the industrial process, to analyze the stability, conversion and selectivity to DME of the catalyst under these extreme reaction conditions. This way, the active surface centers of the catalyst for the methanol dehydration to DME were defined and coke deposition on these actives surface sites for different operation conditions was analyzed. Carbonaceous deposits on the active surface sites proved to be the main source of catalyst deactivation and determined the change in textural properties and surface chemistry of the catalyst. On the other hand, the regeneration of the deactivated catalyst by air oxidation at low temperature was also studied, analyzing the effect of this regeneration process on the active surface sites, as well as on the carbonaceous support properties.

This thesis is structured in 4 chapters. The Introduction constitutes the first one, in which the motivation of this thesis was proposed and the state of the art was also showed. In the second chapter, the main experimental methods used in the development of this thesis are shown, as well as the experimental equipment and characterization techniques used. The third chapter shows the experimental results obtained and the discussion of these results.

Chapter 3.1 collects the study of the kinetics of the oxidation and decomposition of phosphorus surfaces groups on a biomass-derived porous carbon material, given that P-surface groups have been described as very active for the selective dehydration of methanol to DME. These P-surface groups are generated on the carbon materials

UNIVERSIDAD DE MÁLAGA

by the activation process itself using phosphoric acid as an activating agent. In this sense, a methodology has been proposed to be able to follow the isothermal specific oxidation of reduced P-surface groups under different operation conditions and the non-isothermal decomposition of the oxidized ones by Thermal-Programed-Desorption (TPD). Activation energies for the isothermal oxidation of reduced P-surface groups were obtained using the Elovich equation. A non-isothermal kinetic model was used to evaluate the activation energies for the decomposition of oxidized phosphorus-surface groups and other carbon-oxygen surface groups to CO_x. These results are of great interest for the study of the stability of these surface groups on carbon materials when they act as catalysts in reactions of industrial interest, such as the dehydration of methanol to DME. Chapter 3.2 shows a study on the stability of Zr-loaded P-containing biomass-derived catalyst for the dehydration of methanol at operation conditions close to those of the industrial process, very high conversions of methanol at relatively high reaction temperatures. It is also described the different surface active phases for this reaction, C-O-P and Zr-O-P types, which showed a very high selectivity to DME at these operation conditions, and how these surface active phases are affected (deactivated by coke deposition) by reaction temperature and time on stream. A regeneration step by an air oxidation process was attempted. Besides, a reaction pathway for the deactivation process was proposed. Chapter 3.3 complete the study started on chapter 3.2 and a kinetic model based on a proposed reaction mechanism that predicts yields to different products was stablished. The kinetic model quantifies deactivation effect of coke deposition as well as the effect of water in the reaction medium. Each chapter presents a short introduction and conclusions.

A final chapter provides with the general conclusions and gives a brief insight in the remaining and future work that could be derived as a result of this thesis.

UNIVERSIDAD DE MÁLAGA

Chapter 1

Introduction

UNIVERSIDAD DE MÁLAGA

1.1. The problem with fossil fuels

Nowadays, fossil fuel derivatives are present in every facet of our lives. From diesel to refuel our cars to the vanilla flavor, going through the fabric we used to be dressed, all comes from petrol. Moreover, natural gas and coal are additionally used to be burned in order to obtain energy.

Fossil fuels are used both for energy and chemical production. Regarding to energy, Figure 1.1. shows that, before 1850, only biomass was used as primary energy. After that, coal was introduced as primary energy source, and after 1900, fossil fuels were the main source of primary energy, increasing their percentage year after year. Although traditional biomass consumption has been more or less maintained (with a slight increase in the last years), the increasing energy demand from a growing population and their lifestyle in an electric world, has led to the use of fossil fuel sources.

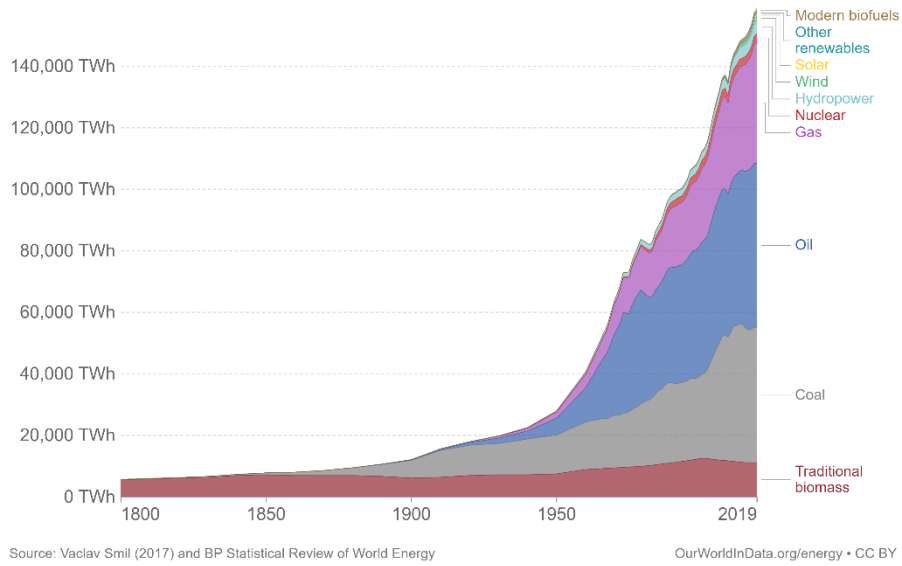

Figure 1. 1. Global direct primary energy consumption. Extracted from [1].

Besides, in the following years, this primary energy demand is expected to still be growing [2], increasing nearly a 50% between 2018 and 2050. This high increase was mainly caused by the strong economic growth

UNIVERSIDAD DE MÁLAGA

of Asia. However, although a high rise of renewable energy was expected for 2050 (from 15% to 28%), it would not even cover the increase in the demand, so coal, natural gas and petroleum consumption would also be expanded.

On the other hand, fossil fuels are not only used as combustible sources. Fossil fuels, especially petroleum, are the feedstock for the obtention of a huge variety of petrochemicals, which can be classified in three types [3]. The first one is olefins, such as ethylene and propylene using as feedstock in the plastic industry, or butadiene, used in synthetic rubber production. The second one is aromatics, such as benzene, toluene and xylenes, that could be used to produce dyes, synthetic detergents, isocyanates, plastics or synthetic fibers. The last type is the synthesis gas (syngas), a mixture of CO and H_2 that is used as a feedstock for the Fischer-Tropsch reaction or for production of ammonia, methanol or dimethyl ether (DME).

All of those uses of fossil fuels contribute to a high level of dependency from those resources. This implies a series of drawbacks that must be taken into account.

The first problem is the pollution they produce. When energy want to be obtained from those fossil fuels, they need to be burned, releasing CO_2 that contributes to the greenhouse effect, and this way, to the increase in the global temperature. Temperature has been rising since 1980 and, in particular, in 2020, the increase in temperature was of +1.2 ºC compared to the period 1951-1981 [4,5]. In an attempt to avoid the continuous increasing of temperature, United Nations included an specific goal covering this topic [6]. In this sense, some international agreements have been promoted, like the already finished Kyoto Protocol, which covered from 2008 to 2012, but was extended until 2020, and whose goal was the reduction of the CO_2 emissions and other greenhouse gases [7]. After Kyoto Protocol, Paris Agreement is already ongoing. This new international treaty aim not only to reduce greenhouse gas emissions, but also to limit global warming below 2 ºC (trying to be under 1.5 ºC) [8]. Nevertheless, as Figure 1.2 shows [9], although global CO_2 emissions seems to be stabilizing from 2012 (although it decay in 2020 due to the impact of Covid-19 pandemic), their amount is still too high, and far from the United Nations goals.

UNIVERSIDAD DE MÁLAGA

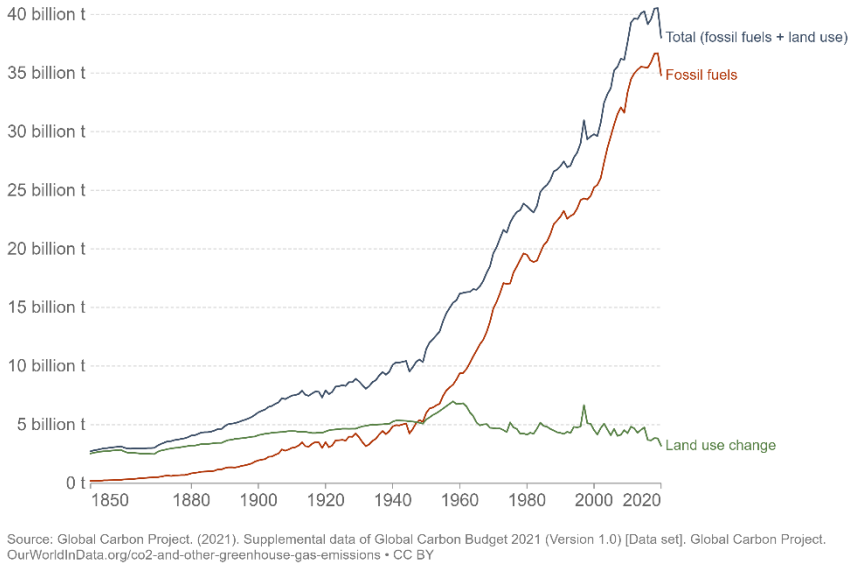

Figure 1. 2. Global CO_2 emissions from fossil fuels and land use change. Extracted from [9].

Other of the biggest problems of those fossil fuels is their shortage. According to MET group [10], oil and natural gas will ran out in about 50 years, while coal will last for 114 years. A worst scenario is depicted in an article by Standford University [11], which reduce that time to 30 years for oil, 40 years for gas and 70 years for coal. However, the years proposed in those studies could be longer as some new reserved might be discovered [12]. For example, in 2000 the total oil reserves were 1300.9 thousand million barrels, while in 2010, that number increase to1636.9 thousand million barrels and in 2020 to 1732.4 thousand million barrels. But the rate of new reserves discovering is decaying and no much more fossil fuel sources is expected to be found [12].

Directly related to the latter problem was the price. Figure 1.3. shows how the crude oil price has been oscillating in the last years [12] and, due to its depletion, it is expected that the barrel prices go on growing. That price was also hardly affected by different events, as Figure 1.2. shows, and this is caused by the oil reserves concentration, which are mainly in Venezuela, Middle East (Saudi Arabia, Iran, Iraq and Kuwait), Canada and Russia. For this reason, when an event happened on those zones, the oil price was hardly affected and it strongly affect the economies of those country that import those fuels.

UNIVERSIDAD DE MÁLAGA

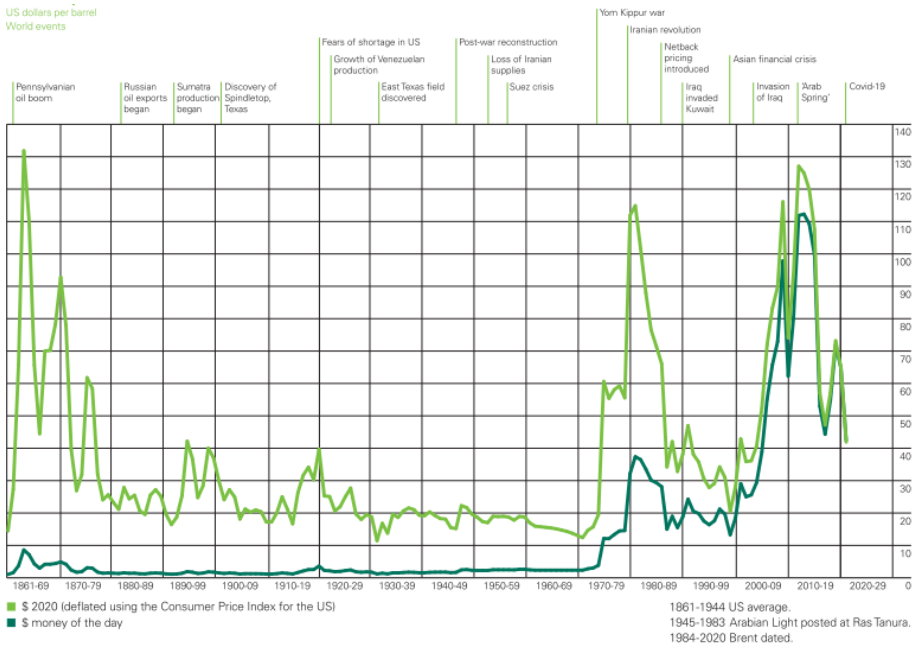

Figure 1. 3. Crude oil prices 1861-2020 (US dollars per barrel). Extracted from [12].

Similar behavior can be found for the natural gas and coal prices. In particular, in Spain, natural gas price is of special importance. The Spanish electricity price is calculated by a marginalist market, which means that the most costly energy is the one which stablish the price [13], and the increase in natural gas price has a negative effect on the electricity price [14].

1.2. The biorefinery concept

A solution for these problems is the implementation of waste refineries, that employ used plastics and tires as feedstock [15,16], or, even better, biorefineries. In a biorefinery plant, renewable biomass is used instead of petroleum to obtain fuels, chemicals and materials [17]. This way, those energy can be obtained without a net contribution to CO_2 levels, as the CO_2 produced by burning those fuels was the same that was removed when growing the biomass. Moreover, although the production of biomass is a seasonal event that implies the intermittent function of

UNIVERSIDAD DE MÁLAGA

those biorefineries or a stabilization of the feedstock capacity, the biomass can be grown up in every part of the globe, avoiding long transportation costs and allowing a potential infinite production of that renewable feedstock, as well as the independence of the few countries which have fossil fuel reserves [18]. Nevertheless, at the moment, this technology is already more expensive than fossil fuels, so more researching must be done in this aspect to reduce its costs [19].

According to their feedstock, different types of biorefineries has been developed. The first generation biorefineries are those which used vegetable oils and edible sugar as feedstock to produce biodiesel or ethanol. Those biorefineries present the huge problem of the competition with the food industry, so their use should be minimized. Second generation or lignocellulosic biorefineries goes a little step further and avoid competition with food industry by using waste biomass as feedstock to produce a huge variety of chemicals, biofuels and materials. Third generation biorefineries use algae as a feedstock to produce biodiesel, ethanol, hydrogen and methane [20]. In the last years an additional type has been added, the fourth generation biorefineries which would use genetically modified crops and advance technology to capture more CO_2 from the environment than the one produced during the burning processes [21].

Among all of these biorefinery types, that of lignocellulosic waste seems to be one of the most interesting alternatives and is able to be implemented in a short/medium term, as they use already mature technology. The process employed on these plants could be differentiated between physical conversion (mechanical extraction of oils, distillation and briquetting), thermo-chemical conversion (combustion, gasification, pyrolysis, liquefaction), chemical conversion (hydrolysis and supercritical water conversion), bio-chemical conversion (microbial and enzymatic processes for sugar obtention and fermentation of sugars), hydrotreating of oils and Fischer-Tropsch reactions [22].

In the particular case of Spain, and specially in Andalusia, with a well-developed agroindustry, the implementation of lignocellulosic refineries present a high interest, as several articles show [23,24].

UNIVERSIDAD DE MÁLAGA

1.3. Dimethyl ether

DME is one of the petrochemicals that can be obtained from petroleum through synthesis gas. However, in the context of a biorefinery, it can be also obtained from syngas originating from biomass gasification [25,26].

DME (CH_3OCH_3) is the simplest ether, with a density of 0.661 g/cm^3 at standard conditions and a boiling point of -25 ºC at atmospheric pressure, so it is normally stored at high pressure. It has no color and a sweet ether-like odor. Its flame is blue without peroxide formation and its heating value is 28,620 kJ/kg. It is non-carcinogenic, non-teratogenic, non-mutagenic and non-toxic and, although it has a greenhouse effect, its global warming potential is similar to that of CO_2 at a 20 years horizon, but ten times lower at a 500 years horizon [27].

1.3.1. DME applications

All of the aforementioned properties encourage the use of DME in a wide range of activities:

- Diesel substitute in engines

DME presents a cetane number between 55-60, higher than traditional diesel (40-55), which together with its low boiling point make DME a good candidate for its substitution in compression-ignition engines. Moreover, DME has no C-C bonds, which produce a smokeless combustion, as well as low formation and high oxidation rate of particles. DME is also non-corrosive for engines and produce less NOx and combustion noise than diesel, probably due to its short ignition delay. However, it presents some drawbacks compared with conventional diesel, being the main one its lower heating values (around a 33% lower), which needs a higher injected volume for the same amount of energy. Another one is its low compressibility, which needs a work of 10% higher in the diesel pump, and its low viscosity and lubricity, which needs the addition of some additives to avoid leakage or surface wear. However, this problems can be easily solved with small changes in the conventional compression-ignition engine [28–30].

- Liquefied petroleum gas (LPG) substitute

Physical properties of DME are quite similar than LPG, so technology developed to store, handle and transport LPG can be directly applied to DME [29]. The most common use of LPG is domestic, being reported

UNIVERSIDAD DE MÁLAGA

that a 20 % blending with DME can be directly used, but higher percentages, or even pure DME, can be used with only small changes in the already implanted infrastructure. Conversely, DME has also been proposed as spark ignition engine blended with LPG, showing that no modification was needed if percentage of DME was lower than 20% [31–33].

- Fuel in power turbines

As DME is a gaseous compound at normal conditions, it can be used as combustible in turbines of electricity generation. It has been successfully used in gas turbines which used methane, with a small modifications to achieve a clean and stable performance [34–36].

- Hydrogen vector

The absence of supply infrastructure and the problems related to the storage and transportation (hard liquefaction and low mass energy density), makes difficult to commercialize hydrogen directly. Due to its high hydrogen content (13 wt%) and its ability to be stored and transported in a liquified form, DME is a good candidate to produce hydrogen by steam reforming [37,38]. So this way, hydrogen is produced in-situ in the location where it needs to be used, like for example in a hydrogen fuel cell vehicle [39–42]

- Propellant

Due to its boiling point, one of the most common uses of DME is as aerosol propellant. It is specially used at a high purity for hygiene or cosmetic products, as is non-toxic. The main reason is because it is non-harmful to the ozone layer (contrary to CFC gases) and it is degraded in the troposphere [43,44]. Moreover, it does not contribute to the greenhouse effect in a high extend.

- Platform

DME can be used as a reactant for a wide range of reactions. The most common reactions are olefins, gasolines or hydrocarbon production [45–50], that are produced by acidic catalyst (like zeolites or SAPO) at relatively high temperatures (between 350-500 ºC). Other reactions are also studied which uses DME as reagent: methyl acetate is produced by carbonylation of DME with CO, using a zeolite as catalyst [51,52]; or the methylation of ethene by DME in a HZSM-5 zeolite [53].

UNIVERSIDAD DE MÁLAGA

1.3.2. DME production from syngas

Nowadays, DME is produced from syngas, but there also are some studies about CO_2 conversion into DME. When DME is produced from syngas, two main routes are employed: the direct and the indirect via.

1.3.2.1. Indirect via of DME production

This way of DME production is the most industrially widespread and consist of two steps carried out in different reactors. The first one is the methanol synthesis from syngas (eq. 1.1), and the second one is the methanol dehydration (eq. 1.2).

$$CO + 2H_2 \leftrightarrow CH_3OH \quad \Delta H° = -90.6\ kJ/mol \qquad (1.1)$$

$$2CH_3OH \leftrightarrow CH_3OCH_3\ \Delta H° = -23.4\ kJ/mol \qquad (1.2)$$

This way of DME production has the advantage of working under the best operating condition for every step. Moreover, as methanol production is a mature technology, its production is already well optimized.

The first step, the synthesis of methanol from syngas, is an industrial process that has been studied long time [54]. The first industrial catalyst for methanol synthesis from syngas was ZnO/Cr_2O_3 [55], that was fast replace by Cu around 1960, due to its higher activity. At the moment, it is carried out exclusively using $Cu\text{-}ZnO/Al_2O_3$ (CZA) catalyst, in which alumina act as support and as promoter too [56,57]. Lots of parameters have been study in order to obtain the best performance: coprecipitation at neutral pH and sol-gel precipitation seem to be the best catalyst preparation method [58,59], Al_2O_3 the best support [60] and 2:1 of Cu:Zn the best molar ratio [55]. Also, beneficial effects on catalyst has been shown by promoting the CZA catalyst with Mn [61], B [62], Pd [63] and, even, carbon nanotubes [64].

Other non-Cu based catalyst have also shown activity in the syngas to methanol reaction. Among all of them, Pd supported on ZnO [65] or CeO_2 [66] have shown good activity, although less selective to methanol than the commercial CZA. Molybdenum disulfide [67], as well as Rh, Pd or Pt sulfides [68] have also shown an acceptable performance.

For the second step, the most commonly used catalyst is the $\gamma\text{-}Al_2O_3$ [69,70], which possesses a Lewis acidity adequate for methanol dehydration. However, its main drawback is its water hydrophilicity, competing water and methanol for its adsorption on the active site

UNIVERSIDAD DE MÁLAGA

[69,71] and its deactivation by coke deposition on strong acid sites [72,73]. As the most commonly used catalyst, several studies have been carried out modifying its synthesis method [74,75], synthesis temperature [76], material precursors [77], the effect of promoters [78–80] and the presence of other alumina phases [81]. Modified alumina with Si or aluminosilicates have also been tested [82–84].

Zeolites have also been employed for methanol dehydration, being ZSM5 [85] the most spread one, but also using Y [86], mordenite [87], clionoptilolite [88] and nordstrandite [89]. Their main advantage is that they have both Lewis and Bronsted acidic sites, which seems to decrease the deactivating effect of water [90]. The increase in acidic strength enhance the activity of the zeolites, but also its tendency to be deactivated by coke deposition [91]. Modification of zeolites with Na [90] seems to increase the selectivity to DME by blockage of strong Bronsted acidic sites, but modification with metals, [92–94], as well as halogens [95] have also been assessed with some good results. Related to zeolites, modified silica (normally with Al) can also be used to dehydrate methanol to DME [96–98].

Metal phosphates can also be used as catalyst, presenting a high selectivity and resistance to water, as well as low coke formation. Aluminum phosphate [99–102], Silicoaluminophosphates (SAPO, which are normally used in the methanol to olefins process) [101,103,104] and zirconium phosphate [105–107], have shown promising performances in this reaction.

Finally, other active catalyst for the methanol dehydration can be found. Heteropoly acids (HPAs), very strong Bronsted acidic catalyst, shows activity at low temperatures (at >200 ºC, hydrocarbons are formed) but are hardly affected by water [91,108–110]. Some Ti and Nb oxides can be provided of Bronsted acidic sites, which gives them acceptable DME yields [79,111–113]. Ion exchange resins, with strong Bronsted acidic character have shown good catalytic performance, but some of them suffer from water deactivation [85,114,115].

1.3.2.2. Direct via of DME production

In the production of DME through the direct via, the syngas stream is in contact with a bifunctional catalyst, which is formed from a mix of metallic and acidic phase [116–118]. This via present important advantages versus the indirect via, like the reduction of the thermodynamic constraints of methanol. This is beneficial because the

UNIVERSIDAD DE MÁLAGA

conversion is risen, and it could work at lower H_2/CO ratios. An additional advantage is the use of only one reactor, which reduces the infrastructure cost. The overall reaction is represented in eq. 1.3.

$$3CO + 3H_2 \leftrightarrow CH_3OCH_3 + CO_2 \;\; \Delta H° = -245.8\, kJ/mol \quad (1.3)$$

However, due to the presence of water and CO_2, the water gas shift (and its reverse reaction) could also happen.

$$H_2O + CO \leftrightarrow H_2 + CO_2 \;\; \Delta H° = -41.2\, kJ/mol \quad (1.4)$$

A huge variety of catalyst have been used in the direct production of DME from syngas. As happened for the methanol hydrogenation from syngas, Cu/ZnO-based catalyst are the most commonly used as metallic phase in the hybrid catalyst, in particular, those supported in alumina (CZA catalysts). Conversely, γ-Al_2O_3 and zeolites are also the most widely used as acidic phase. For this reason, a lot of papers studied the use of a physical mix of CZA and γ-Al_2O_3 [119–121] as a catalyst, although other contact methods, like wet mixing [122,123] or kneading [124,125] have also been tested. All of them shows similar yields to DME around 50 %, working at temperatures between 240-275 ºC, a total pressure between 30 and 50 bar and a H_2/CO ratio of 2/1 or 3/1.

Some dopants have been added to those catalysts to enhance their performance. Related to the acidic phase, it is interesting to avoid high acidic character sites that convert methanol or dimethyl ether into hydrocarbons and olefins, producing deactivation by coke deposition. Another problem that is intended to avoid is the competitive adsorption of water in the dehydration sites of γ-Al_2O_3 [117]. Addition of mixed oxides [82,126] or some anions [127–129] seems to enhance the catalyst performance. Related to the metal phase, enhancing the structure of alumina also increase the resistance of Cu particles to sintering [117,130], but the addition of some modifiers to Cu, like Zr, Ga, Y, Mn, Pd or MgO also seems to be beneficial for the catalyst performance [131–136].

Some innovations have been performed lately, as the use of colloids directly deposited on the γ-Al_2O_3 [137], showing high reactivity but low stability. CZA catalyst can also act itself as catalyst if some acidic character is given to the alumina [138] or use only Cu and γ-Al_2O_3 synthesized in a mesoporous form [139].

Another important group of hybrid catalyst for syngas to DME are those which mix of CZA with zeolites. The advantage of those materials is their

UNIVERSIDAD DE MÁLAGA

better stability and hydrophobic character, avoiding competitive adsorption on the methanol active sites and producing a higher activity [117]. Among all of the zeolite-containing catalyst, CZA mixed with HZSM-5 [140–142] or modified HZSM-5 [143–146] are the most commonly used due to its resistance to coke deposition. Ferrierite [147–150], HY [93,94] and other zeolites [151] are also being used as acidic phase, as well as silicoaluminophosphates [152]. All of them show a good performance, being the acidic strength and the crystallite size the most important parameter to modify the selectivity of the catalyst [117].

Some other catalysts are produced applying the core shell concept, in which the metallic phase is in the inner part of the particle and the acidic part in the outer part. This way, methanol produced in the interior of the particle is transformed to DME in its way out of the particle. Good results have been shown in a encapsulated CZA catalyst with H-ZSM-5 [153–155], SAPO-11 [156,157] or other core-shell systems [158,159]. A step further goes some works, which implement a membrane CZA+HZSM-5 microreactor that selectively remove the water present in the medium, enhancing this way the conversion [160–162]. Similar to this core-shell concept, fibrillar Cu-ZnO/ZrO_2 with HZSM-5 zeolite catalyst was prepared, allowing a short distance between the centers of both phases [163].

1.3.3. DME production from CO_2

In the recent years the growing concern about CO_2 emissions has boost the researching for utilization of CO_2 as feedstock. Production of DME from CO_2 rich syngas could mean an interesting way of valorization and, for this reason, a high amount of recent publications related to this topic can be found [164–167] .

CO_2 can react directly with H_2 to produce methanol, as eq. 1.5 shows, but it is thermodynamically less favorable than the syngas reaction. The additional production of water negatively affect the second part, the methanol dehydration [168].

$$CO_2 + 3H_2 \leftrightarrow CH_3OH + H_2O \quad \Delta H° = -49.5\ kJ/mol \qquad (1.5)$$

The bifunctional catalysts that have shown activity in that reaction are similar to the one used in the syngas to DME reaction. The main problems are the damage produced by water on those catalysts and that the metal phase of those catalysts promote the water gas shift reaction (eq. 1.4), reducing CO_2 concentration and the overall yield to methanol

UNIVERSIDAD DE MÁLAGA

[168]. For this reason, some modification has been done on the conventional Cu-ZnO phase, to enhance the reaction with CO_2 instead of CO [169], like the addition of Ga^{3+} [170], Pt, Rh or Pd [171,172]. Moreover, the use of ZrO_2 as support instead of Al_2O_3 (prepared by different methods) has shown further increase in activity [173,174], although mesopores silica [175], TiO_2 [176] and carbon [177] supports have also been found as good supports. Some alternatives to Cu catalysts have also been found, apart from noble metals [178–180], Co [181], Ni [182,183] or In [184] have shown promising yields to methanol production from CO_2.

Related to the acidic phase of the catalyst, as the reaction is the same than when syngas is feed, not many changes could be found. The main problems associated to the use of CO_2 instead of CO is the additional presence of water, specially detrimental for γ-Al_2O_3 [185]. In this sense, γ-Al_2O_3 and HZSM-5 are the most widely used catalyst for this reaction [168].

1.3.4. Kinetic Model of DME production

Kinetic models have been widely used to predict the behavior of a catalyst in a reaction under certain operation conditions. By its use, it is possible to optimize temperature, space time or reactive partial pressure, but also the catalyst formulation. In the literature, several kinetic study of methanol dehydration to DME has been previously reported. Kinetics models ranged from a simple kinetic model that only adjust experimental data to mathematical equations as a function of temperature [186] or semiempirical equations [187,188] to more complex models, extracted from intrinsic mechanisms. Several equations are extracted from Langmuir-Hinschelwood [187,189] or Eley-Rideal concept [70,85,190,191], also taking into account dissociative or molecular adsorption [192,193]. Lu et al. and other authors [104,194,195] employed a 7 step non-dissociative adsorption mechanism. Sierra et al. [196] proposed a model extracted from the assumption of elementary reactions and isothermal plug flow, introducing a factor that highlights the water effect. Ha et al. [197,198] proposed a non-dissociative methanol adsorption mechanism in which methanol is converted into a methyl carboxonium ion intermediate on ZSM-5. A mechanism for methanol dehydration on Zr-loaded P-containing carbon al low temperatures has been proposed [107], based in Langmuir-Hinschelwood concept. The mechanism consists of a dissociative adsorption of a first methanol molecule in the phosphorus

UNIVERSIDAD DE MÁLAGA

part of the active site to produce a methoxy specie, which reacts with a second non-dissociative methanol adsorbed in the zirconium part of the active site. Reaction of both methanol molecules produce DME and regenerate the active site by water release. At higher temperatures, some coke deposition is observed, so a different mechanism seems to be present [199].

1.3.5. DME market

DME global market has been increasing in the recent years [200], only negatively affected by Corona disease, that caused a reduction of crude oil price and demand, and so to the DME demand. Nevertheless, it is expected that, in the near future, DME market continue increasing from USD 4001.89 million in 2020 to USD 8755.17 million in 2028 [201], as well as its demand, expected to grow at a compound annual growth rate (CAGR) of 10.5% [201].

Besides, a renewable dimethyl ether (rDME) producer recently started using primarily waste methanol [202] to produce DME, with the main goal of developing the hydrogen economy, as DME is an interesting hydrogen vector [40].

1.4. Carbon materials as catalysts and catalyst supports

The efficient use of residual biomass resources in future biorefineries to sustainable produce not only fuels and chemicals, but other bioproducts (such as, advanced catalytic materials) involves also a relevant strategy for boosting the bio-based circular economy. In this sense, intensive research is taking place on the preparation of carbon catalysts from biomass as they present several advantages versus conventional inorganic materials [203–205]. Activated carbons are highly thermal and chemically stable carbonaceous materials with a developed porous texture, which have been traditionally use as adsorbent (both in gas [206,207] or liquid phase [208–210]) or catalyst supports [211]. In the context of a biorefinery, those materials can be the final product obtained from pyrolysis or partial gasification of biomass waste. Moreover, the control of the operating conditions during its obtention allows the generation of an specific surface chemistry that can be used as anchor points for different active phases [212]. Additionally, at the

UNIVERSIDAD DE MÁLAGA

end of its life, they can be gasified, recovering the active phases and producing syngas than can be used as feedstock for methanol or DME production [213,214].

The development of a porous texture can be tailored to cover some specific requirements [215]. This process is called activation. Depending on the activation process, it can be classified as physical or chemical.

In a physical activation, a partial gasification is produced, in which an oxidizing agent stream is in contact with the carbonaceous precursor. Temperature and oxidizing time are the most important parameters for a determined agent. The most common agents are CO_2 or steam. Regarding to the selective dehydration reaction of methanol to DME, Moreno-Castilla et al. prepared acid surface carbon catalysts by oxidation of biomass-derived activated carbons with different liquid oxidants and acids. Those carbonaceous materials presented some activity for this reaction, related to the presence of carboxyl acid surface groups on the carbon catalysts [216]. However, the catalysts were rapidly deactivated due to the partial decomposition of these oxygen surface groups at the reaction temperatures.

In a chemical activation, the carbon precursor is physically mixed with an activation substance and then, heated in an inert atmosphere. Several activation chemicals can be used, as $ZnCl_2$ [217], sulfuric acid [218,219], KOH [220,221] or phosphoric acid [222,223].

1.4.1. Phosphoric acid chemical activation

Phosphoric acid activated carbons have been widely studied due to its high versatility [224], as it can be produced carbons with a remarkable micropore and mesoporous texture [225–227]. In the 1980's Professor Laine [222] and Professor Sing [228] started to be interested in the porous texture development of carbonaceous materials by phosphoric acid. After that, Jagtoyen et al. [229] proposed a mechanism for pore development in hardwoods, in which during its activation process, phosphoric acid catalyzes bond cleavage and formation of phosphate and polyphosphate crosslinks due to cyclization and condensation reactions. The P-related bridges produce a dilation of the carbon structure that results in a well-developed pore structure after their removal in the washing step.

Phosphorus, a well-known fire inhibitor, can be used to reduce graphite powder oxidation rate by different treatments with phosphorus compounds [230,231]. In this sense, Professor Radovic el al. [232] studied the phosphorus groups that are able to inhibit the oxidation process and conclude that C-O-PO_3 and C-PO_3 groups can block the

UNIVERSIDAD DE MÁLAGA

active site for oxidation. Puziy and Poddubnaya [233] also observed the presence of those phosphorus groups on activated carbons obtained from P-containing polymers carbonization, which were associated to an acidic character and enhanced thermal and chemical stability. Tascón and his research group [234], observed shortly after the fixation of some phosphorus groups in the carbon surface of synthetic activated carbon produced by chemical activation with H_3PO_4. Those phosphorus groups show a high thermal and chemical stability. Moreover, they studied the carbonization temperature and observed that, at 800 ºC, the higher amount of phosphorus was retained. They also studied on nomex, apple pulp and coffee bean husk [235–237] the effect of changing the phosphoric acid/carbon precursor ratio, the activation temperature, the activation time and the phosphorus contact time before activation. They found that by increasing the ratio acid/precursor, the porous texture became wider, as already observed Rodríguez-Reinoso and Molina-Sabio [238], but also remarked the importance of the washing step after activation to free the pores. Professor Cordero and his research group [239,240] also studied the effect on porosity of lignin from eucalyptus and hemp canes monoliths, and they observed that increasing the H_3PO_4/precursor ratio from 1 to 3 at 425 ºC, the mesoporous volume of the sample was augmented.

Particularly interesting is the phosphorus remained in the lignocellulosic-derived phosphorus acid activated carbons [241], which provides the carbon with an acidic character. Those phosphorus groups, thermally and chemically stable, are present on the carbon surface, in the form of C-O-P (C-O-PO_3, (C-O)$_2$-PO_2 or (C-O)$_3$-PO) or C-P (C_3-PO, C_2-PO_2, C-PO_3) groups [234,242]. Those groups, were also observed by Professor Cordero on phosphorus acid activated carbon from hemp [207], olive stone [243] and lignin, and also provide the activated carbon with a higher oxidation resistance, acting as a physical barrier. They also use the unreacted shrinking core model to predict accurately the carbon oxidation and proposed that, in a thermal treatment at 900 ºC in inert atmosphere, phosphorus remains linked to the carbon, but C-O-P were reduced to C-P groups, causing a slight delay of the oxidation in a subsequent oxidation process [244]. In this sense, they studied in deep the cycle C-O-P to C-P by an inert atmosphere thermal treatment, followed by a relatively low temperature oxidation. They observed that the oxidation of C-P was produced even at ambient temperature (as samples were auto-heated in contact with air after the inert atmosphere thermal treatment), and only after all the C-P groups were oxidized (by the effect of higher temperatures or time) another carbon-oxygen group appears on the carbon surface [245]. Moreover, those phosphorus

UNIVERSIDAD DE MÁLAGA

groups can be used as “anchor” points to functionalize the carbon with nitrogen groups [246] or with some active metal phases [247].

Another important point of those phosphorus groups is their catalytic behavior. Professor Cordero et al. observed the dehydration activity of those acidic phosphorus containing carbons in the dehydration of several alcohols, like isopropanol and ethanol [248,249]. They also used those activated carbons in the production of DME from methanol, but their activity strongly decayed unless an oxidant atmosphere was used. Puziy and Poddubnaya [250], on their behalf, also observed catalytic activity in the synthesis of ethyl-tert-butyl from isobutene.

1.5. Catalyst deactivation

Deactivation is the process by which the catalyst reduces its activity as the time on stream goes by. The mechanism of deactivation depends on the reaction submitted to study. Deactivation is one of the main problems in industrial catalysis and force to replace the catalyst after certain working time. This deactivation can be reversible or irreversible, depending on its possibility to recover the initial activity or not. Conversely, it can also be uniform or selective, if the whole catalyst is affected or only a part of the active site [251].

1.5.1. Classification of catalyst deactivation

Although every reaction has their own mechanism of catalyst deactivation, several common type of deactivation can be named [252,253].

1.5.1.1. Poisoning

This happens when an impurity present in feed is adsorbed irreversibly on the active site, avoiding that this active site could catalyze the main reaction. That type of contaminations is observed in Cu/ZnO by sulfur compounds, phosphine, methyl chloride and methyl fluoride [254]. Another example is the deactivation of Cu by its oxidation with impurities of oxygen [142].

1.5.1.2. Sintering

It consists of the loss of surface area by support collapse or the aggregation of catalyst particles. Some authors [252] divided the sintering process between the migration of the crystallites and their coalescence and the ripening, which involve the movement of atoms to

UNIVERSIDAD DE MÁLAGA

form larger crystallites. This deactivation process also happened in the Cu part of the catalyst [142,255] and some general quantification of that process has been modeled [256–259].

1.5.1.3. Phase change

This happens in catalyst having different phases and, by the action of temperatures, one phase is transformed into another, which may be thermodynamically more stable. A typical case of that deactivation is the transformation of γ-Al_2O_3 into α-Al_2O_3 by the action of temperature [252].

1.5.1.4. Active phase migration

It consists of the movement of certain atoms in the active sites by the action of other compounds present in the medium. This is what happened in zeolites by the action of steam, which tends to dealuminate the zeolite [260,261]. Another problem related to that is the ion exchange between Cu^{2+} and the hydroxyl group of zeolites in bifunctional catalysts [142,262].

1.5.1.5. Coke deposition

This process occurred when an organic compound is adsorbed on the active site and subsequently reacts and polymerize to form coke. Coke has not a definite form and is a general word that describe the deactivation by organic compounds deposition on the active site. It is typical of acidic catalysts [263], and is already observed in the acidic catalyst which converts methanol in DME [91,260,264].

As this type of deactivation is reversible, its quantification and the evaluation of its effect in the catalyst is interesting. In this sense, several models have been proposed for coke modelling. The first, and the simplest one, was the empirical Voorhies equation [265] in which carbon deposited over the catalyst during oil cracking was only correlated to residence time. Chen et al. [266] and Qi et al. [267] modified that equation changing residence time for cumulative amount of hydrocarbon formed or cumulative amount of methanol feed, respectively, to be applied in the methanol to olefins reaction. Some semi-theoretical models have been developed for coke production in different reactions [268,269]. Prof. Holmen proposed a simple method to predict yields to different product in a relatively complex reaction matrix, taking into account the deactivation by adding a “deactivation vector” in every step [270]. Prof. Octave Levenspiel [251] proposed a method for deactivation quantification, which consisted of the addition of an “activity” factor in every reaction affected by the deactivation

UNIVERSIDAD DE MÁLAGA

process. This factor is then quantified empirically by a constant and the concentrations of the different possible deactivation precursors. This methodology has been widely used in literature [260,271]. Prof. Bilbao and his research group, based on that ideas, developed several kinetic studies for direct DME synthesis from syngas in fixed bed reactors [272–274], and in fixed bed reactors equipped with highly hydrophilic membrane reactors for in-situ removal of water, allowing the displacement of the equilibrium to selective DME production and reverse water-gas shift [161,162,275]. They have also proposed the obtention of kinetic parameters in complex reaction networks, including deactivation in different reactor configurations [276–278]. Prof. Froment, Bischoff and De Wilde [252] proposed a methodology for assessment of deactivation by coke deposition. They relate empirically coke concentration with decay in activity and modelled kinetically coke as any other product. This has also been widely used in coke deposition modeling [266,269]. Another methods can be also found in literature [268].

1.5.2. Catalyst regeneration

Catalyst regeneration is the process by which the catalyst recovers totally or partially its activity at zero time on stream. Not all of the deactivated catalyst can be regenerated, and some of them could only be recycled. Among them the most used regeneration happens on coke deposited catalyst (and sometimes in reversible poisoned) and consists of the contact of an oxidizing stream at high temperatures with the deactivated catalyst, which gasifies the coke, recovering the initial catalyst.

1.6. Objective

This thesis is focused on the study of lignocellulose waste-derived catalysts for the production of dimethyl ether (DME), as in the Methanol-to-DME process (MTD), as a high valuable chemical that can be used as renewable alternative for conventional diesel or liquified petroleum gases (LPG), given that methanol can be obtained from syngas produced from biomass residues gasification. In this sense, a Zr-loaded P-containing biomass-derived carbon catalyst has been studied under severe operation conditions (high temperature and long time on stream),

UNIVERSIDAD DE MÁLAGA

in order to achieve high methanol conversions, similar to those that usually take place in the industrial process, to analyze the stability, methanol conversion and selectivity to DME of the catalyst under these extreme reaction conditions.

The active surface centers of the biomass-derived catalyst for the methanol dehydration to DME have been defined and coke deposition on these actives surface sites for different operation conditions has been analyzed. Carbonaceous deposits on the active surface sites have proved to be the main sources of catalyst deactivation and determined the change in textural properties and surface chemistry of the catalyst and in products distribution.

On the other hand, the regeneration of the deactivated catalyst by air oxidation at low temperature has been also studied, analyzing the effect of this regeneration process on the active surface sites, as well as on the carbonaceous support properties. A kinetic model based on a proposed reaction mechanism that predicts yields to different products and quantify the deactivation effect of coke deposition and of presence of water on products distribution has been stablished.

References

1. Global direct primary energy consumption Available online: https://ourworldindata.org/grapher/global-primary-energy?country=~OWID_WRL (accessed on Jan 2, 2022).
2. Administration, U.S.E.I. EIA projects nearly 50% increase in world energy usage by 2050, led by growth in Asia Available online: https://www.eia.gov/todayinenergy/detail.php?id=41433 (accessed on Jan 2, 2022).
3. Speight, J.G. Petrochemicals. *Handb. Ind. Hydrocarb. Process.* **2011**, 429–466, doi:10.1016/B978-0-7506-8632-7.10012-X.
4. Blunden, J.; Boyer, T. State of the Climate in 2020. *Bull. Am. Meteorol. Soc.* **2021**, *102*, S1–S475, doi:10.1175/2021BAMSStateoftheClimate.1.
5. Hansen, J.; Sato, M. Global Temperature Available online: http://www.columbia.edu/~mhs119/Temperature/ (accessed on Dec 30, 2021).
6. Nations, U. Goal 13: Climate Action - United Nations Sustainable Development Available online: https://www.un.org/sustainabledevelopment/climate-change/ (accessed on Dec 30, 2021).

UNIVERSIDAD DE MÁLAGA

7. Comission, E. Progress made in cutting emissions Available online: https://ec.europa.eu/clima/eu-action/climate-strategies-targets/progress-made-cutting-emissions_en (accessed on Dec 30, 2021).

8. Nations, U. Key aspects of the Paris Agreement Available online: https://cop23.unfccc.int/process-and-meetings/the-paris-agreement/the-paris-agreement/key-aspects-of-the-paris-agreement (accessed on Dec 30, 2021).

9. CO2 emissions Available online: https://ourworldindata.org/co2-emissions (accessed on Dec 30, 2021).

10. Group, M. When will fossil fuels run out? Available online: https://group.met.com/fyouture/when-will-fossil-fuels-run-out/68 (accessed on Dec 31, 2021).

11. MAHB When Fossil Fuels Run Out, What Then? Available online: https://mahb.stanford.edu/library-item/fossil-fuels-run/ (accessed on Dec 31, 2021).

12. BP Full report – Statistical Review of World Energy 2021.

13. OMIE Mercado de electricidad Available online: https://www.omie.es/es/mercado-de-electricidad (accessed on Jan 1, 2022).

14. ¿Por qué el precio del gas está disparando la factura de la luz en España? Available online: https://www.antena3.com/noticias/economia/que-precio-gas-esta-disparando-factura-luz-espana_20210912613e3b0969e535000128b5b3.html (accessed on Jan 1, 2022).

15. Lopez, G.; Artetxe, M.; Amutio, M.; Alvarez, J.; Bilbao, J.; Olazar, M. Recent advances in the gasification of waste plastics. A critical overview. *Renew. Sustain. Energy Rev.* **2018**, *82*, 576–596, doi:10.1016/j.rser.2017.09.032.

16. Lee, U.; Chung, J.N.; Ingley, H.A. High-temperature steam gasification of municipal solid waste, rubber, plastic and wood. *Energy & Fuels* **2014**, *28*, 4573–4587, doi:10.1021/ef500713j.

17. Saral, J.S.; Ajmal, R.S.; Ranganathan, P. Bioeconomy of hydrocarbon biorefinery processes. *Hydrocarb. Biorefinery* **2022**, 355–385, doi:10.1016/B978-0-12-823306-1.00011-X.

18. Cherubini, F. The biorefinery concept: Using biomass instead of oil for producing energy and chemicals. *Energy Convers. Manag.* **2010**, *51*, 1412–1421, doi:10.1016/j.enconman.2010.01.015.

UNIVERSIDAD DE MÁLAGA

19. Stichnothe, H.; Meier, D.; de Bari, I. Biorefineries: Industry Status and Economics. *Dev. Glob. Bioeconomy Tech. Mark. Environ. Lessons from Bioenergy* **2016**, 41–67, doi:10.1016/B978-0-12-805165-8.00003-3.

20. Suganya, T.; Varman, M.; Masjuki, H.H.; Renganathan, S. Macroalgae and microalgae as a potential source for commercial applications along with biofuels production: A biorefinery approach. *Renew. Sustain. Energy Rev.* **2016**, *55*, 909–941, doi:10.1016/J.RSER.2015.11.026.

21. Cuellar-Bermudez, S.P.; Garcia-Perez, J.S.; Rittmann, B.E.; Parra-Saldivar, R. Photosynthetic bioenergy utilizing CO2: an approach on flue gases utilization for third generation biofuels. *J. Clean. Prod.* **2015**, *98*, 53–65, doi:10.1016/J.JCLEPRO.2014.03.034.

22. Naik, S.N.; Goud, V. V.; Rout, P.K.; Dalai, A.K. Production of first and second generation biofuels: A comprehensive review. *Renew. Sustain. Energy Rev.* **2010**, *14*, 578–597, doi:10.1016/J.RSER.2009.10.003.

23. Gutiérrez, M.C.; Rosas, J.M.; Rodríguez-Cano, M.A.; López-Luque, I.; Rodríguez-Mirasol, J.; Cordero, T. Strategic situation, design and simulation of a biorefinery in Andalusia. *Energy Convers. Manag.* **2019**, *182*, 201–214, doi:10.1016/j.enconman.2018.12.038.

24. Cardoza, D.; Romero, I.; Martínez, T.; Ruiz, E.; Gallego, F.J.; López-Linares, J.C.; Manzanares, P.; Castro, E. Location of Biorefineries Based on Olive-Derived Biomass in Andalusia, Spain. *Energies 2021, Vol. 14, Page 3052* **2021**, *14*, 3052, doi:10.3390/EN14113052.

25. Basu, P. *Biomass Gasification and Pyrolysis. Practical Design and Theory.*; Elsevier, Ed.; 2010;

26. Huber, G.W.; Iborra, S.; Corma, A. Synthesis of Transportation Fuels from Biomass: Chemistry, Catalysts, and Engineering. **2006**, doi:10.1021/cr068360d.

27. Semelsberger, T.A.; Borup, R.L.; Greene, H.L. Dimethyl ether (DME) as an alternative fuel. *J. Power Sources* **2006**, *156*, 497–511, doi:10.1016/j.jpowsour.2005.05.082.

28. Arcoumanis, C.; Bae, C.; Crookes, R.; Kinoshita, E. The potential of di-methyl ether (DME) as an alternative fuel for compression-ignition engines: A review. *Fuel* **2008**, *87*, 1014–1030, doi:10.1016/j.fuel.2007.06.007.

UNIVERSIDAD DE MÁLAGA

29. Park, S.H.; Lee, C.S. Applicability of dimethyl ether (DME) in a compression ignition engine as an alternative fuel. *Energy Convers. Manag.* **2014**, *86*, 848–863, doi:10.1016/j.enconman.2014.06.051.

30. Styring, P.; Dowson, G.R.M.; Tozer, I.O. Synthetic Fuels Based on Dimethyl Ether as a Future Non-Fossil Fuel for Road Transport From Sustainable Feedstocks. *Front. Energy Res.* **2021**, *9*, 240, doi:10.3389/FENRG.2021.663331/BIBTEX.

31. Anggarani, R.; Wibowo, C.S.; Rulianto, D. Application of dimethyl ether as LPG substitution for household stove. *Energy Procedia* **2014**, *47*, 227–234, doi:10.1016/j.egypro.2014.01.218.

32. Marchionna, M.; Patrini, R.; Sanfilippo, D.; Migliavacca, G. Fundamental investigations on di-methyl ether (DME) as LPG substitute or make-up for domestic uses. *Fuel Process. Technol.* **2008**, *89*, 1255–1261, doi:10.1016/J.FUPROC.2008.07.013.

33. Lee, S.; Oh, S.; Choi, Y.; Kang, K. Effect of n-Butane and propane on performance and emission characteristics of an SI engine operated with DME-blended LPG fuel. *Fuel* **2011**, *90*, 1674–1680, doi:10.1016/J.FUEL.2010.11.040.

34. Lee, M.C.; Seo, S. Bin; Chung, J.H.; Joo, Y.J.; Ahn, D.H. Industrial gas turbine combustion performance test of DME to use as an alternative fuel for power generation. *Fuel* **2009**, *88*, 657–662, doi:10.1016/J.FUEL.2008.10.027.

35. Gökalp, I.; Lebas, E. Alternative fuels for industrial gas turbines (AFTUR). *Appl. Therm. Eng.* **2004**, *24*, 1655–1663, doi:10.1016/J.APPLTHERMALENG.2003.10.035.

36. Kobayashi, N.; Inoue, H.; Koizumi, H.; Watanabe, T. Robust Design of the Coaxial Jet Cluster Nozzle Burner for DME (Dimethyl Ether) Fuel. *Am. Soc. Mech. Eng. Int. Gas Turbine Institute, Turbo Expo IGTI* **2009**, *2*, 333–338, doi:10.1115/GT2003-38410.

37. Vicente, J.; Gayubo, A.G.; Ereña, J.; Aguayo, A.T.; Olazar, M.; Bilbao, J. Improving the DME steam reforming catalyst by alkaline treatment of the HZSM-5 zeolite. *Appl. Catal. B Environ.* **2013**, *130–131*, 73–83, doi:10.1016/j.apcatb.2012.10.019.

38. Ereña, J.; Vicente, J.; Aguayo, A.T.; Olazar, M.; Bilbao, J.; Gayubo, A.G. Kinetic behaviour of catalysts with different CuO-ZnO-Al2O3 metallic function compositions in DME steam reforming in a fluidized bed. *Appl. Catal. B Environ.* **2013**, *142–143*, 315–322, doi:10.1016/j.apcatb.2013.05.034.

UNIVERSIDAD DE MÁLAGA

39. Li, J.; Zhang, Q.; Zhao, Y.; Qi, P.; Shao, C. Alkaline earth metal oxide modification of Ni/Al2O3 for hydrogen production from the partial oxidation and reforming of dimethyl ether. *React. Kinet. Mech. Catal.* **2017**, *122*, 1193–1202, doi:10.1007/s11144-017-1272-1.

40. Kim, D.; Park, G.; Choi, B.; Kim, Y.B. Reaction characteristics of dimethyl ether (DME) steam reforming catalysts for hydrogen production. *Int. J. Hydrogen Energy* **2017**, *42*, 29210–29221, doi:10.1016/j.ijhydene.2017.10.020.

41. Takeishi, K.; Suzuki, H. Steam reforming of dimethyl ether. *Appl. Catal. A Gen.* **2004**, *260*, 111–117, doi:10.1016/J.APCATA.2003.10.006.

42. Galvita, V. V.; Semin, G.L.; Belyaev, V.D.; Yurieva, T.M.; Sobyanin, V.A. Production of hydrogen from dimethyl ether. *Appl. Catal. A Gen.* **2001**, *216*, 85–90, doi:10.1016/S0926-860X(01)00540-3.

43. Fleisch, T.H.; Basu, A.; Gradassi, M.J.; Masin, J.G. Dimethyl ether: A fuel for the 21st century. *Stud. Surf. Sci. Catal.* **1997**, *107*, 117–125, doi:10.1016/S0167-2991(97)80323-0.

44. Yeoman, A.M.; Lewis, A.C. Global emissions of VOCs from compressed aerosol products. *Elem. Sci. Anthr.* **2021**, *9*, doi:10.1525/ELEMENTA.2020.20.00177.

45. Hajjar, Z.; Khodadadi, A.; Mortazavi, Y.; Tayyebi, S.; Soltanali, S. Artificial intelligence modeling of DME conversion to gasoline and light olefins over modified nano ZSM-5 catalysts. *Fuel* **2016**, *179*, 79–86, doi:10.1016/j.fuel.2016.03.046.

46. Haro, P.; Trippe, F.; Stahl, R.; Henrich, E. Bio-syngas to gasoline and olefins via DME - A comprehensive techno-economic assessment. *Appl. Energy* **2013**, *108*, 54–65, doi:10.1016/j.apenergy.2013.03.015.

47. Zhou, H.; Wang, Y.; Wei, F.; Wang, D.; Wang, Z. In situ synthesis of SAPO-34 crystals grown onto α-Al2O3 sphere supports as the catalyst for the fluidized bed conversion of dimethyl ether to olefins. *Appl. Catal. A Gen.* **2008**, *341*, 112–118, doi:10.1016/j.apcata.2008.02.030.

48. Ortega, C.; Hessel, V.; Kolb, G. Dimethyl ether to hydrocarbons over ZSM-5: Kinetic study in an external recycle reactor. *Chem. Eng. J.* **2018**, *354*, 21–34, doi:10.1016/j.cej.2018.07.178.

49. Pérez-Uriarte, P.; Gamero, M.; Ateka, A.; Díaz, M.; Aguayo, A.T.; Bilbao, J. Effect of the Acidity of HZSM-5 Zeolite and the Binder

UNIVERSIDAD DE MÁLAGA

in the DME Transformation to Olefins. *Ind. Eng. Chem. Res.* **2016**, *55*, 1513–1521, doi:10.1021/acs.iecr.5b04477.

50. Pérez-Uriarte, P.; Ateka, A.; Gamero, M.; Aguayo, A.T.; Bilbao, J. Effect of the Operating Conditions in the Transformation of DME to olefins over a HZSM-5 Zeolite Catalyst. *Ind. Eng. Chem. Res.* **2016**, *55*, 6569–6578, doi:10.1021/acs.iecr.6b00627.

51. Cheung, P.; Bhan, A.; Sunley, G.J.; Iglesia, E. Selective Carbonylation of Dimethyl Ether to Methyl Acetate Catalyzed by Acidic Zeolites. *Angew. Chemie Int. Ed.* **2006**, *45*, 1617–1620, doi:10.1002/ANIE.200503898.

52. Zhan, E.; Xiong, Z.; Shen, W. Dimethyl ether carbonylation over zeolites. *J. Energy Chem.* **2019**, *36*, 51–63, doi:10.1016/J.JECHEM.2019.04.015.

53. Maihom, T.; Boekfa, B.; Sirijaraensre, J.; Nanok, T.; Probst, M.; Limtrakul, J. Reaction mechanisms of the methylation of ethene with methanol and dimethyl ether over h-zsm-5: An ONIOM study. *J. Phys. Chem. C* **2009**, *113*, 6654–6662, doi:10.1021/JP809746A/SUPPL_FILE/JP809746A_SI_001.PDF.

54. Klier, K. Methanol Synthesis. *Adv. Catal.* **1982**, *31*, 243–313, doi:10.1016/S0360-0564(08)60455-1.

55. BASF German Patents 1923.

56. Behrens, M.; Zander, S.; Kurr, P.; Jacobsen, N.; Senker, J.; Koch, G.; Ressler, T.; Fischer, R.W.; Schlögl, R. Performance improvement of nanocatalysts by promoter-induced defects in the support material: Methanol synthesis over Cu/ZnO:Al. *J. Am. Chem. Soc.* **2013**, *135*, 6061–6068, doi:10.1021/JA310456F/SUPPL_FILE/JA310456F_SI_001.PDF.

57. Hansen, J.B.; Hojlund Nielsen, P.E. Methanol Synthesis. *Handb. Heterog. Catal.* **2008**, 2920–2949, doi:10.1002/9783527610044.HETCAT0148.

58. Li, J.L.; Inui, T. Characterization of precursors of methanol synthesis catalysts, copper/zinc/aluminum oxides, precipitated at different pHs and temperatures. *Appl. Catal. A Gen.* **1996**, *137*, 105–117, doi:10.1016/0926-860X(95)00284-7.

59. Zhang, Y.; Sun, Q.; Deng, J.; Wu, D.; Chen, S. A high activity Cu/ZnO/Al2O3 catalyst for methanol synthesis: Preparation and catalytic properties. *Appl. Catal. A Gen.* **1997**, *158*, 105–120, doi:10.1016/S0926-860X(96)00362-6.

UNIVERSIDAD DE MÁLAGA

60. Robinson, W.R.A.M.; Mol, J.C. Support effects in methanol synthesis over copper-containing catalysts. *Appl. Catal.* **1991**, *76*, 117–129, doi:10.1016/0166-9834(91)80008-K.

61. Chen, H.Y.; Lin, J.; Tan, K.L.; Li, J. Comparative studies of manganese-doped copper-based catalysts: the promoter effect of Mn on methanol synthesis. *Appl. Surf. Sci.* **1998**, *126*, 323–331, doi:10.1016/S0169-4332(97)00692-2.

62. Wu, J.; Saito, M.; Mabuse, H. Activity and stability of Cu/ZnO/Al2O3 catalyst promoted with B2O3 for methanol synthesis. *Catal. Lett. 2000 681* **2000**, *68*, 55–58, doi:10.1023/A:1019010831562.

63. Sahibzada, M.; Chadwick, D.; Metcalfe, I.S. Hydrogenation of carbon dioxide to methanol over palladium-promoted Cu/ZnO/A12O3 catalysts. *Catal. Today* **1996**, *29*, 367–372, doi:10.1016/0920-5861(95)00306-1.

64. Dong, X.; Zhang, H. Bin; Lin, G.D.; Yuan, Y.Z.; Tsai, K.R. Highly Active CNT-Promoted Cu–ZnO–Al2O3 Catalyst for Methanol Synthesis from H2/CO/CO2. *Catal. Lett. 2003 853* **2003**, *85*, 237–246, doi:10.1023/A:1022158116871.

65. Fujita, S.; Usui, M.; Hanada, T.; Takezawa, N. Methanol synthesis from CO2-H2 and from CO-H2 under atmospheric pressure over Pd and Cu catalysts. *React. Kinet. Catal. Lett. 1995 561* **1995**, *56*, 15–19, doi:10.1007/BF02066946.

66. Shen, W.J.; Ichihashi, Y.; Matsumura, Y. A Comparative Study of Palladium and Copper Catalysts in Methanol Synthesis. *Catal. Lett. 2002 791* **2002**, *79*, 125–127, doi:10.1023/A:1015334914620.

67. Youchang, X.; Naasz, B.N.; Somorjai, G.A. Alcohol synthesis from Co and H2 over molybdenum sulfide. The effect of pressure and promotion by potassium carbonate. *Appl. Catal.* **1986**, *27*, 233–241, doi:10.1016/S0166-9834(00)82920-6.

68. Koizumi, N.; Murai, K.; Ozaki, T.; Yamada, M. Development of sulfur tolerant catalysts for the synthesis of high quality transportation fuels. *Catal. Today* **2004**, *89*, 465–478, doi:10.1016/J.CATTOD.2004.02.002.

69. Akarmazyan, S.S.; Panagiotopoulou, P.; Kambolis, A.; Papadopoulou, C.; Kondarides, D.I. Methanol dehydration to dimethylether over Al_2O_3 catalysts. *Appl. Catal. B Environ.* **2014**, *145*, 136–148, doi:10.1016/j.apcatb.2012.11.043.

70. Alamolhoda, S.; Kazemeini, M.; Zaherian, A.; Zakerinasab, M.R.

UNIVERSIDAD DE MÁLAGA

Reaction kinetics determination and neural networks modeling of methanol dehydration over nano γ-Al2O3 catalyst. *J. Ind. Eng. Chem.* **2012**, *18*, 2059–2068, doi:10.1016/J.JIEC.2012.05.027.

71. Sung, D.M.; Kim, Y.H.; Park, E.D.; Yie, J.E. Role of surface hydrophilicity of alumina in methanol dehydration. *Catal. Commun.* **2012**, *20*, 63–67, doi:10.1016/J.CATCOM.2012.01.005.

72. Guisnet, M.; Magnoux, P. Coking and Deactivation of Zeolites Influence of the Pore Structure. *Appl. Catal. Elsevier Sci. Publ. B.V* **1989**, *54*, 1–27.

73. Müller, S.; Liu, Y.; Vishnuvarthan, M.; Sun, X.; Van Veen, A.C.; Haller, G.L.; Sanchez-Sanchez, M.; Lercher, J.A. Coke formation and deactivation pathways on H-ZSM-5 in the conversion of methanol to olefins. *J. Catal.* **2015**, *325*, 48–59, doi:10.1016/j.jcat.2015.02.013.

74. Sanchez-Valente, J.; Bokhimi, X.; Toledo, J.A. Synthesis and catalytic properties of nanostructured aluminas obtained by sol–gel method. *Appl. Catal. A Gen.* **2004**, *264*, 175–181, doi:10.1016/J.APCATA.2003.12.041.

75. Keshavarz, A.R.; Rezaei, M.; Yaripour, F. Nanocrystalline gamma-alumina: A highly active catalyst for dimethyl ether synthesis. *Powder Technol.* **2010**, *199*, 176–179, doi:10.1016/J.POWTEC.2010.01.003.

76. Kim, S.M.; Lee, Y.J.; Bae, J.W.; Potdar, H.S.; Jun, K.W. Synthesis and characterization of a highly active alumina catalyst for methanol dehydration to dimethyl ether. *Appl. Catal. A Gen.* **2008**, *348*, 113–120, doi:10.1016/J.APCATA.2008.06.032.

77. Hosseini, S.Y.; Khosravi Nikou, M.R. Investigation of different precipitating agents effects on performance of γ-Al2O3 nanocatalysts for methanol dehydration to dimethyl ether. *J. Ind. Eng. Chem.* **2014**, *20*, 4421–4428, doi:10.1016/J.JIEC.2014.02.010.

78. Jun, K.W.; Lee, H.S.; Roh, H.S.; Park, S.E. Catalytic Dehydration of Methanol to Dimethyl Ether (DME) over Solid-Acid Catalysts. *Bull. Korean Chem. Soc.* **2002**, *23*, 803–807, doi:10.5012/BKCS.2002.23.6.803.

79. Fu, Y.; Hong, T.; Chen, J.; Auroux, A.; Shen, J. Surface acidity and the dehydration of methanol to dimethyl ether. *Thermochim. Acta* **2005**, *434*, 22–26, doi:10.1016/J.TCA.2004.12.023.

80. Aboul-Fotouh, S.M.K. Effect of ultrasonic irradiation and/or

UNIVERSIDAD DE MÁLAGA

halogenation on the catalytic performance of γ-Al2O3 for methanol dehydration to dimethyl ether. *J. Fuel Chem. Technol.* **2013**, *41*, 1077–1084, doi:10.1016/S1872-5813(13)60045-6.

81. Sung, D.M.; Kim, Y.H.; Park, E.D.; Yie, J.E. Correlation between acidity and catalytic activity for the methanol dehydration over various aluminum oxides. *Res. Chem. Intermed.* **2010**, *36*, 653–660, doi:10.1007/S11164-010-0201-Y/FIGURES/5.

82. Takeguchi, T.; Yanagisawa, K.I.; Inui, T.; Inoue, M. Effect of the property of solid acid upon syngas-to-dimethyl ether conversion on the hybrid catalysts composed of Cu–Zn–Ga and solid acids. *Appl. Catal. A Gen.* **2000**, *192*, 201–209, doi:10.1016/S0926-860X(99)00343-9.

83. Tokay, K.C.; Dogu, T.; Dogu, G. Dimethyl ether synthesis over alumina based catalysts. *Chem. Eng. J.* **2012**, *184*, 278–285, doi:10.1016/J.CEJ.2011.12.034.

84. Alba, M.D.; Romero, A.A.; Occelli, M.L.; Klinowski, J. Kinetic studies of the dehydration of methanol over aluminosilicate and gallosilicate offretites. *J. Chem. Soc. Faraday Trans.* **1997**, *93*, 1221–1224, doi:10.1039/A607290I.

85. Hosseininejad, S.; Afacan, A.; Hayes, R.E. Catalytic and kinetic study of methanol dehydration to dimethyl ether. *Chem. Eng. Res. Des.* **2012**, *90*, 825–833, doi:10.1016/j.cherd.2011.10.007.

86. Vanoye, L.; Favre-Réguillon, A.; Munno, P.; Rodríguez, J.F.; Dupuy, S.; Pallier, S.; Pitault, I.; De Bellefon, C. Methanol dehydration over commercially available zeolites: Effect of hydrophobicity. *Catal. Today* **2013**, *215*, 239–242, doi:10.1016/J.CATTOD.2013.01.012.

87. Sofianos, A.C.; Scurrell, M.S. Conversion of synthesis gas to dimethyl ether over bifunctional catalytic systems. *Ind. Eng. Chem. Res.* **2002**, *30*, 2372–2378, doi:10.1021/IE00059A002.

88. Khoshbin, R.; Haghighi, M. Direct syngas to DME as a clean fuel: The beneficial use of ultrasound for the preparation of CuO–ZnO–Al2O3/HZSM-5 nanocatalyst. *Chem. Eng. Res. Des.* **2013**, *91*, 1111–1122, doi:10.1016/J.CHERD.2012.11.017.

89. Seo, C.W.; Jung, K.D.; Lee, K.Y.; Yoo, K.S. Dehydration of methanol over Nordstrandite based catalysts for dimethyl ether synthesis. *J. Ind. Eng. Chem.* **2009**, *15*, 649–652, doi:10.1016/J.JIEC.2009.09.037.

90. Jiang, S.; Hwang, J.S.; Jin, T.; Cai, T.; Cho, W.; Baek, Y.S.; Park, S.E. Dehydration of Methanol to Dimethyl Ether over ZSM-5

UNIVERSIDAD DE MÁLAGA

Zeolite. *Bull. Korean Chem. Soc.* **2004**, *25*, 185–189, doi:10.5012/BKCS.2004.25.2.185.

91. Alharbi, W.; Kozhevnikova, E.F.; Kozhevnikov, I. V. Dehydration of Methanol to Dimethyl Ether over Heteropoly Acid Catalysts: The Relationship between Reaction Rate and Catalyst Acid Strength. *ACS Catal.* **2015**, *5*, 7186–7193, doi:10.1021/acscatal.5b01911.

92. Khandan, N.; Kazemeini, M.; Aghaziarati, M. Determining an optimum catalyst for liquid-phase dehydration of methanol to dimethyl ether. *Appl. Catal. A Gen.* **2008**, *349*, 6–12, doi:10.1016/J.APCATA.2008.07.029.

93. Fei, J.; Hou, Z.; Zhu, B.; Lou, H.; Zheng, X. Synthesis of dimethyl ether (DME) on modified HY zeolite and modified HY zeolite-supported Cu–Mn–Zn catalysts. *Appl. Catal. A Gen.* **2006**, *304*, 49–54, doi:10.1016/J.APCATA.2006.02.019.

94. Jin, D.; Zhu, B.; Hou, Z.; Fei, J.; Lou, H.; Zheng, X. Dimethyl ether synthesis via methanol and syngas over rare earth metals modified zeolite Y and dual Cu–Mn–Zn catalysts. *Fuel* **2007**, *86*, 2707–2713, doi:10.1016/J.FUEL.2007.03.011.

95. Aboul-Fotouh, S.M.K.; Aboul-Gheit, N.A.K.; Hassan, M.M.I. Conversion of Methanol Using Modified H-MOR Zeolite Catalysts. *Chinese J. Catal.* **2011**, *32*, 412–417, doi:10.1016/S1872-2067(10)60187-8.

96. Sabour, B.; Peyrovi, M.H.; Hamoule, T.; Rashidzadeh, M. Catalytic dehydration of methanol to dimethyl ether (DME) over Al-HMS catalysts. *J. Ind. Eng. Chem.* **2014**, *20*, 222–227, doi:10.1016/J.JIEC.2013.03.044.

97. Macina, D.; Piwowarska, Z.; Tarach, K.; Góra-Marek, K.; Ryczkowski, J.; Chmielarz, L. Mesoporous silica materials modified with alumina polycations as catalysts for the synthesis of dimethyl ether from methanol. *Mater. Res. Bull.* **2016**, *74*, 425–435, doi:10.1016/J.MATERRESBULL.2015.11.018.

98. Naik, S.P.; Bui, V.; Ryu, T.; Miller, J.D.; Zmierczak, W. Al-MCM-41 as methanol dehydration catalyst. *Appl. Catal. A Gen.* **2010**, *381*, 183–190, doi:10.1016/J.APCATA.2010.04.007.

99. Yaripour, F.; Mollavali, M.; Jam, S.M.; Atashi, H. Catalytic Dehydration of Methanol to Dimethyl Ether Catalyzed by Aluminum Phosphate Catalysts. *Energy and Fuels* **2009**, *23*, 1896–1900, doi:10.1021/EF800856C.

100. Lertjiamratn, K.; Praserthdam, P.; Arai, M.; Panpranot, J.

UNIVERSIDAD DE MÁLAGA

Modification of acid properties and catalytic properties of AlPO4 by hydrothermal pretreatment for methanol dehydration to dimethyl ether. *Appl. Catal. A Gen.* **2010**, *378*, 119–123, doi:10.1016/J.APCATA.2010.02.013.

101. Dai, W.; Kong, W.; Wu, G.; Li, N.; Li, L.; Guan, N. Catalytic dehydration of methanol to dimethyl ether over aluminophosphate and silico-aluminophosphate molecular sieves. *Catal. Commun.* **2011**, *12*, 535–538, doi:10.1016/J.CATCOM.2010.11.019.

102. Kikhtyanin, O. V.; Mastikhin, V.M.; Ione, K.G. Methanol conversion on aluminophosphates with zeolite structure. *Appl. Catal.* **1988**, *42*, 1–13, doi:10.1016/S0166-9834(00)80071-8.

103. Yoo, K.S.; Kim, J.H.; Park, M.J.; Kim, S.J.; Joo, O.S.; Jung, K.D. Influence of solid acid catalyst on DME production directly from synthesis gas over the admixed catalyst of Cu/ZnO/Al2O3 and various SAPO catalysts. *Appl. Catal. A Gen.* **2007**, *330*, 57–62, doi:10.1016/J.APCATA.2007.07.007.

104. Pop, G.; Bozga, G.; Ganea, R.; Natu, N. Methanol Conversion to Dimethyl Ether over H-SAPO-34 Catalyst. *Ind. Eng. Chem. Res.* **2009**, *48*, 7065–7071, doi:10.1021/IE900532Y.

105. Cheng, S.; Peng, G.Z.; Clearfield, A. Decomposition of alcohols over zirconium and titanium phosphates. *Ind. Eng. Chem. Prod. Res. Dev.* **1984**, *23*, 219–225, doi:10.1021/i300014a008.

106. Palomo, J.; Rodríguez-Mirasol, J.; Cordero, T. Methanol Dehydration to Dimethyl Ether on Zr-Loaded P-Containing Mesoporous Activated Carbon Catalysts. *Materials (Basel).* **2019**, *12*, 2204, doi:10.3390/ma12132204.

107. Palomo, J.; Rodríguez-Cano, M.A.; Rodríguez-Mirasol, J.; Cordero, T. On the kinetics of methanol dehydration to dimethyl ether on Zr-loaded P-containing mesoporous activated carbon catalyst. *Chem. Eng. J.* **2019**, *378*, 122198, doi:10.1016/j.cej.2019.122198.

108. Ladera, R.M.; Ojeda, M.; Fierro, J.L.G.; Rojas, S. TiO2-supported heteropoly acid catalysts for dehydration of methanol to dimethyl ether: relevance of dispersion and support interaction. *Catal. Sci. Technol.* **2014**, *5*, 484–491, doi:10.1039/C4CY00998C.

109. Ivanova, S.; Nitsch, X.; Romero-Sarria, F.; Louis, B.; Centeno, M.A.; Roger, A.C.; Odriozola, J.A. New class of acid catalysts for methanol dehydration. *Stud. Surf. Sci. Catal.* **2010**, *175*, 601–604, doi:10.1016/S0167-2991(10)75117-X.

UNIVERSIDAD DE MÁLAGA

110. Anwar, A.; Abdel-Ghaffar, A.; Aboul-Fotouh, S.; Fikry, E. Surface Studies and Nature of Active Sites of Supported Heteropolyacids as Catalysts in Methanol Dehydration. *Collect. Czechoslov. Chem. Commun.* **1994**, *59*, 820–832, doi:10.1135/CCCC19940820.

111. Vishwanathan, V.; Roh, H.-S.; Kim, J.-W.; Jun, K.-W. Surface Properties and Catalytic Activity of TiO2–ZrO2 Mixed Oxides in Dehydration of Methanol to Dimethyl Ether. *Catal. Lett. 2004 961* **2004**, *96*, 23–28, doi:10.1023/B:CATL.0000029524.94392.9F.

112. Sun, Q.; Fu, Y.; Yang, H.; Auroux, A.; Shen, J. Dehydration of methanol to dimethyl ether over Nb2O5 and NbOPO4 catalysts: Microcalorimetric and FT-IR studies. *J. Mol. Catal. A Chem.* **2007**, *275*, 183–193, doi:10.1016/J.MOLCATA.2007.06.008.

113. Ladera, R.; Finocchio, E.; Rojas, S.; Fierro, J.L.G.; Ojeda, M. Supported niobium catalysts for methanol dehydration to dimethyl ether: FTIR studies of acid properties. *Catal. Today* **2012**, *192*, 136–143, doi:10.1016/J.CATTOD.2012.01.025.

114. Ciftci, A.; Sezgi, N.A.; Dogu, T. Nafion-Incorporated Silicate Structured Nanocomposite Mesoporous Catalysts for Dimethyl Ether Synthesis. *Ind. Eng. Chem. Res.* **2010**, *49*, 6753–6762, doi:10.1021/IE9015667.

115. VARIŞLI, D.; DOĞU, T. Production of Clean Transportation Fuel Dimethylether by Dehydration of Methanol Over Nafion Catalyst. *Gazi Univ. J. Sci.* **2010**, *21*, 37–41.

116. Ng, K.L.; Chadwick, D.; Toseland, B.A. Kinetics and modelling of dimethyl ether synthesis from synthesis gas. *Chem. Eng. Sci.* **1999**, *54*, 3587–3592, doi:10.1016/S0009-2509(98)00514-4.

117. Saravanan, K.; Ham, H.; Tsubaki, N.; Bae, J.W. Recent progress for direct synthesis of dimethyl ether from syngas on the heterogeneous bifunctional hybrid catalysts. *Appl. Catal. B Environ.* **2017**, *217*, 494–522, doi:10.1016/j.apcatb.2017.05.085.

118. Azizi, Z.; Rezaeimanesh, M.; Tohidian, T.; Rahimpour, M.R. Dimethyl ether: A review of technologies and production challenges. *Chem. Eng. Process. Process Intensif.* **2014**, *82*, 150–172, doi:10.1016/J.CEP.2014.06.007.

119. Moradi, G.R.; Nazari, M.; Yaripour, F. The interaction effects of dehydration function on catalytic performance and properties of hybrid catalysts upon LPDME process. *Fuel Process. Technol.* **2008**, *89*, 1287–1296, doi:10.1016/J.FUPROC.2008.09.014.

120. Stiefel, M.; Ahmad, R.; Arnold, U.; Döring, M. Direct synthesis of

UNIVERSIDAD DE MÁLAGA

dimethyl ether from carbon-monoxide-rich synthesis gas: Influence of dehydration catalysts and operating conditions. *Fuel Process. Technol.* **2011**, *92*, 1466–1474, doi:10.1016/J.FUPROC.2011.03.007.

121. Wang, D.; Han, Y.; Tan, Y.; Tsubaki, N. Effect of H2O on Cu-based catalyst in one-step slurry phase dimethyl ether synthesis. *Fuel Process. Technol.* **2009**, *90*, 446–451, doi:10.1016/J.FUPROC.2008.11.007.

122. Ereña, J.; Sierra, I.; Olazar, M.; Gayubo, A.G.; Aguayo, A.T. Deactivation of a CuO−ZnO−Al2O3/γ-Al2O3 Catalyst in the Synthesis of Dimethyl Ether. *Ind. Eng. Chem. Res.* **2008**, *47*, 2238–2247, doi:10.1021/IE071478F.

123. Sierra, I.; Er Na, J.; Aguayo, A.T.; Arandes, J.M.; Olazar, M.; Bilbao, J.; Ereña, J.; Aguayo, A.T.; Arandes, J.M.; Olazar, M.; et al. Co-feeding water to attenuate deactivation of the catalyst metallic function (CuO–ZnO–Al 2 O 3) by coke in the direct synthesis of dimethyl ether. *"Applied Catal. B, Environ.* **2011**, *106*, 167–173, doi:10.1016/j.apcatb.2011.05.021.

124. Abu-Dahrieh, J.; Rooney, D.; Goguet, A.; Saih, Y. Activity and deactivation studies for direct dimethyl ether synthesis using CuO–ZnO–Al2O3 with NH4ZSM-5, HZSM-5 or γ-Al2O3. *Chem. Eng. J.* **2012**, *203*, 201–211, doi:10.1016/J.CEJ.2012.07.011.

125. Jung, H.; Lee, S.M.; Yang, D.R.; Jung, K.D. Relative Roles of Methanol Synthesis and Solid Acid Catalysts in the Direct DME Synthesis from Syngas. *Bull. Korean Chem. Soc.* **2015**, *36*, 1221–1225, doi:10.1002/BKCS.10235.

126. Lima, S.H.; Forrester, A.M.S.; Palacio, L.A.; Faro, A.C. Niobia-alumina as methanol dehydration component in mixed catalyst systems for dimethyl ether production from syngas. *Appl. Catal. A Gen.* **2014**, *488*, 19–27, doi:10.1016/J.APCATA.2014.09.022.

127. Xia, J.; Mao, D.; Zhang, B.; Chen, Q.; Zhang, Y.; Tang, Y. Catalytic properties of fluorinated alumina for the production of dimethyl ether. *Catal. Commun.* **2006**, *7*, 362–366, doi:10.1016/J.CATCOM.2005.12.011.

128. Mao, D.; Yang, W.; Xia, J.; Zhang, B.; Lu, G. The direct synthesis of dimethyl ether from syngas over hybrid catalysts with sulfate-modified γ-alumina as methanol dehydration components. *J. Mol. Catal. A Chem.* **2006**, *250*, 138–144, doi:10.1016/J.MOLCATA.2006.01.053.

129. Montesano, R.; Chadwick, D. Combined methanol and dimethyl

UNIVERSIDAD DE MÁLAGA

ether synthesis from CO/H2: Phosphorus mediated deactivation. *Catal. Commun.* **2012**, *29*, 137–140, doi:10.1016/J.CATCOM.2012.09.031.

130. Twigg, M. V.; Spencer, M.S. Deactivation of supported copper metal catalysts for hydrogenation reactions. *Appl. Catal. A Gen.* **2001**, *212*, 161–174, doi:10.1016/S0926-860X(00)00854-1.

131. Kang, S.H.; Bae, J.W.; Kim, H.S.; Dhar, G.M.; Jun, K.W. Enhanced Catalytic Performance for Dimethyl Ether Synthesis from Syngas with the Addition of Zr or Ga on a Cu−ZnO−Al2O3/γ-Al2O3 Bifunctional Catalyst. *Energy and Fuels* **2010**, *24*, 804–810, doi:10.1021/EF901133Z.

132. Venugopal, A.; Palgunadi, J.; Deog, J.K.; Joo, O.S.; Shin, C.H. Dimethyl ether synthesis on the admixed catalysts of Cu-Zn-Al-M (M = Ga, La, Y, Zr) and γ-Al2O3: The role of modifier. *J. Mol. Catal. A Chem.* **2009**, *302*, 20–27, doi:10.1016/J.MOLCATA.2008.11.038.

133. Song, F.; Tan, Y.; Xie, H.; Zhang, Q.; Han, Y. Direct synthesis of dimethyl ether from biomass-derived syngas over Cu–ZnO–Al2O3–ZrO2(x)/γ-Al2O3 bifunctional catalysts: Effect of Zr-loading. *Fuel Process. Technol.* **2014**, *126*, 88–94, doi:10.1016/J.FUPROC.2014.04.021.

134. Tan, Y.; Xie, H.; Cui, H.; Han, Y.; Zhong, B. Modification of Cu-based methanol synthesis catalyst for dimethyl ether synthesis from syngas in slurry phase. *Catal. Today* **2005**, *104*, 25–29, doi:10.1016/J.CATTOD.2005.03.033.

135. Palgunadi, J.; Yati, I.; Jung, K.D. Catalytic activity of Cu-Zn-Al-Mn admixed with gamma-alumina for the synthesis of DME from syngas: Manganese effect or just method of preparation? *React. Kinet. Mech. Catal.* **2010**, *101*, 117–128, doi:10.1007/S11144-010-0205-Z/FIGURES/8.

136. Asthana, S.; Samanta, C.; Bhaumik, A.; Banerjee, B.; Voolapalli, R.K.; Saha, B. Direct synthesis of dimethyl ether from syngas over Cu-based catalysts: Enhanced selectivity in the presence of MgO. *J. Catal.* **2016**, *334*, 89–101, doi:10.1016/J.JCAT.2015.10.020.

137. Gentzen, M.; Habicht, W.; Doronkin, D.E.; Grunwaldt, J.D.; Sauer, J.; Behrens, S. Bifunctional hybrid catalysts derived from Cu/Zn-based nanoparticles for single-step dimethyl ether synthesis. *Catal. Sci. Technol.* **2016**, *6*, 1054–1063, doi:10.1039/C5CY01043H.

UNIVERSIDAD DE MÁLAGA

138. Gao, Z.H.; Hao, L.F.; Huang, W.; Xie, K.C. A novel liquid-phase technology for the preparation of slurry catalysts. *Catal. Lett. 2005 1023* **2005**, *102*, 139–141, doi:10.1007/S10562-005-5845-7.

139. Jiang, H.; Bongard, H.; Schmidt, W.; Schüth, F. One-pot synthesis of mesoporous Cu–γ-Al2O3 as bifunctional catalyst for direct dimethyl ether synthesis. *Microporous Mesoporous Mater.* **2012**, *164*, 3–8, doi:10.1016/J.MICROMESO.2012.08.004.

140. Chen, W.H.; Lin, B.J.; Lee, H.M.; Huang, M.H. One-step synthesis of dimethyl ether from the gas mixture containing CO2 with high space velocity. *Appl. Energy* **2012**, *98*, 92–101, doi:10.1016/J.APENERGY.2012.02.082.

141. Ramos, F.S.; Farias, A.M.D. De; Borges, L.E.P.; Monteiro, J.L.; Fraga, M.A.; Sousa-Aguiar, E.F.; Appel, L.G. Role of dehydration catalyst acid properties on one-step DME synthesis over physical mixtures. *Catal. Today* **2005**, *101*, 39–44, doi:10.1016/J.CATTOD.2004.12.007.

142. Ordomsky, V. V.; Cai, M.; Sushkevich, V.; Moldovan, S.; Ersen, O.; Lancelot, C.; Valtchev, V.; Khodakov, A.Y. The role of external acid sites of ZSM-5 in deactivation of hybrid CuZnAl/ZSM-5 catalyst for direct dimethyl ether synthesis from syngas. *"Applied Catal. A, Gen.* **2014**, *486*, 266–275, doi:10.1016/j.apcata.2014.08.030.

143. Mao, D.; Guo, X. Dimethyl Ether Synthesis from Syngas over the Admixed Cu/ZnO/Al2O3 Catalyst and Alkaline Earth Oxide-Modified HZSM-5 Zeolite. *Energy Technol.* **2014**, *2*, 882–888, doi:10.1002/ENTE.201402071.

144. Mao, D.; Xia, J.; Zhang, B.; Lu, G. Highly efficient synthesis of dimethyl ether from syngas over the admixed catalyst of CuO–ZnO–Al2O3 and antimony oxide modified HZSM-5 zeolite. *Energy Convers. Manag.* **2010**, *51*, 1134–1139, doi:10.1016/J.ENCONMAN.2009.12.022.

145. García-Trenco, A.; Martínez, A. Direct synthesis of DME from syngas on hybrid CuZnAl/ZSM-5 catalysts: New insights into the role of zeolite acidity. *Appl. Catal. A Gen.* **2012**, *411–412*, 170–179, doi:10.1016/J.APCATA.2011.10.036.

146. Ereña, J.; Garoña, R.; Arandes, J.M.; Aguayo, A.T.; Bilbao, J. Effect of operating conditions on the synthesis of dimethyl ether over a CuO-ZnO-Al2O3/NaHZSM-5 bifunctional catalyst. *Catal. Today* **2005**, *107–108*, 467–473, doi:10.1016/j.cattod.2005.07.116.

UNIVERSIDAD DE MÁLAGA

147. Lee, Y.J.; Jung, M.H.; Lee, J.B.; Jeong, K.E.; Roh, H.S.; Suh, Y.W.; Bae, J.W. Single-step synthesis of dimethyl ether from syngas on Al2O3-modified CuO–ZnO–Al2O3/ferrierite catalysts: Effects of Al2O3 content. *Catal. Today* **2014**, *228*, 175–182, doi:10.1016/J.CATTOD.2013.11.015.

148. Flores, J.H.; Peixoto, D.P.B.; Appel, L.G.; De Avillez, R.R.; Silva, M.I.P. Da The influence of different methanol synthesis catalysts on direct synthesis of DME from syngas. *Catal. Today* **2011**, *172*, 218–225, doi:10.1016/J.CATTOD.2011.02.063.

149. Jung, J.W.; Lee, Y.J.; Um, S.H.; Yoo, P.J.; Lee, D.H.; Jun, K.W.; Bae, J.W. Effect of copper surface area and acidic sites to intrinsic catalytic activity for dimethyl ether synthesis from biomass-derived syngas. *Appl. Catal. B Environ.* **2012**, *126*, 1–8, doi:10.1016/J.APCATB.2012.06.026.

150. Montesano, R.; Narvaez, A.; Chadwick, D. Shape-selectivity effects in syngas-to-dimethyl ether conversion over Cu/ZnO/Al2O3 and zeolite mixtures: Carbon deposition and by-product formation. *Appl. Catal. A Gen.* **2014**, *482*, 69–77, doi:10.1016/J.APCATA.2014.05.009.

151. Mao, D.; Xia, J.; Chen, Q.; Lu, G. Highly effective conversion of syngas to dimethyl ether over the hybrid catalysts containing high-silica HMCM-22 zeolites. *Catal. Commun.* **2009**, *10*, 620–624, doi:10.1016/J.CATCOM.2008.11.003.

152. Ateka, A.; Sierra, I.; Ereña, J.; Bilbao, J.; Aguayo, A.T. Performance of CuO–ZnO–ZrO2 and CuO–ZnO–MnO as metallic functions and SAPO-18 as acid function of the catalyst for the synthesis of DME co-feeding CO2. *Fuel Process. Technol.* **2016**, *152*, 34–45, doi:10.1016/j.fuproc.2016.05.041.

153. Yang, G.; Tsubaki, N.; Shamoto, J.; Yoneyama, Y.; Zhang, Y. Confinement effect and synergistic function of H-ZSM-5/Cu-ZnO-Al 2O3 capsule catalyst for one-step controlled synthesis. *J. Am. Chem. Soc.* **2010**, *132*, 8129–8136, doi:10.1021/JA101882A/SUPPL_FILE/JA101882A_SI_001.PDF .

154. Yang, G.; Thongkam, M.; Vitidsant, T.; Yoneyama, Y.; Tan, Y.; Tsubaki, N. A double-shell capsule catalyst with core–shell-like structure for one-step exactly controlled synthesis of dimethyl ether from CO2 containing syngas. *Catal. Today* **2011**, *171*, 229–235, doi:10.1016/J.CATTOD.2011.02.021.

155. Nie, R.; Lei, H.; Pan, S.; Wang, L.; Fei, J.; Hou, Z. Core–shell structured CuO–ZnO@H-ZSM-5 catalysts for CO hydrogenation

UNIVERSIDAD DE MÁLAGA

to dimethyl ether. *Fuel* **2012**, *96*, 419–425, doi:10.1016/J.FUEL.2011.12.048.

156. Phienluphon, R.; Pinkaew, K.; Yang, G.; Li, J.; Wei, Q.; Yoneyama, Y.; Vitidsant, T.; Tsubaki, N. Designing core (Cu/ZnO/Al2O3)–shell (SAPO-11) zeolite capsule catalyst with a facile physical way for dimethyl ether direct synthesis from syngas. *Chem. Eng. J.* **2015**, *270*, 605–611, doi:10.1016/J.CEJ.2015.02.071.

157. Sánchez-Contador, M.; Ateka, A.; Aguayo, A.T.; Bilbao, J. Direct synthesis of dimethyl ether from CO and CO2 over a core-shell structured CuO-ZnO-ZrO2@SAPO-11 catalyst. *Fuel Process. Technol.* **2018**, *179*, 258–268, doi:10.1016/j.fuproc.2018.07.009.

158. Du, C.; Hondo, E.; Chizema, L.G.; Wang, C.; Tong, M.; Xing, C.; Yang, R.; Lu, P.; Tsubaki, N. Developing Cu-MOR@SiO2 Core-Shell Catalyst Microcapsules for Two-Stage Ethanol Direct Synthesis from DME and Syngas. *Ind. Eng. Chem. Res.* **2020**, *59*, 3293–3300, doi:10.1021/ACS.IECR.9B05663/SUPPL_FILE/IE9B05663_SI_001.PDF.

159. Tan, L.; Zhang, P.; Suzuki, Y.; Li, H.; Guo, L.; Yoneyama, Y.; Chen, J.; Peng, X.; Tsubaki, N. Bifunctional Capsule Catalyst of Al2O3@Cu with Strengthened Dehydration Reaction Field for Direct Synthesis of Dimethyl Ether from Syngas. *Ind. Eng. Chem. Res.* **2019**, *58*, 22905–22911, doi:10.1021/ACS.IECR.9B04864/SUPPL_FILE/IE9B04864_SI_001.PDF.

160. Koybasi, H.H.; Avci, A.K. Modeling of a membrane integrated catalytic microreactor for efficient DME production from syngas with CO2. *Catal. Today* **2022**, *383*, 133–145, doi:10.1016/J.CATTOD.2020.10.020.

161. Diban, N.; Urtiaga, A.M.; Ortiz, I.; Ereña, J.; Bilbao, J.; Aguayo, A.T. Influence of the membrane properties on the catalytic production of dimethyl ether with in situ water removal for the successful capture of co2. *Chem. Eng. J.* **2013**, *234*, 140–148, doi:10.1016/j.cej.2013.08.062.

162. Rodriguez-Vega, P.; Ateka, A.; Kumakiri, I.; Vicente, H.; Ereña, J.; Aguayo, A.T.; Bilbao, J. Experimental implementation of a catalytic membrane reactor for the direct synthesis of DME from H2+CO/CO2. *Chem. Eng. Sci.* **2021**, *234*, 116396, doi:10.1016/j.ces.2020.116396.

163. Palomo, J.; Rodríguez-Cano, M.Á.; Rodríguez-Mirasol, J.;

UNIVERSIDAD DE MÁLAGA

Cordero, T. ZSM-5-decorated CuO/ZnO/ZrO2 fibers as efficient bifunctional catalysts for the direct synthesis of DME from syngas. *Appl. Catal. B Environ.* **2020**, *270*, 118893, doi:10.1016/j.apcatb.2020.118893.

164. Koybasi, H.H.; Hatipoglu, C.; Avci, A.K. Sustainable DME synthesis from CO2–rich syngas in a membrane assisted reactor–microchannel heat exchanger system. *J. CO2 Util.* **2021**, *52*, 101660, doi:10.1016/J.JCOU.2021.101660.

165. Koybasi, H.H.; Hatipoglu, C.; Avci, A.K. Comparison of intensified reactor systems for one–step conversion of CO2–containing syngas to DME. *Chem. Eng. Process. - Process Intensif.* **2021**, *167*, 108538, doi:10.1016/J.CEP.2021.108538.

166. Delgado Otalvaro, N.; Sogne, G.; Herrera Delgado, K.; Wild, S.; Pitter, S.; Sauer, J. Kinetics of the direct DME synthesis from CO2 rich syngas under variation of the CZA-to-γ-Al2O3 ratio of a mixed catalyst bed. *RSC Adv.* **2021**, *11*, 24556–24569, doi:10.1039/D1RA03452A.

167. Wild, S.; Polierer, S.; Zevaco, T.A.; Guse, D.; Kind, M.; Pitter, S.; Delgado, K.H.; Sauer, J. Direct DME synthesis on CZZ/H-FER from variable CO2/CO syngas feeds. *RSC Adv.* **2021**, *11*, 2556–2564, doi:10.1039/D0RA09754C.

168. Mota, N.; Ordoñez, E.M.; Pawelec, B.; Fierro, J.L.G.; Navarro, R.M. Direct Synthesis of Dimethyl Ether from CO2: Recent Advances in Bifunctional/Hybrid Catalytic Systems. *Catal. 2021, Vol. 11, Page 411* **2021**, *11*, 411, doi:10.3390/CATAL11040411.

169. Lee, J.S.; Moon, K.I.; Lee, S.H.; Lee, S.Y.; Kim, Y.G. Modified Cu/ZnO/Al2O3 catalysts for methanol synthesis from CO2/H2 and CO/H2. *Catal. Lett. 1995 341* **1995**, *34*, 93–99, doi:10.1007/BF00808326.

170. Schumann, J.; Eichelbaum, M.; Lunkenbein, T.; Thomas, N.; Álvarez Galván, M.C.; Schlögl, R.; Behrens, M. Promoting strong metal support interaction: Doping ZnO for enhanced activity of Cu/ZnO:M (M = Al, Ga, Mg) catalysts. *ACS Catal.* **2015**, *5*, 3260–3270, doi:10.1021/ACSCATAL.5B00188/SUPPL_FILE/CS5B00188_SI_001.PDF.

171. Fierro, J.L.G.; Melián-Cabrera, I.; López Granados, M. Pd-Modified Cu–Zn Catalysts for Methanol Synthesis from CO2/H2 Mixtures: Catalytic Structures and Performance. *J. Catal.* **2002**, *210*, 285–294, doi:10.1006/JCAT.2002.3677.

UNIVERSIDAD DE MÁLAGA

172. Liu, L.; Fan, F.; Bai, M.; Xue, F.; Ma, X.; Jiang, Z.; Fang, T. Mechanistic study of methanol synthesis from CO2 hydrogenation on Rh-doped Cu(111) surfaces. *Mol. Catal.* **2019**, *466*, 26–36, doi:10.1016/J.MCAT.2019.01.009.

173. Frusteri, F.; Cordaro, M.; Cannilla, C.; Bonura, G. Multifunctionality of Cu–ZnO–ZrO2/H-ZSM5 catalysts for the one-step CO2-to-DME hydrogenation reaction. *Appl. Catal. B Environ.* **2015**, *162*, 57–65, doi:10.1016/J.APCATB.2014.06.035.

174. Kornas, A.; Grabowski, R.; Śliwa, M.; Samson, K.; Ruggiero-Mikołajczyk, M.; Żelazny, A. Dimethyl ether synthesis from CO2 hydrogenation over hybrid catalysts: effects of preparation methods. *React. Kinet. Mech. Catal.* **2017**, *121*, 317–327, doi:10.1007/S11144-017-1153-7/TABLES/5.

175. Barroso-Martín, I.; Infantes-Molina, A.; Fini, F.J.; Ballesteros-Plata, D.; Rodríguez-Castellón, E.; Moretti, E. Silica-Related Catalysts for CO2 Transformation into Methanol and Dimethyl Ether. *Catal. 2020, Vol. 10, Page 1282* **2020**, *10*, 1282, doi:10.3390/CATAL10111282.

176. Xiao, J.; Mao, D.; Guo, X.; Yu, J. Methanol Synthesis from CO2 Hydrogenation over CuO–ZnO–TiO2 Catalysts: The Influence of TiO2 Content. *Energy Technol.* **2015**, *3*, 32–39, doi:10.1002/ENTE.201402091.

177. Deerattrakul, V.; Puengampholsrisook, P.; Limphirat, W.; Kongkachuichay, P. Characterization of supported Cu-Zn/graphene aerogel catalyst for direct CO2 hydrogenation to methanol: Effect of hydrothermal temperature on graphene aerogel synthesis. *Catal. Today* **2018**, *314*, 154–163, doi:10.1016/J.CATTOD.2017.12.010.

178. Xu, J.; Su, X.; Liu, X.; Pan, X.; Pei, G.; Huang, Y.; Wang, X.; Zhang, T.; Geng, H. Methanol synthesis from CO2 and H2 over Pd/ZnO/Al2O3: Catalyst structure dependence of methanol selectivity. *Appl. Catal. A Gen.* **2016**, *514*, 51–59, doi:10.1016/J.APCATA.2016.01.006.

179. Rui, N.; Wang, Z.; Sun, K.; Ye, J.; Ge, Q.; Liu, C. jun CO2 hydrogenation to methanol over Pd/In2O3: effects of Pd and oxygen vacancy. *Appl. Catal. B Environ.* **2017**, *218*, 488–497, doi:10.1016/J.APCATB.2017.06.069.

180. Baiker, A.; Kilo, M.; Maciejewski, M.; Menzi, S.; Wokaun, A. Hydrogenation of CO2 Over Copper, Silver and Gold/Zirconia Catalysts: Comparative Study of Catalyst Properties and Reaction Pathways. *Stud. Surf. Sci. Catal.* **1993**, *75*, 1257–1272,

UNIVERSIDAD DE MÁLAGA

doi:10.1016/S0167-2991(08)64449-3.

181. Li, C.S.; Melaet, G.; Ralston, W.T.; An, K.; Brooks, C.; Ye, Y.; Liu, Y.S.; Zhu, J.; Guo, J.; Alayoglu, S.; et al. High-performance hybrid oxide catalyst of manganese and cobalt for low-pressure methanol synthesis. *Nat. Commun. 2015 61* **2015**, *6*, 1–5, doi:10.1038/ncomms7538.

182. Choi, H.; Oh, S.; Trung Tran, S.B.; Park, J.Y. Size-controlled model Ni catalysts on Ga2O3 for CO2 hydrogenation to methanol. *J. Catal.* **2019**, *376*, 68–76, doi:10.1016/J.JCAT.2019.06.051.

183. Studt, F.; Sharafutdinov, I.; Abild-Pedersen, F.; Elkjær, C.F.; Hummelshøj, J.S.; Dahl, S.; Chorkendorff, I.; Nørskov, J.K. Discovery of a Ni-Ga catalyst for carbon dioxide reduction to methanol. *Nat. Chem. 2014 64* **2014**, *6*, 320–324, doi:10.1038/nchem.1873.

184. Chen, T.Y.; Cao, C.; Chen, T.B.; Ding, X.; Huang, H.; Shen, L.; Cao, X.; Zhu, M.; Xu, J.; Gao, J.; et al. Unraveling Highly Tunable Selectivity in CO2 Hydrogenation over Bimetallic In-Zr Oxide Catalysts. *ACS Catal.* **2019**, *9*, 8785–8797, doi:10.1021/ACSCATAL.9B01869/SUPPL_FILE/CS9B01869_SI_001.PDF.

185. Xu, M.; Lunsford, J.H.; Goodman, D.W.; Bhattacharyya, A. Synthesis of dimethyl ether (DME) from methanol over solid-acid catalysts. *Appl. Catal. A Gen.* **1997**, *149*, 289–301, doi:10.1016/S0926-860X(96)00275-X.

186. Raoof, F.; Taghizadeh, M.; Eliassi, A.; Yaripour, F. Effects of temperature and feed composition on catalytic dehydration of methanol to dimethyl ether over γ-alumina. *Fuel* **2008**, *87*, 2967–2971, doi:10.1016/j.fuel.2008.03.025.

187. Bercic, G.; Levec, J. Intrinsic and global reaction rate of methanol dehydration over γ-alumina pellets. *Ind. Eng. Chem. Res.* **1992**, *31*, 1035–1040, doi:10.1021/IE00004A010.

188. Klusáček, K.; Schneider, P. Stationary catalytic kinetics via surface concentrations from transient data: Methanol dehydration. *Chem. Eng. Sci.* **1982**, *37*, 1523–1528, doi:10.1016/0009-2509(82)80010-9.

189. Migliori, M.; Aloise, A.; Catizzone, E.; Giordano, G. Kinetic Analysis of Methanol to Dimethyl Ether Reaction over H-MFI Catalyst. *Ind. Eng. Chem. Res.* **2014**, *53*, 14885–14891, doi:10.1021/IE502775U.

UNIVERSIDAD DE MÁLAGA

190. Gates, B.C.; Johanson, L.N. Langmuir-hinshelwood kinetics of the dehydration of methanol catalyzed by cation exchange resin. *AIChE J.* **1971**, *17*, 981–983, doi:10.1002/AIC.690170435.

191. An, W.; Chuang, K.T.; Sanger, A.R. Dehydration of Methanol to Dimethyl Ether by Catalytic Distillation. *Can. J. Chem. Eng.* **2004**, *82*, 948–955, doi:10.1002/CJCE.5450820510.

192. Lee, E.-Y.; Park, Y.-K.; Joo, O.-S.; Jung, and K.-D. Methanol dehydration to produce dimethyl ether over g -Al 2 O 3. *React. Kinet. Catal. Lett. 2006 891* **2006**, *89*, 115–121, doi:10.1007/S11144-006-0093-4.

193. Zhang, L.; Zhang, H.; Ying, W.; Fang, D. Dehydration of methanol to dimethyl ether over γ-Al2O3 catalyst: Intrinsic kinetics and effectiveness factor. *Can. J. Chem. Eng.* **2013**, *91*, 1538–1546, doi:10.1002/CJCE.21760.

194. Lu, W.Z.; Teng, L.H.; Xiao, W. De Simulation and experiment study of dimethyl ether synthesis from syngas in a fluidized-bed reactor. *Chem. Eng. Sci.* **2004**, *59*, 5455–5464, doi:10.1016/J.CES.2004.07.031.

195. Majid Mollavali, *,†; Fereydoon Yaripour, *,‡; Hossein Atashi, † and; Sahebdelfar‡, S. Intrinsic Kinetics Study of Dimethyl Ether Synthesis from Methanol on γ-Al2O3 Catalysts. *Ind. Eng. Chem. Res.* **2008**, *47*, 3265–3273, doi:10.1021/IE800051H.

196. Sierra, I.; Ereña, J.; Aguayo, A.T.; Ateka, A.; Bilbao, J. *Kinetic Modelling for the Dehydration of Methanol to Dimethyl Ether over γ-Al2O3*; 2013; Vol. 32, pp. 613–618;.

197. Ha, K.S.; Lee, Y.J.; Bae, J.W.; Kim, Y.W.; Woo, M.H.; Kim, H.S.; Park, M.J.; Jun, K.W. New reaction pathways and kinetic parameter estimation for methanol dehydration over modified ZSM-5 catalysts. *Appl. Catal. A Gen.* **2011**, *395*, 95–106, doi:10.1016/J.APCATA.2011.01.025.

198. Ortega, C.; Rezaei, M.; Hessel, V.; Kolb, G. Methanol to dimethyl ether conversion over a ZSM-5 catalyst: Intrinsic kinetic study on an external recycle reactor. *Chem. Eng. J.* **2018**, *347*, 741–753, doi:10.1016/J.CEJ.2018.04.160.

199. Torres-Liñán, J.; García-Rollán, M.; Rosas, J.M.; Rodríguez-Mirasol, J.; Cordero, T. Deactivation of a biomass-derived zirconium-doped phosphorus-containing carbon catalyst in the production of dimethyl ether from methanol dehydration. *Energy and Fuels* **2021**, *35*, 17225–17240, doi:10.1021/ACS.ENERGYFUELS.1C01721/SUPPL_FILE/EF1

UNIVERSIDAD DE MÁLAGA

C01721_SI_001.PDF.

200. Imarc Dimethyl Ether Market: Global Industry Trends, Share, Size, Growth, Opportunity and Forecast 2021-2026 Available online: https://www.imarcgroup.com/dimethyl-ether-market (accessed on Nov 4, 2021).

201. Fortune Business Insight Dimethyl Ether Market Size, Share & COVID-19 Impact Analysis, By Application (LPG Blending, Aerosol Propellant, Transportation Fuel, and Others), and Regional Forectas, 2021-2028 Available online: https://www.fortunebusinessinsights.com/dimethyl-ether-market-104309 (accessed on Aug 18, 2021).

202. Oberon Fuels Oberon Fuels Starts Commercial Production of Renewable Dimethyl Ether (rDME), a Pivotal Step Towards a Net-Zero Future Available online: https://oberonfuels.com/2021/06/10/oberon-fuels-starts-commercial-production-of-renewable-dimethyl-ether-rdme-a-pivotal-step-towards-a-net-zero-future/ (accessed on Aug 18, 2021).

203. De, S.; Balu, A.M.; van der Waal, J.C.; Luque, R. Biomass-Derived Porous Carbon Materials: Synthesis and Catalytic Applications. *ChemCatChem* **2015**, *7*, 1608–1629, doi:10.1002/cctc.201500081.

204. Lee, J.; Kim, K.H.; Kwon, E.E. Biochar as a Catalyst. *Renew. Sustain. Energy Rev.* **2017**, *77*, 70–79, doi:10.1016/j.rser.2017.04.002.

205. Lam, E.; Luong, J.H.T. Carbon materials as catalyst supports and catalysts in the transformation of biomass to fuels and chemicals. *ACS Catal.* **2014**, *4*, 3393–3410, doi:10.1021/cs5008393.

206. Calvo-Muñoz, E.M.; García-Mateos, F.J.; Rosas, J.M.; Rodríguez-Mirasol, J.; Cordero, T. Biomass Waste Carbon Materials as adsorbents for CO2 Capture under Post-Combustion Conditions. *Front. Mater.* **2016**, *3*, 23, doi:10.3389/fmats.2016.00023.

207. Rosas, J.M.; Bedia, J.; Rodríguez-Mirasol, J.; Cordero, T. HEMP-derived activated carbon fibers by chemical activation with phosphoric acid. *Fuel* **2009**, *88*, 19–26, doi:10.1016/j.fuel.2008.08.004.

208. Almarri, M.; Ma, X.; Song, C. Role of surface oxygen-containing functional groups in liquid-phase adsorption of nitrogen compounds on carbon-basedadsorbents. *Energy and Fuels*

UNIVERSIDAD DE MÁLAGA

2009, *23*, 3940–3947, doi:10.1021/ef900051r.

209. Wan, C.; Xie, Q.; Liu, J.; Liang, D.; Huang, X.; Zhou, H.; Tang, Y.; Liu, D. Pilot-scale combined adsorption columns using activated carbon and zeolite for hazardous trace elements removal from wastewater of entrained-flow coal gasification. *Process Saf. Environ. Prot.* **2021**, *147*, 439–449, doi:10.1016/j.psep.2020.09.053.

210. de Camargo Lima Beluci, N.; Tonial dos Santos, T.R.; Marcuzzo, J.S.; Bergamasco, R. Facile filtration system to remove Diuron in aqueous solutions. *J. Hazard. Mater.* **2021**, *404*, 124163, doi:10.1016/j.jhazmat.2020.124163.

211. Valero-Romero, M.J.; Rodríguez-Cano, M.Á.; Palomo, J.; Rodríguez-Mirasol, J.; Cordero, T. Carbon-Based Materials as Catalyst Supports for Fischer–Tropsch Synthesis: A Review. *Front. Mater.* **2021**, *7*, 455, doi:10.3389/FMATS.2020.617432/BIBTEX.

212. Rodríguez-Reinoso, F. The role of carbon materials in heterogeneous catalysis. *Carbon N. Y.* **1998**, *36*, 159–175, doi:10.1016/S0008-6223(97)00173-5.

213. Umeki, K.; Yamamoto, K.; Namioka, T.; Yoshikawa, K. High temperature steam-only gasification of woody biomass. *Appl. Energy* **2010**, *87*, 791–798, doi:10.1016/J.APENERGY.2009.09.035.

214. Chen, W.H.; Lin, B.J. Hydrogen and synthesis gas production from activated carbon and steam via reusing carbon dioxide. *Appl. Energy* **2013**, *101*, 551–559, doi:10.1016/J.APENERGY.2012.06.030.

215. Marsh, H.; Rodríguez-Reinoso, F. *Activated Carbon*; Elsevier, 2006; ISBN 9780080444635.

216. Moreno-Castilla, C.; Carrasco-Marín, F.; Parejo-Pérez, C.; López Ramón, M. V. Dehydration of methanol to dimethyl ether catalyzed by oxidized activated carbons with varying surface acidic character. *Carbon N. Y.* **2001**, *39*, 869–875, doi:10.1016/S0008-6223(00)00192-5.

217. Köseoɬlu, E.; Akmil-Başar, C. Preparation, structural evaluation and adsorptive properties of activated carbon from agricultural waste biomass. *Adv. Powder Technol.* **2015**, *26*, 811–818, doi:10.1016/J.APT.2015.02.006.

218. Suzuki, R.M.; Andrade, A.D.; Sousa, J.C.; Rollemberg, M.C. Preparation and characterization of activated carbon from rice

UNIVERSIDAD DE MÁLAGA

bran. *Bioresour. Technol.* **2007**, *98*, 1985–1991, doi:10.1016/J.BIORTECH.2006.08.001.

219. Karagöz, S.; Tay, T.; Ucar, S.; Erdem, M. Activated carbons from waste biomass by sulfuric acid activation and their use on methylene blue adsorption. *Bioresour. Technol.* **2008**, *99*, 6214–6222, doi:10.1016/J.BIORTECH.2007.12.019.

220. Boyjoo, Y.; Cheng, Y.; Zhong, H.; Tian, H.; Pan, J.; Pareek, V.K.; Jiang, S.P.; Lamonier, J.F.; Jaroniec, M.; Liu, J. From waste Coca Cola® to activated carbons with impressive capabilities for CO2 adsorption and supercapacitors. *Carbon N. Y.* **2017**, *116*, 490–499, doi:10.1016/J.CARBON.2017.02.030.

221. Wang, R.; Wang, P.; Yan, X.; Lang, J.; Peng, C.; Xue, Q. Promising porous carbon derived from celtuce leaves with outstanding supercapacitance and CO2 capture performance. *ACS Appl. Mater. Interfaces* **2012**, *4*, 5800–5806, doi:10.1021/AM302077C/SUPPL_FILE/AM302077C_SI_001.PDF.

222. Laine, J.; Calafat, A.; Labady, M. Preparation and characterization of activated carbons from coconut shell impregnated with phosphoric acid. *Carbon N. Y.* **1989**, *27*, 191–195, doi:10.1016/0008-6223(89)90123-1.

223. Nahil, M.A.; Williams, P.T. Pore characteristics of activated carbons from the phosphoric acid chemical activation of cotton stalks. *Biomass and Bioenergy* **2012**, *37*, 142–149, doi:10.1016/J.BIOMBIOE.2011.12.019.

224. Puziy, A.M.; Poddubnaya, O.I.; Gawdzik, B.; Tascón, J.M.D. Phosphorus-containing carbons: Preparation, properties and utilization. *Carbon N. Y.* 2020, *157*, 796–846.

225. Guo, Y.; Rockstraw, D.A. Physicochemical properties of carbons prepared from pecan shell by phosphoric acid activation. *Bioresour. Technol.* **2007**, *98*, 1513–1521, doi:10.1016/J.BIORTECH.2006.06.027.

226. Ibeh, P.O.; García-Mateos, F.J.; Ruiz-Rosas, R.; Rosas, J.M.; Rodríguez-Mirasol, J.; Cordero, T. Acid Mesoporous Carbon Monoliths from Lignocellulosic Biomass Waste for Methanol Dehydration. *Mater. 2019, Vol. 12, Page 2394* **2019**, *12*, 2394, doi:10.3390/MA12152394.

227. Zhu, G.Z.; Deng, X.L.; Hou, M.; Sun, K.; Zhang, Y.P.; Li, P.; Liang, F.M. Comparative study on characterization and adsorption properties of activated carbons by phosphoric acid activation from

UNIVERSIDAD DE MÁLAGA

corncob and its acid and alkaline hydrolysis residues. *Fuel Process. Technol.* **2016**, *144*, 255–261, doi:10.1016/J.FUPROC.2016.01.007.

228. Freeman, J.J.; Gimblett, F.G.R.; Roberts, R.A.; Sing, K.S.W. Studies of activated charcoal cloth. III. Mesopore development induced by phosphate impregnants. *Carbon N. Y.* **1988**, *26*, 7–11, doi:10.1016/0008-6223(88)90003-6.

229. Jagtoyen, M.; Derbyshire, F. Activated carbons from yellow poplar and white oak by H3PO4 activation. *Carbon N. Y.* **1998**, *36*, 1085–1097, doi:10.1016/S0008-6223(98)00082-7.

230. McKee, D.W.; Spiro, C.L.; Lamby, E.J. The inhibition of graphite oxidation by phosphorus additives. *Carbon N. Y.* **1984**, *22*, 285–290, doi:10.1016/0008-6223(84)90172-6.

231. Oh, S.G.; Rodriguez, N.M.; Baker, R.T.K. In-situ electron microscopy studies of surface segregation in bimetallic catalyst particles. *J. Catal.* **1992**, *136*, 584–597, doi:10.1016/0021-9517(92)90088-Y.

232. Lee, Y.-J.; Radovic, L.R. Oxidation inhibition effects of phosphorus and boron in different carbon fabrics. *Carbon N. Y.* **2003**, *41*, 1987–1997, doi:10.1016/S0008-6223(03)00199-4.

233. Puziy, A.M.; Poddubnaya, O.I. The properties of synthetic carbon derived from nitrogen- and phosphorus-containing polymer. *Carbon N. Y.* **1998**, *36*, 45–50, doi:10.1016/S0008-6223(97)00149-8.

234. Puziy, A..; Poddubnaya, O..; Martínez-Alonso, A.; Suárez-García, F.; Tascón, J.M.. Synthetic carbons activated with phosphoric acid. *Carbon N. Y.* **2002**, *40*, 1493–1505, doi:10.1016/S0008-6223(01)00317-7.

235. Suárez-García, F.; Martínez-Alonso, A.; Tascón, J.M.D. Pyrolysis of apple pulp: chemical activation with phosphoric acid. *J. Anal. Appl. Pyrolysis* **2002**, *63*, 283–301, doi:10.1016/S0165-2370(01)00160-7.

236. Baquero, M.C.; Giraldo, L.; Moreno, J.C.; Suárez-García, F.; Martínez-Alonso, A.; Tascón, J.M.D. Activated carbons by pyrolysis of coffee bean husks in presence of phosphoric acid. *J. Anal. Appl. Pyrolysis* **2003**, *70*, 779–784, doi:10.1016/S0165-2370(02)00180-8.

237. Suárez-García, F.; Martínez-Alonso, A.; Tascón, J.M.D. Nomex polyaramid as a precursor for activated carbon fibres by phosphoric acid activation. Temperature and time effects.

UNIVERSIDAD DE MÁLAGA

Microporous Mesoporous Mater. **2004**, *75*, 73–80, doi:10.1016/J.MICROMESO.2004.07.004.

238. Molina-Sabio, M.; Rodríguez-Reinoso, F.; Caturla, F.; Sellés, M.J. Porosity in granular carbons activated with phosphoric acid. *Carbon N. Y.* **1995**, *33*, 1105–1113, doi:10.1016/0008-6223(95)00059-M.

239. Gonzalez-Serrano, E.; Cordero, T.; Rodriguez-Mirasol, J.; Cotoruelo, L.; Rodriguez, J.J. Removal of water pollutants with activated carbons prepared from H3PO4 activation of lignin from kraft black liquors. *Water Res.* **2004**, *38*, 3043–3050, doi:10.1016/J.WATRES.2004.04.048.

240. Juana M. Rosas; Jorge Bedia; José Rodríguez-Mirasol; Cordero, T.; Rosas, J.M.; Bedia, J.; Rodríguez-Mirasol, J.; Cordero, T. Preparation of hemp-derived activated carbon monoliths. Adsorption of water vapor. *Ind. Eng. Chem. Res.* **2008**, *47*, 1288–1296, doi:10.1021/ie070924w.

241. Puziy, A.M.; Poddubnaya, O.I.; Martínez-Alonso, A.; Suárez-García, F.; Tascón, J.M.D. Surface chemistry of phosphorus-containing carbons of lignocellulosic origin. *Carbon N. Y.* **2005**, *43*, 2857–2868, doi:10.1016/J.CARBON.2005.06.014.

242. Valero-Romero, M.J.M.J.; Calvo-Muñoz, E.M.; Ruiz-Rosas, R.; Rodríguez-Mirasol, J.; Cordero, T. Phosphorus-Containing Mesoporous Carbon Acid Catalyst for Methanol Dehydration to Dimethyl Ether. *Ind. Eng. Chem. Res.* **2019**, *58*, 4042–4053, doi:10.1021/acs.iecr.8b05897.

243. Bedia, J.; Rosas, J.M.; Márquez, J.; Rodríguez-Mirasol, J.; Cordero, T. Preparation and characterization of carbon based acid catalysts for the dehydration of 2-propanol. *Carbon N. Y.* **2009**, *47*, 286–294, doi:10.1016/j.carbon.2008.10.008.

244. Rosas, J.M.; Ruiz-Rosas, R.; Rodríguez-Mirasol, J.; Cordero, T. Kinetic study of the oxidation resistance of phosphorus-containing activated carbons. *Carbon N. Y.* **2012**, *50*, 1523–1537, doi:10.1016/j.carbon.2011.11.030.

245. Valero-Romero, M.J.; García-Mateos, F.J.; Rodríguez-Mirasol, J.; Cordero, T. Role of surface phosphorus complexes on the oxidation of porous carbons. *Fuel Process. Technol.* **2017**, *157*, 116–126, doi:10.1016/j.fuproc.2016.11.014.

246. Ternero-Hidalgo, J.J.; Rosas, J.M.; Palomo, J.; Valero-Romero, M.J.; Rodríguez-Mirasol, J.; Cordero, T. Functionalization of activated carbons by HNO3 treatment: Influence of phosphorus

UNIVERSIDAD DE MÁLAGA

surface groups. *Carbon N. Y.* **2016**, *101*, 409–419, doi:10.1016/j.carbon.2016.02.015.

247. Bedia, J.; Rosas, J.M.; Rodríguez-Mirasol, J.; Cordero, T. Pd supported on mesoporous activated carbons with high oxidation resistance as catalysts for toluene oxidation. *Appl. Catal. B Environ.* **2010**, *94*, 8–18, doi:10.1016/j.apcatb.2009.10.015.

248. Bedia, J.; Rosas, J.M.; Vera, D.; Rodríguez-Mirasol, J.; Cordero, T. Isopropanol decomposition on carbon based acid and basic catalysts. *Catal. Today* **2010**, *158*, 89–96, doi:10.1016/j.cattod.2010.04.043.

249. Bedia, J.; Barrionuevo, R.; Rodríguez-Mirasol, J.; Cordero, T. Ethanol dehydration to ethylene on acid carbon catalysts. *Appl. Catal. B, Environ.* **2011**, *103*, 302–310, doi:10.1016/j.apcatb.2011.01.032.

250. Puziy, A.M.; Poddubnaya, O.I.; Kochkin, Y.N.; Vlasenko, N.V.; Tsyba, M.M. Acid properties of phosphoric acid activated carbons and their catalytic behavior in ethyl-tert-butyl ether synthesis. *Carbon N. Y.* **2010**, *48*, 706–713, doi:10.1016/j.carbon.2009.10.015.

251. Levenspiel, O. *Chemical Reaction Engineering*; 3rd Editio.; John Wiley & Sons, 1999;

252. Froment, G.F.; Bischoff, K.B.; De Wilde, J. *Chemical Reactor Analysis and Design*; 3rd ed.; John Wiley & Sons, 2011; ISBN 978-0-470-56541-4.

253. Argyle, M.D.; Bartholomew, C.H. Heterogeneous Catalyst Deactivation and Regeneration: A Review. *Catal. 2015, Vol. 5, Pages 145-269* **2015**, *5*, 145–269, doi:10.3390/CATAL5010145.

254. Quinn, R.; Dahl, T.A.; Toseland, B.A. An evaluation of synthesis gas contaminants as methanol synthesis catalyst poisons. *Appl. Catal. A Gen.* **2004**, *272*, 61–68, doi:10.1016/J.APCATA.2004.05.015.

255. Luan, Y.; Xu, H.; Yu, C.; Li, W.; Hou, S. Effects and control of steam in the systems of methanol and DME synthesis from syngas over Cu-based catalysts. *Catal. Letters* **2008**, *125*, 271–276, doi:10.1007/S10562-008-9529-Y/FIGURES/7.

256. Dadyburjor, D.B. Multiparticle-Based Models for Sintering of Supported Metal Catalysts. *Stud. Surf. Sci. Catal.* **1987**, *34*, 21–38, doi:10.1016/S0167-2991(09)60349-9.

257. Wang, H.T.; Liu, X.Q.; Chen, F.L.; Meng, G.Y.; Sørensen, O.T.

UNIVERSIDAD DE MÁLAGA

Kinetics and Mechanism of a Sintering Process for Macroporous Alumina Ceramics by Extrusion. *J. Am. Ceram. Soc.* **1998**, *81*, 781–784, doi:10.1111/J.1151-2916.1998.TB02412.X.

258. Bartholomew, C.H. Sintering kinetics of supported metals: new perspectives from a unifying GPLE treatment. *Appl. Catal. A Gen.* **1993**, *107*, 1–57, doi:10.1016/0926-860X(93)85114-5.

259. Flynn, P.C.; Wanke, S.E. Experimental studies of sintering of supported platinum catalysts. *J. Catal.* **1975**, *37*, 432–448, doi:10.1016/0021-9517(75)90180-3.

260. Gayubo, A.G.; Aguayo, A.T.; Olazar, M.; Vivanco, R.; Bilbao, J. Kinetics of the irreversible deactivation of the HZSM-5 catalyst in the MTO process. *Chem. Eng. Sci.* **2003**, *58*, 5239–5249, doi:10.1016/J.CES.2003.08.020.

261. Silaghi, M.C.; Chizallet, C.; Raybaud, P. Challenges on molecular aspects of dealumination and desilication of zeolites. *Microporous Mesoporous Mater.* **2014**, *191*, 82–96, doi:10.1016/J.MICROMESO.2014.02.040.

262. García-Trenco, A.; Vidal-Moya, A.; Martínez, A. Study of the interaction between components in hybrid CuZnAl/HZSM-5 catalysts and its impact in the syngas-to-DME reaction. *Catal. Today* **2012**, *179*, 43–51, doi:10.1016/J.CATTOD.2011.06.034.

263. Guisnet, M.; Magnoux, P.; Martin, D. Roles of acidity and pore structure in the deactivation of zeolites by carbonaceous deposits. *Stud. Surf. Sci. Catal.* **1997**, *111*, 1–19, doi:10.1016/S0167-2991(97)80138-3.

264. Barbosa, F.S.R.; Ruiz, V.S.O.; Monteiro, J.L.F.; De Avillez, R.R.; Borges, L.E.P.; Appel, L.G. The deactivation modes of Cu/ZnO/Al2O3 and HZSM-5 physical mixture in the one-step DME synthesis. *Catal. Letters* **2008**, *126*, 173–178, doi:10.1007/S10562-008-9601-7/TABLES/1.

265. Jr, A.V.; Voorhies, A.J. Carbon Formation in Catalytic Cracking. *Ind. Eng. Chem.* **1945**, *37*, 318–322, doi:10.1021/IE50424A010.

266. Chen, D.; Rebo, H.P.P.; Grønvold, A.; Moljord, K.; Holmen, A. Methanol conversion to light olefins over SAPO-34: kinetic modeling of coke formation. *Microporous Mesoporous Mater.* **2000**, *35–36*, 121–135, doi:10.1016/S1387-1811(99)00213-9.

267. Qi, G.; Xie, Z.; Yang, W.; Zhong, S.; Liu, H.; Zhang, C.; Chen, Q. Behaviors of coke deposition on SAPO-34 catalyst during methanol conversion to light olefins. *Fuel Process. Technol.* **2007**, *88*, 437–441, doi:10.1016/J.FUPROC.2006.11.008.

UNIVERSIDAD DE MÁLAGA

268. Simón, E.; Rosas, J.M.; Santos, A.; Romero, A. Coke formation in copper catalyst during cyclohexanol dehydrogenation: Kinetic deactivation model and catalyst characterization. *Chem. Eng. J.* **2013**, *214*, 119–128, doi:10.1016/j.cej.2012.10.040.

269. Gao, Y.; Chen, S.L.; Wei, Y.; Wang, Y.; Sun, W.; Cao, Y.; Zeng, P. Kinetics of coke formation in the dimethyl ether-to-olefins process over SAPO-34 catalyst. *Chem. Eng. J.* **2017**, *326*, 528–539, doi:10.1016/j.cej.2017.05.158.

270. Chen, D.; Grønvold, † A; Moljord, K.; Holmen, A. Methanol Conversion to Light Olefins over SAPO-34: Reaction Network and Deactivation Kinetics. **2007**, doi:10.1021/ie0610748.

271. Pérez-Uriarte, P.; Ateka, A.; Gayubo, A.G.; Cordero-Lanzac, T.; Aguayo, A.T.; Bilbao, J. Deactivation kinetics for the conversion of dimethyl ether to olefins over a HZSM-5 zeolite catalyst. *Chem. Eng. J.* **2017**, *311*, 367–377, doi:10.1016/j.cej.2016.11.104.

272. Aguayo, A.T.; Ereña, J.; Mier, D.; Arandes, J.M.; Olazar, M.; Bilbao, J. Kinetic modeling of dimethyl ether synthesis in a single step on a CuO-ZnO-Al2O3/γ-Al2O3 catalyst. *Ind. Eng. Chem. Res.* **2007**, *46*, 5522–5530, doi:10.1021/ie070269s.

273. Ereña, J.; Sierra, I.; Aguayo, A.T.; Ateka, A.; Olazar, M.; Bilbao, J. Kinetic modelling of dimethyl ether synthesis from (H2+CO2) by considering catalyst deactivation. *Chem. Eng. J.* **2011**, *174*, 660–667, doi:10.1016/j.cej.2011.09.067.

274. Pérez-Uriarte, P.; Ateka, A.; Aguayo, A.T.; Gayubo, A.G.; Bilbao, J. Kinetic model for the reaction of DME to olefins over a HZSM-5 zeolite catalyst. *Chem. Eng. J.* **2016**, *302*, 801–810, doi:10.1016/j.cej.2016.05.096.

275. Gayubo, A.G.; Vicente, J.; Ereña, J.; Oar-Arteta, L.; Azkoiti, M.J.; Olazar, M.; Bilbao, J. Causes of deactivation of bifunctional catalysts made up of CuO-ZnO-Al 2O3 and desilicated HZSM-5 zeolite in DME steam reforming. *Appl. Catal. A Gen.* **2014**, *483*, 76–84, doi:10.1016/j.apcata.2014.06.031.

276. Cordero-Lanzac, T.; Aguayo, A.T.; Gayubo, A.G.; Castaño, P.; Bilbao, J. Simultaneous modeling of the kinetics for n-pentane cracking and the deactivation of a HZSM-5 based catalyst. *Chem. Eng. J.* **2018**, *331*, 818–830, doi:10.1016/j.cej.2017.08.106.

277. Cordero-Lanzac, T.; Aguayo, A.T.; Gayubo, A.G.; Castaño, P.; Bilbao, J. A comprehensive approach for designing different configurations of isothermal reactors with fast catalyst deactivation. *Chem. Eng. J.* **2020**, *379*, 122260,

UNIVERSIDAD DE MÁLAGA

doi:10.1016/j.cej.2019.122260.

278. Cordero-Lanzac, T.; Hita, I.; García-Mateos, F.J.; Castaño, P.; Rodríguez-Mirasol, J.; Cordero, T.; Bilbao, J. Adaptable kinetic model for the transient and pseudo-steady states in the hydrodeoxygenation of raw bio-oil. *Chem. Eng. J.* **2020**, *400*, 124679, doi:10.1016/j.cej.2020.124679.

UNIVERSIDAD DE MÁLAGA

UNIVERSIDAD DE MÁLAGA

Chapter 2

Experimental Methods

UNIVERSIDAD DE MÁLAGA

2.1. Materials preparation

2.1.1. Activated carbon preparation

The carbon used in this thesis was prepared from an abundant and low-cost biomass waste from olive oil industry, olive stone supplied by Sociedad Cooperativa Andaluza Olivarera y Frutera San Isidro, Periana (Málaga), Spain. The carbon precursor, after washing with distilled water, was impregnated at a mass ratio 2/1 (H_3PO_4/olive stone) with a solution of H_3PO_4 (85% w/w, Panreac) and dried overnight in an oven at 60 ºC. Then, it was heated at 800 ºC (heating rate 10 ºC/min) in a tubular furnace with an inert atmosphere flow (150ºC Ncm^3/min N_2 99.999%, Linde) and kept at that temperature for 2 h. After that, the activated sample was washed with distilled water at 60 ºC until a stable pH was reached in the residual water. Finally, the chemically activated carbon (ACP) was grinded and sieved between 100-300 µm.

2.1.2. Catalyst preparation

The chemically activated carbon (ACP), prepared in section 2.1.1. of this thesis, was used as support for the preparation of the catalyst. For this reason, it was impregnated by the incipient wetness method with zirconium (IV) oxynitrate hydrate ($N_2O_7Zr{\cdot}xH_2O$, purity 99%, Sigma Aldrich). The sample was loaded with a 5.25% of zirconium, which turned out to be the optimum amount of deposited zirconium for methanol to DME reaction at lower temperatures. The impregnated samples were then dried for 12 h at 120 ºC and treated in a muffle furnace at 250 ºC for 2 h under air atmosphere.

2.2. Characterization

2.2.1. Porous texture

N_2 adsorption-desorption at -196 ºC and CO_2 adsorption isotherms at 0 ºC were used to evaluate the porous texture of the carbon by using an ASAP 2020 instrument (Micromeritics). Samples were outgassed, at least, for 8 h at 150 ºC before the analysis. From the N_2 isotherm data, apparent surface area (A_{BET}) was obtained from N_2 isotherm data by using Brunauer, Emmett and Teller equation; t-method was used to assess micropore volume (V_t) and external surface area (A_t); mesopore volume (V_{mes}) was obtained as the difference between maximum volume adsorbed (V_{tot}) at a relative pressure of 0.995 and micropore volume.

UNIVERSIDAD DE MÁLAGA

From the CO_2 isotherm data, narrow micropore volume (V_{DR}) and narrow surface area (A_{DR}) was evaluated from CO_2 isotherm data applying Dubinin-Radushkevich equation. Pore size distributions were obtained from N_2 isotherms data by using 2D-NLDFT heterogeneous adsorption models for carbon slit-shaped pores.

2.2.1. Surface chemistry by XPS

X-ray photoelectron spectroscopy (XPS) was used to determine surface species and concentrations of different elements in the materials before and after every process. XPS analyses were performed in a spectrophotometer 5700C (Physical Electronics) with MgK α radiation (1253.6 eV). C_{1s} peak, set at 284.5 eV, was used as a reference for the rest of the peaks. Peaks were deconvoluted using Gaussian-Lorentzian curves and Shirley type background line.

2.2.2. Surface chemistry by TPD

Temperature programmed desorption (TPD) was used to determine and quantify different oxygen functional groups present on the carbon surface. In a typical experiment, between 50-150 mg of dried carbon was introduced in a 4 mm crucible and heated from room temperature to 1000-1500ºC at a heating rate of 10 ºC/min, under a helium flow (200 Ncm^3/min 99.999% He, Linde). CO and CO_2 released due to the decomposition of carbon-oxygen surface groups were measured by a mass spectrometer (Pfeiffer Omnistar).

2.2.3. Composition by MAS-NMR

^{31}P Magic angle spinning NMR spectroscopy was carried out at room temperature to assess phosphorus groups, using a High-Resolution Bruker AXS Spectrometer, model AVANCEIII HD 600 (narrow bore). The magnetic field was 14.1 T corresponding to a ^{31}P resonance frequency of 242.92 MHz. The spinning rate was 15 kHz. $NH_4H_2PO_4$ was used as a reference at 0 ppm. ^{31}P-^{1}H HETCOR-NMR spectra were also recorded using a triple resonance CP-MAS probe of 3.2 mm.^{31}P MAS NMR spectra were recorded with a 2 ms contact pulse and 1 s delay with ^{1}H decoupling (^{31}P HPDEC with spinal decoupling sequence 64 for P) and summing up 200 scans.

UNIVERSIDAD DE MÁLAGA

2.3. Catalytic experiments

2.3.1. Carbon oxidation

ACP was submitted to different oxygen oxidation processes. First of all, the samples were thermally treated at 1000 ºC in order to remove most of the oxygen groups presented in the carbon surface, obtaining a "clean surface". After that, the oxidation was performed under a 100 cm^3/min stream of diluted air (3% oxygen, 97% nitrogen). Temperature ranged from 30 ºC to 340 ºC, while oxidation times varied from 30 s to 24 h. 50 mg of silicon carbide was carefully mixed with 50 mg of carbon samples to avoid hot spots and autothermal heating of the carbon during oxidation. Finally, DTP were performed on oxidized carbons to quantify the different carbon-oxygen groups presented in the carbon surface.

2.3.2. Catalytic dehydration of methanol

Catalytic performance of the zirconium impregnated P-containing activated carbons was evaluated for the dehydration of methanol to dimethyl ether reaction. The experiments were carried out in a fixed bed microreactor (4 mm i.d.) located in a vertical furnace, working under atmospheric pressure, with a catalyst mass between 50-300 mg. Methanol (CH_3OH, purity 99.9%, Carlo Erba) or a mixture of methanol and distilled water was fed to the reactor by using a syringe pump (Cole-Parmer® 74900-00-05 model) and the inlet stream was maintained at a methanol partial pressure between 0.015-0.08 atm in a 70 Ncm^3/min Helium flow (purity 99.999%, Linde). The reaction temperature was ranged from 450 ºC to 600 ºC, and a space time from 50-100 $g_{cat}{\cdot}s/mmol_{CH3OH}$ was used. All the pipelines were heated at 120 ºC to avoid methanol or any other product condensation.

2.3.3. Products identification and quantification

Concentrations of gas reactants and products were measured by an on-line Varian CP-4900 gas micro-chromatograph (Agilent), equipped with capillary columns: 5A molsieve, PPQ and wax columns. This equipment allowed sampling the gas outlet concentration every 4 minutes. Coke content was quantified by direct weighing of the catalyst before and after reaction and coke selectivity was calculated by assuming that the produced coke consisted of pure carbon.

Conversion, selectivity and yield were defined by the following expressions:

UNIVERSIDAD DE MÁLAGA

$$X = \frac{F_{CH_3OH_0} - F_{CH_3OH}}{F_{CH_3OH_0}} \quad (2.1)$$

$$S = \frac{n_i \cdot F_i}{\sum n_i \cdot F_i} \quad (2.2)$$

$$y = X \cdot S \quad (2.3)$$

where X represents the conversion, S denotes the selectivity and y the yield. $F_{CH_3OH_0}$ is the methanol molar flow fed to the reactor and F_{CH_3OH} the methanol molar flow in the outlet stream, F_i stands for the molar flow of the product i in the outlet stream and n_i represents the number of carbon atoms in the corresponding i molecule.

2.3.4. Regeneration experiments

Air treatment of the deactivated catalysts after reaction was carried out in-situ by an air flow (purity 99.999%, Linde) of 70 cm^3/min. Samples, after reaction at different experimental conditions, were exposed to air at 200 ºC followed by a temperature increase to 350 ºC at a heating rate of 10 ºC/min. This temperature was kept for 2 h.

2.4. Experimental set-up

2.4.1. Carbonization/Activation/Calcination

Figure 2.1. shows the experimental set-up used in the carbonization, activation or calcination process. It consisted of:

- Nitrogen or synthetic air cylinder
- Mass flow controller (Bronkshorst High-Tech)
- Horizontal tubular furnace (Carbolite Furnace, CFT model; 75 mm inner diameter, 750 mm heated length)

UNIVERSIDAD DE MÁLAGA

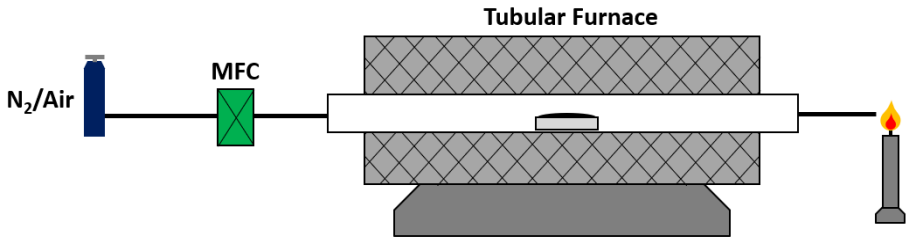

Figure 2. 1. Experimental set-up for carbonization/activation/calcination

2.4.2. Methanol dehydration

Figure 2.2. shows the experimental set-up used in the methanol dehydration reaction. It consisted of:

- Nitrogen, helium, oxygen or other cylinders
- Mass flow controllers (Bronkshorst High-Tech)
- Syringe pump (Cole-Parmer 74900-00-05 model)
- Custom quartz tubular reactor (inner diameter 4 mm; length 400 mm)
- Vertical furnace (Hobersal, ST18VO-0A PAD P DS PAD)
- Heating cable
- Gas chromatograph (Agilent, CP-4900) equipped with molecular sieve, PPQ and was columns.

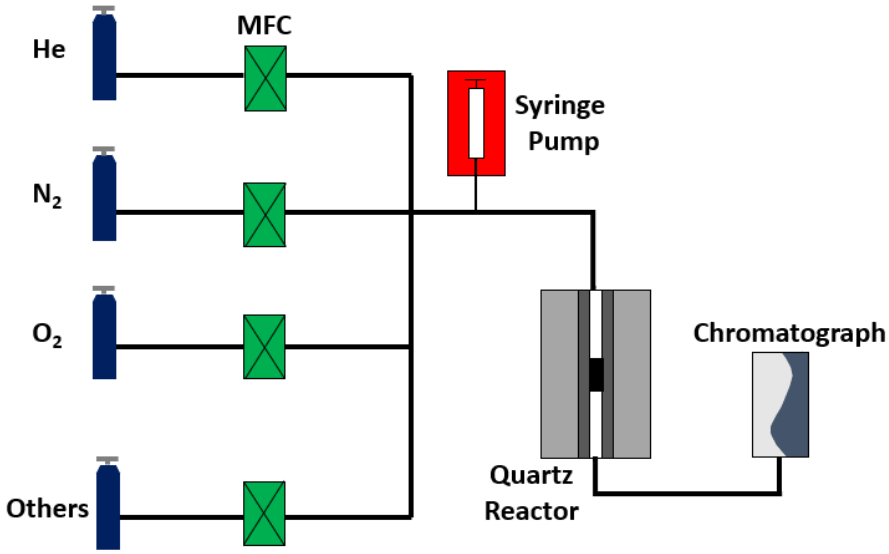

Figure 2. 2. Experimental set-up for methanol dehydration

UNIVERSIDAD DE MÁLAGA

2.4.3. TPD

The experimental set up used to carry out TPD experiments was similar to the one observed in Figure 2.2, but instead of a chromatograph, the detection equipment was a mass spectrophotometer (Pfeiffer Vacuum, Omnistar).

UNIVERSIDAD DE MÁLAGA

UNIVERSIDAD DE MÁLAGA

Chapter 3

Experimental results and discussion

UNIVERSIDAD DE MÁLAGA

3.1. ON THE KINETICS OF OXIDATION AND DECOMPOSITION OF PHOSPHORUS SURFACE GROUPS ON CARBON MATERIALS

As was presented in the introduction (section 1.4.2.1), the most important functional groups generated on the surface of the H_3PO_4 chemically activated carbons are the C-O-P and C-P type groups. Those groups provide the carbon with a high oxidation resistance [1,2], as well as an acidic character [3] of great interest in oxidation reactions and heterogeneous catalysis. Nevertheless, in addition to the presence of these phosphorus groups, those activated carbon also present the typical carbon-oxygen surface groups on the carbon surface [4,5] that also affect carbon properties like wettability or electrical properties [6]. Some of them have also catalytic activity, as the carbonyl one in partial oxidation of ethylbenzene to styrene [7], or carboxylic acids, able to catalyze methanol dehydration to dimethyl ether [8].

For all of these reasons, identification of surface groups is an interesting task. Bohem and Potentiometric titrations, X-ray photoelectron spectrometry (XPS), Fourier transform infrared spectroscopy (FTIR) and thermogravimetric analysis (TGA) can be used with this purpose, but all of these techniques have their own problems [9–11]: Titrations can only account acidic/basic groups; XPS and FTIR are able to identify and quantify every group, but their interpretation could be difficult as many interaction are detected in a small region; TGA allows an easy quantification of mass loss, but the simultaneous emission of CO, CO_2, CH_4 and water (among others) makes very difficult to associate those mass losses to an specific group [12,13]. To solve the aforementioned problems, TGA/Mass spectrometry (MS) [14] and TPD [4,15] can be used to determine and quantify carbon-oxygen groups presented on the carbon surface, being the later and easy and non-expensive alternative. In a TPD, CO and CO_2 signals can be assigned to the evolution of different oxygen groups as a function of temperature [11]. The contribution of every group is usually quantified as isometric peaks [12,14,16], but, that way of quantification is not strictly correct, as the profile obtained by TPD should be the addition of the different non-isothermal reactions produced (evolution of functional groups to CO_x). A more accurate quantification can be made assuming that every

UNIVERSIDAD DE MÁLAGA

reaction takes place independently from the others, having their own preexponential factor and activation energy.

On the other hand, several papers look for the production of these oxygen groups on carbon surface. Nitric acid [6,17–19], sulfuric acid (and mixtures with nitric acid) [20,21], ozone [22–24], electrooxidation [25,26], H_2O_2 [27], other compounds [19,28], or even air can be used for the partial oxidation of surface carbon to produce different carbon-oxygen groups. Moreover, the study of the production and the decomposition of those oxygen surface groups, provides meaningful information about their behavior in the gasification or combustion process [29]. In our research group, Valero et al. [15] used the inert atmosphere TPD to study the oxidation of a P-containing biomass-derived carbon. After the TPD, the initial C-O-P groups present on the carbon surface were reduce to C'-P, but those groups were reoxidized to C'-O-P groups when they were exposed to air, even at 20 ºC. Moreover, several cycles reduction-oxidation were undergo without any phosphorus loss and obtaining the same carbon-oxygen surface groups.

This chapter, deepen in the reduction-oxidation process of the tandem C-P/C-O-P groups, and how it affects the production of other carbon-oxygen surface groups. With this goal, a non-isothermal kinetic model of the decomposition of the C-O-P groups and of the carbon-oxygen surface groups was used to predict and quantify the groups produced after diluted air oxidation at different times and temperatures on the clean surface (thermal treated at 1000 ºC in a 150 cm^3/min of helium flow) of a phosphorus acid activated carbon. With the data obtained, the Elovich equation was used to obtain the activation energy and the preexponential factor of every carbon-oxygen functional group produced on the surface.

The preparation of the P-containing activated carbon was described in section 2.1.1 and the characterization techniques in section 2.2. The oxidation process to those activated carbon has been submitted is described in section 2.3.1.

3.1.1. Carbon characterization

Table 3.1 collects the textural parameters obtained from N_2 adsorption isotherm at -196 ºC and CO_2 adsorption isotherm at 0 ºC. A_{BET} shows a high development of porosity on this kind of carbons, as was already reported on similar activated carbons [30,31]. This carbon also shows a ratio V_t/V_{DR} higher than one (2.7) which means a higher prominence of wide microporous (0.7 – 2 nm) versus narrow ones (around 0.7 nm) [32].

UNIVERSIDAD DE MÁLAGA

The high value of the external surface area (A_t) suggests a high presence of mesopores, which is in agreement with the higher mesopore volume compared to the micropore volume [33].

Table 3. 1. Textural parameter values derived from N_2 at -196 ºC and CO_2 at 0 ºC adsorption isotherms.

N_2 Isotherm					CO_2 Isotherm	
A_{BET} (m^2/g)	A_t (m^2/g)	V_t (cm^3/g)	V_{mes} (cm^3/g)	V_{tot} (cm^3/g)	A_{DR} (m^2/g)	V_{DR} (cm^3/g)
1232	437	0.41	0.64	1.05	363	0.15

Table 3.2 collects the XPS surface concentration of the initial activated carbon. The main component was carbon with a 91.3%. Although it was heated at 800 ºC during the preparation process, it also showed a considerable amount of oxygen, around 6.9%. This is typical on that kind of phosphorus-containing activated carbons, as was observed before [15]. Some nitrogen was also detected (0.7%), probably originating from the biomass precursor. Moreover, around 1.1% of phosphorus was detected on the carbon surface, produced because of the activation process with phosphoric acid. These phosphorus groups are strongly bonded to the surface and remained in the surfaced even after several washes with water at 60 ºC [1,2].

Figure 3.1 a represents the O_{1s} spectra of the activated carbon ACP2800. Two main contributions can be seen: at 532.6 eV the most prominent one, which was associated to oxygen linked to carbon, like in C-OH, C-O-C and C-O-P groups; and the other one at 530.9 eV, associated to an oxygen doble bond, like in C=O and P=O. The band at 532.6 eV, attributed to chemisorbed water or O_2 was only hardly detected in the sample [15].

Figure 3.1 b shows the P_{2p} spectra of the initial activated carbon. A wide peak can be observed, formed by different contributions: a very small band at 131.1 eV, associated to C_3P groups; a band at 132.1 eV associated to C_3PO groups; a contribution at 133.2 eV from $C\text{-}PO_3$ and $C_2\text{-}PO_2$; and the peak at 134.1 eV associated to C-O-P groups (like $C\text{-}O\text{-}PO_3$, $(C\text{-}O)_2\text{-}PO_2$ or $(C\text{-}O)_3\text{-}PO$) [34]. The most important contribution was associated to $C\text{-}PO_3$ and $C_2\text{-}PO_2$ groups, which is an intermediate compound between the reduced phosphorus, in which phosphorus is

UNIVERSIDAD DE MÁLAGA

directly linked to carbon (except for the double bonded oxygen) and the oxidized group, in which, except for the double bond oxygen, phosphorus is linked to oxygen.

Table 3. 2. Atomic surface concentration determined by XPS analysis.

Sample	Atomic surface concentration (%)				
	C_{1s}	O_{1s}	P_{2p}	N_{1s}	O/P
ACP2800	91.3	6.9	1.1	0.7	6.3
ACP2800-TT	91.2	6.6	1.7	0.5	3.9
ACP2800-OX50	89.7	8.3	1.8	0.3	4.6
ACP2800-OX180	89.4	8.4	1.7	0.4	4.9
ACP2800-OX340	86.5	11.5	1.7	0.3	6.8

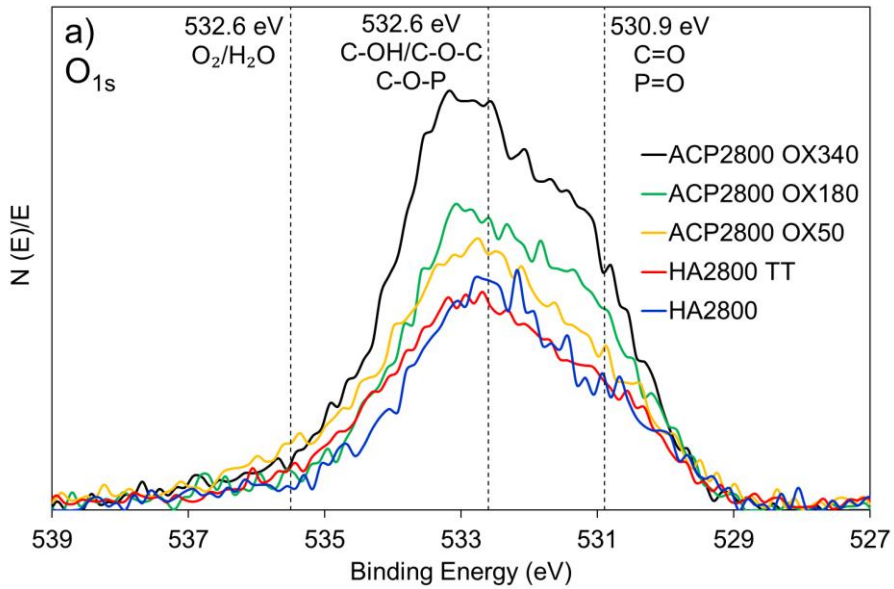

UNIVERSIDAD DE MÁLAGA

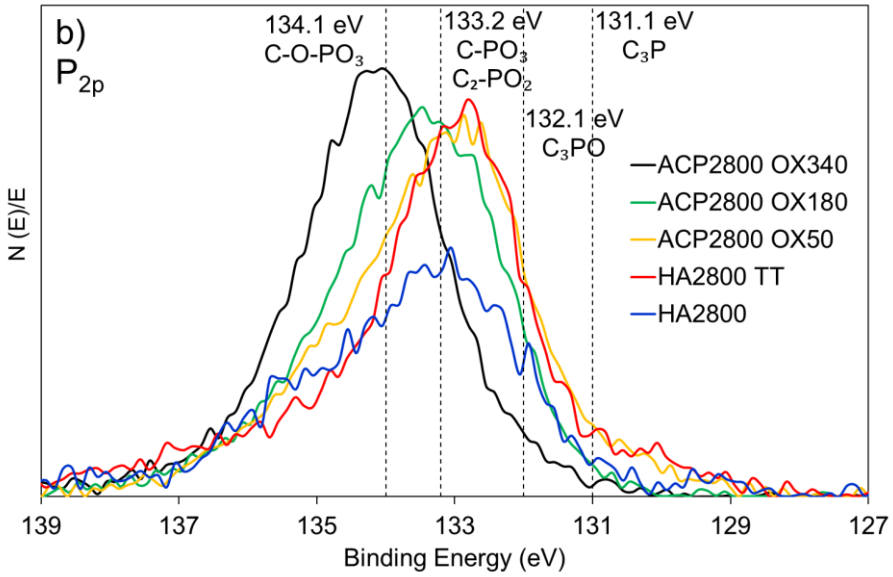

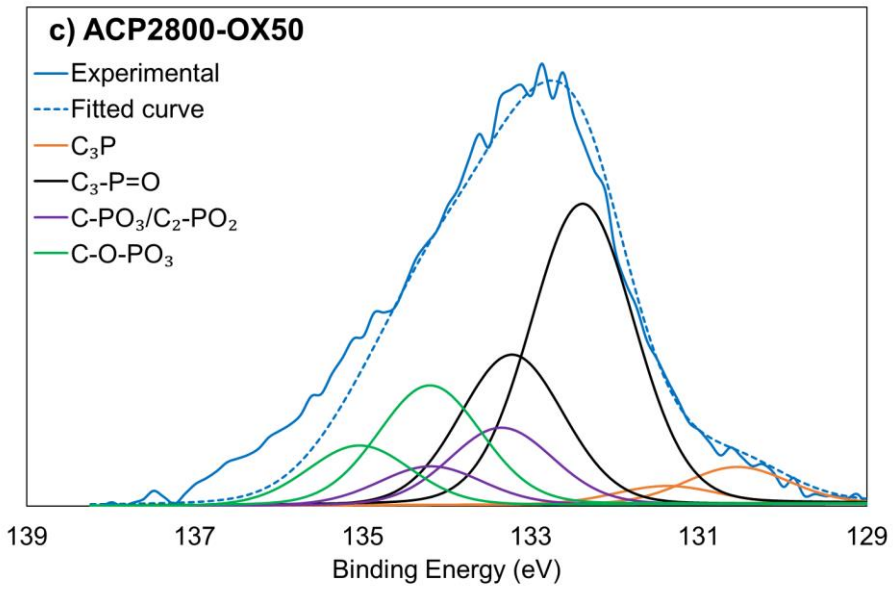

UNIVERSIDAD DE MÁLAGA

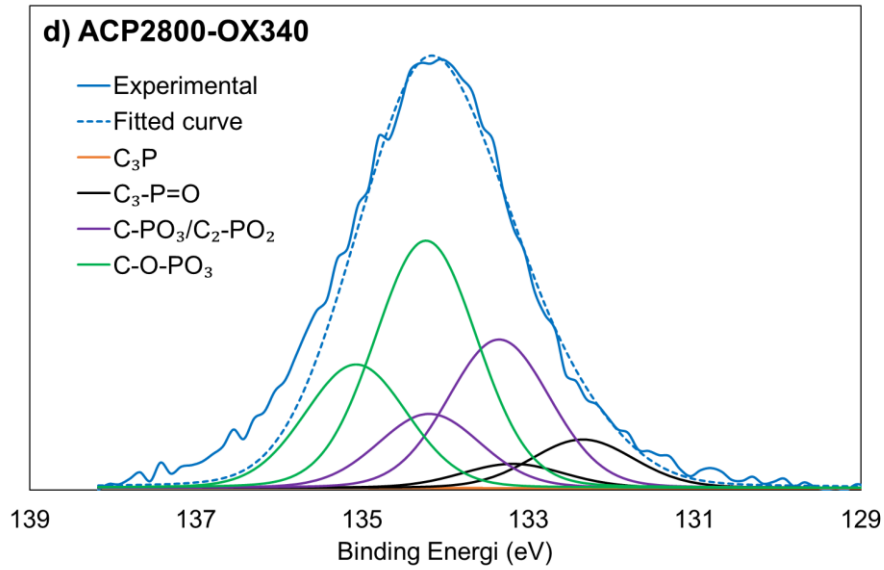

Figure 3. 1. XPS spectra of a) O_{1s} and b) P_{2p} of fresh, thermal treated and samples thermal treated and oxidized for 12 h at different temperatures and deconvolution of P_{2p} curves of sample oxidized 12 h at c) 50 ºC and d) 340 ºC (0.03 atm_{O2})

Figure 3.2 represents the TPD profile for the ACP2800 activated carbon. As already commented in the introduction section, the concentration of CO and CO_2 obtained during the heating of a carbonaceous sample at a controlled heating rate in an inert atmosphere, can be directly correlated to the oxygenated group presented in the carbon surface. Moreover, in activated carbons without phosphorus, the evolved CO_2 account for the number of acidic groups on the carbon surface [6].

In this sense, to avoid any error in the experimental set-up, two consecutive TPD were performed on the same carbon. This second TPD is represented in Figure 3.2 as ACP2800-TT, showing only a small CO and CO_2 evolution. This evolution can be related to small quantities of oxygen presented in the inert stream that, during the cooling and subsequent heating process was adsorbed mainly by the C'-P group [15], evolving to CO at high temperatures. With only small trace concentrations of oxygen, at such high temperatures, the carbon surface can be oxidized. Another explanation is related to the possible oxygen spill-over, as some groups are still stable at temperatures above 1000 ºC (like some pyran or benzopyran groups [35,36]). Those groups, remain unaltered after the TPD process, and then, during the cooling process, the high reactivity with oxygen of C_3PO groups [15] can take

UNIVERSIDAD DE MÁLAGA

those oxygen atoms from those high stable carbon-oxygen groups and then, during the second heating process, evolve as CO.

According to the literature, several contributions can be detected in the CO and CO_2 TPD profile. Focusing on the CO profile, the most prominent peak is observed at 870 ºC, and this peak can be associated to C-O-P groups [37]. At lower temperatures, at 800 ºC, a shoulder can be seen related to carbonyl or quinone groups. At 655 ºC, a small peak, associated to phenol or ether groups can be detected. At 450 ºC, a small interaction can be hardly seen that is associated to anhydride groups [4,15]. Finally, around 350 ºC, a minimal evolution can be seen, that can be associated to α-substituted aldehyde or ketone groups [38,39], but other authors suggest that those interactions were produced by decomposition of carboxylic acid groups, as their evolution temperature is similar to the one for those groups in CO_2 [28,40].

Focusing on the CO_2 evolution profile, the most important change compared to CO profile is the difference in concentration. The main peak for CO groups was around 3.5 μmol/g·s, for CO_2 groups the maximum was around 0.2 μmol/g·s. This implies that those kinds of carbons do not present much carbon-oxygen acidic groups (except for the C-O-P) as acidic groups appear in the CO_2 profile [6]. As happened in the CO profile, the profile is the sum of several interactions. At 870 ºC, the main peak observed was related to C-O-P groups, as happened for the CO evolution profile. That could be associated to the reaction of a CO molecule with an oxygen surface group to produce a CO_2 molecule and carbon deposited [37]. Another explanation is the evolution of C-O-P groups next to a carbon-oxygen functional group, like stable O=C-O-P groups, evolving as CO_2 instead of only CO [15]. At lower temperatures, at 690 ºC, the evolution of lactones to CO_2 groups can be detected. After that, at 450 ºC, the evolution of anhydride groups can be seen [4]. The disposition of that kind of groups promotes its evolution to both CO and CO_2 at the same time. Nevertheless, although in this work both CO and CO_2 evolution has been considered coincident, some authors suggest that their evolution should not be simultaneous, as they are linked to the carbon with different strength [41]. Finally, at 280 ºC a peak, higher than the two latter can be seen, that was associated to carboxylic acid groups. Moreover, that peak can be again divided into two, one smaller at 230 ºC and another one at 330 ºC, which means that there is a labile (Low stability) and a strong (high stability) carboxylic acid group [28,35,36].

UNIVERSIDAD DE MÁLAGA

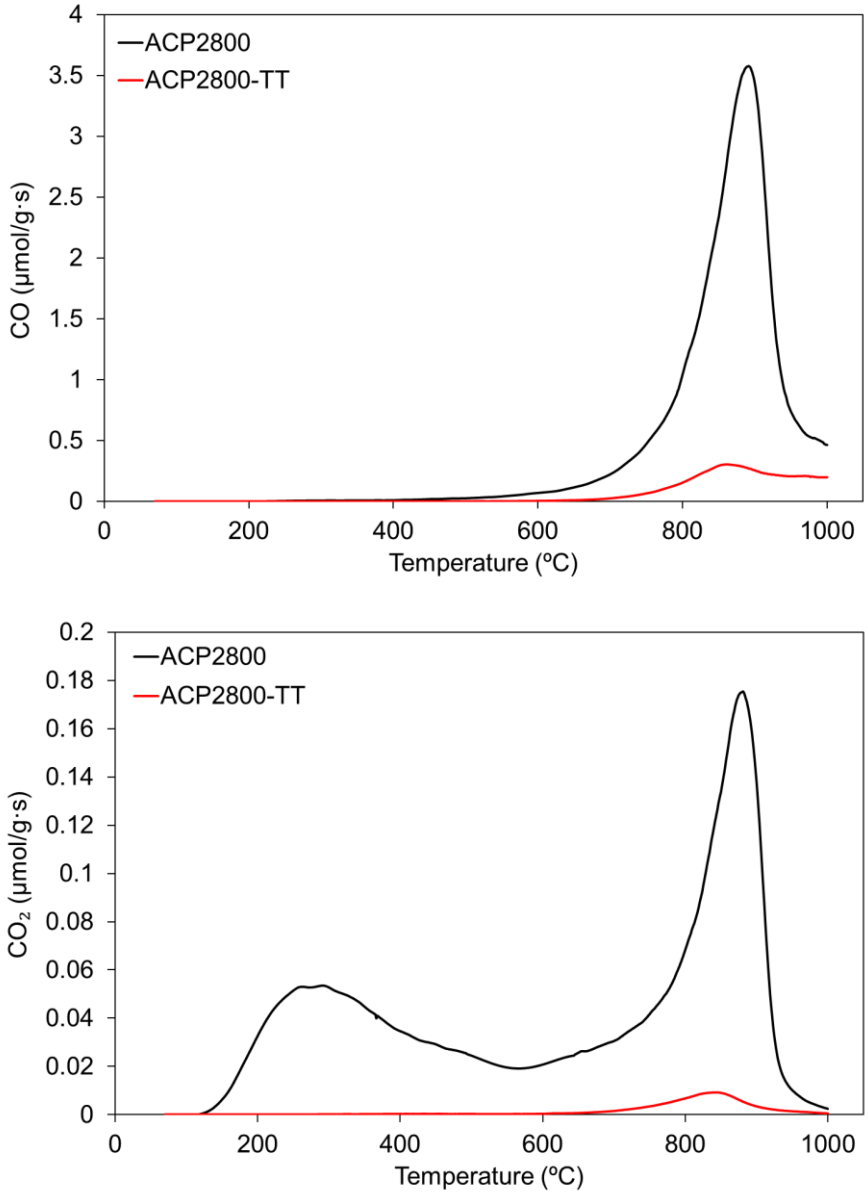

Figure 3. 2. TPD evolution profile for initial and thermal treated ACP2800

UNIVERSIDAD DE MÁLAGA

3.1.2. Non-isothermal decomposition of oxygen surface groups

In the previous section, CO and CO_2 TPD profile were described as the sum of different functional oxygen-carbon groups evolution to CO_x. Moreover, every kind of functional oxygen group evolved at different temperatures, which suggest that different kinetic parameters could described those evolutions. In this sense, a kinetic modelling of the non-isothermal decomposition of oxygen surface groups has been performed, following the methodology used in previous papers [42]. The assumptions taken into account for the development of the kinetic study were a negligible heat and mass transfer limitations and ideal flow, without radial gradients of concentrations. The experimental conditions used for the kinetic model were: inlet inert atmosphere flow of 200 Ncm^3/min, 100 mg of sample and increasing temperatures from 70 to 1000 ºC at a heating rate of 10 ºC/min.

Taking into account the aforementioned conditions, and the independence of each functional group to evolve to CO_X, a batch reactor can be used to describe the data and the mass balance equation for every functional group take the form of eq. 3.1.

$$(-R_i) = N_{i,0}\frac{dX_i}{dt} \tag{3.1}$$

where X_i represents the conversion of the functional group and $-R_i$ is the kinetic rate of consumption of the i functional group (µmol/g·s), t is the time (s) and $N_{i,0}$ is the molar amount of the functional group i (µmol/g). Temperature dependence of kinetic constant is considered to follow Arrhenius law (eq. 3.2), while relation between temperature and time follow eq. 3.3.

$$k_i = k'_{0,i} \cdot exp\left(\frac{-E_{a,i}}{R \cdot T}\right) \tag{3.2}$$

$$T = T_0 + \beta \cdot t \tag{3.3}$$

where k_i is the kinetic constant, $k'_{0,i}$ is the apparent preexponential factor, $E_{a,i}$ is the activation energy of reaction i, R is the universal gas constant (J/mol·K), T is the temperature (K), T_0 is the initial temperature (K), β is the heating rate (K/s) and t is the time (s).

All of the functional groups are supposed to react to CO_x without interaction among each other, this way, equations 4-11 collects all of the functional groups presented in the carbon surface (see section 3.1) and its evolution to CO_x.

UNIVERSIDAD DE MÁLAGA

Carboxylic acid	$-COOH \rightarrow CO_2$	(3.4)
Aldehyde	$-CHO \rightarrow CO$	(3.5)
Anhydride	$-CO-O-OC- \rightarrow CO + CO_2$	(3.6)
Phenol/Ether	$-C-OH/-C-O-C- \rightarrow CO$	(3.7)
Lactone	$-COO- \rightarrow CO_2$	(3.8)
Carbonyl/Quinone	$-CO- \rightarrow CO$	(3.9)
Phosphorus (CO)	$-C-O-P- \rightarrow CO$	(3.10)
Phosphorus (CO_2)	$O=C-O-P- \rightarrow CO_2$	(3.11)

Assuming all of the reactions were simple steps, their reaction rate can be described as first order equations (eq. 3.12).

$$-R_i = k \cdot N_i = k \cdot N_{i,0} \cdot (1 - X_i) \quad (3.12)$$

where R_i is the reaction rate (μmole/g·s), k is the kinetic constant (s^{-1}), N_i is the amount of functional group i (μmol/g) and $N_{i,0}$ is the initial amount of the functional group i.

Taking into account eq. 3.1-3 and eq. 3.12, the equation that describes every reaction is collected in eq. 3.13.

$$\frac{dX_i}{dt} = k_{i,0} \cdot \exp\left(\frac{-E_{a,i}}{R \cdot (T_0 + \beta \cdot t)}\right) \cdot (1 - X_i) \quad (3.13)$$

where X_i is the conversion of group i, $k_{i,0}$ is the preexponential factor and $E_{a,i}$ is the activation energy of group i.

To obtain the kinetic parameters of every reaction, the objective function was minimized (eq. 3.14), which consisted of the square difference between the experimental CO or CO_2 concentration and the sum of the calculated CO or CO_2 evolved from the different reactions.

$$OF = \sum \left(CO_{x,exp} - CO_{x,calc}\right)^2 \quad (3.14)$$

Table 3.3 collects the best fit parameters for the different carbon-oxygen functional groups present on the carbon surface. The first thing that can be observed is that the activation energy for the decomposition of every group ranged from 30 to 100 kJ/mol, except for the phosphorus group, whose value is around 250 kJ/mol. That can be associated the high

UNIVERSIDAD DE MÁLAGA

thermal stability of those phosphorus groups in comparison with the others.

On the other hand, for a specific group, as the temperature for their maximum rate of decomposition increases, their activation energy also increases. That does not happen for lactone groups, and that can be attributed to the decomposition of several type of lactone groups, which distort its activation energy [43,44]. A similar behavior can be seen for the carboxylic acid group, as the “high stability” group presented a lower activation energy than the “low stability”. That can be associated to the temperatures used in this study. Probably, “low stability” carboxylic groups started to decompose at temperatures below room temperature, so, at the temperatures starting temperature used in this work, the peak was deformed, and the activation energy was not adequately associated.

Comparison of those activation energies obtained in this work with bibliography shows different activation energies for the same groups, that can be associated in a first step to the different kinetic models used on their calculation, as some of them proposed a changing activation energy as a function of oxygen coverage. For example, Barton et al. [45] observed an E_a of 75 to 420 kJ/mol (average 275 kJ/mol) for evolution of carbon-oxygen surface groups to CO_x for oxidized thermal treated graphite. Similar to this, Kelemen et al. [46,47] proposed an E_a ranged from 242 to 334 kJ/mol (average 272 kJ/mol). Focusing on activating energy for the evolution of different carbon-oxygen groups, Marchon et al. [44] proposed a three activation energies for CO groups decomposition of 238, 267, 309 kJ/mol and for CO_2 groups of 108, 138, 163, 192 and 222 kJ/mol, although they associated those CO groups to semiquinones and CO_2 to lactones. Perrard et al [19] proposed an E_a for carboxylic and anhydride evolution to CO_x of 142 kJ/mol. Finally, Chernyak et al [48] proposed decreasing activation energies as a function of increasing oxygen coverage for different functional groups: 46-74 keto/hydroxyl acids, 79-101 kJ/mol for carboxylic acids, 92-160 kJ/mol anhydrides and 106-234 kJ/mol for phenol, pyran and carbonyl groups. All of the activation energies obtained in this work for the evolution of the different carbon-oxygen functional groups are lower than the one already shows by Chernyak but are not far from the values obtained at the highest coverage (lower E_a). This can suggest that the groups obtained in this work has a similar behavior than high oxygen coverage on his work. Nevertheless, a more logic explanation is that phosphorus groups (presented on this carbon but not on the carbons on

UNIVERSIDAD DE MÁLAGA

the bibliography) somehow distort the evolution of those groups, as phosphorus has a high appetence for oxygen.

Table 3. 3 Best fit parameters for the decomposition of different functional groups

Group	E_a (kJ/mol)	k_0 (s^{-1})
L Carboxylic acid	42	456
H Carboxylic acid	30	1.0
Aldehyde	45	395
Anhydride	62	66
Phenol/Ether	93	386
Lactone	55	1.2
Carbonyl/Quinone	97	94
Phosphorus (CO)	249	$9.22 \cdot 10^8$
Phosphorus (CO_2)	259	$4.60 \cdot 10^9$

Figure 3.3 collects the experimental and the calculated profile of the TPD for the ACP2800 with the best fit parameters collected in Table 3.3. A good agreement between the experimental and the calculated curve can be observed. The most prominent group was the phosphorus one, followed by the carbonyl/quinone groups. They both showed a big difference between their width, as phosphorus groups decomposed forming a thinner peak than the carbonyl/quinone groups. This was already observed in previous works [15] as carbonyl/quinone groups presented a wide profile in the absence of phosphorus.

UNIVERSIDAD DE MÁLAGA

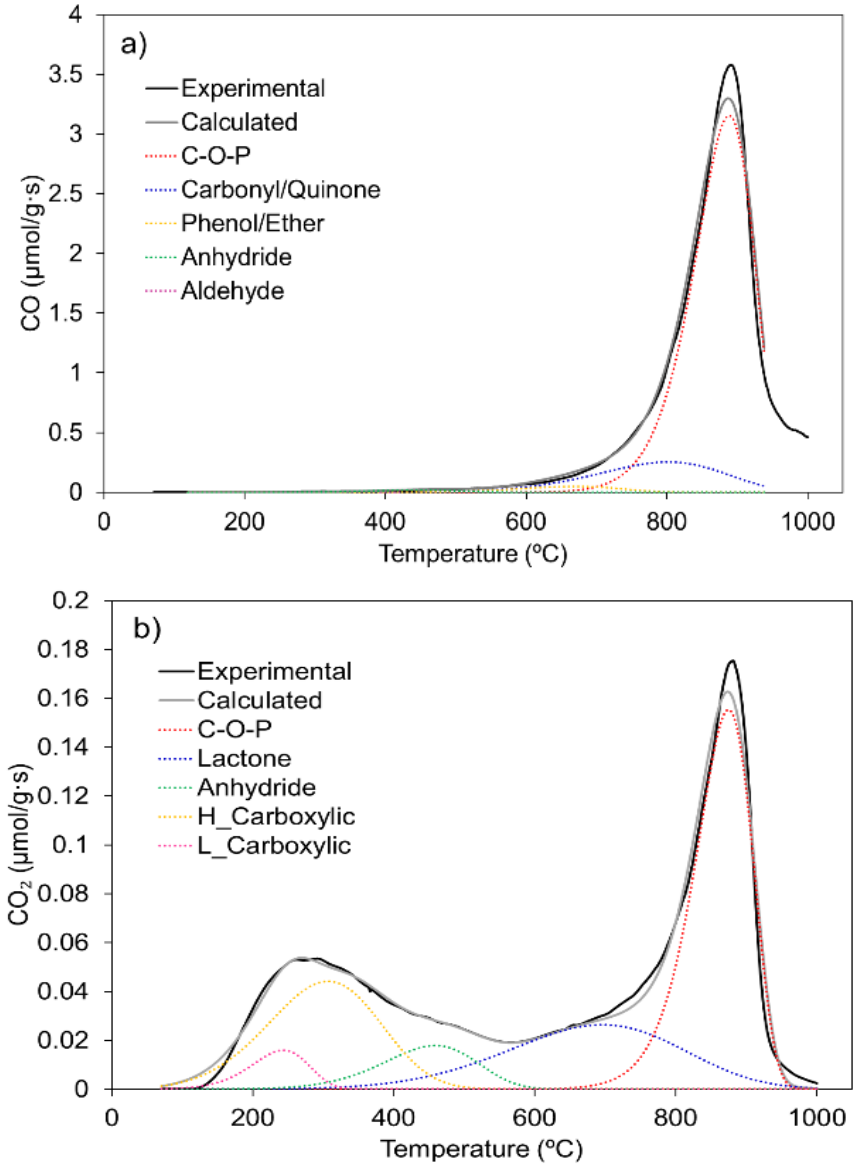

Figure 3. 3. Experimental TPD evolution profile and the calculated profile for the initial ACP2800 with the best fit parameters for the decomposition of every functional group

3.1.3. Carbon oxidation

In a previous paper [15], a biomass-derived P-containing activated carbon was submitted to several oxidation processes. As the oxidation temperature increased, the evolution of CO and CO_2 at temperatures

UNIVERSIDAD DE MÁLAGA

around 860 ºC also increased. When the oxidation treatment was performed at temperatures above 300 ºC, the peak related to carbonyl/quinones could be clearly observed as an increasing shoulder around 750 ºC. Nevertheless, in that work, the oxidation took place on the initial catalyst, so interaction between different carbon-oxygen surface groups could happened. To avoid those interaction between groups, a different methodology has been used in this study. In a first place, an inert atmosphere thermal treatment at 1000 ºC was performed on the activated carbon, sample that was called ACP2800-TT. After that, the oxidation process took place and then, the TPD was performed on the oxidized sample. It is worth mention, that those type of experiment needed to be done using a small amount of sample diluted with silicon carbide under a diluted air stream. This way, only <5 ºC of temperature increase in the first minutes of oxidation was observed. Otherwise, the temperature increase when the oxidizing stream was in contact with the sample could be higher than 100 ºC. That happened because phosphorus oxidation from C-P groups to C-O-P groups is a highly exothermic reaction that is carried out even at low temperature.

Figure 3.4 collects the data of the TPD profiles after the oxidation of ACP2800-TT for 30 minutes (Figures 3.4 a and c) and 12 h (Figures 3.4 b and d) at different temperatures. As described before, when the temperature increased, the peak at 860 ºC associated to phosphorus groups increased. Moreover, an evident shoulder appears at oxidizing temperatures above 300 ºC, although, this shoulder was also observed at 240 ºC for longer oxidizing times (12 h). It is also interesting that, after an oxidation of 12 h at 300 ºC and at 340 ºC, the peak at 860 ºC, associated with phosphorus, did not increase (as happened with the increase of the oxidizing temperature below 300 ºC). That could suggest the saturation of oxygen in the phosphorus groups, which means that all of the C-P groups susceptible to be converted into C-O-P were already converted. However, that saturation was not observed when the oxidizing time was only 30 minutes, meaning that 30 minutes was not enough time to saturate all of the C-P sites. The most interesting part is that, only after saturation of the C-O-P group, the shoulder observed at lower temperatures started to increase. This suggests that phosphorus increase the oxidation resistance by its preferential oxidation versus the formation of other carbon-oxygen groups that evolved at lower temperatures and could begin to gasify the carbon.

Focusing on figures 3.4 c and d, a clear delay in the evolution of groups can be seen as the oxidizing temperature increased. That could be explained due to the evolution temperature of those labile groups, which

UNIVERSIDAD DE MÁLAGA

was similar to the one used during the oxidation process. In that case, at the same time that those groups were formed, they were volatilized and decomposed as CO or CO_2.

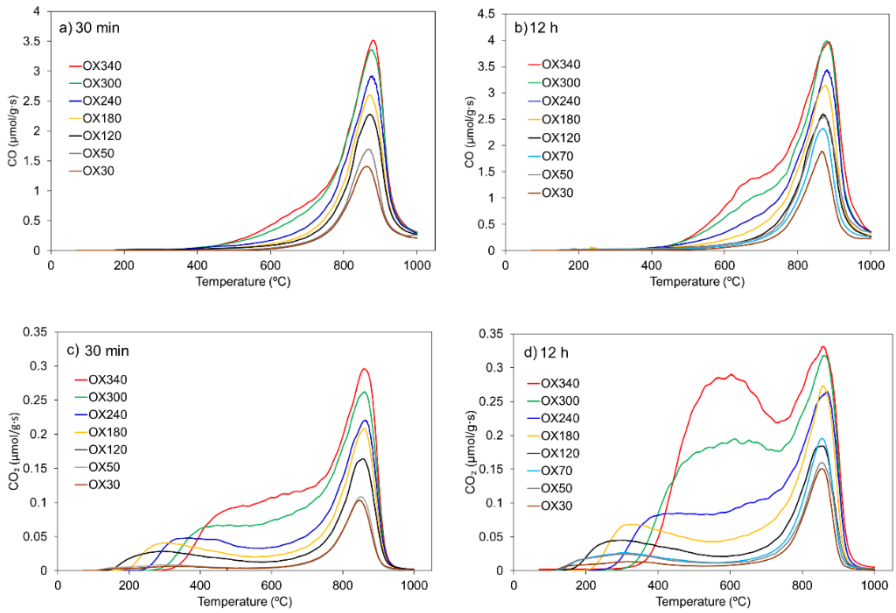

Figure 3. 4. TPD profiles after oxidation of ACP2800-TT at a) and c) 30 min and b) and d) 12 h at different temperatures

As was said before, the oxidizing time was an important factor to produce the different carbon-oxygen surface groups. For this reason, a series of experiments were performed, in which the oxidizing time was varied from 30 seconds to 24 h at different temperatures. The results of those series of experiment were collected in Figure 3.5. Figure 3.5 a, shows that, only after 30 s of oxidating treatment at only 30 ºC, a certain uptake of oxygen was observed. Nevertheless, it takes more than 24 h to double the amount of oxygen uptake. Conversely, both in CO and CO_2 profile, only the peak located at 860 ºC, associated to C-O-P groups could be clearly seen, an no other carbon-oxygen groups were produced at 30 ºC (except for a small quantity of carboxylic acid).

On the other hand, in Figures 3.5 c and d, the oxidation was performed at 300 ºC and, apart from the C-O-P peak, a big shoulder, that increased with time of oxidation, could be seen. These shoulders were associated with carbonyl/quinone and phenol/ether groups in the CO profile. Nevertheless, as the sample were oxidized in absence of a hydrogen source, those groups could not be phenols and must be carbonyl/quinone and ethers. The shoulders in the CO_2 profile could be

UNIVERSIDAD DE MÁLAGA

associated to lactones and anhydrides. Low stability groups, like carboxylic acid, did not appear due to the high temperature of the oxidation. This behavior of increasing functional groups with increasing time of oxidation was the same described when the temperature was increasing.

Some authors also observed the increasing carbon-oxygen groups formation as temperature or time was increased [15]. Nevertheless, depending on the oxidation treatment, different functional groups were detected on the carbon surface. Li et al. [49] compared the formation of carbon-oxygen groups on the carbon surface by titration after treatment with ammonia, sodium hydroxide, nitric acid, sulfuric acid and phosphoric acid. Ammonia treatment reduced phenolic groups; sodium hydroxide removed phenolic groups while increased lactones; treatment with those three acids produce similar groups, with a high amount of carboxylic groups, while lactone and phenolic groups were also increased with respect to the initial carbon. Moreno-Castilla et al. [27] treated activated carbons with nitric acid, hydrogen peroxide and $(NH_4)_2S_2O_8$. Nitric acid added the higher amount of oxygen to the carbon surface (mainly as carboxylic acids, anhydride and lactones, but also as carbonyl/quinone and phenol/ethers), while $(NH_4)_2S_2O_8$ only added a low amount of oxygen to the surface, similar to the results obtained by Salame et al. [9]. Hydrogen peroxide showed an intermediate effect. Zhuang et al. [11] studied the carbon-oxygen surface groups during carbon gasification with air by TPD and showed a higher evolution of CO than CO_2 (10 times higher), as happened in our work. This observation was also supported by Otake et al. [6]. Berenguer et al. [25] compared the chemical methods of oxidation with electrochemical methods, showing with the latter an easy selectivity of different carbon-oxygen groups. Valdés et al. [24] detected a high increase in carboxyl acid with ozone treatment, as well as an increase in anhydride and lactones while basic groups where decreased. Finally, Jaramillo et al [50] compared wet and dry oxidations and found that nitric acid and, especially, ozone increased the oxygen content (mainly as carboxylic acids) in the carbon surface in a high degree than O_2 or H_2O_2.

UNIVERSIDAD DE MÁLAGA

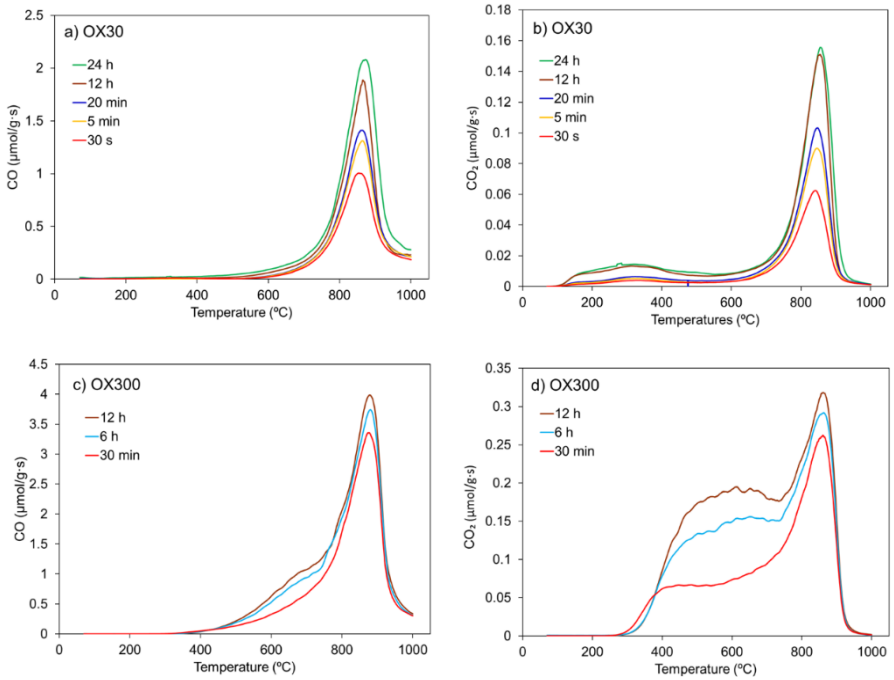

Figure 3. 5. TPD profiles after oxidation of ACP2800-TT at a) and b) 30 ºC and c) and d) 300 ºC for different times

Figure 3.1 shows the O_{1s} and P_{2p} spectra of ACP2800, ACP2800-TT and ACP2800-TT after oxidation for 12 h at 50 ºC, 180 ºC and 340 ºC. It is difficult to distinguish between oxygen bands in the O_{1s} spectrum, but a clear increase in the oxygen amount with the oxidation temperature can be observed. That was also shown in Table 3.2, in which surface atomic concentrations of oxygen follows the same trend. One of the most remarkable things is the high amount of oxygen presented in the ACP2800-TT. This behavior was already described in a previous paper [15], but was easily explained as only 30 s of oxidation with diluted air at 30 ºC was necessary to present an important amount of CO evolved during the TPD, specially at temperatures where C-O-P groups were decomposed. For this reason, although a careful handling of ACP2800-TT was done, it was impossible to avoid its contact with air before the XPS analysis and, therefore, the oxidation of a high amount of C-P to C-O-P. In particular, similar profiles for ACP2800 (initial catalyst) and ACP2800-TT (thermal treated at 1000 ºC) were observed. That could be explained with the activation temperature of the initial activated carbon, that was 800 ºC. For this reason, when the carbon was removed from the furnace, it should present reduced C-P species, that in contact with the air were transformed into C-O-P groups, the same

UNIVERSIDAD DE MÁLAGA

procedure that happened after ACP2800-TT was handled to obtain the XPS spectrum.

Focusing the P_{2p} spectrum, and due to the oxygen uptake when ACP2800-TT was being handled, ACP2800 and ACP2800-TT presented a similar profile, only with a higher amount of phosphorus presented in the thermal treated sample, mainly in the form of C-PO_3, C_2-PO_2 and C_3-PO. That could be associated to the elimination of some carbon-oxygen groups presented in the sample that, initially, hindered some phosphorus, and, after the remotion of those carbon-oxygen groups, more phosphorus could be detected in the XPS. Sample after oxidation at 50 ºC (ACP2800 OX50) shows an almost identical profile than ACP2800-TT, having only a slightly high amount of C-O-PO_3. This could be attributed to the similar temperature of oxidation, as ACP2800 OX50 was obtained after exposure to diluted air at 50 ºC and ACP2800 TT was exposed to air while handling to obtain the XPS spectra. Moreover, ACP2800 OX50 was also exposed to air while handling, with the possible modification of its carbon surface.

More differences can be found by seeing samples oxidized at 180 ºC and 340 ºC. As the temperature increased, the maximum of the peak was shifted to more oxidized species. For this reason, after oxidation at 340 ºC, more than a 55% of the phosphorus was in the form of C-O-PO_3 and only a 10% remains as C_3-P=O. This was in concordance with TPD analysis, by increasing the temperature, the peak at 860 ºC related to C-O-P groups was increased.

With the aim of a better description of the different carbon-oxygen groups presented after the different oxidizing treatments, the best fit parameters collected in Table 3.3, obtained with eq. 3.13, were used to predict the rate of decomposition of those surface groups and its quantity. The amount of every functional group after the oxidation of ACP2800-TT at different operation conditions was collected in Figure 3.6. This figure also includes the oxygen desorbed, which correspond to the sum of all of the groups that evolve to CO_x.

After the oxidation at 30 ºC for 30 minutes (Figure 3.6 a), C-O-P appears as the main peak, and only a small quantity of carbonyl/quinone were also presented in the CO profile; in the CO_2 profile (Figure 3.6 e), C-O-P appears again as the main group, but small quantities of lactone and high stability carboxylic acid were observed. If the ACP2800-TT was submitted to 12 h of oxidation at 30 ºC (Figure 3.6 b) in the CO profile, apart from the main peak of C-O-P groups and the small contribution of carbonyl/quinone, the peak related to ether was also observed, although

UNIVERSIDAD DE MÁLAGA

in a small amount. In the CO_2 profile (Figure 3.6 f) a small increase in every group can be observed, and low stability carboxylic acid and anhydrides can be detected, although at a low concentration.

Figure 3.6 c shows the CO profile of the ACP2800-TT oxidized for 30 min at 300 ºC. C-O-P is the highest peak, but carbonyl/quinone and ether are presented in a high amount. Anhydrides are also detected, but no aldehydes, because they evolved at temperatures lower than 300 ºC. In the CO_2 profile (Figure 3.6 g), again C-O-P groups are the most prominent, but a relatively high number of lactones and anhydrides are observed. At those temperatures only a small amount of high stability carboxylic acids was observed, because they started to evolve, but the time was not enough to be completely eliminated. Figure 3.6 d shows the same sample than Figure 3.6 c but oxidized during 12 h. This profile shows the same functional groups than the sample oxidized at shorter times, but all of the groups presented a higher amount. That is also what happened between Figure 3.6 g and Figure 3.6 h, the latter showing higher amount of C-O-P, lactones and anhydrides, but in this case, the time was enough to completely convert carboxylic acid groups into CO_2.

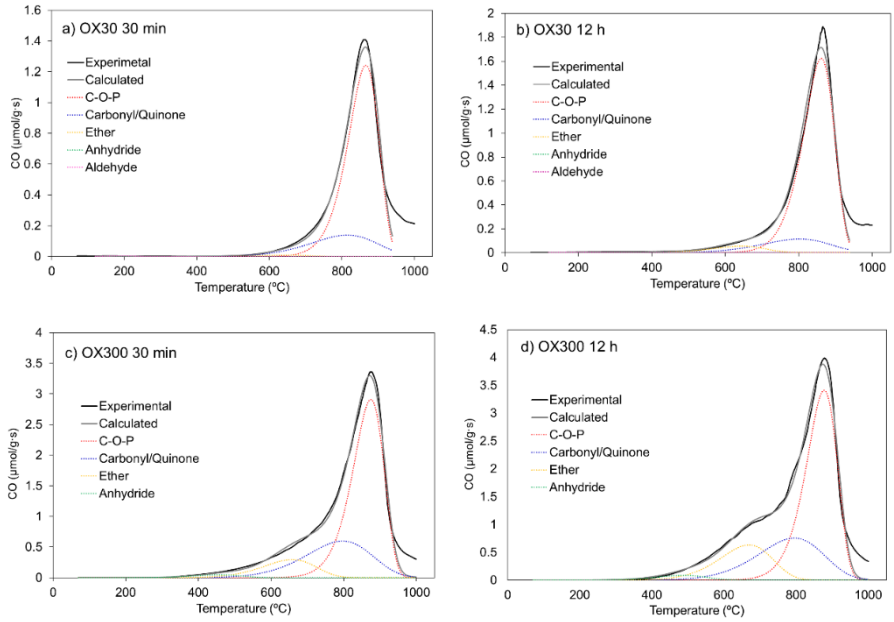

UNIVERSIDAD DE MÁLAGA

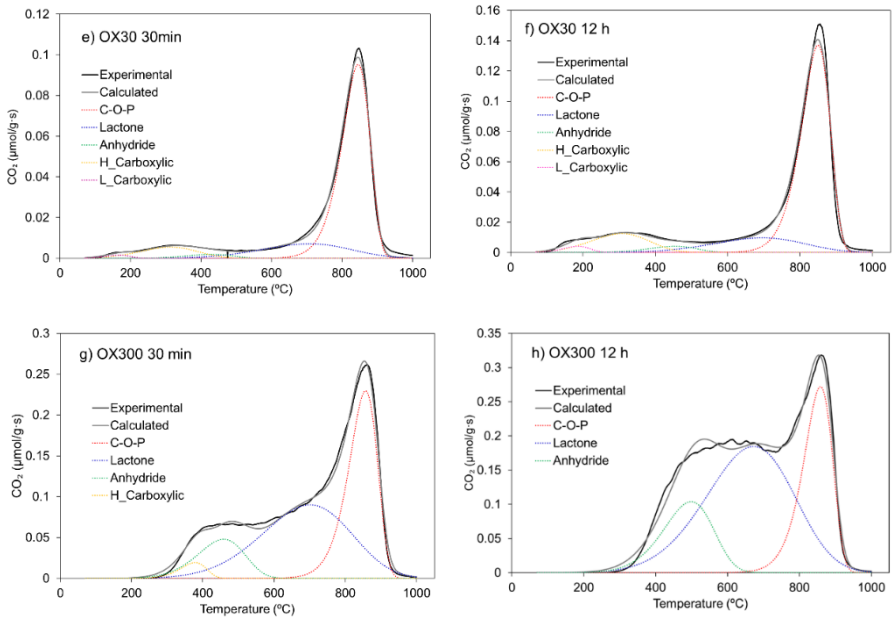

Figure 3. 6. Experimental TPD evolution profile and the calculated profile for the oxidized ACP2800-TT after different times and temperatures, using the best fit parameters for the decomposition of every functional group

The same methodology used to predict the rate of decomposition of every carbon-oxygen group and their amount, was applied to every oxidized sample. To confirm the correct quantification of those groups, XPS and TPD analyses after oxidation of 340 ºC were compared. The oxygen desorbed by the C-O-P groups in the TPD was 0.12 mmol/g·s while the oxygen associated to those phosphorus groups by XPS was 0.11 mmol/g·s, both similar values. This suggests that the TPD quantification of C-O-P groups was adequate.

3.1.4. Kinetics of surface carbon oxidation

Several authors have looked for the kinetics of carbon surface oxidation. The more commonly used models were Sestak-Berggren [51], pseudo n^{th} order [43,52,53] or Elovich equations [54,55]. Both three equations were employed to predict the kinetic data of the production of carbon-surface groups, nevertheless, in our case, with Sestak-Berggren or pseudo n^{th} order, the parameters obtained did not have physical meaning. For this reason, in this work, to describe the amount of every group formed as a function of time and temperature, the semiempirical Elovich equation [56] (eq. 3.15) has been used.

UNIVERSIDAD DE MÁLAGA

$$\frac{dq_i}{dt} = a_i \cdot \exp(-b_i \cdot q_i) \quad (3.15)$$

where q_i is the amount of the functional group i, t is the time (min), a_i is the initial rate of the formation of group i and b_i is a constant that accounts for the non-uniformity of the surface.

This eq. 3.15 can be integrated in the form of eq. 3.16, where a_i, as the initial rate, takes the form of eq. 3.17.

$$q_i = \frac{1}{b} \cdot \ln(\, a_i \cdot b_i \cdot t + 1) \quad (3.16)$$

$$a_i = \frac{k_i'}{b_i} \cdot \exp\left(-\frac{E_{a_i}}{R \cdot T}\right) \quad (3.17)$$

where k_i' is the apparent preexponential factor, E_{ai} is the activation energy for the production of this carbon-oxygen surface group, R is the universal gas constant (J/mol·K) and T is the temperature (K).

As was mentioned before, the constant b_i refers to a constant related to the non-uniformity of the surface where those carbon-oxygen groups were formed. In particular, if the surface was divided into "patches" with the same activation energy for the production of those groups and assuming that, at certain time, patches with activation energies below a certain E_t were saturated, while patches with activation energies above that E_t value were empty, the constant b_i takes the form of eq. 3.18.

$$b_i = \frac{\alpha}{R \cdot T} \quad (3.18)$$

where α is a constant that accounts for the step between activation energy of two consecutive patches.

To obtain the kinetic parameters of the formation of the different surface groups, and considering eq. 3.16-18, the OF2 has been minimized (eq. 3.19).

$$OF2 = \sum\left(q_{exp} - q_{calc}\right)^2 \quad (3.19)$$

UNIVERSIDAD DE MÁLAGA

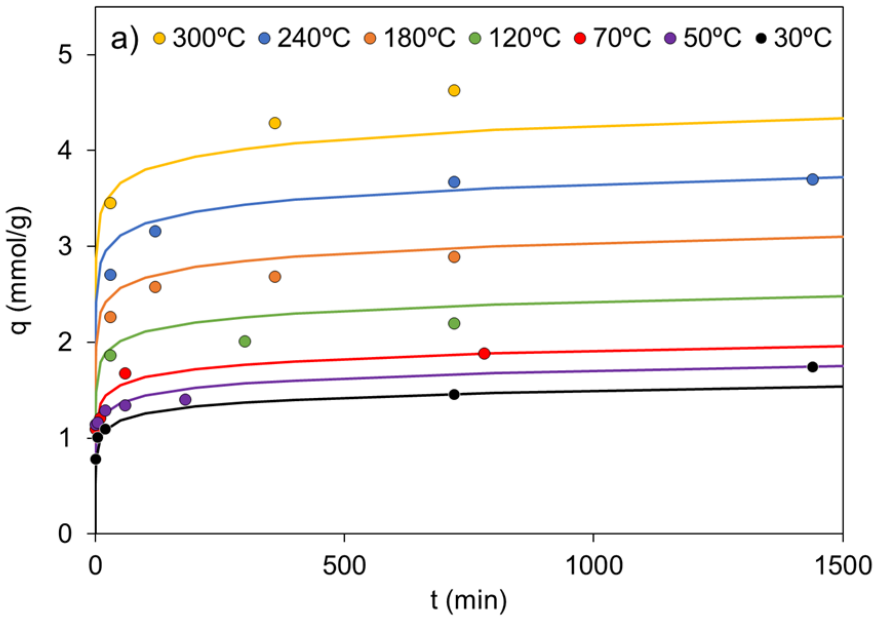

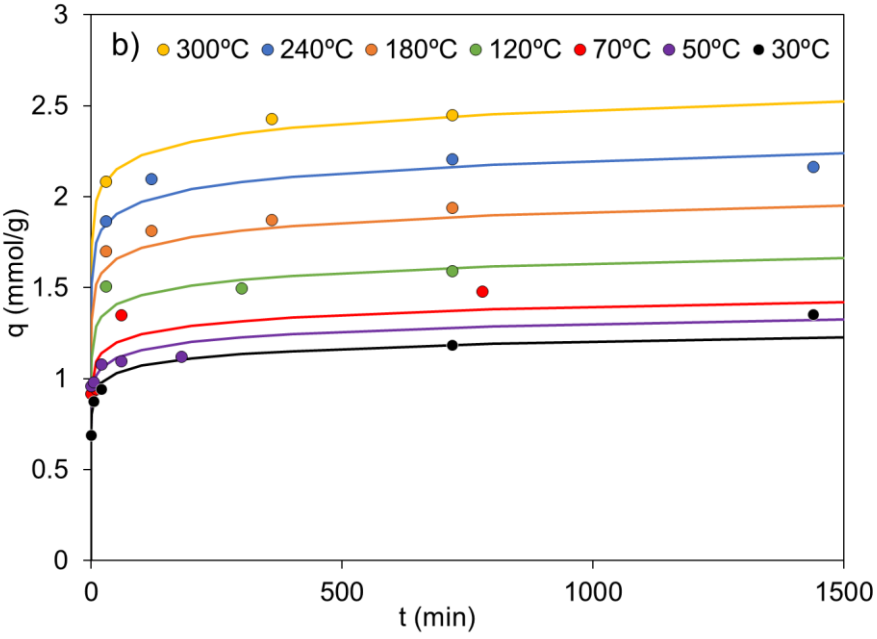

UNIVERSIDAD DE MÁLAGA

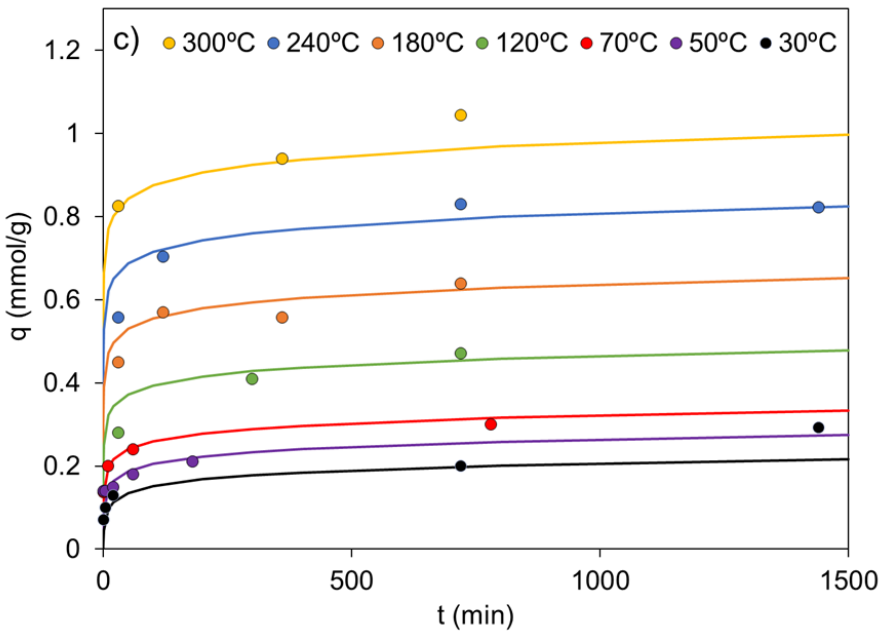

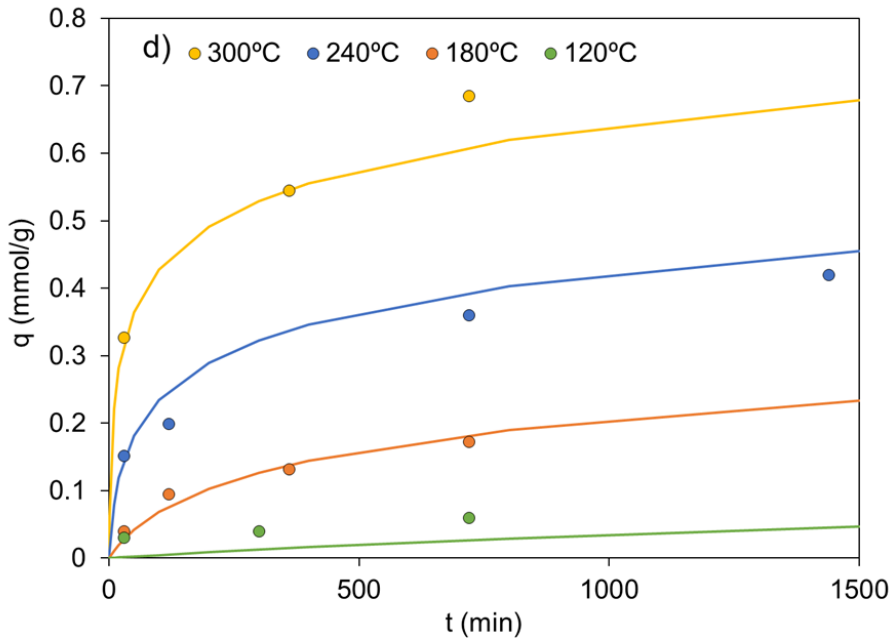

UNIVERSIDAD DE MÁLAGA

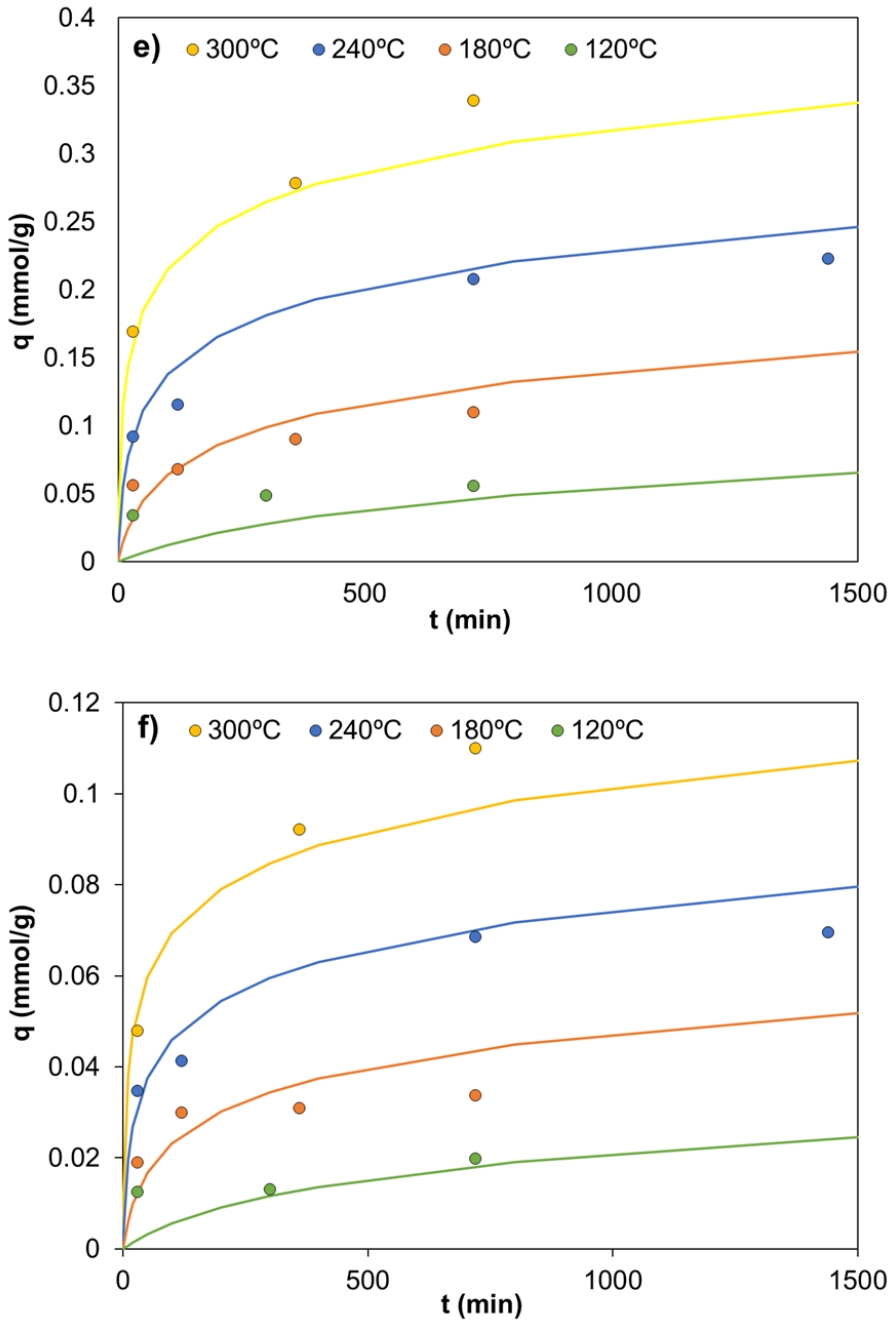

Figure 3. 7. Amount of a) all oxygen desorbed, b) C-O-P, c) Carboxyl/quinone, d) ether, e) Anhydride and f) Lactone groups after oxidation of ACP2800-TT at different times and temperatures.

UNIVERSIDAD DE MÁLAGA

Table 3.4 collects the kinetic parameters for eq. 3.16-19 and lines in Figure 3.7 represents the curves predicted by those parameters and equations. As was mentioned before, kinetic parameters for carboxylic acids and aldehydes have not been obtained because they decomposed at temperatures so low that they were not present after the oxidized treatment when it was above 250 ºC. Moreover, at lower temperatures, their amount was low and, thus, the experimental error was high. An analogous behavior happened with ether, anhydride and lactones groups at temperatures below 120 ºC, as their amounts at those low temperatures were not high enough to describe a clear tendency, with a high experimental error. For this reason, only amount at temperatures above 120 ºC has been taking into account to obtain their kinetic parameters. Oxidation process above 300 ºC have not neither be taken into account due to their appreciable gasification during the oxidation process. This way, the activated carbon mass could not be supposed constant.

As can be seen, Figure 3.7 shows a good agreement between experimental and calculated data. It also describes the sum of all of the oxygen desorbed and the data at different order of magnitude.

Activation energies collected in Table 3.4 shows a small value for the production of C-O-P groups from C-P ones, more similar to an enthalpy of adsorption value. This is in agreement with their experimental behavior, as they are able to be fast oxidized at low temperatures (as Figure 3.6 a shows). Anhydride and lactone groups present a similar tendency as well as similar activation energies (58 and 61 kJ/mol, respectively). Their amount is always low compared with other groups and are not present below 120 ºC. Ether groups present an activation energy of 79 kJ/mol, higher than carbonyl/quinone groups (73 kJ/mol), which also corresponds with their experimental behavior. As shows the TPD profile after oxidation at 30 ºC for 30 min (Figure 3.6 a), carbonyl/quinone groups were already present in the sample, while ether needed higher times (Figure 3.6 b) or temperatures (Figure 3.6 c) to be detected. That explain their higher value of activation energy. Finally, the activation energy for the sum of all groups shows an intermediate value of 42 kJ/mol. This value is quite low because C-O-P groups are the most abundant groups presented in the carbon, and their activation energy is quite low.

Several authors obtained the kinetics of carbon surface oxidation. Hotová et al. [51] proposed, on a carbon cryogel, an activation energy for the production of those carbon-surface groups of 77 kJ/mol, while Cheng et al. [53] obtained a value around 133 kJ/mol for different

UNIVERSIDAD DE MÁLAGA

carbons. Zabuga et al. [57] compared the oxidation of carbon black with nanodiamonds, obtaining an activation energy of 168 kJ/mol and 98 kJ/mol respectively. Kelemen et al. [47] obtained 134 kJ/mol on a glassy carbon with a high oxygen coverage, but this value decrease to 54 kJ/mol at low oxygen coverage. The latter being a more similar value than the one obtained in this work (42 kJ/mol), in which the coverage of oxygen is low due to the thermal treatment carried out before oxidation. In this sense, Hart et al. [43] obtained an activation energy on well cleaned graphon surface of 31 kJ/mol, also closer to the one obtained in our study. This similarity in activation energies when carbon surface has a low oxygen coverage could suggest that, after the remotion of oxygen from the carbon, several edge carbons, easy to be oxidized, remain on the carbon surface. Another explanation was the presence of phosphorus, with a high appetence for oxygen, that could act as an anchor point for oxygen that, subsequently, is displaced to the surface.

The comparison of activation energies for the production and the decomposition of the C-O-P group presented inverse tendency. As their decomposition showed the higher value (249 kJ/mol) and their production shows the lower activation energy value (13 kJ/mol). That corroborate the high appetence of phosphorus for oxygen, as the stability of the C-P bond is very low in the presence of oxygen while the reduction of C-O-P groups again to C-P groups needed a high temperature even in the absence of oxygen. This explain the high oxidation resistance of those P-containing activated carbon, as only after the C-P groups is completely oxidized, no other low stability carbon-oxygen surface group is produced, and due to the high stability of those C-O-P groups, no gasification is produced on those carbons.

Table 3. 4. Best fit parameters for the formation of different carbon-oxygen groups with time under oxidized atmosphere

Group	E_a (kJ/mol)	k_0	α
Sum of all	42	$2.36 \cdot 10^{9}$	$2.39 \cdot 10^{4}$
C-O-P	13	$1.30 \cdot 10^{7}$	$4.36 \cdot 10^{4}$
Carbonyl/Quinone	73	$4.74 \cdot 10^{11}$	$1.05 \cdot 10^{5}$
Ether	79	$1.50 \cdot 10^{6}$	$5.12 \cdot 10^{4}$
Anhydride	58	$3.54 \cdot 10^{3}$	$3.38 \cdot 10^{5}$
Lactone	61	$1.85 \cdot 10^{4}$	$1.05 \cdot 10^{5}$

UNIVERSIDAD DE MÁLAGA

3.1.4. Conclusion

The oxidation-decomposition of phosphorus groups on the surface of P-containing activated carbon has been carried out. The influence of this phosphorus groups on the oxidation of the carbon surface has also been addressed. For this reason, it has been performed a non-isothermal kinetic study of the decomposition of carbon-oxygen surface groups in inert atmosphere. XPS showed that the phosphorus present in the carbon, thermically and chemically stable, was linked to the carbon in the form of C-P or C-O-P groups due to the chemical activation process with H_3PO_4. Reduction of C-O-P bonds, by inert atmosphere thermal treatment, and reoxidation of those C'-P to C'-O-P bonds, by air flow, was observed. In addition to the phosphorus groups, the carbon present other carbon-oxygen groups, like carboxylic acids, anhydrides, lactones, phenols, ethers, carbonyls and quinones, as was shown by XPS and TPD. The proposed non-isothermal first order kinetic model was based on the fact that the decomposition of a determined group does not affect the others and this model reproduced successfully the experimental data. The activation energies for the reduction of C-O-P groups to C'-P showed a high value, around 250 kJ/mol, which is in concordance with the high temperature needed to carry out that reduction (around 860 ºC in TPD). Activation energies for the decomposition of the other carbon-oxygen surface groups ranged from 30 to 97 kJ/mol.

Oxidation of thermal treated carbon (whose most of the carbon-oxygen surface groups were removed) as a function of time and temperature was carried out. By means of TPD analysis and using the kinetic parameters obtained for the decomposition of each carbon-oxygen group, the amount of every group was quantified. The Elovich equation was used to obtain the kinetic parameters of the oxidation and successfully reproduces the experimental points. The activation energy for C-P oxidation to C-O-P was the lowest obtained, around 13 kJ/mol, which explain the high oxidation of those groups in contact with air even at low temperatures. The activation energy for the production of the other carbon-oxygen groups ranged from 58 to 79 kJ/mol. This fast oxidation of C-P groups (low E_a) in contrast with their high decomposition from C-O-P to C-P (high E_a), much higher than the other groups decomposition, could explain the high oxidation resistance that those groups provide to the activated carbon. For this reason, only after total oxidation of C-P to C-O-P groups, no other low stability groups are formed.

UNIVERSIDAD DE MÁLAGA

References

1. J.M. Rosas, R. Ruiz-Rosas, J. Rodríguez-Mirasol, T. Cordero, Kinetic study of the oxidation resistance of phosphorus-containing activated carbons, Carbon N. Y. 50 (2012) 1523–1537. https://doi.org/10.1016/j.carbon.2011.11.030.

2. X. Wu, L.R. Radovic, Inhibition of catalytic oxidation of carbon/carbon composites by phosphorus, Carbon N. Y. 44 (2006) 141–151. https://doi.org/10.1016/j.carbon.2005.06.038.

3. A.M. Puziy, O.I. Poddubnaya, A.M. Ziatdinov, On the chemical structure of phosphorus compounds in phosphoric acid-activated carbon, Appl. Surf. Sci. 252 (2005) 8036–8038. https://doi.org/10.1016/j.apsusc.2005.10.044.

4. J.. Figueiredo, M.F.. Pereira, M.M.. Freitas, J.J.. Órfão, Modification of the surface chemistry of activated carbons, Carbon N. Y. 37 (1999) 1379–1389. https://doi.org/10.1016/S0008-6223(98)00333-9.

5. A.M. Puziy, O.I. Poddubnaya, R.P. Socha, J. Gurgul, M. Wisniewski, XPS and NMR studies of phosphoric acid activated carbons, Carbon N. Y. 46 (2008) 2113–2123. https://doi.org/10.1016/j.carbon.2008.09.010.

6. Y. Otake, R.G. Jenkins, Characterization of oxygen-containing surface complexes created on a microporous carbon by air and nitric acid treatment, Carbon N. Y. 31 (1993) 109–121. https://doi.org/10.1016/0008-6223(93)90163-5.

7. M.F.R. Pereira, J.J.M. Órfão, J.L. Figueiredo, Oxidative dehydrogenation of ethylbenzene on activated carbon catalysts. I. Influence of surface chemical groups, Appl. Catal. A Gen. 184 (1999) 153–160. https://doi.org/10.1016/S0926-860X(99)00124-6.

8. C. Moreno-Castilla, F. Carrasco-Marín, C. Parejo-Pérez, M. V. López Ramón, Dehydration of methanol to dimethyl ether catalyzed by oxidized activated carbons with varying surface acidic character, Carbon N. Y. 39 (2001) 869–875. https://doi.org/10.1016/S0008-6223(00)00192-5.

9. I.I. Salame, T.J. Bandosz, Surface Chemistry of Activated Carbons: Combining the Results of Temperature-Programmed

UNIVERSIDAD DE MÁLAGA

Desorption, Boehm, and Potentiometric Titrations, J. Colloid Interface Sci. 240 (2001) 252–258. https://doi.org/10.1006/jcis.2001.7596.

10. P.E. Fanning, M.A. Vannice, A DRIFTS study of the formation of surface groups on carbon by oxidation, Carbon N. Y. 31 (1993) 721–730. https://doi.org/10.1016/0008-6223(93)90009-Y.

11. Q.-L. Zhuang, T. Kyotani, A. Tomita, DRIFT and TK/TPD Analyses of Surface Oxygen Complexes Formed during Carbon Gasification, Energy & Fuels. 8 (1994) 714–718. http://pubs.acs.org/doi/pdf/10.1021/ef00045a028 (accessed April 27, 2017).

12. E.A. Arkhipova, A.S. Ivanov, N.E. Strokova, S.A. Chernyak, A. V. Shumyantsev, K.I. Maslakov, S. V. Savilov, V. V. Lunin, Structural evolution of nitrogen-doped carbon nanotubes: From synthesis and oxidation to thermal defunctionalization, Carbon N. Y. 125 (2017) 20–31. https://doi.org/10.1016/j.carbon.2017.09.013.

13. S. Ghosh, F. Wei, S.M. Bachilo, R.H. Hauge, W.E. Billups, R.B. Weisman, Structure-Dependent Thermal Defunctionalization of Single-Walled Carbon Nanotubes, ACS Nano. 9 (2015) 6324–6332. https://doi.org/10.1021/acsnano.5b01846.

14. S.A. Chernyak, A.S. Ivanov, N.E. Strokova, K.I. Maslakov, S. V. Savilov, V. V. Lunin, Mechanism of Thermal Defunctionalization of Oxidized Carbon Nanotubes, J. Phys. Chem. C. 120 (2016) 17465–17474. https://doi.org/10.1021/acs.jpcc.6b05178.

15. M.J. Valero-Romero, F.J. García-Mateos, J. Rodríguez-Mirasol, T. Cordero, Role of surface phosphorus complexes on the oxidation of porous carbons, Fuel Process. Technol. 157 (2017) 116–126. https://doi.org/10.1016/j.fuproc.2016.11.014.

16. V. Likodimos, T.A. Steriotis, S.K. Papageorgiou, G.E. Romanos, R.R.N. Marques, R.P. Rocha, J.L. Faria, M.F.R. Pereira, J.L. Figueiredo, A.M.T. Silva, P. Falaras, Controlled surface functionalization of multiwall carbon nanotubes by HNO3 hydrothermal oxidation, Carbon N. Y. 69 (2014) 311–326. https://doi.org/10.1016/j.carbon.2013.12.030.

17. Y. Kanai, V.R. Khalap, P.G. Collins, J.C. Grossman, Atomistic oxidation mechanism of a carbon nanotube in nitric acid, Phys. Rev. Lett. 104 (2010) 066401. https://doi.org/10.1103/PHYSREVLETT.104.066401/FIGURES/

UNIVERSIDAD DE MÁLAGA

4/MEDIUM.

18. P. Vinke, M. van der Eijk, M. Verbree, A.F. Voskamp, H. van Bekkum, Modification of the surfaces of a gas-activated carbon and a chemically activated carbon with nitric acid, hypochlorite, and ammonia, Carbon N. Y. 32 (1994) 675–686. https://doi.org/10.1016/0008-6223(94)90089-2.

19. A. Perrard, L. Retailleau, R. Berjoan, J.P. Joly, Liquid phase oxidation kinetics of an ex-cellulose activated carbon cloth by NaOCl, Carbon N. Y. 50 (2012) 2226–2234. https://doi.org/10.1016/j.carbon.2012.01.039.

20. I. Mazov, V.L. Kuznetsov, I.A. Simonova, A.I. Stadnichenko, A. V. Ishchenko, A.I. Romanenko, E.N. Tkachev, O.B. Anikeeva, Oxidation behavior of multiwall carbon nanotubes with different diameters and morphology, Appl. Surf. Sci. 258 (2012) 6272–6280. https://doi.org/10.1016/j.apsusc.2012.03.021.

21. S. Karagöz, T. Tay, S. Ucar, M. Erdem, Activated carbons from waste biomass by sulfuric acid activation and their use on methylene blue adsorption, Bioresour. Technol. 99 (2008) 6214–6222. https://doi.org/10.1016/J.BIORTECH.2007.12.019.

22. F. Cataldo, M. V. Putz, O. Ursini, G. Angelini, Surface modification of activated carbon fabric with ozone, part 1: Kinetics and oxidation degree, Fullerenes, Nanotub. Carbon Nanostructures. 24 (2016) 313–323. https://doi.org/10.1080/1536383X.2016.1154849.

23. P. Manoj Kumar Reddy, K. Krushnamurty, S.K. Mahammadunnisa, A. Dayamani, C. Subrahmanyam, Preparation of activated carbons from bio-waste: effect of surface functional groups on methylene blue adsorption, Int. J. Environ. Sci. Technol. 12 (2015) 1363–1372. https://doi.org/10.1007/s13762-014-0506-2.

24. H. Valdés, M. Sá Nchez-Polo, J. Rivera-Utrilla, C.A. Zaror, Effect of Ozone Treatment on Surface Properties of Activated Carbon, (2002). https://doi.org/10.1021/la010920a.

25. R. Berenguer, E. Morallón, Oxidation of different microporous carbons by chemical and electrochemical methods, Front. Mater. 6 (2019) 130. https://doi.org/10.3389/FMATS.2019.00130/BIBTEX.

UNIVERSIDAD DE MÁLAGA

26. R. Berenguer, R. Ruiz-Rosas, A. Gallardo, D. Cazorla-Amorós, E. Morallón, H. Nishihara, T. Kyotani, J. Rodríguez-Mirasol, T. Cordero, Enhanced electro-oxidation resistance of carbon electrodes induced by phosphorus surface groups, Carbon N. Y. 95 (2015) 681–689. https://doi.org/10.1016/j.carbon.2015.08.101.

27. C. Moreno-Castilla, M.A. Ferro-García, J.P. Joly, I. Bautista-Toledo, F. Carrasco-Marín, J. Rivera-Utrilla, Activated Carbon Surface Modifications by Nitric Acid, Hydrogen Peroxide, and Ammonium Peroxydisulfate Treatmenss, Langmuir. 11 (1995) 4386–4392. https://doi.org/10.1021/la00011a035.

28. G. Hotová, V. Slovák, O.S.G.P. Soares, J.L. Figueiredo, M.F.R. Pereira, Oxygen surface groups analysis of carbonaceous samples pyrolysed at low temperature, Carbon N. Y. 134 (2018) 255–263. https://doi.org/10.1016/J.CARBON.2018.03.067.

29. Q.-L. Zhuang, T. Kyotani, A. Tomita, The change of TPD pattern of O2-gasified carbon upon air exposure, Carbon N. Y. 32 (1994) 539–540. https://doi.org/10.1016/0008-6223(94)90177-5.

30. M.J. Valero-Romero, E.M. Calvo-Muñoz, R. Ruiz-Rosas, J. Rodríguez-Mirasol, T. Cordero, Phosphorus-Containing Mesoporous Carbon Acid Catalyst for Methanol Dehydration to Dimethyl Ether, Ind. Eng. Chem. Res. 58 (2019) 4042–4053. https://doi.org/10.1021/acs.iecr.8b05897.

31. J. Palomo, J. Rodríguez-Mirasol, T. Cordero, Methanol Dehydration to Dimethyl Ether on Zr-Loaded P-Containing Mesoporous Activated Carbon Catalysts, Materials (Basel). 12 (2019) 2204. https://doi.org/10.3390/ma12132204.

32. F.J. García-Mateos, R. Ruiz-Rosas, J. María Rosas, E. Morallón, D. Cazorla-Amorós, J. Rodríguez-Mirasol, T. Cordero, Activation of electrospun lignin-based carbon fibers and their performance as self-standing supercapacitor electrodes, Sep. Purif. Technol. 241 (2020) 116724. https://doi.org/10.1016/J.SEPPUR.2020.116724.

33. F.J. García-Mateos, R. Ruiz-Rosas, J.M. Rosas, J. Rodríguez-Mirasol, T. Cordero, Phosphorus containing carbon (submicron)fibers as efficient acid catalysts, Catal. Today. 383 (2022) 308–319. https://doi.org/10.1016/J.CATTOD.2020.10.025.

UNIVERSIDAD DE MÁLAGA

34. J. Bedia, R. Barrionuevo, J. Rodríguez-Mirasol, T. Cordero, Ethanol dehydration to ethylene on acid carbon catalysts, Appl. Catal. B, Environ. 103 (2011) 302–310. https://doi.org/10.1016/j.apcatb.2011.01.032.

35. U. Zielke, K.J. Hüttinger, W.P. Hoffman, Surface-oxidized carbon fibers: I. Surface structure and chemistry, Carbon N. Y. 34 (1996) 983–998. https://doi.org/10.1016/0008-6223(96)00032-2.

36. J.L. Figueiredo, M.F. R Pereira, M.M. A Freitas, J.J. M O Ä rfão, Characterization of Active Sites on Carbon Catalysts, (2007). https://doi.org/10.1021/ie061071v.

37. J. Bedia, J.M. Rosas, J. Márquez, J. Rodríguez-Mirasol, T. Cordero, Preparation and characterization of carbon based acid catalysts for the dehydration of 2-propanol, Carbon N. Y. 47 (2009) 286–294. https://doi.org/10.1016/j.carbon.2008.10.008.

38. C. Moreno-Castilla, F. Carrasco-Marín, F.J. Maldonado-Hódar, J. Rivera-Utrilla, Effects of non-oxidant and oxidant acid treatments on the surface properties of an activated carbon with very low ash content, Carbon N. Y. 36 (1998) 145–151. https://doi.org/10.1016/S0008-6223(97)00171-1.

39. G.S. Szymański, Z. Karpiński, S. Biniak, A. Świątkowski, The effect of the gradual thermal decomposition of surface oxygen species on the chemical and catalytic properties of oxidized activated carbon, Carbon N. Y. 40 (2002) 2627–2639. https://doi.org/10.1016/S0008-6223(02)00188-4.

40. P. Valle-Vigón, M. Sevilla, A.B. Fuertes, Carboxyl-functionalized mesoporous silica–carbon composites as highly efficient adsorbents in liquid phase, Microporous Mesoporous Mater. 176 (2013) 78–85. https://doi.org/10.1016/J.MICROMESO.2013.03.049.

41. J.H. Zhou, Z.J. Sui, J. Zhu, P. Li, D. Chen, Y.C. Dai, W.K. Yuan, Characterization of surface oxygen complexes on carbon nanofibers by TPD, XPS and FT-IR, Carbon N. Y. 45 (2007) 785–796. https://doi.org/10.1016/j.carbon.2006.11.019.

42. T. Cordero, F. García, J.J. Rodríguez, A kinetic study of holm oak wood pyrolysis from dynamic and isothermal TG experiments, Thermochim. Acta. 149 (1989) 225–237. https://doi.org/10.1016/0040-6031(89)85284-0.

UNIVERSIDAD DE MÁLAGA

43. P.J. Hart, F.J. Vastola, P.L. Walker, Oxygen chemisorption on well cleaned carbon surfaces, Carbon N. Y. 5 (1967) 363–371. https://doi.org/10.1016/0008-6223(67)90052-8.

44. B. Marchon, J. Carrazza, H. Heinemann, G.A. Somorjai, TPD and XPS studies of O2, CO2, and H2O adsorption on clean polycrystalline graphite, Carbon N. Y. 26 (1988) 507–514. https://doi.org/10.1016/0008-6223(88)90149-2.

45. S.S. Barton, B.H. Harrison, J. Dollimore, Surface studies on graphite. Desorption of surface oxides formed on the clean surface at 300 K, J. Phys. Chem. 82 (1978) 290–294. https://doi.org/10.1021/j100492a008.

46. S.R. Kelemen, H. Freund, O2 oxidation studies of the edge surface of graphite, Carbon N. Y. 23 (1985) 619–625. https://doi.org/10.1016/0008-6223(85)90221-0.

47. S.R. Kelemen, H. Freund, A comparison of O2 and CO2 oxidation of glassy carbon surfaces, Carbon N. Y. 23 (1985) 723–729. https://doi.org/10.1016/0008-6223(85)90234-9.

48. S.A. Chernyak, A.S. Ivanov, A.M. Podgornova, E.A. Arkhipova, S.Y. Kupreenko, A. V. Shumyantsev, N.E. Strokova, K.I. Maslakov, S. V. Savilov, V. V. Lunin, Kinetics of the defunctionalization of oxidized few-layer graphene nanoflakes, Phys. Chem. Chem. Phys. 20 (2018) 24117–24122. https://doi.org/10.1039/c8cp05149f.

49. L. Li, S. Liu, J. Liu, Surface modification of coconut shell based activated carbon for the improvement of hydrophobic VOC removal, J. Hazard. Mater. 192 (2011) 683–690. https://doi.org/10.1016/j.jhazmat.2011.05.069.

50. J. Jaramillo, P.M. Álvarez, V. Gómez-Serrano, Oxidation of activated carbon by dry and wet methods, Fuel Process. Technol. 91 (2010) 1768–1775. https://doi.org/10.1016/j.fuproc.2010.07.018.

51. G. Hotová, V. Slovák, Optimization of oxygen chemisorption on the carbon surface based on kinetic analysis of isothermal thermogravimetry, Thermochim. Acta. 666 (2018) 82–90. https://doi.org/10.1016/j.tca.2018.06.007.

52. V. Slovák, B. Taraba, Effect of experimental conditions on parameters derived from TG-DSC measurements of low-

UNIVERSIDAD DE MÁLAGA

temperature oxidation of coal, (n.d.). https://doi.org/10.1007/s10973-010-0878-6.

53. A. Cheng, P. Harriott, Kinetics of oxidation and chemisorption of oxygen for porous carbons with high surface area, Carbon N. Y. 24 (1986) 143–150. https://doi.org/10.1016/0008-6223(86)90109-0.

54. F.J. Vastola, P.J. Hart, P.L. Walker, A study of carbon-oxygen surface complexes using O18 as a tracer, Carbon N. Y. 2 (1964) 65–71. https://doi.org/10.1016/0008-6223(64)90029-6.

55. N.R. Laine, F.J. Vastola, P.L. Walker, The importance of active surface area in the carbon-oxygen reaction, in: J. Phys. Chem., 1963: pp. 2030–2034. https://doi.org/10.1021/j100804a016.

56. C. Aharoni, F.C. Tompkins, Kinetics of Adsorption and Desorption and the Elovich Equation, Adv. Catal. 21 (1970) 1–49. https://doi.org/10.1016/S0360-0564(08)60563-5.

57. V.Y. Zabuga, O.O. Bochechka, G.G. Tsapyuk, V.E. Diyuk, T.O. Kurylyak, V. V. Lisnyak, Kinetic analysis of nanodiamonds oxidation, Mol. Cryst. Liq. Cryst. 673 (2018) 89–96. https://doi.org/10.1080/15421406.2019.1578497.

UNIVERSIDAD DE MÁLAGA

UNIVERSIDAD DE MÁLAGA

3.2. STUDY OF DEACTIVATION PROCESS OF AN ACTIVATED CARBON CONTAINING ZR AND P IN THE METHANOL TO DIMETHYL ETHER REACTION

Problems associated to fossil fuels consumption have driven the research for the implementation of a new sustainable scenario, in which non-pollution renewable fuels, chemicals and materials were used [1]. In this sense, valorization of industrial waste and lignocellulosic biomass, through waste refineries and biorefineries [2–6] could mean interesting alternatives achieve a circular economy.

In the context of those biorefineries, dimethyl ether (DME), a promising diesel and LPG substitute, can be obtained from syngas that has been produced from biomass gasification [7–10], thus providing that DME from a renewable character. That transformation from syngas to DME can be direct using a bifunctional catalyst [11–16] or indirect, producing methanol in a first stage and, subsequently, DME by dehydration of that methanol [17]. One of the main disadvantages of those catalyst in the industrial environment is the deactivation with time on stream [18–21].

Another important biorefineries product could be activated carbons, that can be used as adsorbent, catalyst supports of catalyst themself [22–24]. Chemical activation of lignocellulosic residues with H_3PO_4 [25,26] under certain operating conditions produce activated carbons with a high porosity, and different thermally stable phosphorus surface groups, responsible for their high oxidation resistance and acidic character [26–29], that can be used as catalyst for alcohol decomposition, and, even in the methanol to dimethyl ether reaction [30–33].

On their part, zirconium phosphate has shown also activity in methanol and other alcohol dehydration [34–38]. For this reason, the addition of zirconium to a P-containing activated carbon allows the production of a highly disperse zirconium phosphate on a carbon support that can be also gasified to obtain syngas and to recover the active phase at the end of its life cycle. This Zr-loaded P-containing activated catalyst showed a stable yield to DME around 50 %, without any other byproduct detected at 350 ºC [39,40]. However, industrial production of DME was performed

UNIVERSIDAD DE MÁLAGA

at higher temperatures in which coke deposition was observed [41–44] on acidic catalyst, especially influenced by temperature [45].

In this chapter, it was assessed the performance of a Zr-loaded P-containing biomass-derived carbon material as catalyst for the methanol dehydration to DME under severe reaction conditions to achieve high methanol conversions. Analyzing both selectivity and stability, as well as, textural properties, surface chemistry and coke content of the catalyst after different reaction temperatures and times on stream. A kinetic model to predict the coke formation at these different operating conditions has been proposed. In addition, the possible regeneration of the deactivated catalyst with an air treatment was assessed.

The catalyst preparation was described in section 2.3.1 and 2.3.2, and the techniques used for characterization in section 2.2. Catalytic experiments were presented in section 2.3.2 and 2.3.3, as well as regeneration experiments in section 2.3.4.

3.2.1. Properties of the catalyst

Figure 3. 8 represents the N_2 adsorption-desorption isotherm at -196 ºC of the fresh catalyst. The catalyst shows a type IV(a) isotherm with a large nitrogen adsorption volume at low relative pressures, evidencing the presence of high micropore volumes. In addition, a H4 hysteresis loop is also observed at medium-high range of relative pressures, associated to the adsorption in mesopores of an in-bottle shape [46]. Table 3. 5 collects the textural parameters derived from the N_2 and CO_2 adsorption isotherms. CO_2 adsorption at low relative pressure (< 0.3) and 0 ºC was used to characterize narrow microporosity (pores lower than 0.7 nm) due to a better diffusion in these narrow micropores compared to that of the N_2 adsorption at -196 ºC. Nevertheless, the catalyst showed a micropore volume value measured by adsorption of N_2 (V_t) significantly higher than the one determined by CO_2 adsorption (V_{DR}), which also suggests the presence of broad microporosity. In addition, the relatively high values of external surface area (A_t) and mesopore volume (V_{mes}) are also indicative of the large contribution of mesoporosity found in this sample. Table 3. 6 summarizes the atomic surface concentrations of the catalyst derived from XPS analysis. The results showed the presence of mainly carbon and oxygen species and, in less extent, phosphorus and zirconium surface groups. In this sense, P/Zr ratio was close to 1, lower than the theoretical zirconium phosphate atomic ratio (it should be 2), which could be attributed to an excess of zirconium deposited during wet impregnation. This result suggests the further formation of other Zr surface groups, like Zr-C/Zr-$(O\text{-}C)_2$ groups,

UNIVERSIDAD DE MÁLAGA

which were also observed in a previous work [40], close to those of zirconium phosphate species, as well as phosphorus-carbon surface groups.

Table 3. 5. Textural parameter values derived from N_2 adsorption isotherm at -196 ºC and CO_2 adsorption isotherm at 0 ºC of fresh and spent catalyst with different coke content, obtained at different reaction temperatures and TOS, at a methanol partial pressure of 0.04 atm and a space time of 75 g_{cat}·s/$mmol_{CH_3OH}$

		N_2 Isotherm					CO_2 Isotherm	
Sample	Coke content (%)	A_{BET} (m^2/g)	A_t (m^2/g)	V_t (cm^3/g)	V_{mes} (cm^3/g)	V_{tot} (cm^3/g)	A_{DR} (m^2/g)	V_{DR} (cm^3/g)
Fresh	-	1130	271	0.44	0.42	0.86	476	0.19
450 ºC 60 h	18	644	215	0.22	0.38	0.60	238	0.10
500 ºC 12 h	18	767	248	0.27	0.43	0.69	281	0.11
550 ºC 4.5 h	18	757	246	0.26	0.43	0.69	273	0.11
500 ºC 3 h	11	909	282	0.32	0.47	0.79	314	0.13
500 ºC 7 h	14	806	257	0.28	0.44	0.72	286	0.11
500 ºC 51 h	23	600	154	0.23	0.26	0.48	236	0.09

Table 3. 6. Atomic surface concentration (%) obtained by XPS of fresh and spent catalysts with different coke content, for a reaction temperature of 500 ºC and different TOS, at a methanol partial pressure of 0.04 atm and a space time of 75 g_{cat}·s/$mmol_{CH_3OH}$

Sample	C_{1s}	O_{1s}	P_{2p}	Zr_{3d}	P/Zr	C/P	C/Zr
Fresh	61.2	30.5	4.4	3.9	1.1	13.9	15.7
3 h	75.1	18.5	4.5	1.9	2.4	16.5	39.5
7 h	81.2	13.8	3.3	1.7	1.9	24.5	47.4
12 h	87.0	9.4	2.3	1.3	1.8	37.8	68.1

UNIVERSIDAD DE MÁLAGA

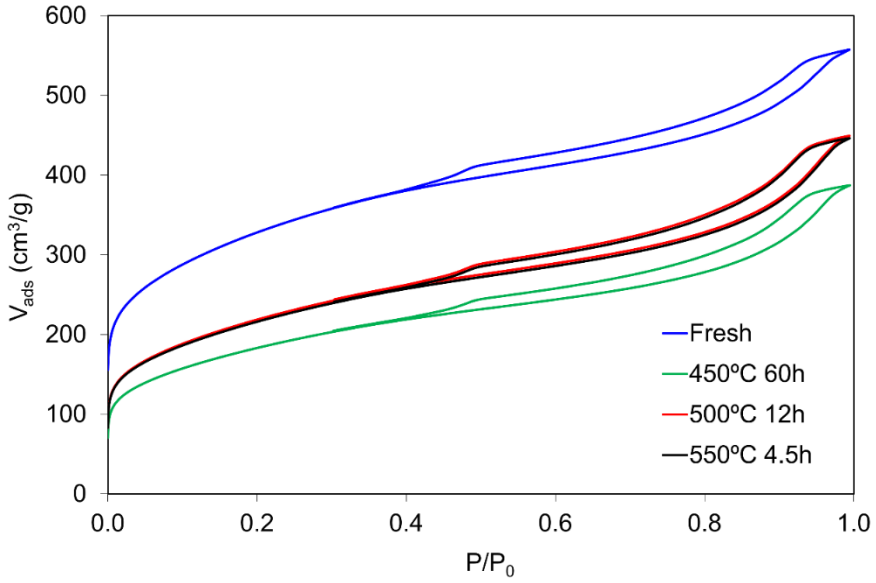

Figure 3. 8. N_2 adsorption-desorption isotherms at -196 ºC of fresh and spent catalyst with the same coke content (18%), obtained at different reaction temperatures and TOS, at a methanol partial pressure of 0.04 atm and a space time of 75 g_{cat}·s/$mmol_{CH3OH}$

3.2.2. Catalyst assessment in MTD

Methanol conversions as a function of time-on-stream (TOS) at temperatures between 300 ºC and 600 ºC are represented in Figure 3. 9 for a methanol partial pressure of 0.04 atm and a space time of 75 g_{cat}·s/$mmol_{CH_3OH}$. Steady state conversions of methanol were observed for temperatures lower than 450 ºC, with a conversion value higher than 60% for a reaction temperature of 400 ºC, which indicates that the catalyst presents a high stability for methanol dehydration in this temperature range. An increase in the reaction temperature produced a significant enhancement of the initial methanol conversion (short TOS), with conversion values of 100% for temperatures higher than 500 ºC. However, a slight reduction of methanol conversion with TOS was observed for a reaction temperature of 450 ºC and this decay was somewhat more pronounced as the temperature increased. In this sense, the methanol conversion value remained higher than 50% at 450 ºC for more than 24 h under the studied conditions. However, this value was lower than 5% at a reaction temperature of 600 ºC for similar TOS (24 h).

UNIVERSIDAD DE MÁLAGA

In this regard, the use of carbons with acid surface groups as catalysts to produce DME from dehydration of methanol was evaluated, but reaction temperatures could not exceed 180 ºC because the catalysts suffered from a strong catalyst deactivation by decomposition of the acid surface groups, showing a maximum conversion of around 13% at this temperature [47]. On the other hand, $H_3PW_{12}O_{40}$ heteropolyacid catalyst also showed faster deactivation during methanol dehydration at milder conditions, with conversion decreasing from 33% to 14% after 2 h at 200 ºC for a W/F_{CH_3OH}=7.33 g_{cat}·s/mmol$_{CH_3OH}$ (although some deactivation was already detected at 150 ºC) [44].

In the present study, the methanol conversion values for temperatures higher than 400 ºC at short TOS exceed those of the methanol-DME reaction equilibrium at the corresponding temperature (represented as dash lines in Figure 3. 9), which suggests that side reactions were been carried out, like those involved in coke production.

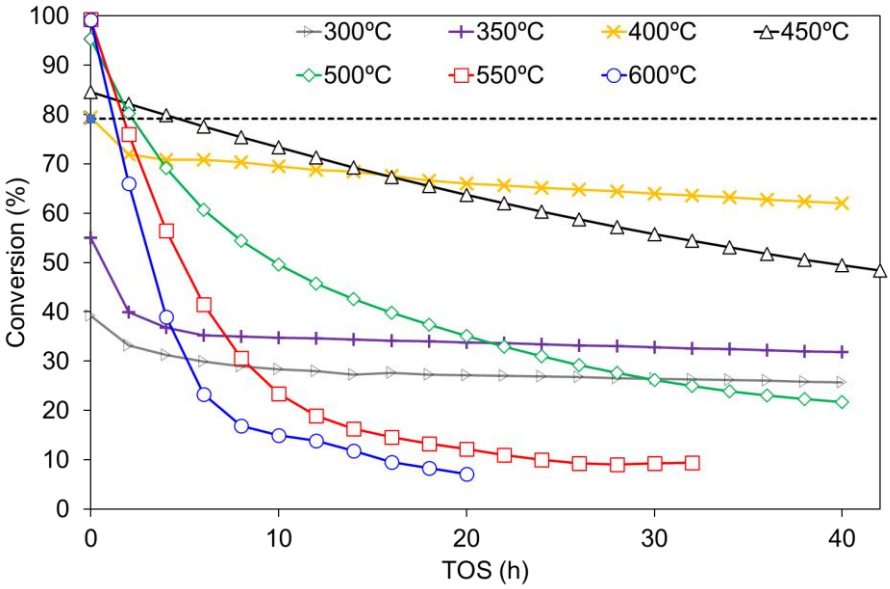

Figure 3. 9. Methanol conversion profile as a function of TOS at different reaction temperatures, at a methanol partial pressure of 0.04 atm and a space time of 75 g_{cat}·s/mmol$_{CH_3OH}$. Dash line shows the equilibrium Methanol-DME conversion at 450 ºC.

Figure 3. 10 shows the gas outlet concentrations, as well as, the selectivity as a function of TOS at different reaction temperatures, including also the selectivity to coke. DME and water were the only

UNIVERSIDAD DE MÁLAGA

products observed at reaction temperature of 400 ºC (Figure 3. 10a), with trace methane at very short TOS, and so with a very high selectivity to DME (99%) with TOS (Figure 3. 10b). Figure 3. 10c shows the gas outlet concentrations as a function of TOS for the catalyst at 450 ºC. A decay of the DME concentration with TOS was observed, as a consequence of a gradual reduction in the methanol conversion, as well (shown in Figure 3. 9). However, the selectivity to DME (Figure 3. 10d) remained stable at this temperature, with values higher than 90% for more than 20 h. A small amount of methane and coke and, in less extent, CO could also be detected. At 550 ºC (Figure 3. 10e and f), DME and water outlet concentrations decreased faster and methane and coke formation become more important than at 450 ºC, although DME selectivity was still quite high, showing values higher than 55% for more than 35 h. Thus, the relatively high selectivity to DME observed for the catalyst studied in the present work should be highlighted, especially, considering that several works found in the literature, which studied different acid catalysts for dehydration of methanol, showed lower selectivity to DME values even at lower temperatures (<350 ºC), although the operation conditions were also different (space time). For example, a γ-Alumina showed a selectivity to DME of 85% at 400 ºC [48], selectivity to DME in several kinds of HZSM-5 decayed almost totally as the temperature increased up to 320 ºC [49], selectivity to DME was also reduced to 80% at 400 ºC for a K-modified H-ZSM5 [50] and that of $H_3PW_{12}O_{40}$ decreased to 70% after 2h at 250 ºC [44].

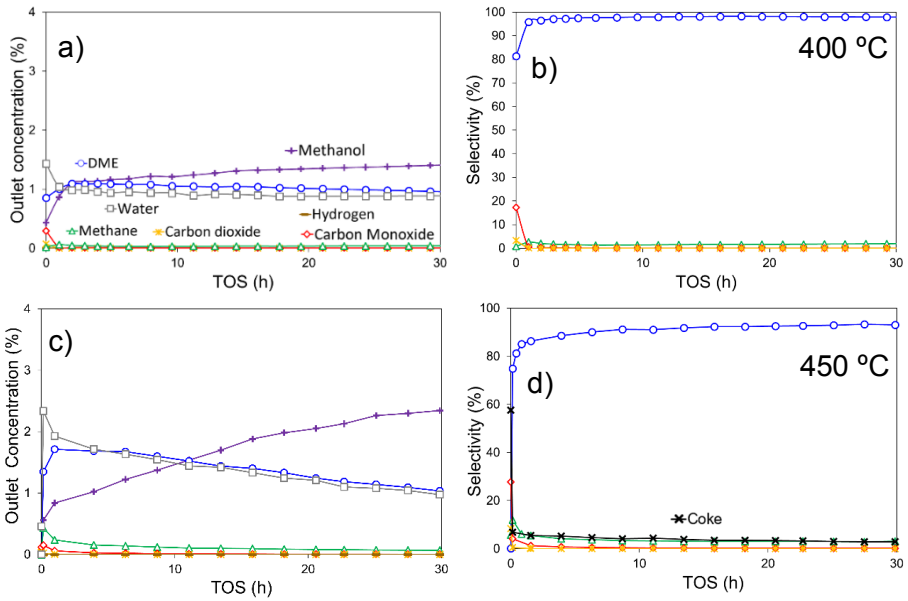

UNIVERSIDAD DE MÁLAGA

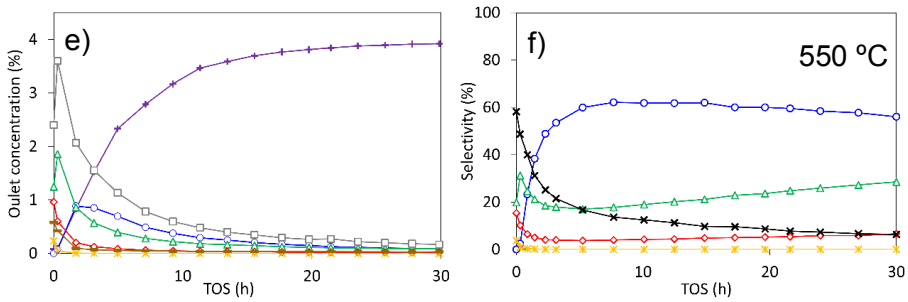

Figure 3. 10. Gas outlet concentrations (a,c,e) and selectivity (b,d,f) to carbon products as a function of TOS at: (a,b) 400 ºC, (c,d) 450 ºC and (e,f) 550 ºC, respectively. Methanol partial pressure of 0.04 atm and a space time of 75 g_{cat}·s/$mmol_{CH3OH.}$ Figure legend: methanol (+), DME (○), methane (△), carbon monoxide (◇), carbon dioxide (✳), hydrogen (–), water (□) and coke (✳).

On the other hand, it was observed that the higher the temperature, the higher the amount of methane formed. In this sense, Akarmazyan et al. [48] associated CO and CH_4 production to a change in mechanism due to the increase in temperature. They reported that CO and CH_4 were produced due to the evolution of surface formate groups, which were formed instead of metoxi groups at high temperatures. In order to evaluate the possible thermal decomposition of DME under the conditions studied, an experiment with 3%v DME up to 600 ºC in the absence of catalyst was carried out. The results indicated that the homogeneous DME thermal decomposition was lower than 1%, producing mainly CH_4 and CO. Therefore, the formation of methane via thermal decomposition of DME was neglected. On the other hand, Akarmazyan et al. [48] proposed that DME adsorbed species could decompose to CH_4, H_2 and CO, but this would require the stoichiometric formation of methane and CO. Other authors suggested also the thermal decomposition of DME into CO and CH_4 or formaldehyde (that decomposes into CO+H_2) [51].The larger observed formation of methane and water than CO and DME, respectively, at 550º C suggests that other reactions might be taking place, like the formation of methane and formaldehyde by decomposition of DME adsorbed species (produced by reaction of methoxy species with methanol through a six-member ring electron transfer process), as suggested by Cheng et al [38]. Formaldehyde would decompose further to CO and H_2 or to coke (C) and H_2O, probably on different acid sites. The results observed in Figure 3. 10 e and f suggest that the second route (producing coke and water) seems the one that occurs to a greater extent. In this sense, the

UNIVERSIDAD DE MÁLAGA

concentration of produced water and DME were very similar at 450 ºC, except for initial TOS (probably due to water can be desorbed easier than DME), evidencing that mostly all the water comes from the methanol dehydration reaction. Nevertheless, the concentration of water greatly exceeded that of DME at 550 ºC, which could be initially associated to the production of light olefins. However, olefins were hardly detected in the gas product at any of the temperatures studied. Thus, the similarities found for the production of water and coke with TOS at 550º C (Figure 3. 10e and f) indicate that coke production and growth (through reaction of coke with oxygenated compounds (methanol and/or DME) seem to be the main responsible for the excess observed in the water production [52].

3.2.3. Deactivated sample characterization

The catalyst was characterized after reaction at different temperatures and TOS. N_2 adsorption-desorption isotherms at -196 ºC of the spent catalyst after reaction at different experimental conditions, but with the same coke content (18%), are also shown in Figure 3. 8. Lower adsorption uptakes at low relative pressures were observed for the spent catalyst samples as compared to that for the fresh one, with the adsorption isotherm profile remaining similar, which suggests that coke deposition took place preferentially in micropores at all the evaluated temperatures. A slightly larger reduction in nitrogen adsorbed volume at low relative pressures was observed for the catalyst deactivated at 450 ºC. The three samples contained the same coke content, but the coke formation rate is obviously slower at 450 ºC, needing more than 60 h to reach this amount (18%) of coke. This lower coke formation rate could favour the diffusion of methanol inside the narrow micropores, producing a higher decrease of the microporosity. The results show that microporosity was reduced by half (V_t from 0.44 to 0.22 cm^3/g), but mesoporosity remained practically the same (V_{mes} from 0.42 to 0.38 cm^3/g). Nevertheless, the remaining surface area on the spent catalysts was high enough to question that the pore filling by coke was the only cause for catalyst deactivation at these temperatures, so the coverage of active site should also play an important role in this process.

The pore size distribution of these samples is collected in Figure 3. 11. The catalyst presents a bimodal distribution, showing two main peaks with two maxima located at 0.63 nm and 2.1 nm, respectively. The spent catalysts obtained after reaction at the different experimental conditions studied showed a similar pore size distribution, but the decrease observed for the shoulder located at lower pore sizes was larger than the peak corresponding to higher pore sizes, suggesting that coke is

UNIVERSIDAD DE MÁLAGA

preferentially deposited in narrow micropores rather than in wider micropores or mesopores.

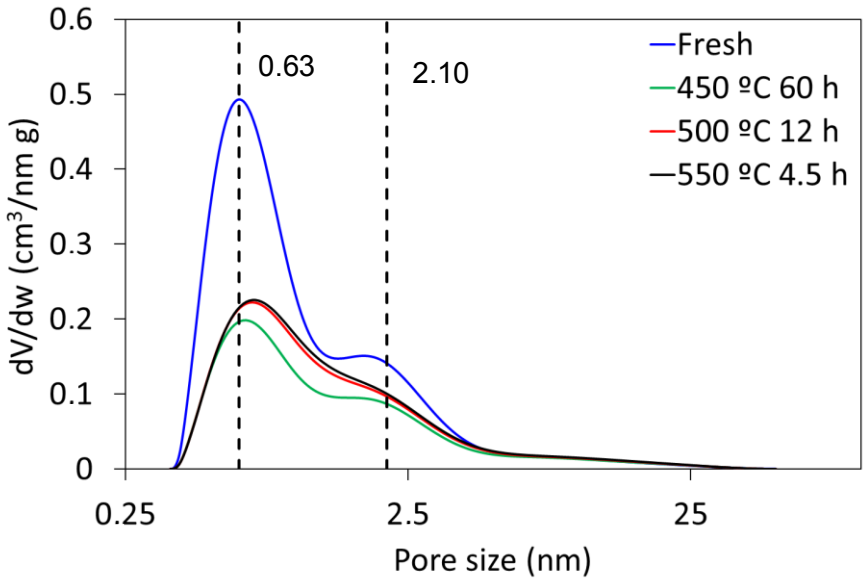

Figure 3. 11. Pore size distribution of fresh and spent catalyst with the same coke content (18%), obtained at different reaction temperatures and TOS, at a methanol partial pressure of 0.04 atm and a space time of 75 g_{cat}·s/mmol$_{CH_3OH}$

Porosity of the catalyst after reacting at 500 ºC for different TOS was also studied. Figure 3. 12 collects their corresponding N_2 adsorption-desorption isotherms obtained at -196 ºC. This temperature (500 ºC) was chosen as the best option between high coke deposition and enough time difference between selected TOS. Percentage of deposited coke was added to the legend of Figure 3. 12. The isotherm profile remained the same, but there was a significant reduction in adsorbed volume at low relative pressures with the increase of the amount of coke deposited on the catalyst, associated to the preferential deposition of the carbonaceous solid on the narrow micropore surface. Table 3. 6 lists the textural parameters of the spent catalyst after reaction at 500 ºC for different TOS. A reduction in the BET surface area and micropore volume measured with N_2 was mainly observed at low TOS, meanwhile mesopore volume slightly increased. With the increase of TOS, the deposition of coke augmented too, taking place on both micropore and mesopore surfaces, as evidenced the reduction observed of about 50% for all the textural parameter values. These results suggest that, initially,

UNIVERSIDAD DE MÁLAGA

coke was deposited mainly on the surface of the micropores and with the course of the reaction, the deposition took place uniformly on all the catalyst surface, reaching an apparent surface area of 600 m^2/g and mesopore volume of 0.26 cm^3/g after ~50 h of reaction at 500º C. Pore size distribution of the spent catalyst at different TOS (Figure 3. 13) also confirmed the preferential deposition of coke in narrow micropores (with a mean pore size of 0.63 nm), in the same way that it happened at different reaction temperatures (Figure 3. 11).

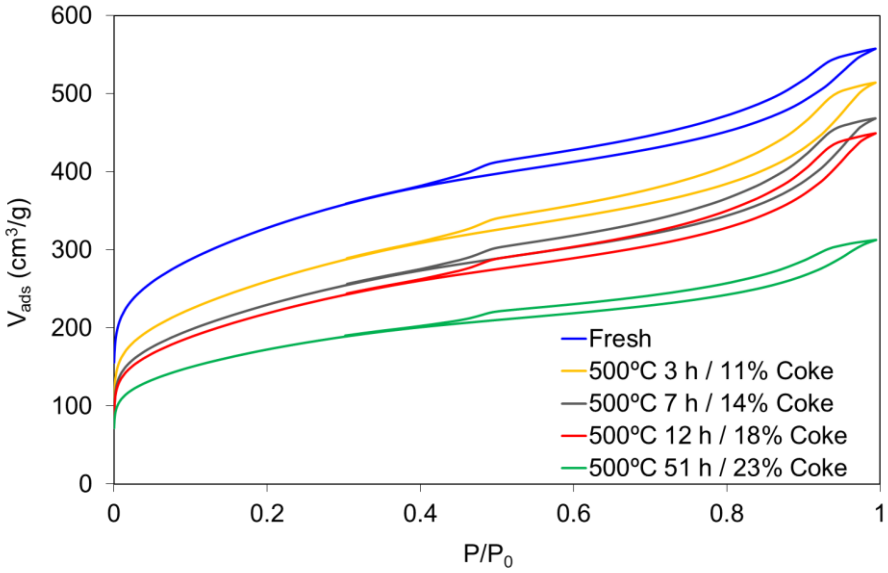

Figure 3. 12. N_2 adsorption-desorption isotherms at -196 ºC of fresh and spent catalyst with different coke content, obtained at 500 ºC and different TOS, at a methanol partial pressure of 0.04 atm and a space time of 75 g_{cat}·s/$mmol_{CH_3OH}$

UNIVERSIDAD DE MÁLAGA

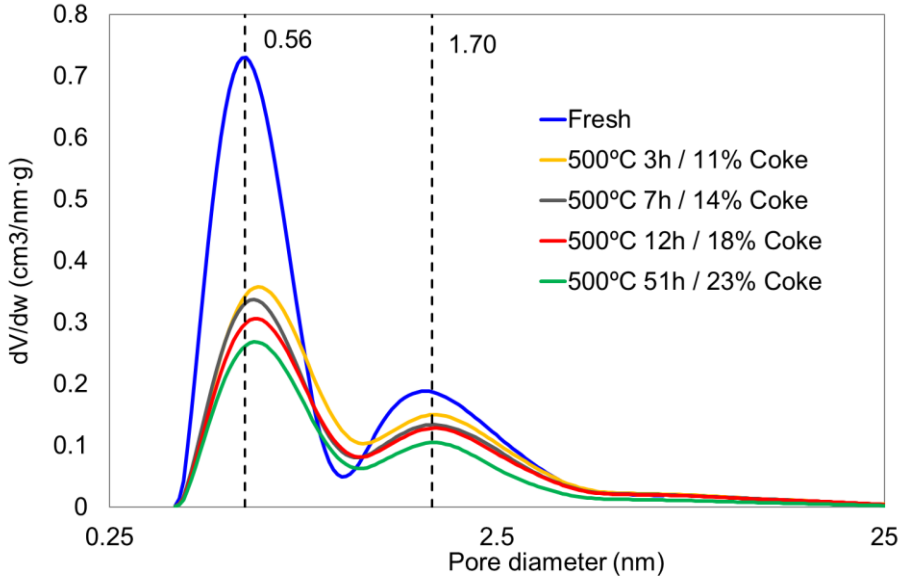

Figure 3. 13. Pore size distribution of fresh and spent catalyst at the same reaction temperature (500 ºC), obtained at different reaction TOS and with different coke content, at a methanol partial pressure of 0.04 atm and a space time of 75 g_{cat}·s/$mmol_{CH_3OH}$

XPS analyses were performed to assess how coke deposition took place on the catalyst surface. Table 3. 5 collects the atomic surface concentration of the catalyst after reaction at 500 ºC and different TOS. As expected, the carbon surface concentration increased with TOS. This increase was accompanied by a reduction in oxygen surface concentration, which seems to indicate that the composition of coke deposited was made up preferentially of less oxygenated species. Phosphorus and zirconium concentrations also decrease with TOS. In this sense, fresh catalyst showed a P/Zr ratio next to 1, but this ratio increases after reaction. Specifically, the P/Zr ratio come closer to 2, which is in concordance with the presence of zirconium phosphate species on the surface of the deactivated catalyst. On the other hand, the rapid increase observed for the P/Zr and C/Zr ratios compared to that of C/P for short TOS (3 h) indicate that the loss of surface concentration of zirconium is much higher than the one of phosphorus at the first stages.

Figure 3. 14 shows XPS spectra of P_{2p} and Zr_{3d} of fresh and spent catalyst. P_{2p} spectrum (Figure 3. 14a) of the fresh sample showed a broad band that suggests the presence of different phosphorus species.

UNIVERSIDAD DE MÁLAGA

The peak located at 133.2 ± 0.2 eV was attributed to C-PO_3/C_2PO_2 surface groups; other appearing at 134.0 ± 0.2 eV to C-O-PO_3 surface groups [31]; and a last contribution at 134.6 ± 0.2 eV was associated to zirconium phosphate surface groups, like in $Zr(HPO_4)_2 \cdot H_2O$ [53]. For the sample obtained after reaction at 450 ºC, a general decrease of the intensity of the whole band was observed, but especially the contribution at lower binding energies, related to the coverage of C-PO_3/C_2PO_2 and C-O-P groups by coke. These results are in concordance with those reported by Valero-Romero et al.[33] with a catalyst similar to the one studied in the present work. They suggested the presence of different P-surface groups (such as, P-OH and C-O-P) with different acid strength, which are very fast deactivated by coke under methanol dehydration reaction, even at lower temperatures.

Focusing on the Zr_{3d} spectrum of the fresh catalyst (Figure 3. 14b), different Zr species could be suggested, given the presence of one peak located at 182.3 ± 0.2 eV attributed to the existence of zirconium-carbon/ZrO_2 species [54]; another one at 183.0 ± 0.2 eV associated to Zr-OH bonds, like in $Zr(HPO_4)_2 \cdot H_2O$ [53], which seems to be the most relevant; and the last one at 184.2 ± 0.2 eV attributed to the presence of Zr(IV) bound to an electroactive species, such as phosphorus in form of pyrophosphates groups [55]. The intensity of the spectrum decreased and shifted at higher binding energies for the sample obtained after reaction at 450 ºC. These results suggest that deposition of coke took place on zirconium phosphate-like active sites and zirconium-carbon/ZrO_2 species. Actually, the band with the peaks associated to these two species almost disappeared after reaction at 450 ºC, shifting to higher binding energies, which suggests the formation of zirconium pyrophosphates-like species, probably due to the attack of oxygenated compounds to the –OH group of zirconium phosphate forming methoxy and other organic groups [56], which would be the precursors of the formed coke.

UNIVERSIDAD DE MÁLAGA

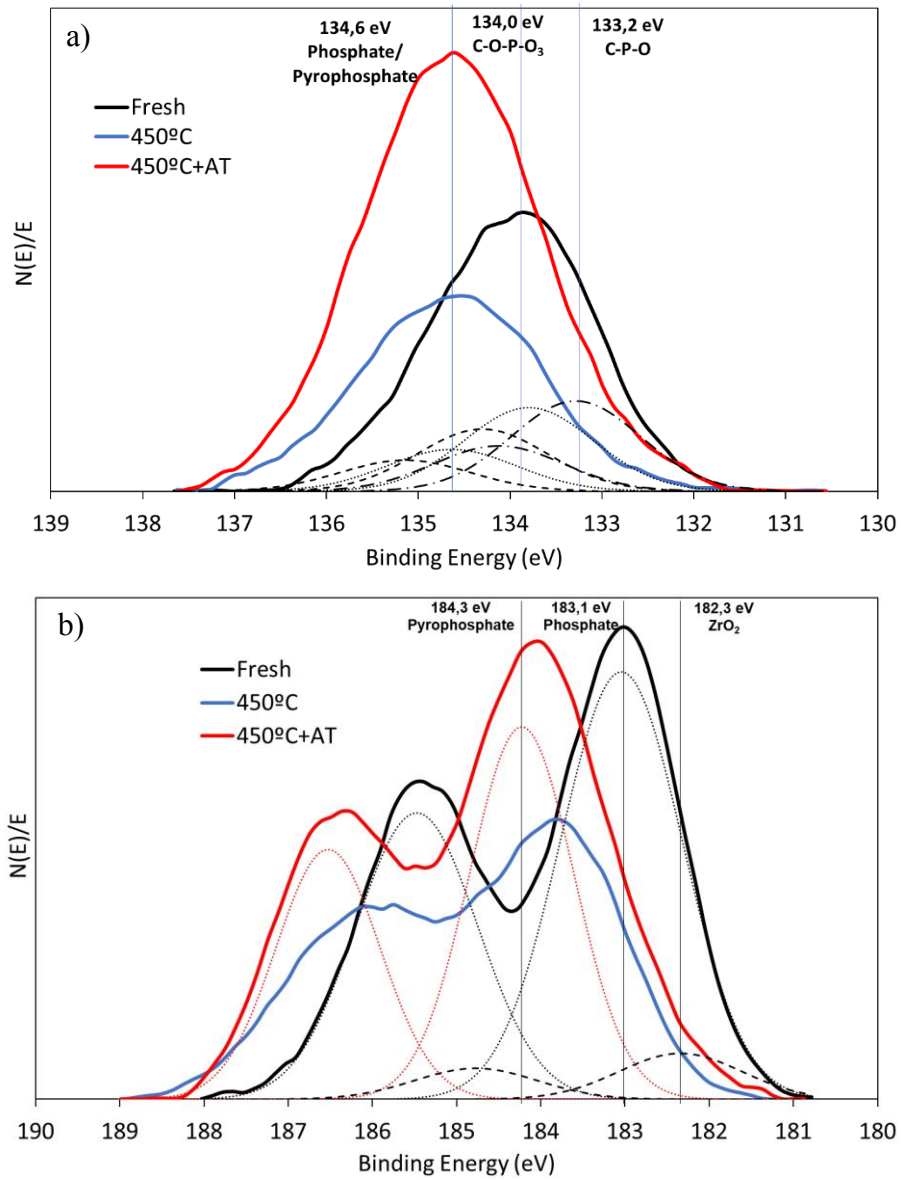

Figure 3. 14. XPS spectra of a) P_{2p} and b) Zr_{3d} of fresh and spent catalyst with different coke content, obtained at 450 ºC for 15 h, at a methanol partial pressure of 0.04 atm and a space time of 75 g_{cat}·s/mmol$_{CH_3OH}$ and after an air treatment at 350 ºC

3.2.4. Deactivated catalysts partial regeneration

By using the catalyst at different temperatures and TOS, catalysts with different degree of deactivation by coke deposition were obtained.

UNIVERSIDAD DE MÁLAGA

These deactivated catalysts were treated under air atmosphere with the goal of oxidizing the coke deposits and regenerating the catalyst. Thus, the catalysts deactivated at 450 ºC (partially) and at 550 ºC (almost totally) for 15 h (containing 9 and 22 % of deposited coke, respectively) were treated with an air flow of 150 cm^3/min at 350 ºC for 2 h (time enough to consume the deposited coke that could be oxidized under these operating conditions). Then, the oxidized catalysts were evaluated again under the same reaction conditions. A blank experiment was also performed (not shown) in which the fresh catalyst was exposed to the same air treatment prior to the dehydration reaction of methanol to DME at 450 ºC. No changes in conversion or selectivity were observed compared to the ones of the fresh catalyst without any treatment. In addition, the analysis of the mass loss during the air treatment of the catalyst obtained after reaction at 450 ºC for 15 h showed a very low catalyst lost, around 4.0%. This value was practically the same than the one observed for the fresh catalyst after the same oxidation treatment (blank experiment), suggesting that gasification of the formed coke was very low at this temperature.

The methanol conversions for the fresh catalyst at 450 ºC and 550 ºC and those of the corresponding deactivated samples followed by the oxidative air treatment are represented in Figure 3. 15. The methanol conversions for the air-treated deactivated catalyst at 450 ºC (second part of Figure 3. 15a) was almost restored (as can be compared to that of the fresh catalyst; first part of Figure 3. 15a) but only initially, decreasing very fast and reaching similar conversion values than those observed for the fresh catalyst after 15 h of reaction at very short TOS. In the case of the reaction temperature of 550 ºC, the conversion of methanol for the oxidized deactivated (almost totally) catalyst could not be totally restored, taking only 3 h to reach the same residual conversion than the one observed for the fresh catalyst after 15 h of reaction.

The catalyst support (not containing Zr but containing P surface groups) oxidized in air flow at the same conditions was also analyzed at these reaction temperatures to be compared to the fresh and to the deactivated catalysts followed by this oxidative treatment, (results included in Figure 3. 15a and b). In this sense, Rosas et al. reported the preferential oxidation of C-P-O groups to C-O-PO ones (to that of other surface groups) on phosphorus-containing activated carbon surfaces under air atmosphere and similar temperature conditions [28]. This C-O-PO surface groups presented also moderate-strength acidity, as reported by Valero-Romero et al. [33]. On the other hand, Palomo et al.[39,40] suggested that Zr-O-P sites, present in zirconium phosphate

UNIVERSIDAD DE MÁLAGA

surface species of carbon-based catalysts, were responsible for the activity of these catalysts for the dehydration of methanol to DME.

Figure 3. 15b show that oxidized catalyst support showed a very fast deactivation for methanol dehydration at both reaction temperatures, showing a conversion profile (in both cases) similar to the one observed for the oxidized deactivated catalyst reacting at 550 ºC. These results suggest the presence of, at least, two types of coke, probably of different nature, on the surface of this catalyst after reaction under these temperatures. A coke deposited on the C-O-P surface centers of the catalytic support that is oxidizable in air at 350ºC and another type of coke very much resistant to oxidation in air at this temperature treatment deposited on the Zr-O-P active sites of the surface groups of zirconium phosphate of the catalyst. In case of the air treated-spent catalyst (at 450 ºC), the methanol conversion profile can be considered as the sum of the residual conversion associated to zirconium phosphate sites and these new C-O-P surface groups, which means that air treatment only affects the first hours, and then, when the support lost its residual activity, conversion will have the same tendency than that observed for the catalyst without air treatment.

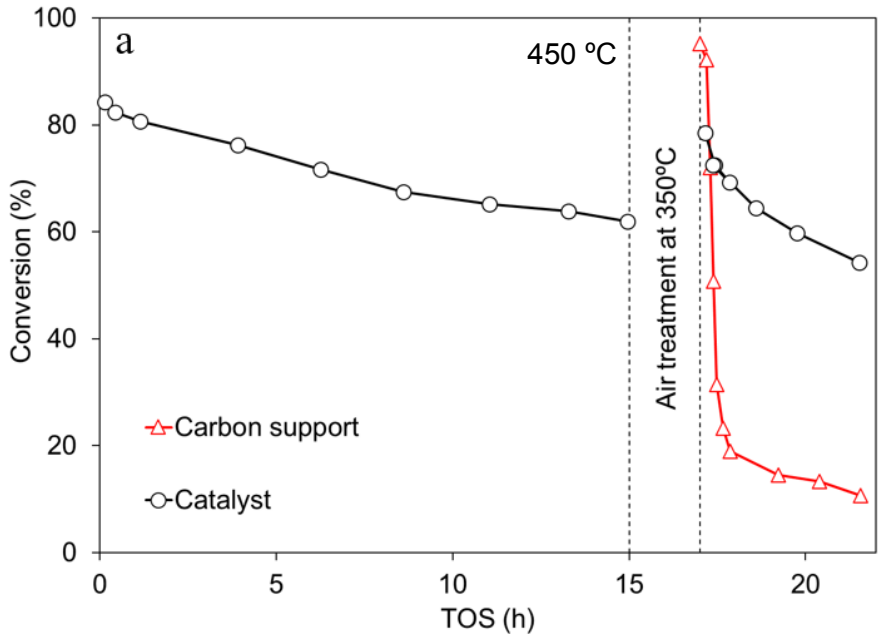

UNIVERSIDAD DE MÁLAGA

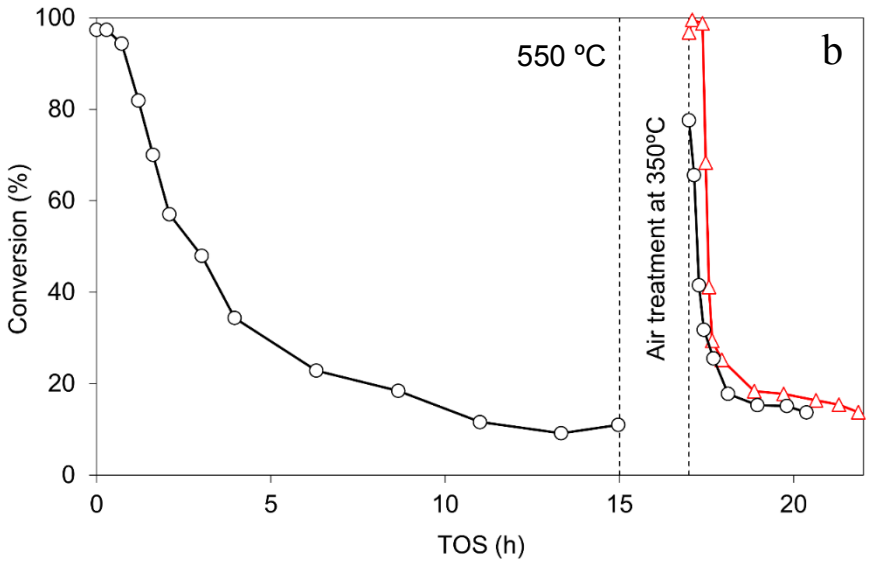

Figure 3. 15. Methanol conversion profiles a) 450 ºC and b) 550 ºC as a function of TOS of carbon support, fresh and air-oxidized spent catalyst, at a methanol partial pressure of 0.04 atm and a space time of 75 g_{cat}·s/$mmol_{CH_3OH}$

On the other hand, no differences were found regarding the selectivity of methanol towards the different products for the samples before and after reaction at 450 ºC and 550 ºC, except for a slightly increases of the selectivity to CH_4 observed for the catalyst deactivated at 550º C with subsequent treatment in air (higher than 60% at 550 ºC), which can be associated to the unsuccessful elimination of coke from zirconium phosphate groups and the appearance of new phosphorus-coke bonds, whose selectivity to methane is quite high.

With this goal, a new experiment was performed (Figure 3. 16) in which the fresh catalyst was used in reaction at 450 ºC, with a 4% methanol partial pressure and a space time of 75 g_{cat}·s/$mmol_{CH_3OH}$, at long TOS (70 h). The catalyst showed a relatively high stability at this temperature, with conversion values higher than 40% for 70 h of TOS, and very high selectivity to DME (values higher than 90% for the whole range of TOS evaluated) under the operation conditions studied.

For the sake of comparison, a similar experiment at the same operation conditions was carried out with the fresh catalyst (Figure 3. 16), but now the catalyst was submitted to a regeneration process by air treatment at

UNIVERSIDAD DE MÁLAGA

350 ºC for 2 h every 15 h of TOS. It was observed that the catalyst was partially regenerated, due to the oxidation of coke deposited on C-O-P active sites, transforming the inactive coke deposited (C-P) surface groups into active C-O-P groups. However, the regenerated catalyst follows the same trend than the fresh catalyst (without any regeneration air treatment during the long TOS experiment) after 5 h of reaction, in all the cases, due to the slow but irreversible deactivation of Zr-O-P active surface groups by deposition of more oxidation resistance coke that cannot be burn-out by the air treatment at 350 ºC.

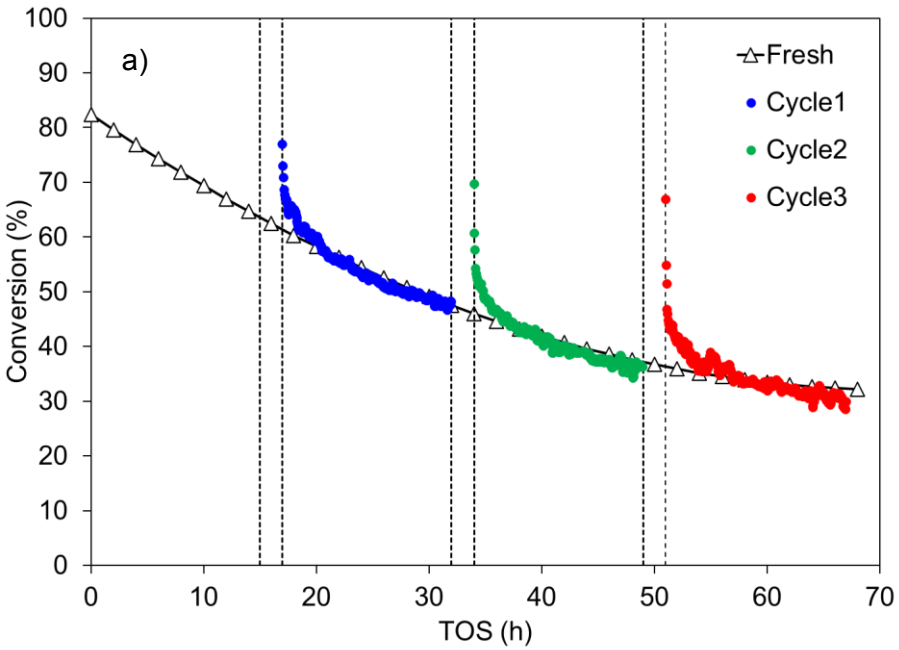

UNIVERSIDAD DE MÁLAGA

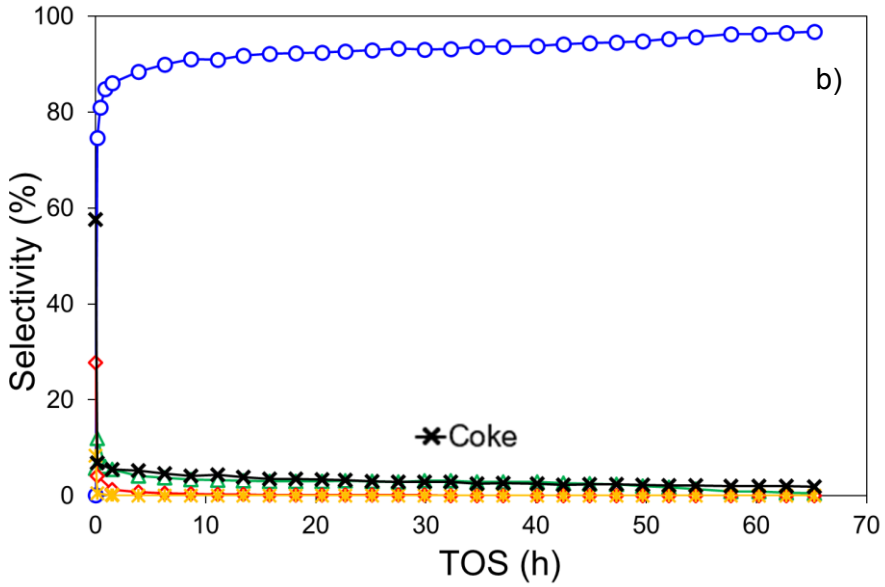

Figure 3. 16. a) Methanol conversion profile as a function of TOS, for long-term experiment and for consecutive cycles of reaction-air treatment; and b) selectivity for long-term experiment. Reaction conditions: 450 ºC at a methanol partial pressure of 0.04 atm and a space time of 75 g_{cat}·s/$mmol_{CH_3OH}$. Air treatment conditions: 350 ºC 2 h

All these results seem to point out that the negligible gasification of coke deposits on the Zr-O-P surface species of zirconium phosphate of the catalyst was the main cause for the poor catalyst regeneration. However, a change in crystallinity of zirconium phosphate due to the high reaction temperature reached could be another possible explanation to the poor regeneration of the catalyst. To assess the influence on activity of a hypothetical change in crystallinity, an experiment in which sample was subjected to a helium treatment at 550 ºC for 15 hours was performed. No change in conversion or selectivity was found between the fresh and the thermal treated sample, ruling out the possibility of a change in crystallinity as responsible for catalyst deactivation.

3.2.5. Air-treated sample characterization

N_2 adsorption-desorption isotherms of the partial and almost totally deactivated catalyst at 450 ºC and 550 ºC, respectively, followed by the

UNIVERSIDAD DE MÁLAGA

oxidative treatment in air at 350 ºC are presented in Figure 3. 17. Their corresponding textural parameters are gathered in

Table 3. 7. For the sake of comparison, N_2 adsorption-desorption isotherm of fresh catalyst after the oxidative treatment was also included in Figure 3. 17. The mild conditions of the oxidation treatment resulted into minimal differences between the isotherms of the fresh and the air treated catalyst. These results are in concordance with the low burn-off observed for the carbon support and the deactivated catalysts (<4%), associated to the high oxidation resistance of the carbon support due to the presence of phosphorus groups on the carbon surface [28].

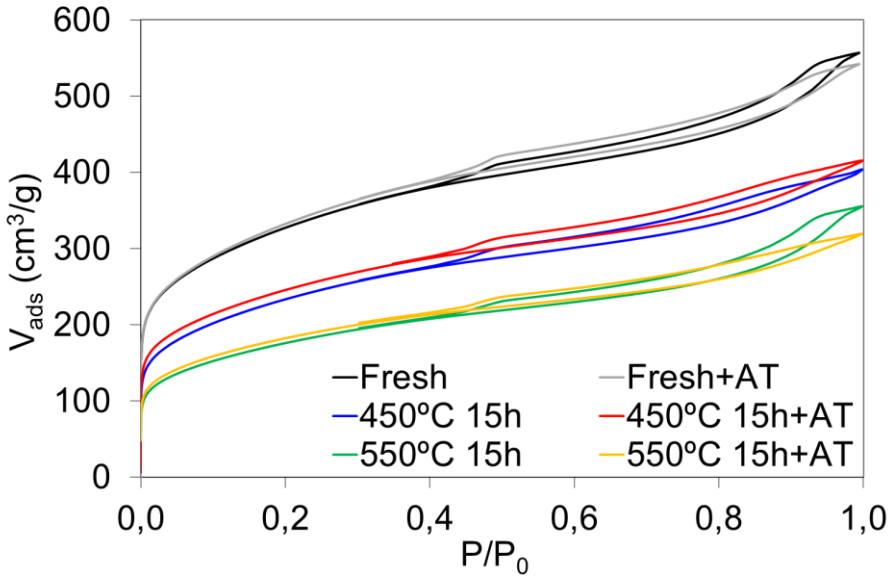

Figure 3. 17. N_2 adsorption-desorption isotherms at -196 ºC of fresh and spent catalyst at 450 ºC and 550 ºC for 15 h, at a methanol partial pressure of 0.04 atm and a space time of 75 g_{cat}·s/mmo$_{lCH_3OH}$, and the same samples after air treatment.

The isotherms of the catalyst used in reaction, before and after the oxidation treatment, presented fairly similarities, showing only a low increase in the N_2 adsorbed volume at low relative pressures. On the other hand, the results presented in

Table 3. 7 show that the oxidative treatment to the fresh catalyst (Fresh+AT) led to a slight decrease in the micropore volume measured with CO_2 and the mesopore volume, which also resulted in a reduction in the narrow micropore area and the external area, suggesting that the oxidation of C-P bonds of the catalyst carbon support to C-O-P ones

UNIVERSIDAD DE MÁLAGA

took place mainly on the narrow micropore and external surfaces of the catalyst support. Furthermore, the oxidative treatment of the partially deactivated catalyst after reacting at 450ºC produced a somewhat more significant increase (14%) in the volume of micropore measured with CO_2 and, to a lesser extent, in the volume of micropore measured with N_2, without any observed modification of the mesopore volume. The effect of the oxidative treatment on the catalyst obtained after reaction at 550º C was mainly focused on the increase of the narrow micropore, although to a lesser degree. These results indicate that the deposition of coke on the phosphorus species of the catalyst surface, the only type of coke that could be removed from the catalyst under the oxidative treatment conditions, took place to a greater extent on the narrow micropore surface of the catalyst. Nevertheless, none of the values of the different textural parameters obtained for the fresh catalyst could be completely restored by the oxidative treatment in air carried out on the partially and almost totally deactivated catalysts (after reaction at 450 and 550º C, respectively), which suggest that the zirconium phosphate surface species were very well dispersed on the whole catalyst surface. The fact that this reduction occurred to a greater extent for the narrow micropores suggests that some of the narrower micropores were blocked, probably due to diffusion limitations to these reaction temperatures.

Table 3. 7. Textural parameters values extracted from N_2 adsorption isotherm at -196 ºC and CO_2 adsorption isotherm at 0 ºC of fresh and deactivated catalyst after reaction at 450 ºC and 550 ºC for 15 h, and the corresponding samples after the oxidative air treatment (AT), at a methanol partial pressure of 0.04 atm and a space time of 75 g_{cat}·s/mmol$_{CH_3OH}$, and followed by air treatment at 350 ºC

	N_2 Isotherm					CO_2 Isotherm	
Sample	A_{BET} (m^2/g)	A_t (m^2/g)	V_{tot} (cm^3/g)	V_{mes} (cm^3/g)	V_t (cm^3/g)	A_{DR} (m^2/g)	V_{DR} (cm^3/g)
Fresh	1130	271	0.86	0.42	0.44	476	0.19
Fresh + AT	1153	262	0.84	0.38	0.46	446	0.18
450 ºC	816	221	0.62	0.32	0.30	290	0.12
450 ºC + AT	852	223	0.64	0.32	0.32	348	0.14
550 ºC	614	187	0.48	0.27	0.22	242	0.10
550 ºC + AT	634	189	0.49	0.27	0.22	273	0.11

TPD experiments were performed for the fresh and deactivated catalysts before and after the oxidizing treatment (Figure 3. 18). The CO TPD profile for the fresh catalyst showed three main peaks. A CO peak

UNIVERSIDAD DE MÁLAGA

evolving around 860 ºC, which was related to decomposition of C-O-P groups; a peak around 1000 ºC, which was attributed to the decomposition of C-O-Zr bonds present in zirconium phosphate groups linked to the carbon surface; and a CO evolution appearing around 1300-1350 ºC, which was correlated to zirconium-carbon/ZrO_2 species and/or to the ZrO_2 carboreduction, occurring at such high temperature [39].

The CO evolution at around 860 ºC, associated to decomposition of C-O-P groups, almost disappeared after reaction at 450 ºC and 550 ºC, which could be related to deactivation of these groups by coke deposition, thus reducing the C-O-P bonds to C-P ones [33]. After the air treatment (AT), only some of these groups were regenerated, suggesting that the complete recovering of the C-O-P groups was not possible, presumably of those groups that were on the surface of the narrower micropores that ended up blocked during the reaction. The CO peak associated to decomposition of zirconium-carbon/ZrO_2 species diminished after reaction and could not be recovered after the oxidative air treatment, showing that the coke layer deposited on these sites was strongly linked. As a consequence of the oxidative air treatment, new carbon-oxygen groups of lower thermal stability, like phenol groups, were produced on the surface of the carbon support, which decomposed as CO at temperatures around 700º C. Interestingly, the peak associated to decomposition of C-O-Zr bonds present in zirconium phosphate groups, which in the fresh catalyst was the largest one, remained practically the same for the profiles of deactivated catalysts and also for those of the samples that were treated in air at 350º C, which indicates the high stability of these bonds compared to that of the C-O-P ones and that these C-O-Zr surface species were not active for the dehydration of methanol to DME.

On the other hand, the CO_2 TPD profile of the fresh catalyst mainly indicated the presence of anhydrides groups (decomposed at around 470 ºC) and carboxylic acid groups (around 310 ºC). However, the intensity of these peaks was much lower than the intensity of CO-evolving groups, which means that their concentrations are considerably lower. Although the formation of the carboxylic groups could be interesting for this reaction, due to their acid character [47], they are not stable at temperatures higher than 350 ºC.

UNIVERSIDAD DE MÁLAGA

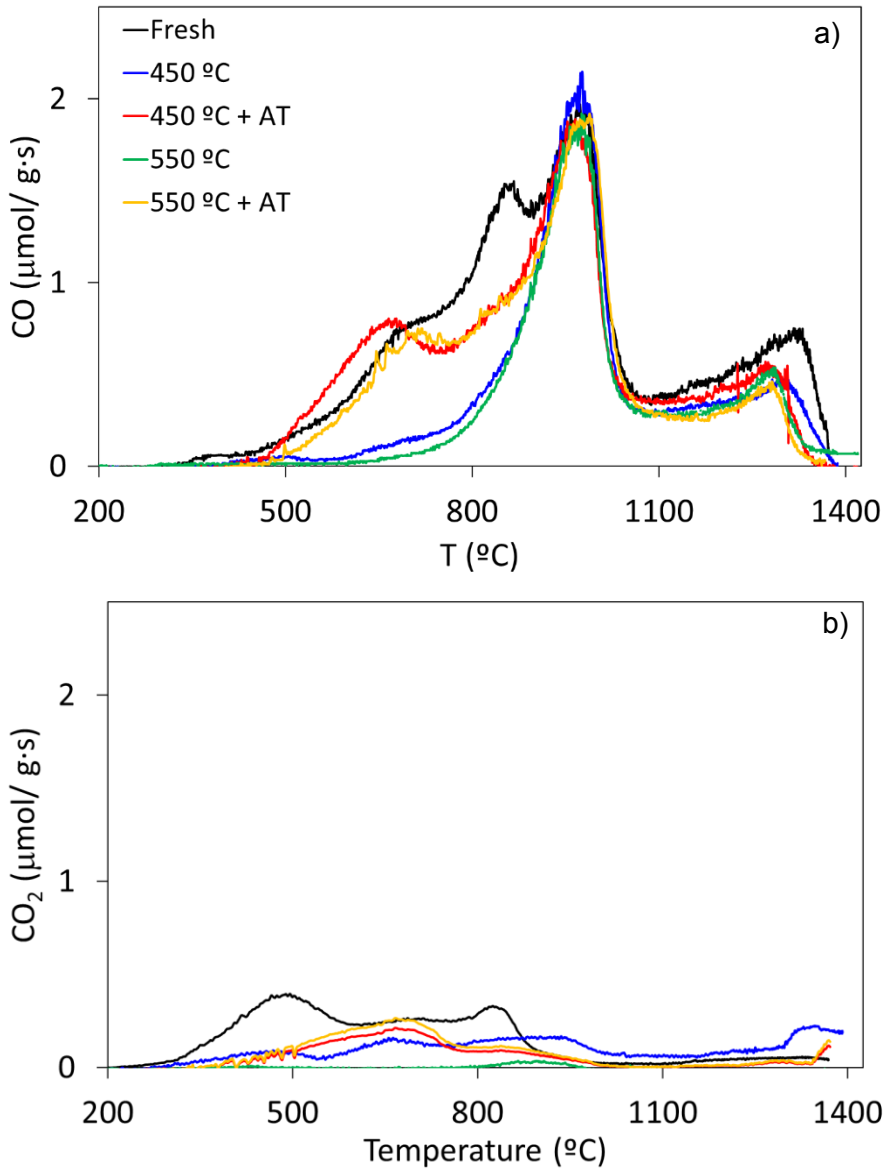

Figure 3. 18. Amount of CO and CO_2 evolved as a function of temperature during TPD of fresh, used samples and air-oxidized samples, at a methanol partial pressure of 0.04 atm and a space time of 75 g_{cat}·s/$mmol_{CH_3OH}$

UNIVERSIDAD DE MÁLAGA

Surface chemistry of deactivated catalysts was studied by XPS analyses (

Table 3. 8). After reaction at 450 ºC and 550 ºC, the catalyst surface oxygen, phosphorus and zirconium concentrations decreased, while carbon content increased due to coke deposition (as was mentioned in section 3.3.) Oxidative treatment of deactivated catalysts (450 ºC+AT and 550 ºC+AT) resulted in a decrease of the surface carbon concentration and an increase of phosphorus, zirconium and, especially, oxygen concentrations. It is important to highlight that after the air treatment at 350 ºC the observed surface phosphorus concentration was even higher than that on the fresh catalyst. Some gasification of the carbon support during the removal of deposited coke, as well as a migration of phosphorus and zirconium from the internal surface to the external one could be responsible for this increase.

Table 3. 8. Atomic surface concentration by XPS of fresh and spent catalyst after reaction at several temperatures and after air treatment at 350 ºC, at a methanol partial pressure of 0.04 atm and a space time of 75 g_{cat}·s/$mmol_{CH_3OH}$

Samples	C_{1s}	O_{1s}	P_{2p}	Zr_{3d}	P/Zr	C/P	C/Zr
Fresh	61.2	30.5	4.4	3.9	1.1	13.9	15.7
450 ºC	78.4	16.1	2.8	2.5	1.1	27.8	31.0
450 ºC + AT	49.8	37.5	8.3	4.4	1.9	6.0	11.4
550 ºC	86.0	10.5	2.3	1.2	2.0	37.1	72.9
550 ºC + AT	57.4	30.9	8.1	3.5	2.3	7.1	16.2

Further information can be obtained from individual XPS spectra. Figure 3. 14 shows also the XPS spectra of Zr_{3d} and P_{2p} of the deactivated catalysts after the air treatment. P_{2p} spectrum after the air treatment (450 ºC+AT) showed an increase of the bands associated to zirconium phosphate, as well as, to C-O-P groups, probably due to the migration of these compounds to the external surface and to the oxidation of C-P-O groups into C-O-PO ones, in agreement with the results obtained from TPD analysis. Furthermore, a small shift of the bands corresponding to zirconium phosphate surface groups can be observed, which could be related to a higher polarization of the environment [57]. Zr_{3d} spectrum of the deactivated catalyst (450 ºC+AT) showed a maximum of the peak appearing at 184.5 eV, which corresponds to the presence of Zr(IV) bound to an electroactive species such as phosphorus in form of pyrophosphates group, with a higher polarization of the environment

UNIVERSIDAD DE MÁLAGA

(Figure 3. 14b) [57]. These results seem to indicate that the –OH group of zirconium phosphate, which was substituted by organic groups (coke), could not be recovered after the air treatment.

With the goal of confirming this hypothesis, ^{31}P-NMR spectra of the carbon support, the fresh catalyst, the deactivated catalysts at 450 ºC and 550 ºC and one of the air oxidized samples (450 ºC+AT) are presented in Figure 3. 19. Two main peaks can be seen in the spectrum of the carbon support, as well as in that of the fresh catalyst. First, a broad band between 20 ppm and -10 ppm was observed, which could be associated to the sum of several species with similar intensities, such as phosphonates, around 20 ppm, and P-esters, around 3 ppm [25,58]. In addition, a narrow peak highlighted at -4 ppm appeared, which could be associated to zirconium phosphate species or some P-esters, like $Zr(HPO_4)_2 \cdot H_2O$ [59] or $(C\text{-}O)_x$-P-OH [60]. The spectrum significantly changed after reaction at 450 ºC and 550 ºC and the broad peak between 20 and -10 ppm, associated to phosphonates and P-esters, almost disappeared, as a consequence of coke deposition. These results were in line with the reduction of C-O-P groups after reaction at these temperatures deduced from the TPD analysis and in agreement with the findings reported by Valero-Romero et al. [33]

For the catalyst used at a reaction temperature of 450 ºC, the sharp peak at -4 ppm was considerably reduced and it was almost negligible for the catalyst after reaction at 550 ºC. It should be noted that the catalyst after reaction at 450 ºC maintained some activity for methanol dehydration reaction. However, after reaction at 550 ºC, the catalyst was practically exhausted, suggesting that zirconium phosphate species was the main responsible for the high activity of this catalyst. Thus, the peak at -4 ppm observed for the partially deactivated catalyst after reaction at 450º C could be ascribed to zirconium phosphate species that still remained on the catalyst surface after 15 h of reaction. Nevertheless, the increase observed for this peak for the sample obtained after the air treatment carried out over the catalyst partially deactivated at 450 ºC was probably due to the presence of C-O-PO surface groups on the sample, appeared as a consequence of oxidation of C-P-O groups to C-O-PO ones, as the results of TPD also indicated, and could explain the slight increase observed in conversion of that oxidized sample that was, however, deactivated very fast. This effect was already observed in P_{2p} XPS spectrum, in which the contribution of C-O-PO groups increased after air treatment of the deactivated catalyst at 450 ºC.

On the other hand, the spectra for the samples exposed to reaction at 450 and 550º C and to the subsequent air treatment showed a peak

UNIVERSIDAD DE MÁLAGA

around -28 ppm, which can be associated with non-hydrogenated phosphate (pyrophosphate) [61,62] or species like P_2O_5 [63]. These results seem to indicate that zirconium phosphates surface groups were converted into zirconium pyrophosphates ones under these operation conditions. The formation of zirconium pyrophosphates groups can be related to the residual conversion of these samples for long TOS.

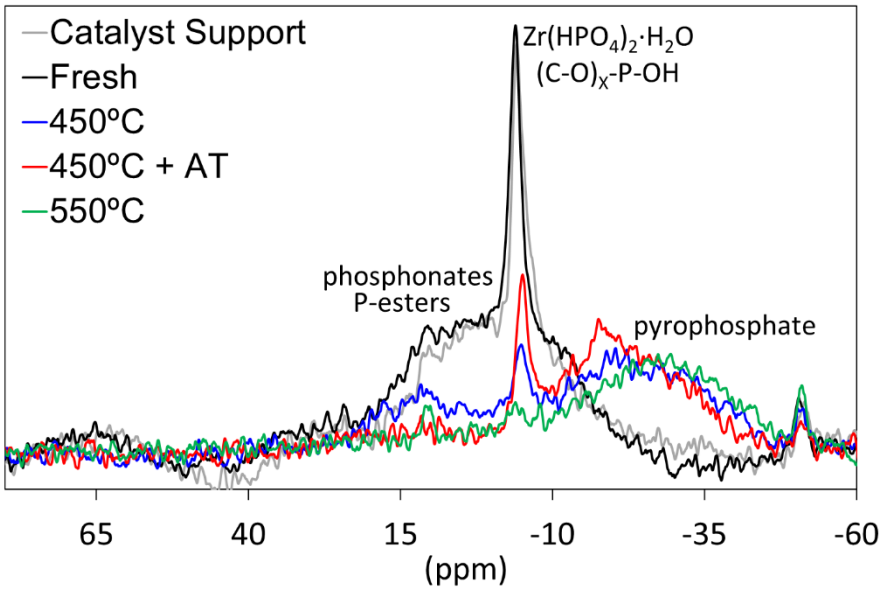

Figure 3. 19. NMR ^{31}P spectra for carbon support, fresh, partially and almost totally deactivated catalyst at 450ºC and 550 ºC, respectively, and oxidized sample after reaction at 450 ºC, at a methanol partial pressure of 0.04 atm and a space time of 75 g_{cat}·s/mmol$_{CH_3OH}$

In order to confirm the above statement, 2D HETCOR ^{31}P-^{1}H NMR was also performed in the fresh and partially deactivated catalyst at 450 ºC and results are shown in Figure 3. 20. A clear connection between the peak of phosphorus at -4 ppm and hydrogen was observed for the fresh catalyst, which is associated to phosphate groups, containing -OH groups. Nevertheless, after reaction at 550º C, when the catalyst presented only a residual activity, this interaction between phosphorus and hydrogen cannot be observed, suggesting the consumption of these –OH bonds.

UNIVERSIDAD DE MÁLAGA

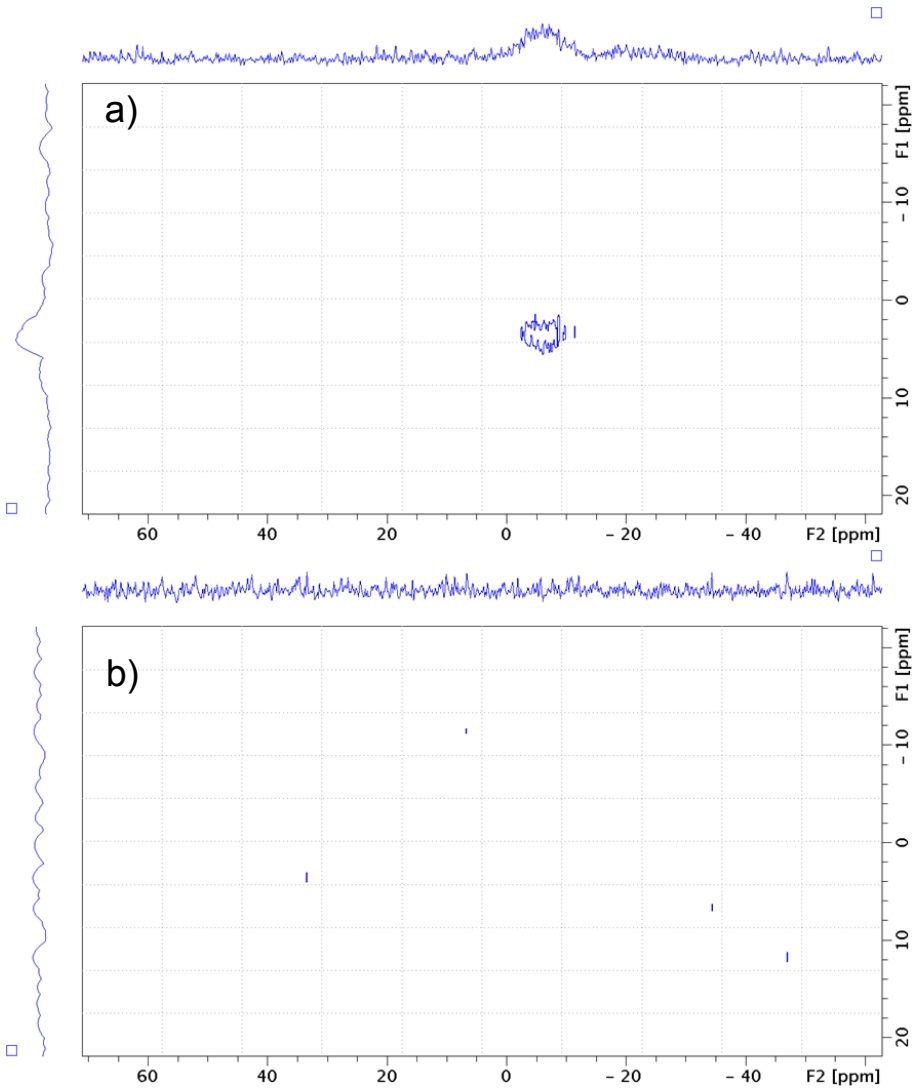

Figure 3. 20. 2D-NMR ^{31}P-^{1}H HETCOR of a) fresh and b) spent catalyst after reaction at 550 ºC 15 h, a methanol partial pressure of 0.04 atm and a space time of 75 g_{cat}·s/mmol$_{CH_3OH}$

3.2.6. Reaction scheme

In a previous paper, a modified Langmuir-Hinshelwood mechanism accounting for two molecules of methanol subsequently on one active site with different adsorption enthalpies and competitive adsorption of water was proposed for MTD reaction on a similar catalyst at low temperatures (250-350º C) and low methanol conversions (<50%) [40].

UNIVERSIDAD DE MÁLAGA

This reaction route considered that Zr-O-P active sites of zirconium phosphate surface groups may reversibly adsorb a methanol molecule in a first step, yielding by cleavage of the site a methoxy group bonded to phosphorus and a vicinal -OH bonded to zirconium. In the next step, a second molecule of methanol is reversible adsorbed on the generated Zr-OH, reacting with the methoxy group to produce reversibly DME and adsorbed water in form of two hydroxyl groups (Zr-OH and P-OH) in a further stage (step 3). In the last step, the hydroxyl groups react to produce water, regenerating, this way, the initial active site.

In this work, based on the experimental catalytic results obtained at higher temperature and the characterization of the catalysts used in reaction, a modified reaction pathway has been proposed, which explains the coke production and deactivation of the catalyst. The higher DME production observed at reaction temperatures above 400° C could lead to a greater stability of the adsorbed DME species, favouring now an irreversible process (see Scheme 1) leading to the formation of methane and adsorbed formaldehyde on the active center. The latter is considered an intermediate product in the production of H_2 and CO and in the formation of coke on the active centers, with water vapor releasing. This would explain the appearance of small amounts of H_2 and CO in the reaction products and the presence of coke and excess of water observed with increasing reaction temperature. Once the catalyst was partially deactivated, the concentration of DME in the gas phase decreased, increasing that of methanol. In this case, the production of coke could also occur through the formation of methoxy species on the active centers of the catalyst (Zr-O-P and/or Zr-OH and P-OH), preventing their regeneration in the reaction.

Ruiz-Rosas et. al [64] reported that Zr-OH species were active for methanol decomposition above 450ºC, although these species were deactivated by coke deposition. Thus, hydroxyl bonded to zirconium can irreversibly interact with methanol, releasing water and letting a methoxy group bonded to zirconium. In this sense, XPS results also pointed out that zirconium atomic concentration was firstly decreased during the reaction, suggesting that the formation of methoxy groups and the consequent growth of coke could be responsible for this decrease. On the other hand, the rapid deactivation of P-OH and C-O-P groups at temperatures even lower than those used in the present study has already been reported in the literature[33]. Cheng et al. also indicated that P-methoxy species ($P\text{-}CH_3$) formed by reaction of methanol on zirconium phosphate catalysts can react with a second methanol molecule through a six-member ring electron transfer process to

UNIVERSIDAD DE MÁLAGA

irreversible produce methane and formaldehyde. These findings also support the reaction scheme proposed in this work (see Scheme 3.1) that accounts for the gas product distribution and the production of coke that generates the deactivation of the catalysts.

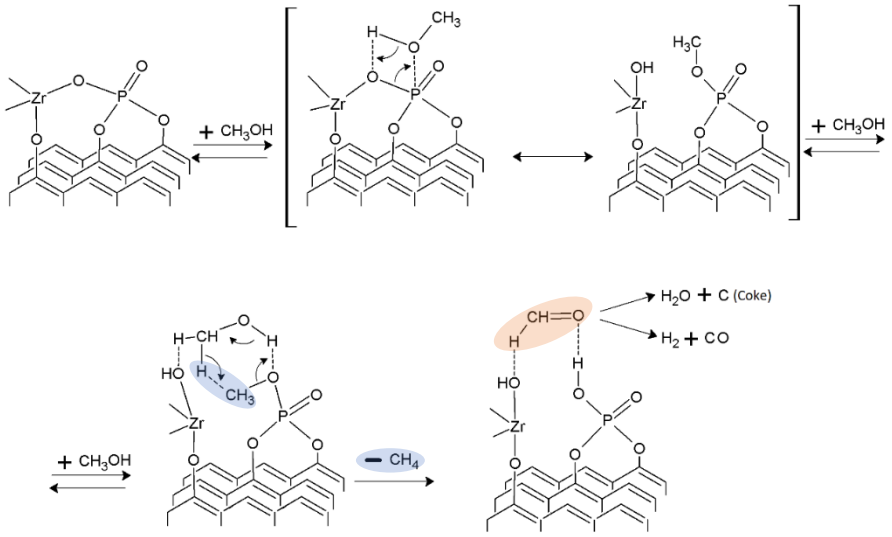

Scheme 3. 1 Reaction pathway for the deactivation of the catalyst in the MTD process.

3.2.7. Kinetics of coke formation

Finally, in order to predict the coke formation experimental results, a kinetic model initially proposed by Froment, Bischoff and De Wilde was used [65]. With this goal, coke content of the catalyst at different reaction temperatures and TOS was quantified. The kinetic model takes into account a deactivation function, which depends on coke content.

$$\frac{dC_c}{dt} = r_C^0 \cdot \Phi_C \tag{3.20}$$

$$\Phi_C = (1 - \alpha \cdot C_C)^2 \tag{3.21}$$

where C_c is the percentage of coke deposited, t the time on stream, r_C^0 is the initial rate of coke production, Φ_C is the deactivation function and α is the deactivation factor. Assuming differential conditions for coke production, the integrated equation takes the form:

$$C_C = \frac{1}{\alpha}\left[1 - \frac{1}{1+\alpha \cdot r_C^0 \cdot t}\right] \tag{3.22}$$

UNIVERSIDAD DE MÁLAGA

where r_C^0 and α are the fitting parameters. It should be pointed that α is considered to be constant in all the experiments [65]. The fitting parameters were calculated by using a Nelder-Mead simplex algorithm, which minimizes the objective function (Eq. 3.23), defined as the sum of quadratic differences between experimental coke content and the calculated values:

$$OF = \sum_{i=1}^{n_T} \left(C_{i,exp} - C_{i,cal}\right)^2 \quad (3.23)$$

where n_T is the total number of experiments and $C_{i,exp}$ and $C_{i,cal}$, the experimental and calculated coke content of the i^{th} experiment, respectively.

The initial rate of coke formation, r_C^0, obtained at different temperatures, can be defined as a simple n-order power law equation and used to obtain the activation energy of the coke formation:

$$r_C^0 = k \cdot P_{MeOH}^n \quad (3.24)$$

where $P_{CH_3OH}^n$ is the fed partial pressure of methanol and k is a kinetic constant that follows Arrhenius law:

$$r_C^0 = k_0 \cdot e^{-\frac{E_a}{R \cdot T}} \cdot P_{MeOH}^n = k_0' \cdot e^{-\frac{E_a}{R \cdot T}} \quad (3.25)$$

being k_0 the preexponential factor, k'_0 the apparent preexponential factor, E_a the activation energy, R the ideal gas constant and T the reaction temperature. In these experiments, partial pressure of methanol was maintained at 0.04 atm.

The amount of coke deposited on the catalyst as a function of TOS for different reaction temperatures is represented in Figure 3. 21. The content of coke deposited on the catalyst and the rate of coke formation increased with TOS and reaction temperature. However, a somewhat saturation level could be observed in the final content of coke deposited on the catalyst with increasing temperature, with a value close to 25%. This behavior could be related to the greater reduction of the narrow microporosity observed with the increase in the reaction rate, probably leaving part of the narrow micropores closed during the process at the highest reaction temperatures. Kinetic parameters are summarized in Table 3. 9. The activation energy value obtained for coke formation was 124 kJ/mol, slightly higher than the activation energies reported for other catalysts at similar experimental conditions [45,66,67]. Experimental and calculated coke contents are represented in Figure 3. 21, showing a good agreement between both values.

UNIVERSIDAD DE MÁLAGA

Table 3. 9. Coke formation kinetic parameters.

Kinetic parameter	Value
Deactivation constant, α	0.038
Coking activation energy, E_a (kJ/mol)	124
Apparent pre-exponential factor, k'_0	$9.5 \cdot 10^8$
R^2	0.97

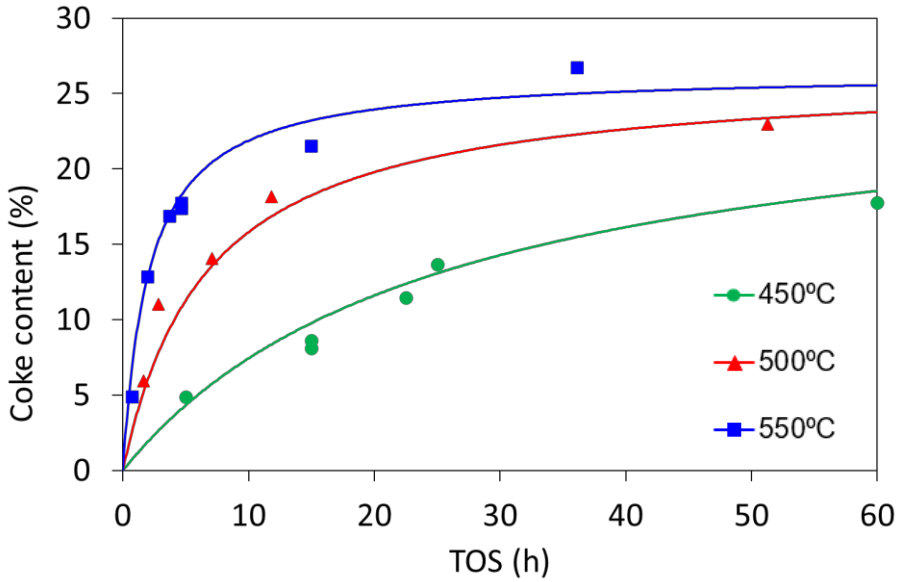

Figure 3. 21. Experimental (points) and calculated (line) coke contents as a function of TOS at different reaction temperatures, at a methanol partial pressure of 0.04 atm and a space time of 75 $g_{cat} \cdot s/mmol_{CH_3OH}$.

3.2.8. Conclusions

Dehydration of methanol to produce dimethyl ether (DME) was studied at different temperatures (300-600º C) on a biomass-derived phosphorus-containing carbon impregnated with a zirconium salt. Highly thermally stable zirconium phosphate surface groups could be obtained on the final catalyst, which were responsible for the high stability and selectivity to DME of the catalyst at temperatures lower than 450º C.

UNIVERSIDAD DE MÁLAGA

However, harder operation conditions, closer to those of the industrial process, were evaluated to analyze the changes of the catalyst surface properties with reaction temperature and the possible causes of deactivation. Thus, high methanol conversion and selectivity to DME were also observed for this biomass-derived catalyst in the temperature range of 450 to 600 ºC, although deactivation was observed. Coke deposition was responsible for a decrease in microporosity and surface concentration of zirconium and phosphorus of the catalyst. TPD, ^{31}P MAS-NMR and XPS results suggest that the Zr-O-P groups from zirconium phosphate species were responsible for the long-term stability of the catalyst and that the C-O-P type active sites deactivated very fast. However, coke deposition on Zr-O-P type active sites during reaction caused a slow and irreversible deactivation, given that removal of the deposited coke from these active sites by gasification in air at 350 ºC proved to be very difficult. Nevertheless, a different nature of deposited coke took place on the C-O-P type active sites, which was easily eliminated by the oxidative treatment in air. A reaction scheme that accounted for the gas product distribution and the production of coke that generated the deactivation of the catalysts was postulated. A kinetic model for coke formation as a function of time on stream that successfully represents the experimental results was also proposed, which yielded a value for the activation energy for the production of coke of 124 kJ/mol.

References

1. UN *Transforming our world: the 2030 Agenda for Sustainable Development*; 2015;

2. Rodríguez, E.; Palos, R.; Gutiérrez, A.; Trueba, D.; Arandes, J.M.; Bilbao, J. Towards waste refinery: Co-feeding HDPE pyrolysis waxes with VGO into the catalytic cracking unit. *Energy Convers. Manag.* **2020**, *207*, 112554, doi:10.1016/j.enconman.2020.112554.

3. Palos, R.; Gutiérrez, A.; Vela, F.J.; Olazar, M.; Arandes, J.M.; Bilbao, J. Waste Refinery: The Valorization of Waste Plastics and End-of-Life Tires in Refinery Units. A Review. *Energy & Fuels* **2021**, *35*, 3529–3557, doi:10.1021/acs.energyfuels.0c03918.

4. De Bhowmick, G.; Sarmah, A.K.; Sen, R. Lignocellulosic biorefinery as a model for sustainable development of biofuels and value added products. *Bioresour. Technol.* **2018**, *247*, 1144–1154, doi:10.1016/j.biortech.2017.09.163.

UNIVERSIDAD DE MÁLAGA

5. FitzPatrick, M.; Champagne, P.; Cunningham, M.F.; Whitney, R.A. A biorefinery processing perspective: Treatment of lignocellulosic materials for the production of value-added products. *Bioresour. Technol.* **2010**, *101*, 8915–8922, doi:10.1016/j.biortech.2010.06.125.

6. Parajuli, R.; Dalgaard, T.; Jørgensen, U.; Adamsen, A.P.S.; Knudsen, M.T.; Birkved, M.; Gylling, M.; Schjørring, J.K. Biorefining in the prevailing energy and materials crisis: A review of sustainable pathways for biorefinery value chains and sustainability assessment methodologies. *Renew. Sustain. Energy Rev.* **2015**, *43*, 244–263, doi:10.1016/j.rser.2014.11.041.

7. Lopez, G.; Artetxe, M.; Amutio, M.; Alvarez, J.; Bilbao, J.; Olazar, M. Recent advances in the gasification of waste plastics. A critical overview. *Renew. Sustain. Energy Rev.* **2018**, *82*, 576–596, doi:10.1016/j.rser.2017.09.032.

8. Lee, U.; Chung, J.N.; Ingley, H.A. High-temperature steam gasification of municipal solid waste, rubber, plastic and wood. *Energy & Fuels* **2014**, *28*, 4573–4587, doi:10.1021/ef500713j.

9. Brachi, P.; Chirone, R.; Miccio, F.; Miccio, M.; Picarelli, A.; Ruoppolo, G. Fluidized bed co-gasification of biomass and polymeric wastes for a flexible end-use of the syngas: Focus on bio-methanol. *Fuel* **2014**, *128*, 88–98, doi:10.1016/j.fuel.2014.02.070.

10. Belgiorno, V.; De Feo, G.; Della Rocca, C.; Napoli, R.M.A. Energy from gasification of solid wastes. *Waste Manag.* **2003**, *23*, 1–15, doi:10.1016/S0956-053X(02)00149-6.

11. Aguayo, A.T.; Ereña, J.; Sierra, I.; Olazar, M.; Bilbao, J. Deactivation and regeneration of hybrid catalysts in the single-step synthesis of dimethyl ether from syngas and CO2. *Catal. Today* **2005**, *106*, 265–270, doi:10.1016/j.cattod.2005.07.144.

12. Sierra, I.; Ereña, J.; Aguayo, A.T.; Arandes, J.M.; Bilbao, J. Regeneration of CuO-ZnO-Al2O3/γ-Al2O3 catalyst in the direct synthesis of dimethyl ether. *Appl. Catal. B Environ.* **2010**, *94*, 108–116, doi:10.1016/j.apcatb.2009.10.026.

13. Sierra, I.; Ereña, J.; Aguayo, A.T.; Arandes, J.M.; Olazar, M.; Bilbao, J. Co-feeding water to attenuate deactivation of the catalyst metallic function (CuO-ZnO-Al2O3) by coke in the direct synthesis of dimethyl ether. *Appl. Catal. B Environ.* **2011**, *106*,

UNIVERSIDAD DE MÁLAGA

167–173, doi:10.1016/j.apcatb.2011.05.021.

14. Ereña, J.; Garoña, R.; Arandes, J.M.; Aguayo, A.T.; Bilbao, J. Effect of operating conditions on the synthesis of dimethyl ether over a CuO-ZnO-Al2O3/NaHZSM-5 bifunctional catalyst. *Catal. Today* **2005**, *107–108*, 467–473, doi:10.1016/j.cattod.2005.07.116.

15. Ateka, A.; Sierra, I.; Ereña, J.; Bilbao, J.; Aguayo, A.T. Performance of CuO–ZnO–ZrO2 and CuO–ZnO–MnO as metallic functions and SAPO-18 as acid function of the catalyst for the synthesis of DME co-feeding CO2. *Fuel Process. Technol.* **2016**, *152*, 34–45, doi:10.1016/j.fuproc.2016.05.041.

16. Sánchez-Contador, M.; Ateka, A.; Aguayo, A.T.; Bilbao, J. Direct synthesis of dimethyl ether from CO and CO2 over a core-shell structured CuO-ZnO-ZrO2@SAPO-11 catalyst. *Fuel Process. Technol.* **2018**, *179*, 258–268, doi:10.1016/j.fuproc.2018.07.009.

17. Sierra, I.; Ereña, J.; Aguayo, A.T.; Ateka, A.; Bilbao, J. Kinetic Modelling for the Dehydration of Methanol to Dimethyl Ether over γ-Al2O3.; 2013; Vol. 32.

18. Gayubo, A.G.; Vicente, J.; Ereña, J.; Oar-Arteta, L.; Azkoiti, M.J.; Olazar, M.; Bilbao, J. Causes of deactivation of bifunctional catalysts made up of CuO-ZnO-Al 2O3 and desilicated HZSM-5 zeolite in DME steam reforming. *Appl. Catal. A Gen.* **2014**, *483*, 76–84, doi:10.1016/j.apcata.2014.06.031.

19. Cordero-Lanzac, T.; Hita, I.; García-Mateos, F.J.; Castaño, P.; Rodríguez-Mirasol, J.; Cordero, T.; Bilbao, J. Adaptable kinetic model for the transient and pseudo-steady states in the hydrodeoxygenation of raw bio-oil. *Chem. Eng. J.* **2020**, *400*, 124679, doi:10.1016/j.cej.2020.124679.

20. Cordero-Lanzac, T.; Aguayo, A.T.; Gayubo, A.G.; Castaño, P.; Bilbao, J. A comprehensive approach for designing different configurations of isothermal reactors with fast catalyst deactivation. *Chem. Eng. J.* **2020**, *379*, 122260, doi:10.1016/j.cej.2019.122260.

21. Cordero-Lanzac, T.; Aguayo, A.T.; Gayubo, A.G.; Castaño, P.; Bilbao, J. Simultaneous modeling of the kinetics for n-pentane cracking and the deactivation of a HZSM-5 based catalyst. *Chem. Eng. J.* **2018**, *331*, 818–830, doi:10.1016/j.cej.2017.08.106.

UNIVERSIDAD DE MÁLAGA

22. De, S.; Balu, A.M.; Van Der Waal, J.C.; Luque, R. Biomass-derived porous carbon materials: Synthesis and catalytic applications. *ChemCatChem* **2015**, *7*, 1608–1629, doi:10.1002/cctc.201500081.

23. Lee, J.; Kim, K.H.; Kwon, E.E. Biochar as a Catalyst. *Renew. Sustain. Energy Rev.* **2017**, *77*, 70–79, doi:10.1016/j.rser.2017.04.002.

24. Lam, E.; Luong, J.H.T. Carbon materials as catalyst supports and catalysts in the transformation of biomass to fuels and chemicals. *ACS Catal.* **2014**, *4*, 3393–3410, doi:10.1021/cs5008393.

25. Puziy, A.M.; Poddubnaya, O.I.; Socha, R.P.; Gurgul, J.; Wisniewski, M. XPS and NMR studies of phosphoric acid activated carbons. *Carbon N. Y.* **2008**, *46*, 2113–2123, doi:10.1016/j.carbon.2008.09.010.

26. Molina-Sabio, M.; Rodríguez-Reinoso, F.; Caturla, F.; Sellés, M.J. Porosity in granular carbons activated with phosphoric acid. *Carbon N. Y.* **1995**, *33*, 1105–1113, doi:10.1016/0008-6223(95)00059-M.

27. Bedia, J.; Rosas, J.M.; Márquez, J.; Rodríguez-Mirasol, J.; Cordero, T. Preparation and characterization of carbon based acid catalysts for the dehydration of 2-propanol. *Carbon N. Y.* **2009**, *47*, 286–294, doi:10.1016/j.carbon.2008.10.008.

28. Rosas, J.M.; Ruiz-Rosas, R.; Rodríguez-Mirasol, J.; Cordero, T. Kinetic study of the oxidation resistance of phosphorus-containing activated carbons. *Carbon N. Y.* **2012**, *50*, 1523–1537, doi:10.1016/j.carbon.2011.11.030.

29. Rosas, J.M.; Bedia, J.; Rodríguez-Mirasol, J.; Cordero, T. HEMP-derived activated carbon fibers by chemical activation with phosphoric acid. *Fuel* **2009**, *88*, 19–26, doi:10.1016/j.fuel.2008.08.004.

30. Bedia, J.; Ruiz-Rosas, R.; Rodríguez-Mirasol, J.; Cordero, T. A kinetic study of 2-propanol dehydration on carbon acid catalysts. *J. Catal.* **2010**, *271*, 33–42, doi:10.1016/j.jcat.2010.01.023.

31. Bedia, J.; Barrionuevo, R.; Rodríguez-Mirasol, J.; Cordero, T. Ethanol dehydration to ethylene on acid carbon catalysts. *Appl. Catal. B, Environ.* **2011**, *103*, 302–310, doi:10.1016/j.apcatb.2011.01.032.

UNIVERSIDAD DE MÁLAGA

32. Soto, J.; Rosas, J.M.; Otero, J.C.; Rodríguez-Mirasol, J.; Cordero, T. Reaction Mechanisms of 2-Butanol Dehydration over a Phosphorus-Containing Activated Carbon Acid Catalyst. *J. Phys. Chem. C* **2018**, *122*, 16772–16778, doi:10.1021/acs.jpcc.8b03700.

33. Valero-Romero, M.J.; Calvo-Muñoz, E.M.; Ruiz-Rosas, R.; Rodríguez-Mirasol, J.; Cordero, T. Phosphorus-Containing Mesoporous Carbon Acid Catalyst for Methanol Dehydration to Dimethyl Ether. *Ind. Eng. Chem. Res.* **2019**, *58*, 4042–4053, doi:10.1021/acs.iecr.8b05897.

34. Nozart, F.; Itoh, T.; Ueda, S. Catalytic Activity of Zirconium Phosphate for Dehydration of 2－Propanol. *Nippon Kagaku Kaishi* **1973**, *1973*, 674–678.

35. Johnstone, R.A.W.; Liu, J.; Whittaker, D. Mechanism of cyclohexanol dehydration catalysed by zirconium phosphate. *J. Chem. Soc., Perkin Trans. 2* **1998**, *0*, 1287–1288.

36. Cheng, L.; Guo, X.; Song, C.; Yu, G.; Cui, Y.; Xue, N.; Peng, L.; Guo, X.; Ding, W. High performance mesoporous zirconium phosphate for dehydration of xylose to furfural in aqueous-phase. *RSC Adv.* **2013**, *3*, 23228–23235, doi:10.1039/c3ra43413c.

37. Ni, W.; Li, D.; Zhao, X.; Ma, W.; Kong, K.; Gu, Q.; Chen, M.; Hou, Z. Catalytic dehydration of sorbitol and fructose by acid-modified zirconium phosphate. *Catal. Today* **2019**, *319*, 66–75, doi:10.1016/j.cattod.2018.03.034.

38. Cheng, S.; Peng, G.Z.; Clearfield, A. Decomposition of alcohols over zirconium and titanium phosphates. *Ind. Eng. Chem. Prod. Res. Dev.* **1984**, *23*, 219–225, doi:10.1021/i300014a008.

39. Palomo, J.; Rodríguez-Mirasol, J.; Cordero, T. Methanol Dehydration to Dimethyl Ether on Zr-Loaded P-Containing Mesoporous Activated Carbon Catalysts. *Materials (Basel).* **2019**, *12*, 2204, doi:10.3390/ma12132204.

40. Palomo, J.; Rodríguez-Cano, M.A.; Rodríguez-Mirasol, J.; Cordero, T. On the kinetics of methanol dehydration to dimethyl ether on Zr-loaded P-containing mesoporous activated carbon catalyst. *Chem. Eng. J.* **2019**, *378*, 122198, doi:10.1016/j.cej.2019.122198.

41. Alharbi, W.; Kozhevnikova, E.F.; Kozhevnikov, I. V. Dehydration

UNIVERSIDAD DE MÁLAGA

of Methanol to Dimethyl Ether over Heteropoly Acid Catalysts: The Relationship between Reaction Rate and Catalyst Acid Strength. *ACS Catal.* **2015**, *5*, 7186–7193, doi:10.1021/acscatal.5b01911.

42. Janssens, T.V.W. A new approach to the modeling of deactivation in the conversion of methanol on zeolite catalysts. *J. Catal.* **2009**, *264*, 130–137, doi:10.1016/j.jcat.2009.03.004.

43. Vanoye, L.; Favre-Réguillon, A.; Munno, P.; Rodríguez, J.F.; Dupuy, S.; Pallier, S.; Pitault, I.; De Bellefon, C. Methanol dehydration over commercially available zeolites: Effect of hydrophobicity. *Catal. Today* **2013**, *215*, 239–242, doi:10.1016/J.CATTOD.2013.01.012.

44. Schnee, J.; Gaigneaux, E.M. Lifetime of the H3PW12O40 heteropolyacid in the methanol-to-DME process: A question of pre-treatment. *Appl. Catal. A Gen.* **2017**, *538*, 174–180, doi:10.1016/j.apcata.2017.03.034.

45. Pérez-Uriarte, P.; Ateka, A.; Gayubo, A.G.; Cordero-Lanzac, T.; Aguayo, A.T.; Bilbao, J. Deactivation kinetics for the conversion of dimethyl ether to olefins over a HZSM-5 zeolite catalyst. *Chem. Eng. J.* **2017**, *311*, 367–377, doi:10.1016/j.cej.2016.11.104.

46. Thommes, M.; Kaneko, K.; Neimark, A. V; Olivier, J.P.; Rodriguez-Reinoso, F.; Rouquerol, J.; Sing, K.S.W. IUPAC Technical Report Physisorption of gases, with special reference to the evaluation of surface area and pore size distribution (IUPAC Technical Report). *Pure Appl. Chem* **2015**, *87*, 1051–1069, doi:10.1515/pac-2014-1117.

47. Moreno-Castilla, C.; Carrasco-Marín, F.; Parejo-Pérez, C.; López Ramón, M. V. Dehydration of methanol to dimethyl ether catalyzed by oxidized activated carbons with varying surface acidic character. *Carbon N. Y.* **2001**, *39*, 869–875, doi:10.1016/S0008-6223(00)00192-5.

48. Akarmazyan, S.S.; Panagiotopoulou, P.; Kambolis, A.; Papadopoulou, C.; Kondarides, D.I. Methanol dehydration to dimethylether over Al2O3catalysts. *Appl. Catal. B Environ.* **2014**, *145*, 136–148, doi:10.1016/j.apcatb.2012.11.043.

49. Rownaghi, A.A.; Rezaei, F.; Stante, M.; Hedlund, J. Selective dehydration of methanol to dimethyl ether on ZSM-5 nanocrystals. *Appl. Catal. B Environ.* **2012**, *119–120*, 56–61,

UNIVERSIDAD DE MÁLAGA

doi:10.1016/J.APCATB.2012.02.017.

50. Kim, S.; Kim, Y.T.; Zhang, C.; Kwak, G.; Jun, K.-W. Effect of Reaction Conditions on the Catalytic Dehydration of Methanol to Dimethyl Ether Over a K-modified HZSM-5 Catalyst. *Catal. Letters* **2017**, *147*, 792–801, doi:10.1007/s10562-017-1981-0.

51. Zhenwei Zhao, Marcos Chaos, Andrei Kazakov, F.L.D. Thermal Decomposition Reaction and a Comprehensive Kinetic Model of Dimethyl Ether. *Wiley Intersci.* **2007**, doi:DOI 10.1002/kin.20285.

52. Martinez-Espin, J.S.; Magnus Mortén, ab; W Janssens, T. V; Svelle, S.; Beato, P.; Olsbye, U. New insights into catalyst deactivation and product distribution of zeolites in the methanol-to-hydrocarbons (MTH) reaction with methanol and dimethyl ether feeds †. *Cite this Catal. Sci. Technol* **2017**, *7*, 2700, doi:10.1039/c7cy00129k.

53. Arfelli, M.; Mattogno, G.; Ferragina, C.; Massucci, M.A. XPS characterization of γ-zirconium phosphate and of some of its intercalation compounds. A comparison with the α-zirconium phosphate analogues. *J. Incl. Phenom. Mol. Recognit. Chem.* **1991**, *11*, 15–27, doi:10.1007/BF01073680.

54. Liu, R.; Yan, C.; Zhang, C.; Cao, Y.; Long, X. Synthesis of zirconium carbide nanoparticles by polymerised complex route. *Adv. Appl. Ceram.* **2016**, *115*, 6–12, doi:10.1179/1743676115Y.0000000039.

55. Colón, J.L.; Thakur, D.S.; Yang, C.-Y.; Clearfield, A.; Martini, C.R. X-ray photoelectron spectroscopy and catalytic activity of α-zirconium phosphate and zirconium phosphate sulfophenylphosphonate. *J. Catal.* **1990**, *124*, 148–159, doi:10.1016/0021-9517(90)90111-V.

56. Xiao, H.; Liu, S. Zirconium phosphate (ZrP)-based functional materials: Synthesis, properties and applications. *Mater. Des.* **2018**, *155*, 19–35, doi:10.1016/j.matdes.2018.05.041.

57. Alberti, G.; Costantino, U.; Marletta, G.; Puglisi, O.; Pignataro, S. ESCA investigations of amorphous and crystalline zirconium acid phosphates. *J. Inorg. Nucl. Chem.* **1981**, *43*, 3329–3334, doi:10.1016/0022-1902(81)80111-X.

58. Sannigrahi, P.; Ingall, E. Polyphosphates as a source of enhanced P fluxes in marine sediments overlain by anoxic

UNIVERSIDAD DE MÁLAGA

waters: Evidence from 31P NMR. *Geochem. Trans.* **2005**, *6*, 52–59, doi:10.1063/1.1946447.

59. Bortun, A.I.; Butler, C.J. Zirconium Phosphate, Hafnium Phosphate and method of makeing same 2005, *U.S. Paten*.

60. Strelko, V.; Streat, M.; Kozynchenko, O. Preparation, characterization and sorptive properties of polymer based phosphorus-containing carbon. *React. Funct. Polym.* **1999**, *41*, 245–253, doi:10.1016/S1381-5148(99)00061-9.

61. Díaz, A.; Mosby, B.M.; Bakhmutov, V.I.; Martí, A.A.; Batteas, J.D.; Clearfield, A. Self-Assembled Monolayers Based Upon a Zirconium Phosphate Platform. *Chem. Mater.* **2013**, *25*, 723–728, doi:10.3949/ccjm.56.2.122.

62. Bakhmutov, V.I.; Clearfield, A. 31P NMR Relaxation and Motions of Phosphate Groups in Layered Zirconium Phosphate Materials. *J. Phys. Chem. C* **2016**, *120*, 19225–19233, doi:10.1021/acs.jpcc.6b06417.

63. Villa, M.; Chiodelli, G.; Scagliotti, M. P2O5 based vitreous electrolytes: structural characterization by 31P NMR and Raman spectroscopies. *Solid State Ionics* **1986**, *18–19*, 382–387.

64. Ruiz-Rosas, R.; Bedia, J.; Rosas, J.M.; Lallave, M.; Loscertales, I.G.; Rodríguez-Mirasol, J.; Cordero, T. Methanol decomposition on electrospun zirconia nanofibers. *Catal. Today* **2012**, *187*, 77–87, doi:10.1016/J.CATTOD.2011.10.031.

65. Froment, G.F.; Bischoff, K.B.; De Wilde, J. *Chemical Reactor Analysis and Design*; 3rd ed.; John Wiley & Sons, 2011; ISBN 978-0-470-56541-4.

66. Gao, Y.; Chen, S.L.; Wei, Y.; Wang, Y.; Sun, W.; Cao, Y.; Zeng, P. Kinetics of coke formation in the dimethyl ether-to-olefins process over SAPO-34 catalyst. *Chem. Eng. J.* **2017**, *326*, 528–539, doi:10.1016/j.cej.2017.05.158.

67. Zhang, G.; Zhang, X.; Bai, T.; Chen, T.; Fan, W. Coking kinetics and influence of reaction-regeneration on acidity, activity and deactivation of Zn/HZSM-5 catalyst during methanol aromatization. *J. Energy Chem.* **2015**, *24*, 108–118, doi:10.1016/S2095-4956(15)60291-1.

UNIVERSIDAD DE MÁLAGA

3.3. KINETIC MODEL CONSIDERING CATALYST DEACTIVATION FOR METHANOL-TO-DIMETHYL ETHER ON A BIOMASS-DERIVED ZR/P-CARBON CATALYST

Dimethyl ether (DME), as an interesting renewable low soot emission diesel substitute, has been widely studied in recent years [1–3]. This DME production can be carried out by one-step syngas to DME process in a bifunctional catalyst or by the two steps process, in which syngas is firstly converted to methanol (in a metallic catalyst like Cu-ZnO/Al_2O_3) [4] and then, methanol is dehydrated to DME (in an acidic catalyst [5,6] like γ- Al_2O_3[7] or zeolites[8]).

In this sense, activated carbon from a non-expensive biomass waste can also be used as catalyst or catalyst support for the methanol to DME reaction [9–13]. This thermal and chemically stable carbonaceous materials move forward a sustainable economy with the advantage of being able to be tailored for different applications [14]. A detailed study of the involved reactions can be very useful in order to optimize the synthesis and stability of the catalysts.

A detailed study of the involved reactions can be very useful in order to optimize the synthesis of the catalysts. The kinetic study of dehydration of methanol to DME has been previously reported in the literature for different inorganic catalysts. In this sense, the determination of the kinetic parameters of this reaction goes from very simple empirical equations, which only fit experimental data to mathematical equations as a function of temperature, to semiempirical equations [15-17] or even more complex models, based on the reaction mechanisms. Several models are derived from Langmuir-Hinshelwood (LH) [17-21] and Eley-Rideal (ER) mechanisms [22-26], also taking into account dissociative or molecular adsorption of methanol [27,28]. In addition, some authors also took into account the influence of water in the inlet stream [11,29].

Deactivation by coke deposition is one of the most common causes of deactivation on these catalysts. For this reason, quantification of coke deposited [30, 31], as well as its effect on the catalyst activity [32-37] has been already addressed in literature.

UNIVERSIDAD DE MÁLAGA

In this chapter, a kinetic model including deactivation for methanol to dimethyl ether reaction over a Zr-loaded P-containing carbon catalyst was proposed. To predict the DME and other products decay with time on stream, a deactivation function determined as a function of coke content was used.

The catalyst preparation was described in section 2.3.1 and 2.3.2, and the techniques used for characterization in section 2.2. Catalytic experiments were presented in section 2.3.2 and 2.3.3.

3.3.1. Catalyst characterization

Table 3. 10 collects the textural parameters obtained from N_2 adsorption isotherm at -196 ºC and CO_2 adsorption isotherm at 0 ºC. The catalyst exhibited an A_{BET} value of 1105 m^2/g, this value is much higher than other inorganic catalysts reported in the literature [7,20,28]. In addition, the contribution of mesopores to the total pore volume is also very significant (almost a 50%), which is favorable for catalytic reactions. On the other hand, the micropore volume measured by N_2, V_t, was more than twice the micropore volume determined by CO_2 adsorption, V_{DR}, which indicated a high preponderance of wide microporosity [39]. Figure 3. 22 shows the N_2 adsorption-desorption isotherm at -196 ºC of the fresh catalyst, that can be associated with a type IV(a) isotherm with a H4 hysteresis loop, evidencing the presence of in-bottle shape mesopores [40].

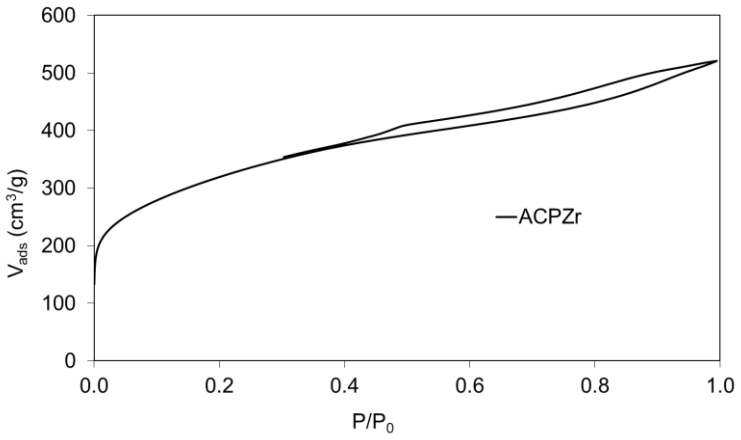

Figure 3. 22. N_2 adsorption-desorption isotherm at -196 ºC of fresh catalyst

UNIVERSIDAD DE MÁLAGA

Table 3. 10 also shows the atomic surface concentration obtained from XPS analysis. Carbon and oxygen were the main compounds detected on the surface, but phosphorus and zirconium were also observed. As can be seen, P/Zr ratio was close to 1. This ratio was quite lower than the theoretical ratio found in zirconium phosphate species, suggesting the possible formation of other Zr surface groups, not bounded to phosphorus. In this sense, Figure 3. 23 shows the individual XPS spectra of P_{2p} and Zr_{3d} of the catalyst. The P_{2p} spectrum (Figure 3. 23a) showed a broad band associated to the presence of different phosphorus compounds, such as C_3PO, $C-PO_3/C_2PO_2$, $C-O-PO_3$ and zirconium phosphate surface groups, like in $Zr(HPO_4)_2 \cdot H_2O$. On the other hand, the Zr_{3d} spectrum (Figure 3. 23b), also presents a broad band attributed to the presence of mainly zirconium-phosphate groups and in less extent $Zr-carbon/ZrO_2$ species and Zr (IV) bound to an electroactive species, like pyrophosphate groups.

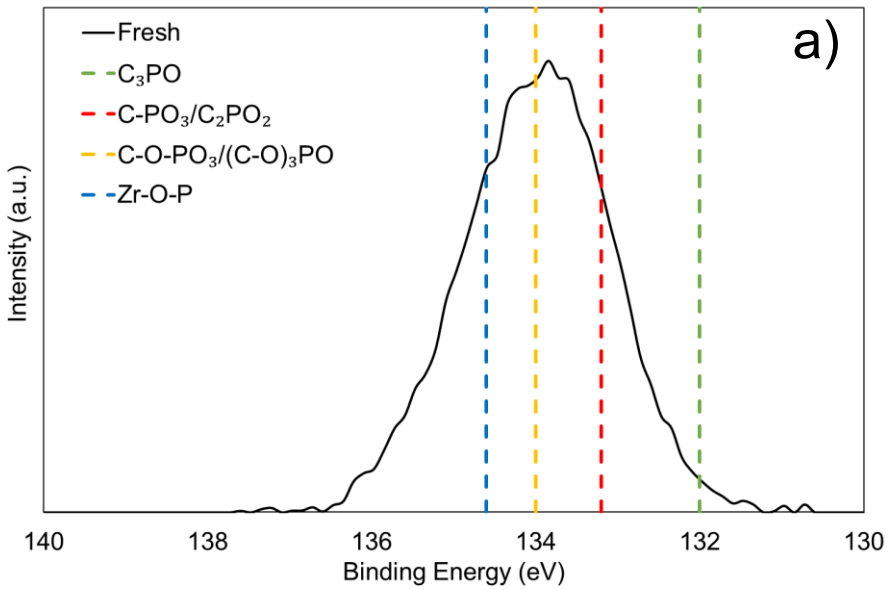

UNIVERSIDAD DE MÁLAGA

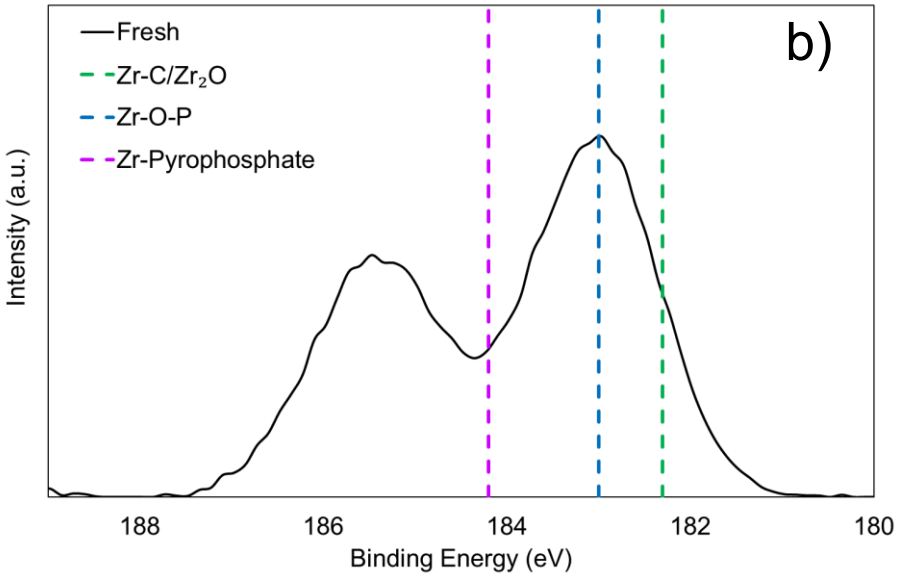

Figure 3. 23. XPS spectra of a) P2p and b) Zr3d of fresh catalyst

Table 3. 10. Textural parameter values derived from N_2 adsorption isotherm at -196 ºC and CO_2 adsorption isotherm at 0 ºC and atomic surface concentration determined by XPS analysis of the catalyst.

N_2 Isotherm					**CO_2 Isotherm**	
A_t (m^2/g)	A_{BET} (m^2/g)	V_t (cm^3/g)	V_{mes} (cm^3/g)	V_{tot} (cm^3/g)	A_{DR} (m^2/g)	V_{DR} (cm^3/g)
279	1105	0.43	0.38	0.80	509	0.20
Atomic surface concentration (%)						
C_{1s}	O_{1s}	P_{2p}	Zr_{3d}	P/Zr		
65.1	27.0	3.9	3.5	1.11		

3.3.2. Dehydration of methanol

This Zr-loaded P-containing biomass-derived catalyst has been already tested at temperatures below 400 ºC for the methanol to DME (MTD) reaction (0.02 atm_{CH3OH} and space time of 75 g_{cat}·s/$mmol_{CH3OH}$) [13]. This catalyst showed a stable and selective DME production for more than 24 h. However, its performance at higher temperatures, where the methanol conversion is very high (100%), closer to that of the industrial

UNIVERSIDAD DE MÁLAGA

process, has been evaluated in this work. Figure 3. 24a shows the gas outlet concentration and Figure 3. 24b represents the product yields as a function of TOS at 500 ºC, 0.04 atm_{CH3OH} and a space time of 75 g_{cat}·s/$mmol_{CH3OH}$. As can be seen, initial methanol concentration is near to zero (very high methanol conversion), being this value even higher than that predicted by methanol-DME equilibrium, possibly due to the presence of side reactions. At higher TOS, methanol concentration slowly increased. In spite of that conversion decrease, methanol conversion was kept higher than 25%, for more than 24 h. This decay in conversion was attributed to catalyst deactivation by the formation of coke.

The main gas products obtained in that reaction were DME, water, methane, CO and hydrogen, with only traces of CO_2, ethane, ethylene, propane and propylene. DME yield reached a maximum around 50% at 3 h. After that TOS, DME yield was gradually reduced. Nevertheless, that yield remained higher than 20%, for more than 24 h, evidencing the high selectivity of this catalyst to DME (around 85%), even in these harder operating conditions. In this sense, the yield to coke and methane was initially significant, but they did not exceed 10% after 5 h. The CO and hydrogen evolution was similar to that found for methane and coke. However, the concentration of water did not present the same tendency as that of DME at the earlier TOS, suggesting that water is also produced by other side-reactions, associated to the formation of coke and methane.

Same trends can be observed at different reaction temperatures (450 ºC and 550 ºC), concentrations (1.5 % and 8%) and space times (50 g_{cat}·s/$mmol_{CH3OH}$ and 100 g_{cat}·s/$mmol_{CH3OH}$), as it was observed from Figure 3. 25.

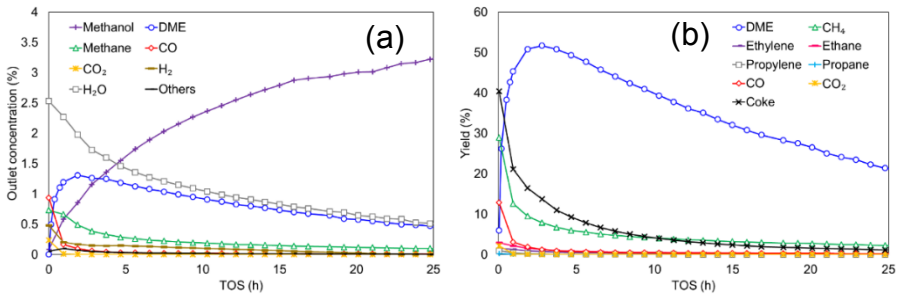

Figure 3. 24. Gas outlet concentration (a) and yield to different products (b) as a function of TOS in the MTD reaction. Reaction conditions: temperature of 500 ºC, methanol partial pressure of 0.04 atm and a space time of 75 g_{cat}·s/$mmol_{CH3OH}$.

UNIVERSIDAD DE MÁLAGA

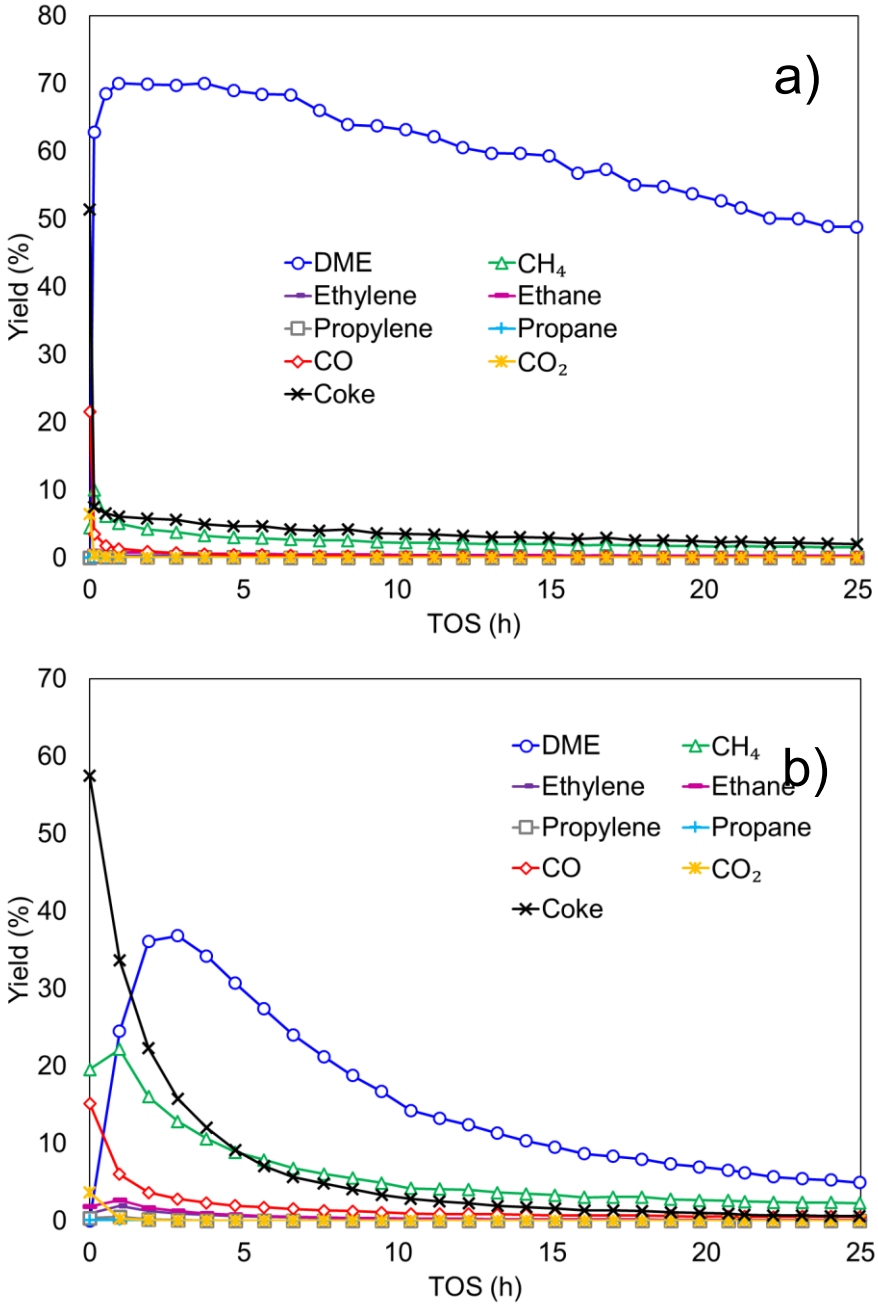

UNIVERSIDAD DE MÁLAGA

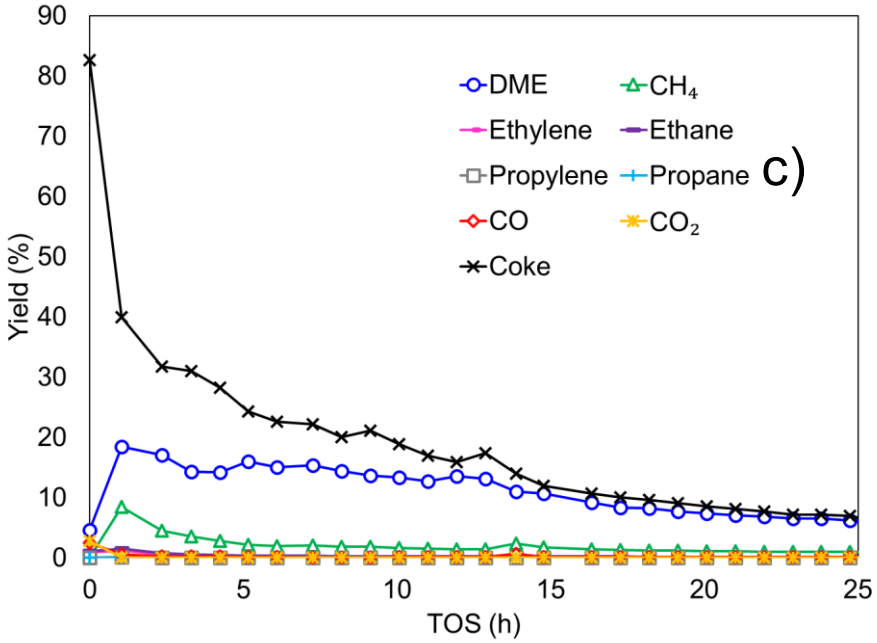

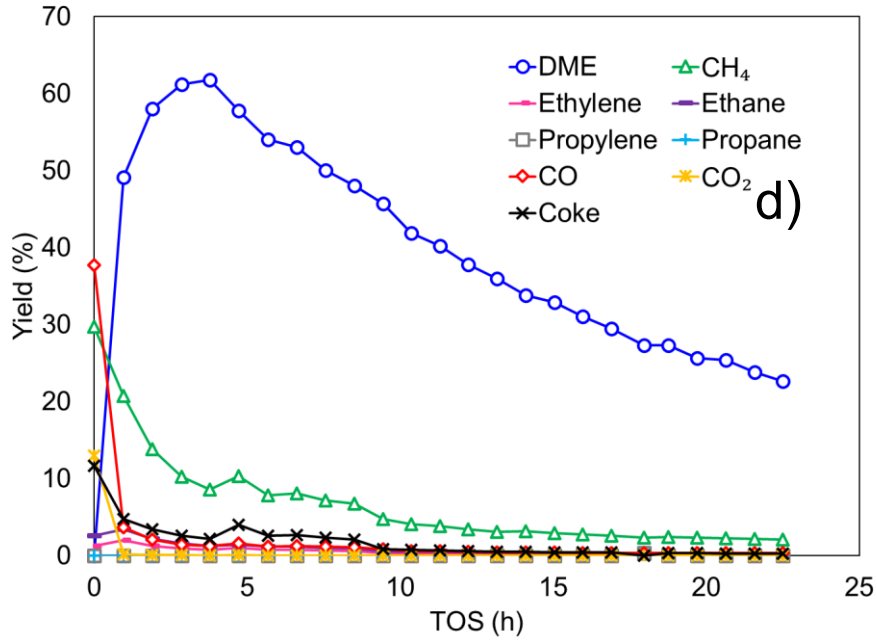

UNIVERSIDAD DE MÁLAGA

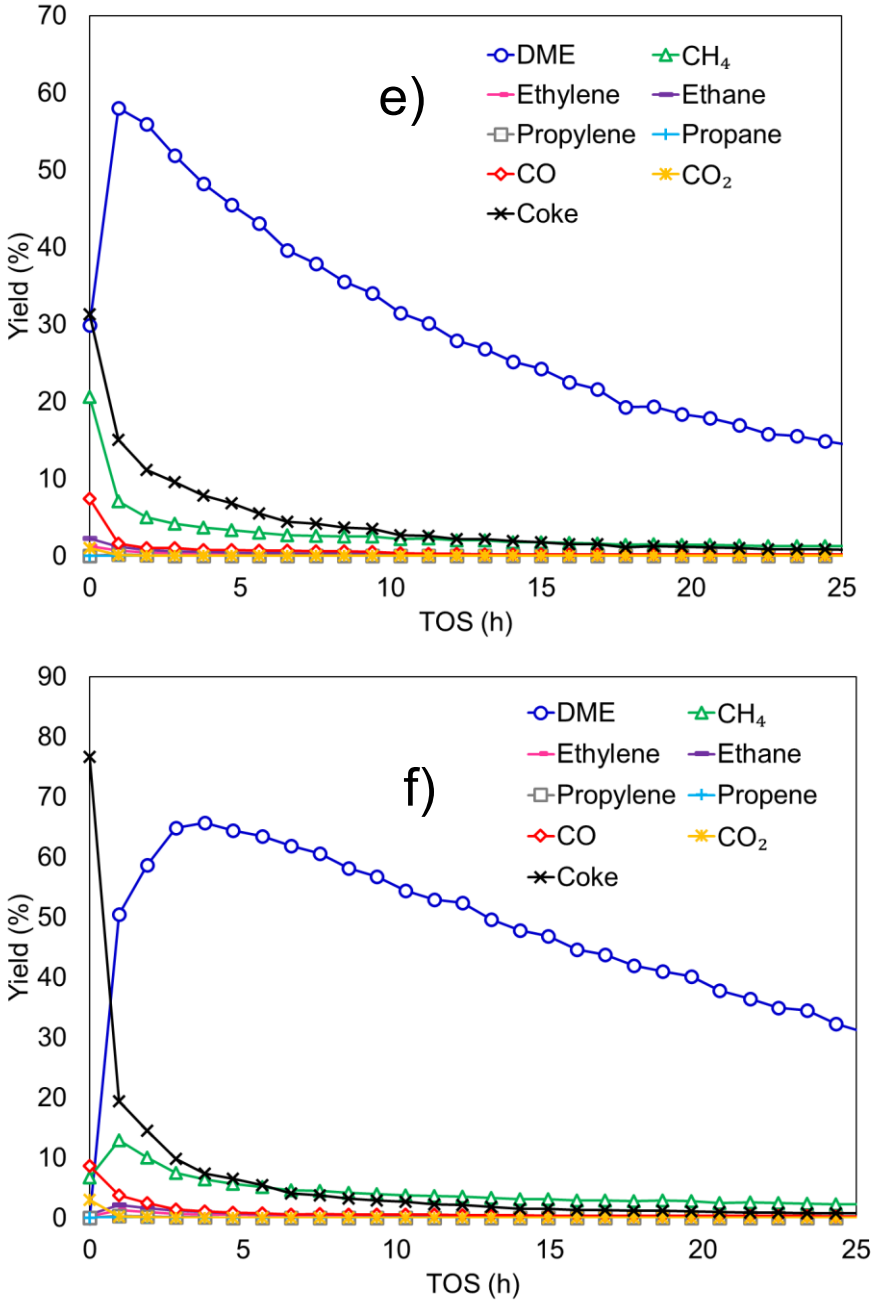

Figure 3. 25. Yield to different products as a function of TOS at different operating conditions in the MTD reaction. a) 450 ºC, 0.04 atm_{CH3OH} and 75 $g_{cat}/mmol_{CH3OH}$ b) 550 ºC, 0.04 atm_{CH3OH} and 75 $g_{cat}/mmol_{CH3OH}$ c) 500 ºC, 0.015 atm_{CH3OH} and 75 $g_{cat}/mmol_{CH3OH}$ d) 500 ºC, 0.08 atm_{CH3OH} and 75 $g_{cat}/mmol_{CH3OH}$ e) 500 ºC, 0.04 atm_{CH3OH} and 50 $g_{cat}/mmol_{CH3OH}$ f) 500 ºC, 0.04 atm_{CH3OH} and 100 $g_{cat}/mmol_{CH3OH}$

UNIVERSIDAD DE MÁLAGA

To explain the main product distribution shown in Figure 3. 24, the following reactions were considered: methanol dehydration to DME (equation 3.26); methane formation, which takes into account the additional formation of water (equation 3.27); CO formation (equation 3.28) and coke production (equation 3.29)[12].

$$2\,CH_3OH_{(ads)} \rightarrow CH_3OCH_3 + H_2O \quad (3.26)$$

$$2\,CH_3OH_{(ads)} \rightarrow CH_4 + H_2O_{(ads)} + CH_2O_{(ads)} \quad (3.27)$$

$$CH_2O_{(ads)} \rightarrow CO + H_2 \quad (3.28)$$

$$CH_2O_{(ads)} \rightarrow C_{coke} + H_2O \quad (3.29)$$

The coke production was considered to take place by an intermediate similar to formaldehyde, as some authors have already reported [41]. This formaldehyde would decompose instantaneously at the operating conditions used in this study, yielding CO and H_2 or coke and water. To validate this assumption, an experiment in which methanol was cofed with formaldehyde and water was carried out and compared to an experiment in which the same partial pressure of methanol and water were added without formaldehyde. Figure 3. 26 collects the coke content as a function of TOS at 500 ºC and 75 g_{cat}·s/$mmol_{CH3OH}$, cofeeding 4% methanol and 2% water without and with 1.5% of formaldehyde. The quantity of coke deposited on the catalyst was 15% higher, in the presence of formaldehyde in the inlet stream, suggesting the significant role of formaldehyde in the coke formation.

UNIVERSIDAD DE MÁLAGA

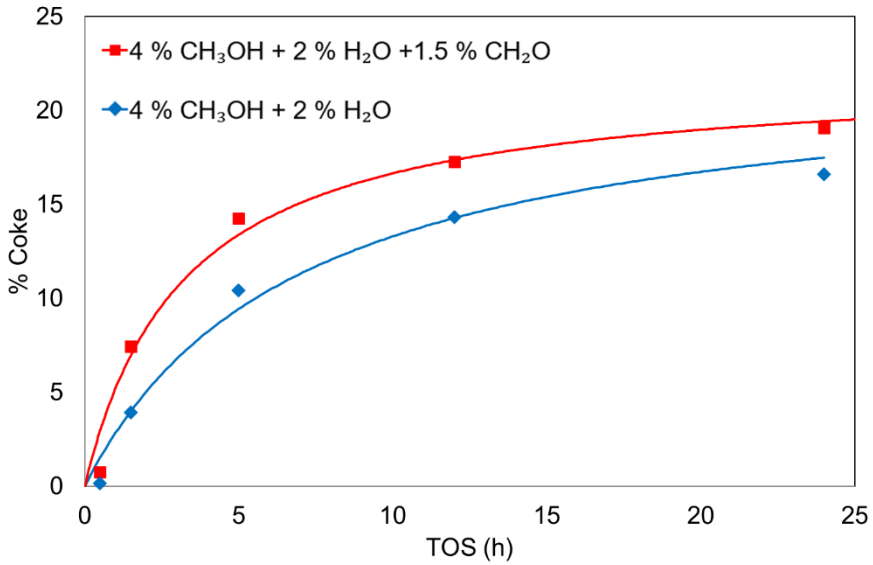

Figure 3. 26. Coke content as a function of TOS for methanol+water fed and methanol+water+formaldehyde; temperature 500 ºC and space time of 75 gcat·s/mmolCH3OH. Experimental data (points) and calculated (lines).

3.3.2.1. Effect of inlet water vapor

Water has been reported to compete with methanol for the active sites of the catalyst, causing a decay in DME production [13,42–44]. The inhibition effect of water is relevant in the experimental conditions here reported, as its concentration is similar to the concentration of DME observed in this work. In this sense, Figure 3. 27a collects the conversion obtained cofeeding methanol (4%) with different water concentrations. When water concentration did not exceed 2%, there were not clear signs of decay in the methanol conversion, probably due to the low differences between the water produced from methanol dehydration and water cofed with methanol. However, a decrease in conversion of around 30% was observed, when a 5% of water was cofed with methanol and, an even higher decay was noticed, when water cofed reached 10%. This data was in concordance with the competitive adsorption of water.

UNIVERSIDAD DE MÁLAGA

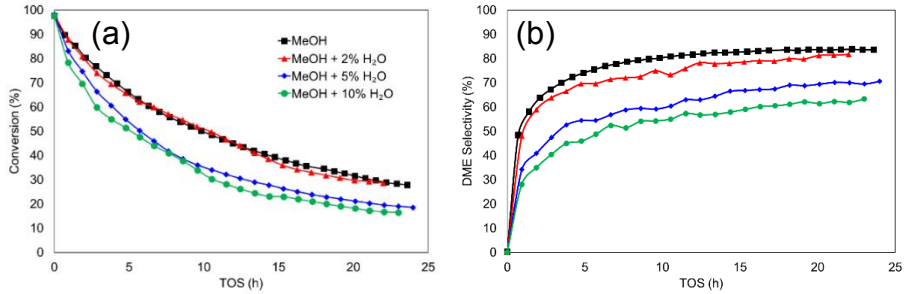

Figure 3. 27. Methanol conversion (a) and DME selectivity (b) as a function of TOS in the MTD reaction with different water concentrations cofed. Reaction conditions: temperature of 500 ºC, methanol partial pressure of 0.04 atm and a space time of 75 g_{cat}·s/$mmol_{CH3OH}$.

The influence of water has been also analyzed in terms of yield and selectivity. Figure 3. 27b shows the selectivity to DME and Figure 3. 28 shows the effect of water concentration on the yields to different products in MTD reaction. The inhibitory effect of water could be clearly seen, if only selectivity or yield to DME was considered. In that case, selectivity or yield to DME decreased as water concentration in the reactor inlet increased. In fact, the maximum of DME yield diminished from 52%, when only methanol was fed, to 25% when a 10% of water was cofed. In this sense, Akarmazyan et al. [7] with a γ-Al_2O_3 catalyst, observed more than a 20 % of methanol conversion decay, after 5 h on stream, when 10 % of inlet water was cofed; Xu et al. [44] with different inorganic solid-acid catalysts observed a decay in more than a 50%, when 3% of water was added; Palomo et al. [13] with a Zr-loaded P-containing activated carbon catalyst, reported a reversible 10% of activity loss, when 2 % of water was cofed with methanol, suggesting, in this case, that the inhibition effect is more related to competitive adsorption, rather than an irreversible deactivation of the active site.

On the other hand, coke yield remained practically the same, when water was cofed, suggesting that the mechanism of coke production was not greatly influenced by the presence of water, probably because the main coke precursor was methanol rather than DME (whose concentration decreased in the presence of water). These results can be apparently in opposition to other results reported in the literature, where the presence of water reduced the coke production. However, as Gayubo et al. reported [45], this reduction can be associated, for example, to a lower reactivity, due to the dealumination of zeolitic type-catalysts.

UNIVERSIDAD DE MÁLAGA

With regard to the formation of methane and CO, their corresponding yields are not affected by the cofeeding of water, independently of the inlet water partial pressure used, which is in agreement with the proposed equations 3.27-29, since coke and CO were probably formed from the formaldehyde intermediate, whose formation implies the simultaneous release of methane, and water is not involved.

All these results seem to point out that the reduction in methanol conversion when water was cofed, shown in Figure 3. 27, can be mainly attributed to the reduction in the selectivity to DME, since no other relevant changes were observed. In this sense, the equilibrium reaction of methanol dehydration could be shifted to the methanol formation from DME in the presence of large quantities of water.

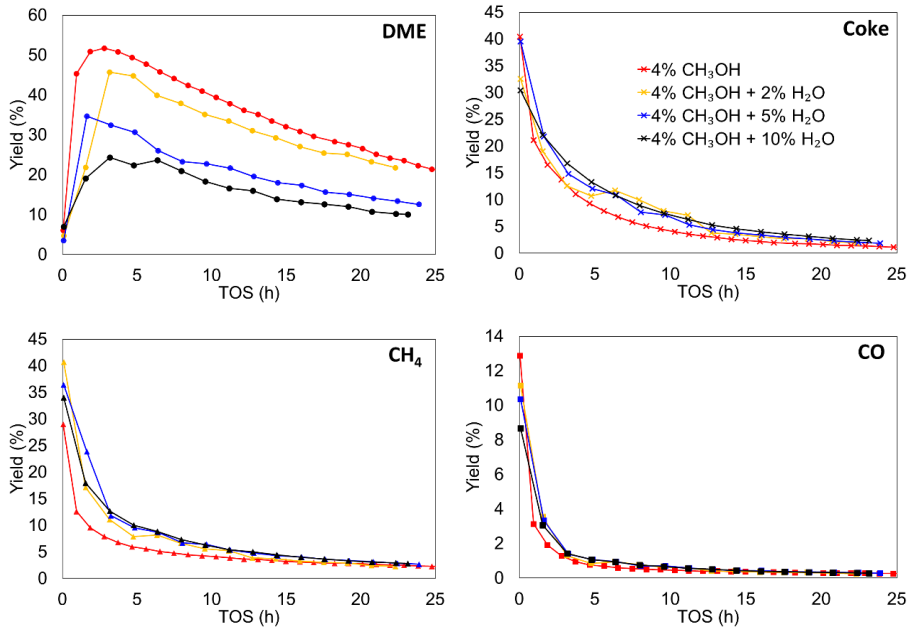

Figure 3. 28. Yield to DME, Coke, Methane and CO as a function of TOS in the MTD reaction with different water concentrations cofed. Reaction conditions: temperature of 500 ºC, methanol partial pressure of 0.04 atm and a space time of 75 g_{cat}·s/$mmol_{CH3OH}$.

3.3.2.2. Stoichiometric study of MTD reaction

A study on the stoichiometry of the MTD reaction has been performed taking into account only the main compounds obtained, in order to

UNIVERSIDAD DE MÁLAGA

validate the reaction pathway proposed in equations 3.26-29. The proposed reaction pathway considers that water release was attributed to methanol dehydration (eq. 3.26) and coke production (eq. 3.51). Olefins production could also produce water, but it has been disregarded because they were detected at very low concentrations (traces) as compared to the formation of DME and coke. Based on these equations, experimental outlet water concentration must be equal to the water released by DME production (equimolar to DME concentration) plus the water released by coke deposition (equimolar to coke precursor). Figure 3. 29a collects experimental and calculated water in the MTD at 450 ºC, 500 ºC and 550 ºC. Both profiles are very similar at every TOS, at 500 and 550 ºC and the slight deviation found at 450 ºC could be related to the lower coke production observed at this temperature, which can induce more experimental error. In any case, these similarities supported the assumption that water was mainly released by DME and coke production.

On the other hand, methane release seems to be associated to the formation of CH_2O(ads) intermediate by eq. 3.27. This CH_2O(ads), subsequently, evolves to CO (eq. 3.28) or coke (eq. 3.29). Figure 3. 29b compares the experimental methane concentration with the sum of CO concentration and coke production (equimolar to coke precursor), at different temperatures. Similar tendency can be seen in both concentration profiles, endorsing, this way, the reaction pathway proposed in equations 3.28 and 3.29. In addition, it is important to highlight that the formation of methane is very low (concentrations lower than 0.3%) from a TOS of 10 h.

Finally, the similarity between the concentrations of hydrogen and carbon monoxide, observed in Figure 3. 24a, was also in accordance with the reaction proposed in eq. 3.26, which predicted the equimolecular release of both compounds. The slight higher release of CO in the earlier times compare to hydrogen evolution can be attributed to the decomposition of oxygen surface groups present on the activated carbon surface, which are evolved as CO at the range of temperatures used in this work [46].

UNIVERSIDAD DE MÁLAGA

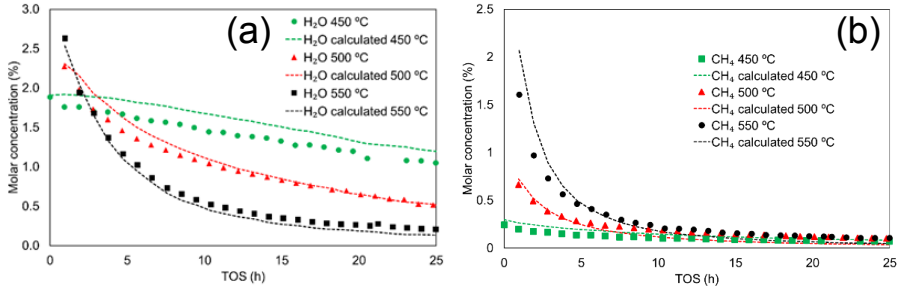

Figure 3. 29. Experimental (symbols) and calculated (dashes lines) molar concentrations of water and methane, respectively, as a function of TOS, at different reaction temperatures. Reaction conditions: methanol partial pressure of 0.04 atm and a space time of 75 g_{cat}·s/$mmol_{CH3OH}$

3.3.3. Kinetic modelling and parameters estimation

Taking into account the aforementioned analysis, a kinetic study was carried out over the ACPZr catalyst for the MTD reaction. With this goal, the reaction pathways previously reported for this catalyst at different experimental conditions were considered. In this sense, Palomo et al. following a Langmuir-Hinshelwood mechanism, proposed a 4 step mechanism for DME production, in which 2 methanol molecules were sequentially adsorbed in the active sites and, then, reacted with each other to produce DME and adsorbed water, which was desorbed to regenerate the initial active sites [11]. On the other hand, at higher temperatures(between 450 ºC and 550 ºC), two adsorbed methanol molecules could also react through a six-member ring, producing methane and an intermediate that evolved mainly to coke and water or CO and hydrogen [12].

For this reason, this model included DME formation, but also coke, methane and CO as the main carbonaceous byproducts. Nevertheless, olefins and paraffins production are not considered, as they are only found in trace levels at the reactor outlet.

Initially, the reaction rate at zero time on stream was predicted by a kinetic study [11,12]. The operating conditions used for the kinetic study were: inlet methanol partial pressure from 0.015 to 0.08 atm and inlet water from 0.02 to 0.1 atm; space times from 50 to 100 g·s/$mmol_{reactive}$; and temperature from 450 ºC to 550 ºC. The assumptions taken into account for the development of the kinetic study were:

UNIVERSIDAD DE MÁLAGA

- A uniform distribution of active sites on the catalyst surface
- Homogeneous distribution of the catalyst in the catalytic bed
- Ideal flow, without radial gradients of concentration
- Isotherm catalytic bed
- Negligible heat and mass transfer limitations

For this reason, plug flow integral reactor can be used to describe the experimental data. The mass balance equation for methanol, DME, methane and CO can be defined in the form of eq. 3.30.

$$-\frac{dX_i}{d\left(\frac{W}{F_{MeOH_0}}\right)} = r_i \tag{3.30}$$

where X_i is extent of reaction, which could account for methanol conversion or DME, methane and CO yield; W is the catalyst mass (g); F_{MeOH_0} accounts for the inlet methanol molar flow (mol/s) and r_i is kinetic rate of consumption or formation for the i species (atm/(g·s)).

Temperature dependence of kinetic constants, k_i, is considered to follow Arrhenius law (eq. 3.31), while adsorption and equilibrium constants, K_i, followed Van't Hoff law (eq. 3.32).

$$k_i = k_{0,i} \cdot \exp\left(\frac{-E_{a,i}}{RT}\right) \tag{3.31}$$

$$K_i = K_{0,i} \cdot \exp\left(\frac{-\Delta H_i}{RT}\right) \tag{3.32}$$

where $k_{0,i}$ and $K_{0,i}$ are the apparent preexponential factor; R is the universal gas constant (J/mol·K); T is the reaction temperature (K); $E_{a,i}$ is the activation energy of reaction i (J/mol) and ΔH_i the adsorption enthalpy of the equilibrium i.

A detailed description of the reactions taking place at higher temperatures, (summarized in eq. 3.26-29), and based on the already described mechanisms, are collected in eq. 3.33-3.39.

$$CH_3OH + * \leftrightarrow * M \tag{3.33}$$

$$CH_3OH + * M \leftrightarrow M * M \tag{3.34}$$

$$M * M \leftrightarrow * W + CH_3OCH_3 \tag{3.35}$$

$$* W \leftrightarrow * + H_2O \tag{3.36}$$

UNIVERSIDAD DE MÁLAGA

$$M * M \rightarrow * I + CH_4 + H_2O \quad (3.37)$$

$$* I \leftrightarrow * + CO + H_2 \quad (3.38)$$

$$* I \rightarrow * C + H_2O \quad (3.39)$$

In this scheme, $*$ stands for free active site; $* M$ represents one adsorbed methanol molecule on the active site; $M * M$ means two adsorbed methanol molecules as described in previous works [11,12]; $* W$ corresponds to an adsorbed water molecule; whereas $* I$ and $* C$ represents a formaldehyde intermediate and coke deposited on the active site, respectively. Eq. 3.33, 3.34 and 3.36 represent methanol and water adsorption equilibria, respectively, while eq. 3.35 accounts for DME formation reaction; eq. 3.37 for the formaldehyde intermediate formation with methane and water evolution; eq. 3.38 for the decomposition of formaldehyde to CO and hydrogen; and eq. 3.39 for the decomposition of formaldehyde intermediate to coke. Moreover, no adsorbed DME step has been taking into account as DME desorption has been considered very fast.

Assuming fast equilibrium for the adsorption of methanol and water, the concentration of adsorbed species can be estimated as follows:

$$C_{*M} = K_{M,1} \cdot P_M \cdot C_* \quad (3.40)$$

$$C_{M*M} = K_{M,2} \cdot P_M \cdot C_{*M} = K_{M,2} \cdot K_{M,1} \cdot P_M^2 \cdot C_* \quad (3.41)$$

$$C_{*W} = K_W \cdot P_W \cdot C_* \quad (3.42)$$

Where C_* is the concentration of free active sites available for adsorption of methanol or water molecules (mol/g); C_{*M} and C_{M*M} are the concentration of active sites with one or two methanol molecules adsorbed, respectively (mol/g); C_{*w} is the concentration of active sites with water adsorbed; $K_{M,1}$ and $K_{M,2}$ stands for the adsorption equilibrium constants of single methanol and a second methanol molecule on the active site (atm^{-1}); K_W represents water equilibrium adsorption constant (atm^{-1}); and P_M and P_W represent the partial pressures of methanol and water (atm). The site balance is described in eq. 3.43.

$$C_{*t} = C_* + C_{*M} + C_{M*M} + C_{*W} + C_{*I} \quad (3.43)$$

In it, C_{*t} represents the total concentration of active sites (mol/g). This equation can be simplified assuming that the surface concentration of

UNIVERSIDAD DE MÁLAGA

the intermediate, C_{*I}, is negligible compared to the other products, as this specie must be similar to an adsorbed formaldehyde, and this molecule is a highly reactive specie that quickly decomposes into products.

The rate equations for each surface reaction step are shown in eq. 3.44-47.

$$r_{13} = k'_{sr} \cdot C_{M*M} - \frac{k'_{sr}}{K_{SR}} \cdot P_{DME} \cdot C_{*W} \quad (3.44)$$

$$r_{15} = k'_{sr2} \cdot C_{M*M} \quad (3.45)$$

$$r_{16} = k'_{sr3} \cdot C_{*I} - \frac{k'_{sr3}}{K_{SR3}} \cdot P_{CO} \cdot P_{H_2} \cdot C_* = k'_{sr3} \cdot C_{*I} - \frac{k'_{sr3}}{K_{SR3}} \cdot P_{CO}^2 \cdot C_* \quad (3.46)$$

$$r_{17} = k'_{sr4} \cdot C_{*I} \quad (3.47)$$

where k'_{sr}, k'_{sr2}, k'_{sr3} and k'_{sr4} are the kinetic constants of the surface reactions (s^{-1}); K_{SR} (atm^{1}), K_{SR3} (atm^{2}) are the equilibrium constant of surface reactions; P_M, P_{DME}, P_W, P_{CO}, P_{H_2} the partial pressures of methanol, DME, water, CO and H_2 (atm) respectively and C_{*I} the surface concentration for the intermediate species, presumably adsorbed formaldehyde, formed on the catalytic site (mol/g). r_{16} has been simplified assuming that the partial pressure of hydrogen must be equal to CO partial pressure, since it is the only reaction in which CO and H_2 are formed, and they are obtained in equimolecular ratio. This assumption has been previously verified in Figure 3. 24a. Thus, the surface concentration of the intermediate was calculated assuming that r_{15} is equal to $r_{16} + r_{17}$:

$$C_{*I} = \frac{k'_{sr2} \cdot K_{M,1} \cdot K_{M,2} \cdot P_M^2 + \frac{k'_{sr3}}{K_{SR3}} \cdot P_{CO}^2}{k'_{sr3} + k'_{sr4}} \cdot C_* \quad (3.48)$$

Combining the site balance equation, Eq. 3.43, with the surface concentration equations, Eq. 3.40-42 and 3.48, the site balance can be rearranged to provide an expression of the free fraction of active sites, θ_*, as eq. 3.49 shows:

$$\frac{C_*}{C_{*t}} = \theta_* = \frac{1}{1 + K_{M,1} \cdot P_M + K_{M,1} \cdot K_{M,2} \cdot P_M^2 + K_W \cdot P_W} \quad (3.49)$$

UNIVERSIDAD DE MÁLAGA

If surface reactions are considered as rate determining steps for every compound, rate expressions for DME (eq. 3.50), CH_4 (eq. 3.51) and CO (eq. 3.52) can be obtained by substituting the fractional coverage values as defined in eq. 3.40-42 and 3.49.

$$r_{DME} = r_{13} = \frac{k_{sr}\cdot\left(K_{M,1}K_{M,2}P_M^2 - \frac{P_{DME}\cdot K_W\cdot P_W}{K_{sr}}\right)}{1+K_{M,1}P_M+K_{M,1}K_{M,2}P_M^2+K_W\cdot P_W} \quad (3.50)$$

$$r_{CH_4} = r_{16} = \frac{k_{sr2}\cdot K_{M,1}\cdot K_{M,2}\cdot P_M^2}{1+K_{M,1}P_M+K_{M,1}K_{M,2}P_M^2+K_W\cdot P_W} \quad (3.51)$$

$$r_{CO} = r_{17} = \frac{\frac{k_{sr2}\cdot k_{sr3}\cdot K_{M,1}\cdot K_{M,2}\cdot P_M^2}{ksr_3+k_{sr4}} + \left(\frac{k_{sr3}}{k_{sr3}+k_{sr4}} - k_{sr3}^{-1}\right)\cdot P_{CO}^2}{1+K_{M,1}P_M+K_{M,1}K_{M,2}P_M^2+K_W\cdot P_W} \quad (3.52)$$

In them, all the kinetic constants (from k_{sr} to k_{sr4}, mol·g^{-1}·s^{-1}) are redefined as the product of $k_i' \cdot C_{*t}$. Finally, methanol decomposition rate can be described attending to the formation rates of the products and taking into consideration the stoichiometry of the MTD reaction as follows:

$$r_{CH_3OH} = -2 \cdot r_{DME} - r_{CH_4} \quad (3.53)$$

To obtain the kinetic parameters, a MATLAB® program based in the Nelder-Mead simplex algorithm, was used. The program minimized the objective function (eq. 3.54), defined as a square difference between experimental and calculated data for every experiment.

$$OF = \sum \left(x_{i,exp} - x_{i,cal}\right)^2 \quad (3.54)$$

where $x_{i,exp}$ is the experimental conversion/yield of the i species, and $x_{i,cal}$ is the conversion yield of the i species estimated from the solution of their respective mass balance equation.

Figure 3. 30 compares the calculated data versus the experimental results at zero time on stream, at different operation conditions. As it can

UNIVERSIDAD DE MÁLAGA

be seen, the model successfully reproduced the experimental data. Only low deviations were found for methane yield obtained at high methanol partial pressures, where the model over predicted the methane conversion, and for the DME yields and methanol conversions obtained at the lowest temperature (450 ºC) and the shortest space time (50 $g \cdot s/mol_{CH3OH}$). For the latter case, it looks like the inhibition effect of water in DME formation via the promotion of DME hydration is stronger in the catalyst than the one predicted by the model.

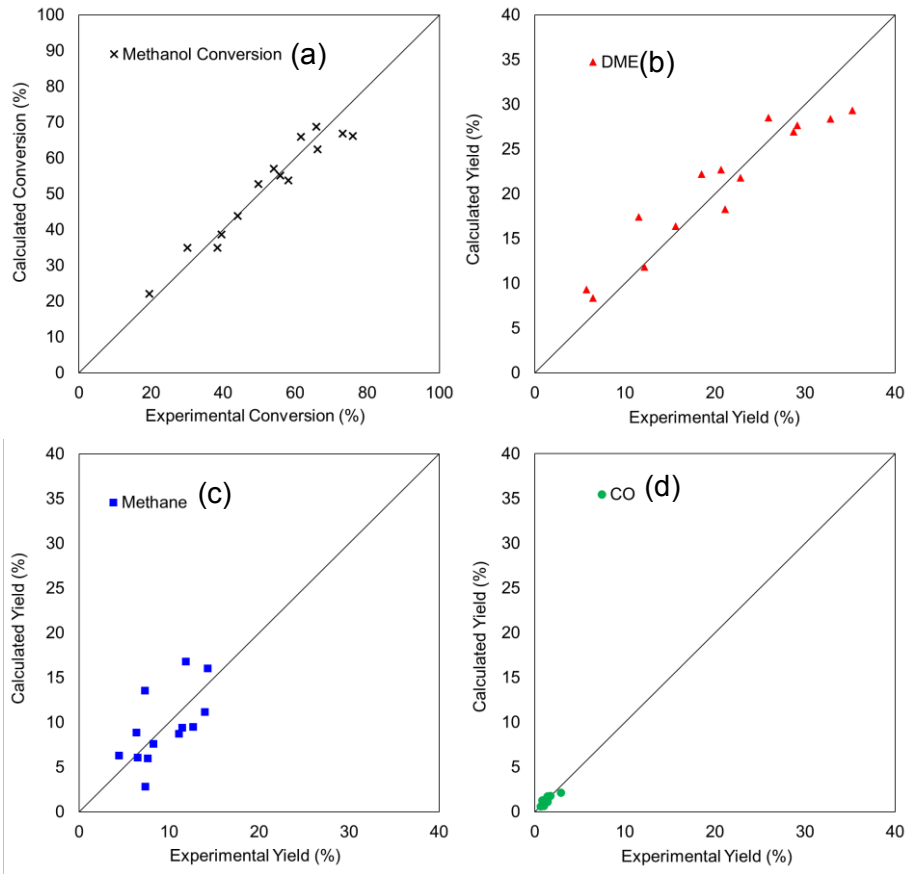

Figure 3. 30. Calculated versus experimental conversion of methanol (a) and yield to DME (b), Methane (c) and CO (d) at zero time on stream for the different operating conditions (temperatures of 450 ºC, 500 ºC and 550 ºC; methanol partial pressure of 1,5 %, 4 % and 8 %; space time of 50, 75 and 10 $g_{cat} \cdot s/mmol_{CH_3OH}$)

UNIVERSIDAD DE MÁLAGA

Table 3. 11 collects the kinetic data at zero time on stream for the reactions proposed in the mechanism. As can be seen, kinetic parameters related to DME formation (k_{sr}, $K_{M,1}$ and $K_{M,2}$) and water desorption ($1/K_W$) are very similar to the kinetic parameters proposed by Palomo et al. [11] at lower temperatures, which corroborated that the same mechanism of DME production takes place at the higher temperatures used in this study. Only some discrepancies can be seen for K_{SR}, as the high preexponential factor and the low adsorption enthalpy reported in their work produced a negligible value of DME hydration reaction. The authors stated that the reverse DME formation reaction can be considered negligible for the operation conditions used in their study [11]. Nevertheless, at the conditions herein tested, this reaction has an important role, as discussed in section 3.2.1. It is also noteworthy that, at these experimental conditions, methanol adsorption on the active site is favored over water adsorption, as suggested by the higher value of $K_{M,1}$ compared to that of K_W, explaining why coke formation was barely affected by water adsorption (see Table 3. 11). Thus, the inhibitory effect of water on DME formation seems to be established via the DME hydrolysis reaction. The evaluation of DME formation rate and the reverse reaction rate (at 500 ºC, a methanol partial pressure of 0.04 atm and methanol conversion of 50%) shows reaction rate values of $1.14 \cdot 10^{-5}$ and $4.02 \cdot 10^{-6}$ atm/g·s, respectively. These results suggest that, even in the absence of water in the inlet stream, nearly 40% of the DME would react to produce methanol at these conditions.

On the other hand, activation energy for k_{sr2} (methane formation) has a lower value than DME formation, which implies that the deactivation rate (triggered by reaction r_{18}, which runs in series with methane formation) is less sensitive to temperature changes. This result indicates that DME formation prevails over deactivation by coke at the highest reaction temperature. Finally, k' value (which corresponded to the ratio k_{sr4}/k_{sr3}, and was related to the selectivity towards coke formation in the decomposition of the intermediate) indicates that activation energy for coke production is higher. Again, this result is in accordance with the experimental data, where coke formation rate becomes faster than CO formation as reaction temperature increases.

UNIVERSIDAD DE MÁLAGA

Table 3. 11. Kinetic parameters of best fit for Eqs. 28-30 and constant value at 500 ºC

	k_0 or K_0	Units	E_a or ΔH (kJ/mol)	Constant value at 500 ºC
k_{sr}	1.3	$mol \cdot g_{cat}^{-1} \cdot s^{-1}$	65	$5.3 \cdot 10^{-5}$
K_{SR}	$5.6 \cdot 10^{-11}$	atm	-123	0.01
k_{sr2}	$2.7 \cdot 10^{-2}$	$mol \cdot g_{cat}^{-1} \cdot s^{-1}$	51	$9.2 \cdot 10^{-6}$
k_{sr3}^{-1}	6.6	$mol \cdot g_{cat}^{-1} \cdot s^{-1}$	15	0.7
k'	69.5	-	19	3.7
$K_{M,1}$	3.0	atm^{-1}	-15	31.1
$K_{M,2}$	3.6	atm^{-1}	-10	17.1
K_W	0.01	atm^{-1}	-41	8.5

Several kinetic studies have been performed for the MTD reaction. Specifically, Hosseininejad et al. [23] with an Amberlist 35 as catalyst, reported an activation energy of 98 kJ/mol at temperatures between 110-135ºC. Lower values of E_a, around 75 kJ/mol, were proposed by Bercic et al. [17] using γ-Al_2O_3, at temperatures between 320-360ºC. This value was similar to the E_a reported by Mollavali et al. [26], for another γ-Al_2O_3, ranged between 57-62 kJ/mol, but far from the value provided by Sierra et al. [29], 264 kJ/mol, for the same reaction. Migliori et al. [47] with a H-FMI catalyst, proposed different activation energy values, between 50-68 kJ/mol, at temperatures between 170ºC to 250ºC, and they related these values with the ratio Si/Al of the zeolite. Pop et al. [21], with H-SAPO-34, obtained an activation energy value of 80 kJ/mol at temperatures between 80-250 ºC. On ZSM-5, Ortega et al. [20] obtained a E_a between 80-130 kJ/mol. Ha et al. [19], with a modified ZSM-5, obtained an activation energy around 55 kJ/mol. With activated carbons, Moreno-Castilla et al. [9] obtained an increasing E_a from 85-115 kJ/mol in the range of temperatures 140-180 ºC. Finally, Palomo obtained an E_a of 70 kJ/mol for the same catalyst, but operating at lower temperatures. Many of these values are similar to the E_a obtained in the present kinetic study for the MTD reaction.

UNIVERSIDAD DE MÁLAGA

All the rates above calculated only account for the zero time on stream, so they are considered initial reaction rates. As the time on stream increased, some loss of activity was observed, associated to the coke deposition on the actives sites. Therefore, to describe the evolution of reactant and product yields with TOS, a deactivation function became necessary. This deactivation function was directly related to the amount of coke deposited, which was described by several empirical equations, proposed by Froment et al. [36]. Once the equation describing the coke evolution with TOS is obtained, it will be used as the model input for the catalyst deactivation function, which relates coke formation with catalyst deactivation. The empirical equations tested for the coke evolution with TOS are collected in eq. 3.55-59.

$$C_{coke} = \frac{1}{\alpha}\ln\left(1 + \alpha \cdot r^0_{coke} \cdot TOS\right) \quad (3.55)$$

$$C_{coke} = \frac{1}{\alpha}\left[1 - \exp\left(-\alpha \cdot r^0_{coke} \cdot TOS\right)\right] \quad (3.56)$$

$$C_{coke} = \frac{1}{\alpha}\left[1 - \frac{1}{1+\alpha \cdot r^0_{coke} \cdot TOS}\right] \quad (3.57)$$

$$C_{coke} = \frac{1}{\alpha}\left[\sqrt{2\alpha \cdot r^0_{coke} \cdot TOS + 1} - 1\right] \quad (3.58)$$

$$C_{coke} = \frac{1}{\alpha}\left[\sqrt[3]{3\alpha \cdot r^0_{coke} \cdot TOS + 1} - 1\right] \quad (3.59)$$

where C_{coke} stands for the percentage of coke deposited on the catalyst; r^0_{coke} is the initial coke production rate and α is a deactivation constant. To predict the data at different operating conditions, initial coke production r^0_{coke} (without deactivation), was predicted using a pseudo n^{th} order equation (eq. 3.60)

$$r^0_{coke} = k' \cdot \exp\left(-\frac{E_a}{RT}\right) \cdot P^n_{CH_3OH} \quad (3.60)$$

where k' is the preexponential factor; E_a is the activation energy of coke production; R is the universal gas constant; T is the temperature (K); P_{CH_3OH} is the partial pressure of methanol and n is the reaction order. The coke formed at different time on streams, inlet methanol pressures and reaction temperatures were determined experimentally by weighing

UNIVERSIDAD DE MÁLAGA

the catalytic bed, and the least square differences between these quantities and the coke predicted by the different models was minimized using the Nelder-Mead simplex algorithm in Matlab®:

$$OF = \sum \left(C_{coke,exp} - C_{coke,cal} \right)^2 \quad (3.61)$$

where $C_{coke,exp}$ is the experimental amount of coke deposited, and $C_{coke,cal}$ is the amount of coke estimated from the Eq. 3.55-59.

Table 3. 12 collects the least square difference (i.e. value of OF at the end of the minimization procedure) and the best fitting parameters for the different coke production equations (eq. 3.55-59), being the deactivation constant (α) the one with a higher impact in the prediction of coke content. The minimal value using as optimization parameter, eq. 3.61, was achieved with eq. 3.57, so this equation was selected as the model input for the development of the catalytic deactivation function.

Table 3. 12. Parameters for coke deposition using different deactivation equations obtained for temperatures between 450 ºC and 550 ºC

	α	$\mathbf{k'_c}$	$\mathbf{E_a}$ **(kJ/mol)**	**n**	**OF**
(3.55)	0.184	$1.24 \cdot 10^{10}$	135	0.88	0.019
(3.56)	0.043	$5.14 \cdot 10^{8}$	122	0.96	0.021
(3.57)	0.038	$2.61 \cdot 10^{9}$	130	0.79	0.015
(3.58)	$5.98 \cdot 10^{14}$	$3.20 \cdot 10^{21}$	87	0.88	0.053
(3.59)	$4.16 \cdot 10^{7}$	$1.91 \cdot 10^{25}$	120	0.98	0.030

Figure 3. 31 represents the coke content as a function of TOS for the MTD reaction and the calculated coke content by using eq. 3.57. A good agreement between experimental and calculated data can be seen. Independently of the equation used, all of them predict a reaction order

UNIVERSIDAD DE MÁLAGA

near to one, which is supported by previous works reported in the literature [48]. The activation energy obtained from the fitting (in the range 450-550 ºC) has a value slightly higher than values reported for other catalysts at similar conditions [33,37,48], probably because this reaction was performed at higher temperatures (450-550 ºC) and the nature of the coke obtained can be different.

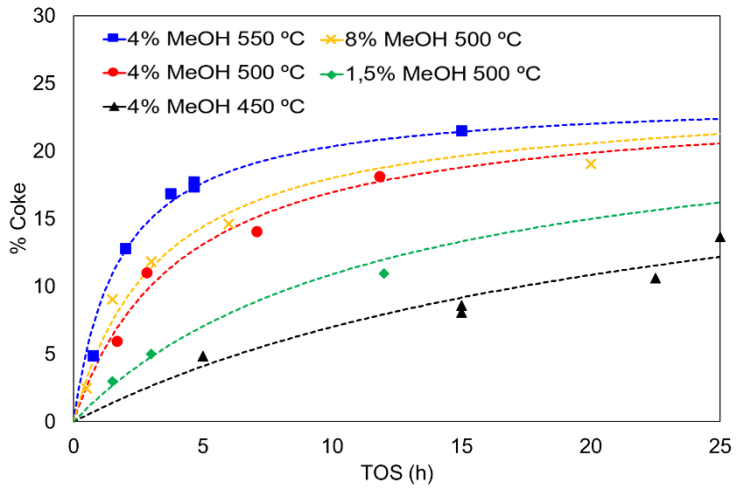

Figure 3. 31. Coke content as a function of TOS for different feeds in the MTD reaction; Reaction conditions: space time of 75 g_{cat}·s/$mmol_{CH3OH}$. Experimental data (points) and calculated (lines)

Once coke content as a function of TOS was successfully modeled, it was used to obtain a deactivation function, which was added to every rate equation, as is shown in eq. 3.62. The expression of the deactivation function Φ_i is represented in eq. 3.63

$$r_i = r_i^0 \cdot \Phi_i\,(C_{coke}) \tag{3.62}$$

$$\Phi_i = \exp\,(-\alpha_i \cdot C_{coke}) \tag{3.63}$$

Where r_i^0 is the rate at zero time on stream for the i product, i.e. DME, CH_4 or CO, and they were predicted by the kinetic model previously developed; and $\Phi_i(C_{coke})$ is the corresponding deactivation function. As can be seen, this deactivation function depends on the coke content,

UNIVERSIDAD DE MÁLAGA

which is a function of TOS and was predicted by eq. 3.57. Finally, α_i is the deactivation constant, which represents the sensitivity of the reaction rate towards deactivation by coke deposition.

The reaction rates for DME, CO and CH_4 as a function of TOS have been determined experimentally at different operating conditions (temperatures, space time, methanol and water inlet pressures) and integrated to obtain the product yields. The least square differences between the experimental reaction rates and the ones predicted by the coke formation model, considering deactivation (Eq. 3.62-63), were minimized again using the algorithm previously mentioned.

Figure 3. 32 shows DME, methane and CO experimental yields (points) as a function of TOS for different reaction conditions and the calculated ones (lines) obtained from the model using the best fitting parameters. It should be noted that the outlet concentrations showed like an induction period, before reaching a semi-steady state, from where the product yield started to show a decay with TOS. The model provides a good description of the decrease in the kinetic rate with TOS, showing a strong reduction in yield for CO and methane, and a soft deactivation for DME yields. It is interesting to highlight that the deactivation constant for methane and CO presented rather similar values, $3.18 \cdot 10^{-1}$, meanwhile a value of $3.51 \cdot 10^{-10}$ was obtained for DME. This result clearly points out that methane and CO are produced through the same reaction pathway, which is severely affected by coke content because coke itself is the final product. In contrast, deactivation of DME production needs a higher amount of coke to achieve the same deactivation degree, and the deactivation could be probably caused by indirect mechanisms, like pore blockage by coke deposition. In this sense, the rate decay for CO and CH_4 is larger with TOS as temperature increases, whereas DME shows small sensitivity to the formation of coke. This latter result seems to confirm that the DME reaction pathway is unconnected to the coke formation in this catalyst. This clear differentiated behaviour might be explained whether mainly methanol and not DME was the main route for coke formation. However, more studies would be needed in order to clarify this point.

UNIVERSIDAD DE MÁLAGA

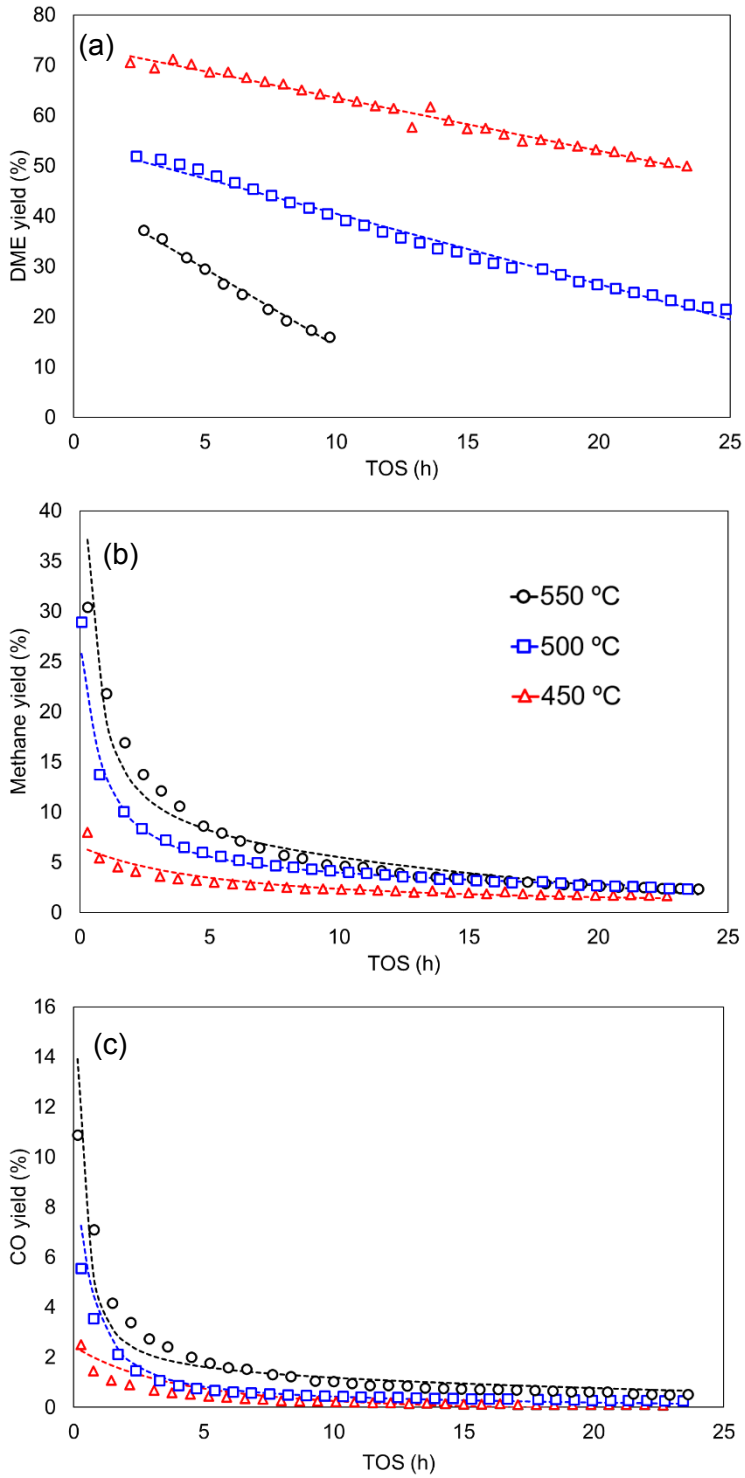

UNIVERSIDAD DE MÁLAGA

Figure 3. 32. a) DME, b) methane and c) CO yield as a function of TOS at different temperatures. Reaction conditions: methanol partial pressure of 0.04 atm and a space time of 75 g_{cat}·s/$mmol_{CH3OH}$

3.3.4. Conclusion

An activated carbon prepared by chemical activation of olive stone waste with phosphoric acid was used as support of a Zr catalyst. This Zr-loaded P-containing biomass-derived activated carbon catalyst (ACPZr) has been tested for methanol dehydration in a wide range of temperature, including those temperatures that produce a very high methanol conversion, closer to those used in the industrial process. The catalyst has shown an excellent performance with high stability and selectivity to DME at temperatures lower than 450 ºC. The conversion of methanol was very high (100%) at higher temperatures and reaction products were mainly DME and in less extent coke, methane, hydrogen and CO, with DME yields higher than 20%, for more than 24 h at 500 ºC.

A kinetic model taking into account the production of the main carbonaceous products (DME, methane, CO and coke) has been proposed, including the inhibition effect of water. The stoichiometric rates pointed out that coke could be produced through a formaldehyde intermediate, which can also decompose into CO. Addition of inlet water affects negatively to the DME production, with a reduction of around 50% for DME yield when a 10% of water was cofed. However, the presence of water did not affect the coke production at temperatures between 450 ºC and 550 ºC.

The model proposed in this work follows a Langmuir-Hinshelwood mechanism, in which two methanol molecules are adsorbed with different adsorption enthalpy values, being the surface reaction, the rate determining step. The model successfully predicts methanol conversion as well as DME, methane and CO yields. The activation energy for DME production was around 65 kJ/mol and that for methane around 51 kJ/mol, in the range 450-550 ºC. The results of the kinetic model allowed to conclude that the water inhibition is mainly related to the formation of methanol through the reverse reaction.

On the other hand, coke formation as a function of TOS was also modelled using an empirical equation, which described very well the coke formation rate using a n^{th} order rate equation, showing an activation energy of 130 kJ/mol and a reaction order close to one. The

UNIVERSIDAD DE MÁLAGA

resulting rate equation of coke formation with TOS was successfully used as the input for the deactivation function of the model, allowing to predict successfully the DME, CH_4 and CO yields in the whole range of TOS evaluated. The similar deactivation rate values obtained for CH_4 and CO confirms that both products are related to coke formation. The lower deactivation rate observed for DME might be related to its higher activation energy, which results in a faster increase of the DME rate with temperature.

References

1. Fortune Business Insight, Dimethyl Ether Market Size, Share & COVID-19 Impact Analysis, By Application (LPG Blending, Aerosol Propellant, Transportation Fuel, and Others), and Regional Forectas, 2021-2028, (2021). https://www.fortunebusinessinsights.com/dimethyl-ether-market-104309 (accessed August 18, 2021).

2. M. Lu, Z. Fu, X. Yuan, G. Sun, G. Jia, Study of the reduced kinetic mechanism of methane/dimethyl ether combustion, Fuel. 303 (2021) 121308. https://doi.org/10.1016/J.FUEL.2021.121308.

3. S. Poto, F. Gallucci, M. Fernanda Neira d'Angelo, Direct conversion of CO2 to dimethyl ether in a fixed bed membrane reactor: Influence of membrane properties and process conditions, Fuel. 302 (2021) 121080. https://doi.org/10.1016/J.FUEL.2021.121080.

4. K. Saravanan, H. Ham, N. Tsubaki, J.W. Bae, Recent progress for direct synthesis of dimethyl ether from syngas on the heterogeneous bifunctional hybrid catalysts, Appl. Catal. B Environ. 217 (2017) 494–522. https://doi.org/10.1016/j.apcatb.2017.05.085.

5. V. V. Volkov, E.G. Novitskii, G.A. Dibrov, P. V. Samokhin, M.A. Kipnis, A.B. Yaroslavtsev, Catalytic conversion of methanol to dimethyl ether on polymer/ceramic composite membranes, Catal. Today. 193 (2012) 31–36. https://doi.org/10.1016/J.CATTOD.2012.05.017.

6. W. Alharbi, E.F. Kozhevnikova, I. V. Kozhevnikov, Dehydration of Methanol to Dimethyl Ether over Heteropoly Acid Catalysts: The Relationship between Reaction Rate and Catalyst Acid Strength, ACS Catal. 5 (2015) 7186–7193.

UNIVERSIDAD DE MÁLAGA

https://doi.org/10.1021/acscatal.5b01911.

7. S.S. Akarmazyan, P. Panagiotopoulou, A. Kambolis, C. Papadopoulou, D.I. Kondarides, Methanol dehydration to dimethylether over Al_2O_3 catalysts, Appl. Catal. B Environ. 145 (2014) 136–148. https://doi.org/10.1016/j.apcatb.2012.11.043.

8. S. Kim, Y.T. Kim, C. Zhang, G. Kwak, K.-W. Jun, Effect of Reaction Conditions on the Catalytic Dehydration of Methanol to Dimethyl Ether Over a K-modified HZSM-5 Catalyst, Catal. Letters. 147 (2017) 792–801. https://doi.org/10.1007/s10562-017-1981-0.

9. C. Moreno-Castilla, F. Carrasco-Marín, C. Parejo-Pérez, M.. López Ramón, Dehydration of methanol to dimethyl ether catalyzed by oxidized activated carbons with varying surface acidic character, Carbon N. Y. 39 (2001) 869–875. https://doi.org/10.1016/S0008-6223(00)00192-5.

10. M.J. Valero-Romero, E.M. Calvo-Muñoz, R. Ruiz-Rosas, J. Rodríguez-Mirasol, T. Cordero, Phosphorus-Containing Mesoporous Carbon Acid Catalyst for Methanol Dehydration to Dimethyl Ether, Ind. Eng. Chem. Res. 58 (2019) 4042–4053. https://doi.org/10.1021/acs.iecr.8b05897.

11. J. Palomo, M.A. Rodríguez-Cano, J. Rodríguez-Mirasol, T. Cordero, On the kinetics of methanol dehydration to dimethyl ether on Zr-loaded P-containing mesoporous activated carbon catalyst, Chem. Eng. J. 378 (2019) 122198. https://doi.org/10.1016/j.cej.2019.122198.

12. J. Torres-Liñán, M. García-Rollán, J.M. Rosas, J. Rodríguez-Mirasol, T. Cordero, Deactivation of a Biomass-Derived Zirconium-Doped Phosphorus-Containing Carbon Catalyst in the Production of Dimethyl Ether from Methanol Dehydration, Energy & Fuels. (2021) acs.energyfuels.1c01721. https://doi.org/10.1021/ACS.ENERGYFUELS.1C01721.

13. J. Palomo, J. Rodríguez-Mirasol, T. Cordero, Methanol Dehydration to Dimethyl Ether on Zr-Loaded P-Containing Mesoporous Activated Carbon Catalysts, Materials (Basel). 12 (2019) 2204. https://doi.org/10.3390/ma12132204.

14. H. Marsh, F. Rodríguez-Reinoso, Activated Carbon, Elsevier, 2006. https://doi.org/10.1016/B978-0-08-044463-5.X5013-4.

UNIVERSIDAD DE MÁLAGA

15. F. Raoof, M. Taghizadeh, A. Eliassi, F. Yariopour, Effects of temperature and feed composition on catalytic dehydration of methanol to dimethyl ether over γ-alumina, Fuel. 87 (2008) 2967–2971. https://doi.org/10.1016/j.fuel.2008.03.025.

16. K. Klusáček, P. Schneider, Stationary catalytic kinetics via surface concentrations from transient data: Methanol dehydration, Chem. Eng. Sci. 37 (1982) 1523–1528. https://doi.org/10.1016/0009-2509(82)80010-9.

17. G. Bercic, J. Levec, Intrinsic and global reaction rate of methanol dehydration over γ-alumina pellets, Ind. Eng. Chem. Res. 31 (1992) 1035–1040. https://doi.org/10.1021/IE00004A010.

18. M. Migliori, A. Aloise, E. Catizzone, G. Giordano, Kinetic Analysis of Methanol to Dimethyl Ether Reaction over H-MFI Catalyst, Ind. Eng. Chem. Res. 53 (2014) 14885–14891. https://doi.org/10.1021/IE502775U.

19. K.S. Ha, Y.J. Lee, J.W. Bae, Y.W. Kim, M.H. Woo, H.S. Kim, M.J. Park, K.W. Jun, New reaction pathways and kinetic parameter estimation for methanol dehydration over modified ZSM-5 catalysts, Appl. Catal. A Gen. 395 (2011) 95–106. https://doi.org/10.1016/J.APCATA.2011.01.025.

20. C. Ortega, M. Rezaei, V. Hessel, G. Kolb, Methanol to dimethyl ether conversion over a ZSM-5 catalyst: Intrinsic kinetic study on an external recycle reactor, Chem. Eng. J. 347 (2018) 741–753. https://doi.org/10.1016/j.cej.2018.04.160.

21. G. Pop, G. Bozga, R. Ganea, N. Natu, Methanol Conversion to Dimethyl Ether over H-SAPO-34 Catalyst, Ind. Eng. Chem. Res. 48 (2009) 7065–7071. https://doi.org/10.1021/IE900532Y.

22. S. Alamolhoda, M. Kazemeini, A. Zaherian, M.R. Zakerinasab, Reaction kinetics determination and neural networks modeling of methanol dehydration over nano γ-Al2O3 catalyst, J. Ind. Eng. Chem. 18 (2012) 2059–2068. https://doi.org/10.1016/J.JIEC.2012.05.027.

23. S. Hosseininejad, A. Afacan, R.E. Hayes, Catalytic and kinetic study of methanol dehydration to dimethyl ether, Chem. Eng. Res. Des. 90 (2012) 825–833. https://doi.org/10.1016/j.cherd.2011.10.007.

24. B.C. Gates, L.N. Johanson, Langmuir-hinshelwood kinetics of the

UNIVERSIDAD DE MÁLAGA

dehydration of methanol catalyzed by cation exchange resin, AIChE J. 17 (1971) 981–983. https://doi.org/10.1002/AIC.690170435.

25. W. An, K.T. Chuang, A.R. Sanger, Dehydration of Methanol to Dimethyl Ether by Catalytic Distillation, Can. J. Chem. Eng. 82 (2004) 948–955. https://doi.org/10.1002/CJCE.5450820510.

26. M. Mollavali, F. Yaripour, H. Atashi, S. Sahebdelfar, Intrinsic Kinetics Study of Dimethyl Ether Synthesis from Methanol on γ-Al2O3 Catalysts, Ind. Eng. Chem. Res. 47 (2008) 3265–3273. https://doi.org/10.1021/IE800051H.

27. E.-Y. Lee, Y.-K. Park, O.-S. Joo, and K.-D. Jung, Methanol dehydration to produce dimethyl ether over g -Al 2 O 3, React. Kinet. Catal. Lett. 2006 891. 89 (2006) 115–121. https://doi.org/10.1007/S11144-006-0093-4.

28. L. Zhang, H. Zhang, W. Ying, D. Fang, Dehydration of methanol to dimethyl ether over γ-Al2O3 catalyst: Intrinsic kinetics and effectiveness factor, Can. J. Chem. Eng. 91 (2013) 1538–1546. https://doi.org/10.1002/CJCE.21760.

29. I. Sierra, J. Ereña, A.T. Aguayo, A. Ateka, J. Bilbao, Kinetic Modelling for the Dehydration of Methanol to Dimethyl Ether over γ -Al2O3, Chem. Eng. Trans. 32 (2013) 613–618.

30. D. Chen, H.P. Rebo, A. Grønvold, K. Moljord, A. Holmen, Methanol conversion to light olefins over SAPO-34: kinetic modeling of coke formation, Microporous Mesoporous Mater. 35–36 (2000) 121–135. https://doi.org/10.1016/S1387-1811(99)00213-9.

31. G. Qi, Z. Xie, W. Yang, S. Zhong, H. Liu, C. Zhang, Q. Chen, Behaviors of coke deposition on SAPO-34 catalyst during methanol conversion to light olefins, Fuel Process. Technol. 88 (2007) 437–441. https://doi.org/10.1016/J.FUPROC.2006.11.008.

32. O. Levenspiel, Chemical reaction engineering, 3rd ed., John Wiley and Sons Inc., 1999. https://doi.org/10.1021/ie990488g.

33. P. Pérez-Uriarte, A. Ateka, A.G. Gayubo, T. Cordero-Lanzac, A.T. Aguayo, J. Bilbao, Deactivation kinetics for the conversion of dimethyl ether to olefins over a HZSM-5 zeolite catalyst, Chem. Eng. J. 311 (2017) 367–377.

UNIVERSIDAD DE MÁLAGA

https://doi.org/10.1016/J.CEJ.2016.11.104.

34. A.G. Gayubo, A.T. Aguayo, M. Olazar, R. Vivanco, J. Bilbao, Kinetics of the irreversible deactivation of the HZSM-5 catalyst in the MTO process, Chem. Eng. Sci. 58 (2003) 5239–5249. https://doi.org/10.1016/J.CES.2003.08.020.

35. M.B. Fichtl, D. Schlereth, N. Jacobsen, I. Kasatkin, J. Schumann, M. Behrens, R. Schlögl, O. Hinrichsen, Kinetics of deactivation on Cu/ZnO/Al2O3 methanol synthesis catalysts, Appl. Catal. A Gen. 502 (2015) 262–270. https://doi.org/10.1016/J.APCATA.2015.06.014.

36. G.F. Froment, K.B. Bischoff, J. De Wilde, Chemical Reactor Analysis and Design, 3rd ed., John Wiley & Sons, 2011.

37. Y. Gao, S.L. Chen, Y. Wei, Y. Wang, W. Sun, Y. Cao, P. Zeng, Kinetics of coke formation in the dimethyl ether-to-olefins process over SAPO-34 catalyst, Chem. Eng. J. 326 (2017) 528–539. https://doi.org/10.1016/j.cej.2017.05.158.

38. E. Simón, J.M. Rosas, A. Santos, A. Romero, Study of the deactivation of copper-based catalysts for dehydrogenation of cyclohexanol to cyclohexanone, Catal. Today. 187 (2012) 150–158. https://doi.org/10.1016/J.CATTOD.2011.10.010.

39. E.M. Calvo-Muñoz, F.J. García-Mateos, J.M. Rosas, J. Rodríguez-Mirasol, T. Cordero, Biomass Waste Carbon Materials as adsorbents for CO2 Capture under Post-Combustion Conditions, Front. Mater. 0 (2016) 23. https://doi.org/10.3389/FMATS.2016.00023.

40. M. Thommes, K. Kaneko, A. V Neimark, J.P. Olivier, F. Rodriguez-Reinoso, J. Rouquerol, K.S.W. Sing, IUPAC Technical Report Physisorption of gases, with special reference to the evaluation of surface area and pore size distribution (IUPAC Technical Report), Pure Appl. Chem. 87 (2015) 1051–1069. https://doi.org/10.1515/pac-2014-1117.

41. J.S. Martinez-Espin, M. Mortén, T.V.W. Janssens, S. Svelle, P. Beato, U. Olsbye, New insights into catalyst deactivation and product distribution of zeolites in the methanol-to-hydrocarbons (MTH) reaction with methanol and dimethyl ether feeds, Catal. Sci. Technol. 7 (2017) 2700–2716. https://doi.org/10.1039/C7CY00129K.

UNIVERSIDAD DE MÁLAGA

42. V. Vishwanathan, K.W. Jun, J.W. Kim, H.S. Roh, Vapour phase dehydration of crude methanol to dimethyl ether over Na-modified H-ZSM-5 catalysts, Appl. Catal. A Gen. 276 (2004) 251–255. https://doi.org/10.1016/J.APCATA.2004.08.011.

43. S.R. Blaszkowski, R.A. Van Santen, The Mechanism of Dimethyl Ether Formation from Methanol Catalyzed by Zeolitic Protons, J. Am. Chem. Soc. 118 (1996) 5152–5153. https://doi.org/10.1021/JA954323K.

44. M. Xu, J.H. Lunsford, D.W. Goodman, A. Bhattacharyya, Synthesis of dimethyl ether (DME) from methanol over solid-acid catalysts, Appl. Catal. A Gen. 149 (1997) 289–301. https://doi.org/10.1016/S0926-860X(96)00275-X.

45. A.G. Gayubo, A.T. Aguayo, A.L. Morán, M. Olazar, J. Bilbao, Role of water in the kinetic modeling of catalyst deactivation in the MTG process, AIChE J. 48 (2002) 1561–1571. https://doi.org/10.1002/AIC.690480718.

46. J.. Figueiredo, M.F.. Pereira, M.M.. Freitas, J.J.. Órfão, Modification of the surface chemistry of activated carbons, Carbon N. Y. 37 (1999) 1379–1389. https://doi.org/10.1016/S0008-6223(98)00333-9.

47. M. Migliori, A. Aloise, G. Giordano, Methanol to dimethylether on H-MFI catalyst: The influence of the Si/Al ratio on kinetic parameters, Catal. Today. 227 (2014) 138–143. https://doi.org/10.1016/j.cattod.2013.09.033.

48. G. Zhang, X. Zhang, T. Bai, T. Chen, W. Fan, Coking kinetics and influence of reaction-regeneration on acidity, activity and deactivation of Zn/HZSM-5 catalyst during methanol aromatization, J. Energy Chem. 24 (2015) 108–118. https://doi.org/10.1016/S2095-4956(15)60291-1.

UNIVERSIDAD DE MÁLAGA

UNIVERSIDAD
DE MÁLAGA

RESUMEN

Alcance de esta tesis

La búsqueda de combustibles alternativos a los combustibles fósiles, que sean renovables y no contribuyan al aumento del efecto invernadero, es la fuerza impulsora para el desarrollo de esta tesis. En particular, la tesis se centra en el estudio de catalizadores de origen biomásico para la producción de dimetileter (DME), compuesto de gran interés industrial como sustituto del diésel convencional o los gases licuados del petróleo. Se estudió por tanto el desempeño de un catalizador carbonoso que contiene fósforo y circonio en su superficie, en condiciones de trabajo de alta conversión (elevada temperatura y largos tiempo de reacción).

Esta tesis por tanto se estructura en 3 capítulos. El primero de ello es una introducción que plantea, en un primer momento, la motivación que ha llevado a la realización de esta tesis, para después mostrar el estado del arte de este tipo de procesos. El segundo capítulo plantea los principales métodos experimentales empleados en el trabajo, así como las instalaciones y técnicas de caracterización. El capítulo tercero, desarrolla los resultados y la discusión suscitada tras el análisis de los resultados. En concreto, la sección 3.1 se fundamenta en el proceso de oxidación y descomposición de la superficie de carbones activados con fósforo en su composición. La sección 3.2 explora la desactivación de un catalizador carbonoso con fósforo y circonio, complementando este estudio con el trabajo presentado en la sección 3.3, en el que se presenta un modelo cinético de dicho catalizador. Finalmente, se concluye con un apartado que enumera las principales conclusiones obtenidas a partir de esta tesis, así como posibles trabajos derivados de los resultados obtenidos.

Introducción

El estilo de vida de la sociedad moderna requiere compuestos químicos y energía que, a día de hoy, se obtienen a partir de combustibles fósiles. En cuestiones energéticas, estos combustibles fósiles (petróleo, gas natural y carbón mineral) representan casi un 80 % del consumo de energía primaria. Además, con el desarrollo en la calidad de vida de ciertos territorios, se espera un incremento en la demanda de energía de alrededor de un 50 % para el año 2050, un incremento de demanda energética que las renovables por si solas no parece que puedan

UNIVERSIDAD DE MÁLAGA

asumir, por lo que, sin vías alternativas, el consumo de combustibles fósiles también se incrementará. Además, estos combustibles fósiles, en especial el petróleo, son una de las materias químicas más empleadas para la producción de plásticos, tintes, detergentes, y reactivos.

Por todo lo anterior, la dependencia actual de los combustibles fósiles y, en especial, del petróleo es muy alta. Esto conlleva una serie de problemas. El primero de ellos es la contaminación por la emisión de gases de efecto invernadero, como el CO_2, y que está provocando un problema de calentamiento global. Se propone para ello la reducción de estas emisiones, promulgadas por el Acuerdo Internacional de París. Otros importantes problemas son el agotamiento de estos combustibles fósiles (que se estima de 30 años para el petróleo, 40 para el gas y 70 para el carbón), así como la concentración de estas reservas en un escaso número de países que marcan su precio, dejando que esos países tengan una gran influencia económica en el resto.

Una posible solución a estos problemas es la implantación de biorrefinerías, que permite obtener todos los combustibles y productos de interés industrial obtenidos en una refinería de petróleo, pero empleando como materia prima biomasa renovable. De esta forma no se contribuye al incremento neto de CO_2 y se distribuye de forma más amplia entre países la capacidad de generar la materia prima (biomasa) para este tipo de industrias. No obstante, solo las biorrefinerías de 2ª generación, que emplean biomasa lignocelulósica residual como materia prima podrían implantarse en un periodo breve de tiempo y de forma que no dañe las reservas mundiales de alimento.

Aplicando este concepto de biorrefinería, el DME se plantea como un prometedor sustituto renovable del diésel convencional, pues presenta un índice de cetano mayor al diesel, su empleo en motores de combustión interna no emite partículas ni humos y emite menores cantidades de NO_x. El DME también se puede emplear como sustituto de los gases licuados del petróleo (GLP), pues comparte características similares a este y podría aprovecharse de la infraestructura ya planteada para los GLP. Debido a su volatilidad, se puede emplear como combustible en turbinas de generación eléctrica o como propelente de aerosoles. Además, debido a su alto ratio H/C, es un buen candidato como vector de hidrógeno. Por último, el DME también se puede emplear como molécula plataforma, siendo materia prima para la producción de olefinas, gasolinas y varios compuestos de interés industrial.

UNIVERSIDAD DE MÁLAGA

La obtención de DME se puede realizar por la que se conoce como “vía indirecta” o por “via directa”. En la vía indirecta, en una primera etapa se obtiene metanol a partir de gas de síntesis, en catalizadores de Cu-ZnO/Al_2O_3.Posteriormente, en una segunda etapa, se deshidrata ese metanol para producir DME. Industrialmente se emplea para ello γ-Al_2O_3, pues este tipo de catalizadores deben presentar una acidez moderada (si la acidez es muy fuerte, se forman olefinas y otros hidrocarburos). Otros catalizadores que presentan gran potencial en deshidratación de metanol son ciertas zeolitas (en especial la HZSM5), fosfatos metálicos de aluminio, silicio-alumino (SAPO) o zirconio, heteropoliácidos (HPA), resinas de intercambio iónico, e incluso ciertos óxidos metálicos.

Aunque la producción industrial se lleve a cabo por el método indirecto, se está promocionando en la actualidad el denominado método directo, en el cual, en un mismo reactor, partiendo de gas de síntesis, se obtiene directamente DME. Para este proceso se requieren catalizadores bifuncionales que deben presentar una fase metálica y una fase ácida, consiguiendo de esta forma desplazar el equilibro hasta la formación de DME y pudiendo suavizar las condiciones de reacción. Los catalizadores empleados para este proceso suelen ser mezclas físicas de los catalizadores empleados en el método indirecto, aunque se están estudiando nuevos métodos de preparación (coprecipitación, sol-gel, electrohilado) que den más rendimiento a DME. Destaca entre todos ellos el concepto de “core-shell”, en el que la fase metálica se encuentra en el interior, recubierto por la fase ácida, obligando así a que el metanol sintetizado pase por la fase ácida donde se realiza su deshidratación.

Similar a la producción de DME a partir de gas de síntesis, en los últimos años, se está estudiando la producción de DME a partir de CO_2, lo que permitiría obtener un combustible renovable a partir este gas de efecto invernadero. Este es un proceso más complejo que la conversión del gas de síntesis, pero para el cual se emplean catalizadores similares, modificados para maximizar la conversión de CO_2.

Otro de los productos de alto interés industrial que se pueden obtener a partir de una biorrefinería son los carbones activos. Estos materiales, empleados tradicionalmente como adsorbentes o soportes catalíticos, presentan una porosidad muy desarrollada y cuyo proceso de activación (generación de porosidad) puede modificarse para adecuarse a unas necesidades determinadas. Los procesos de activación pueden dividirse entre los físicos (gasificación parcial con oxidantes como CO_2 o vapor de agua) o los químicos (pirólisis en presencia de un agente activante, como $ZnCl_2$, ácido sulfúrico, KOH o

UNIVERSIDAD DE MÁLAGA

ácido fosfórico). En particular, la activación con ácido fosfórico a ciertas condiciones de operación proporciona materiales ácidos, mesoporosos y con cierta resistencia a la oxidación que también presentan propiedades catalíticas.

Por último, cuando se trabaja en condiciones industriales, un problema común es la desactivación de catalizadores, que puede dividirse en varias categorías. El envenenamiento de centros activos, que se produce por la adsorción irreversible en el centro activo de ciertos compuestos presentes en el gas de alimento. La sinterización, que consiste en la agregación de partículas catalíticas o en el colapso de estructuras por acción de la temperatura. El cambio de una fase activa a otra no activa, también por efecto de la temperatura. La migración de la fase activa, por la acción de compuestos presentes en el medio que volatilizan ciertos compuestos de la superficie del catalizador. O, por último, la deposición de coque, producido por la adsorción y polimerización de alguno de los reactivos, cubriendo el centro activo e impidiendo que realice su acción de catálisis. Este último tipo de desactivación, observado en catalizadores ácidos, presenta por lo general un carácter reversible, puesto que se pueden gasificar los depósitos de coque empleando una corriente oxidante y por ello es de gran utilidad la cuantificación tanto del carbón depositado como del efecto reductor de actividad en el catalizador.

Objetivo

En la búsqueda de la sostenibilidad global, el uso de catalizadores renovables para producir combustibles renovables que no contaminen es una alternativa interesante. Por ello, en esta tesis se ha estudiado un catalizador carbonoso con fósforo en la reacción de metanol a dimetiléter (MTD) en condiciones donde la conversión sea alta.

En particular, se estudió el proceso de oxidación-descomposición de los grupos C-P/C-O-P de la superficie del carbón, que presentan características catalíticas en la reacción MTD, así como la capacidad de dotar al catalizador de una alta resistencia a la oxidación, muy útil durante el proceso de regeneración.

Debido a las condiciones de alta conversión estudiadas, los catalizadores carbonosos con P y Zr sufren de desactivación por deposición de coque, desactivación que se pretende estudiar para mejorar el proceso de síntesis de los catalizadores y sus condiciones de reacción, así como su posible regeneración.

UNIVERSIDAD DE MÁLAGA

Metodología experimental

Para la preparación del carbón activo con fósforo se ha empleado hueso de aceituna como precursor carbonoso. Este precursor se puso en contacto con ácido fosfórico (ratio másico 2:1 ácido:hueso) durante una noche en estufa a 60 ºC y posteriormente se sometió a 800 ºC (rampa de calentamiento 10 ºC/min) en un horno tubular con un flujo de nitrógeno (150 cm^3/min) durante 2 h. Posteriormente se lavó con agua destilada a 60 ºC hasta pH constante en el agua de lavado y se tamizó entre 100-300 µm. Este carbón se impregnó con oxinitrato de zirconio para obtener una cantidad másica final de Zr del 5.25 % en el catalizador y se estabilizó en una mufla a 250 ºC por 2 h.

Para la caracterización de los materiales se emplearon las siguientes técnicas: isoterma de adsorción-desorción de nitrógeno a -196 ºC y de absorción de CO_2 a 0 ºC; Espectrometría fotoelectrónica de rayos X (XPS); desorción térmica programada (TPD) en atmósfera inerte; y espectroscopía de resonancia nuclear en el ángulo mágico (MAS-NMR).

Los experimentos de oxidación del carbón se llevaron a cabo en 50 mg de carbón en un reactor de cuarzo de 4 mm de diámetro interno tras un tratamiento térmico en 200 cm^3/min de He a 1000 ºC. La oxidación se realizó con una corriente de un 3 % de oxígeno en nitrógeno con un caudal de 100 cm^3/min. La temperatura varió de 30 a 340 ºC y el tiempo de 30 s a 24 h.

Los experimentos catalíticos de deshidratación de metanol se realizaron en el mismo reactor de cuarzo (4 mm d.i.) en el que se introdujeron de 50 a 300 mg de catalizador. Se mantuvo una corriente de 70 cm^3/min de nitrógeno donde se varió la concentración de 0.015 a 0.08 atm de metanol y la temperatura de 450 a 600 ºC. La cuantificación se realizó en un micro-GC con columnas de tamiz molecular, PPQ and wax. El coque se cuantificó por pesada. Los experimentos de regeneración se llevaron a cabo con una corriente de 70 cm^3/min de aire a 350 ºC durante 2 h.

Resultados y discusión

En la primera parte de este capítulo, se aborda el proceso de oxidación de un carbón activo con fósforo, así como la descomposición de sus grupos superficiales, siendo el grupo C-P/C-O-P el de mayor interés pues dota a los catalizadores de una elevada resistencia a la oxidación.

UNIVERSIDAD DE MÁLAGA

La caracterización mediante isotermas de estos materiales carbonosos mostró una desarrollada textura porosa (A_{BET} de 1232 m_2/g), con una mayor predominancia del microporo ancho (0.7-2 nm) frente a los estrechos. La caracterización por XPS mostró la presencia de un 1.1 % atómico de fósforo, que permanecían en el carbón incluso tras un tratamiento térmico a 1000 ºC, y que estaban en la forma de grupos C-P y C-O-P. Además, tras el tratamiento a 1000 ºC aun presentaba entorno a un 7 % másico de oxígeno, que se puede achacar a la oxidación de varios grupos C-P en el manejo de la muestra hasta el análisis XPS.

Por análisis TPD se obtuvieron los grupos superficiales del carbón con fósforo. Para corroborar que no hubiera problemas en la instalación, se realizaron dos TPD consecutivas, observándose una cantidad despreciable de grupos oxigenados tras la segunda TPD. Los grupos detectados y que evolucionan como CO son, en orden creciente de máximo de temperatura de evolución, aldehídos, anhídridos, fenol/eter, carbonil/quinona y grupos C-O-P. Los que evolucionan como CO_2 serían los ácidos carboxílicos, anhídridos, lactonas y grupos de fósforo O=C-O-P. La primera gran diferencia que se observa es la diferencia entre las cantidades que evolucionan como CO y las de CO_2, que son unas 15 veces inferiores. Esto se relaciona directamente con la poca presencia de grupos oxígeno-carbón ácidos, frente al resto de grupos oxígeno-carbón, siendo por tanto el grupo C-O-P el que aporta la acidez del carbón.

Basado en el análisis TPD se planteó un estudio cinético no isotermo para la evolución de cada grupo funcional en CO_x. Las asunciones que se tuvieron en cuenta fueron que no hubiera limitaciones a la transferencia de calor ni materia y flujo ideal. Para el modelo cinético se partió de la ecuación del reactor tipo Batch y la ecuación no-isoterma de Arrhenius.

$$(-R_i) = N_{i,0}\frac{dX_i}{dt}$$

$$k_i = k'_{0,i} \cdot exp\left(\frac{-E_{a,i}}{R \cdot (T_0 + \beta \cdot t)}\right)$$

donde $-R_i$ es la velocidad de descomposición del grupo i (µmol/g·s), $N_{i,0}$ el número de moles de ese grupo funcional i (µmol/g), X_i es la conversión de ese grupo funcional i y t el tiempo (s) ; k_i es la constante cinética de velocidad, $k'_{0,i}$ es el factor preexponencial y $E_{a,i}$ (kJ/mol) la energía de activación del grupo i, R la constante ideal de los gases

UNIVERSIDAD DE MÁLAGA

(J/mol·K), T_0 la temperatura inicial (K) y β la velocidad de calentamiento (º C/min).

Asumiendo que cada una de las reacciones de descomposición transcurre independiente del resto de reacciones y descritas por una ecuación de primer orden, la ecuación que describe cada reacción es:

$$\frac{dX_i}{dt} = k_{i,0} \cdot \exp\left(\frac{-E_{a,i}}{R \cdot (T_0 + \beta \cdot t)}\right) \cdot (1 - X_i)$$

Las energías de activación obtenidas para la descomposición de los diferentes grupos funcionales se muestran en la siguiente tabla:

Grupo	E_a (kJ/mol)	k_0 (s^{-1})
L Acido carboxílico	42	456
H Acido carboxílico	30	1.0
Aldehído	45	395
Anhídrido	62	66
Fenol/éter	93	386
Lactona	55	1.2
Carbonilo/Quinona	97	94
Fósforo (CO)	249	$9.22 \cdot 10^8$
Fósforo (CO_2)	259	$4.60 \cdot 10^9$

Se observa que a mayores temperaturas para la máxima velocidad de evolución de ese grupo funcional a CO_x también aumenta la energía de activación de descomposición de ese grupo funcional.

La oxidación de la superficie limpia (tratada en helio a 1000 ºC) mostró que conforme se aumentaba la temperatura (de 25 a 340 ºC) o el tiempo de oxidación (de 30 s 24 h), el grupo asociado con los C-O-P también aumentaba hasta estabilizarse a 300 ºC y 12 h de oxidación, cantidad que no variaba aunque se aumentara la temperatura, sugiriendo la saturación de dicho grupo. Además, a esas temperaturas se observaba una clara presencia de los grupos carbonil/quinona y fenol/éter.

UNIVERSIDAD DE MÁLAGA

La cantidad de los diferentes grupos oxígeno-carbón se cuantificó mediante TPD y se realizó un estudio cinético para el cual se empleó la ecuación de Elovich:

$$q_i = \frac{1}{b} \cdot \ln(\, a_i \cdot b_i \cdot t + 1)$$

$$a_i = \frac{k'_i}{b_i} \cdot \exp\left(-\frac{E_{a_i}}{R \cdot T}\right) ;\; b_i = \frac{\alpha}{R \cdot T}$$

donde q_i es la cantidad de ese grupo i (mmol/g), t es el tiempo (min), a_i la velocidad inicial del grupo i y b_i una constante relacionada con la heterogeneidad del catalizador; k'_i es el factor preexponencial, $E_{a,i}$ la energía de activación, R la constante de los gases ideales (J/mol·K), T la temperatura (K) y α la constante de heterogeneidad. A partir de esto las energías de activación para la oxidación de la superficie del carbón y la formación de grupos oxígeno-carbón es:

Grupo	$\mathbf{E_a\ (kJ/mol)}$	$\mathbf{k_0}$	$\boldsymbol{\alpha}$
Suma total	42	$2.36 \cdot 10^9$	$2.39 \cdot 10^4$
C-O-P	13	$1.30 \cdot 10^7$	$4.36 \cdot 10^4$
Carbonil/Quinona	73	$4.74 \cdot 10^{11}$	$1.05 \cdot 10^5$
Éter	79	$1.50 \cdot 10^6$	$5.12 \cdot 10^4$
Anhídrido	58	$3.54 \cdot 10^3$	$3.38 \cdot 10^5$
Lactona	61	$1.85 \cdot 10^4$	$1.05 \cdot 10^5$

Se observa un valor muy bajo para la oxidación de los grupos C-P a C-O-P, lo que explicaría su oxidación durante el manejo hasta el análisis XPS. Esto parece indicar que se requiere que todos los grupos C-P se encuentren oxidados en la forma C-O-P para que el oxígeno reaccione con la superficie del carbón y forme otros grupos oxígeno-carbón, explicando así por qué la presencia de estos grupos de fósforo aumenta la resistencia a la oxidación. En concreto, se debe a la necesidad de una alta temperatura para que esos grupos C-O-P se descompongan y, como se ha visto, en presencia de grupos C-P se impide la formación de otros grupos oxigenados que evolucionarían a CO_x a menores temperaturas.

UNIVERSIDAD DE MÁLAGA

La segunda parte del capítulo 3 aborda el empleo de catalizadores carbonosos de fósforo y circonio en la reacción de deshidratación de metanol, con la finalidad de obtener un combustible renovable como el DME, empleando además un catalizador altamente selectivo a DME obtenido a partir de biomasa residual. En concreto, se estudiaron condiciones de elevada conversión, similares a las que se emplean en la industria.

Este catalizador se sintetizó mediante la impregnación con circonio de un carbón activado que contenía fósforo. La caracterización del catalizador mediante isotermas de nitrógeno mostró una isoterma tipo IV(a) con histéresis tipo H4, con un gran desarrollo de la porosidad del catalizador, con un área BET de 1130 m^2/g, mientras que el área de microporo estrecho era de 476 m^2/g. El análisis XPS mostró la presencia mayoritaria de carbón y de alrededor de un 4.4 % de fósforo y un 3.9 % de zirconio atomicos. Los grupos superficiales detectados en el espectro del P eran C-O-P-O_3 principalmente y cantidades similares de C-P-O y fosfato/pirofosfato de circonio. En el espectro del Zr se observa fosfato de circonio y pirofosfato de circonio (en menor medida).

En los experimentos de reacción a diferentes temperaturas (presión parcial de metanol de 0.04 y tiempo espacial de 75 $g_{cat}{\cdot}s/mmol_{CH_3OH}$) se observa que, a temperaturas inferiores a 450 ºC, tras un breve periodo de inducción la conversión se mantiene constante durante al menos 40 h. Sin embargo, a temperaturas mayores a 450 ºC se observa una ligera caída en la conversión con el tiempo, que se intensifica a medida que se aumenta la temperatura. Se observa además como en los primeros momentos la conversión de metanol supera el equilibrio metanol-DME, lo que sugiere la presencia de reacciones secundarias.

Si se centra la atención en la selectividad, se observa que a temperaturas inferiores a 450 ºC, la selectividad es total a DME. A 450 ºC, esta selectividad decae ligeramente, pero se mantiene en torno a un 90 % durante más de 24 h. A 550 ºC este valor disminuye a un 60 %, siendo apreciables las selectividades a coque y metano. Esta presencia de reacciones secundarias se confirma observando la cantidad de DME y agua: a 400 ºC y 450 ºC ambas curvas presentan la misma concentración, mientras que a 550 ºC la cantidad de agua es superior a la de DME. Además, a esos 550 ºC, la concentración de CO e H_2 es, aunque baja, similar. Ciertos estudios previos en fosfato de circonio parecen indicar que la desactivación podría venir por la presencia de un intermediario similar al formaldehido que

UNIVERSIDAD DE MÁLAGA

posteriormente descompone en coque y agua (mayoritariamente) o CO e H_2.

La caracterización de las muestras parcialmente desactivadas determinó que había una disminución en la porosidad a medida que se aumentaba el tiempo de reacción y con ello la cantidad de coque depositada, y que está perdida era mayoritariamente en el microporo. Además, la concentración por XPS muestra que disminuyen las especies superficiales tanto de fósforo como de circonio con el tiempo de reacción, a medida que aumenta la de carbono. La reacción a 450 ºC durante 15 h disminuye eminentemente los grupos C-P-O y C-O-P_3, observables en el espectro XPS del P. En el espectro XPS del Zr se observa también una caída de las especies de fosfato de circonio, pero un ligero aumento de las de pirofosfato de circonio.

A fin de eliminar los depósitos de coque presente en las muestras se realizó una gasificación de los catalizadores parcialmente desactivados (a 450 ºC o 550 ºC) en aire a 350 ºC durante 2 h. Tras el proceso de regeneración de ambas muestras desactivadas a diferentes temperaturas, los catalizadores mostraban un aumento de conversión, pero este decaía al valor anterior a la regeneración tras unas 3 h. Esto se achaca a la presencia adicional de grupos de fósforo no unidos al circonio. Estos grupos presentan también poder catalítico en la reacción de deshidratación de metanol, pero pierden su actividad muy rápidamente, como se corrobora al comparar las muestras regeneradas con el soporte (carbón con fósforo). Sin embargo, estos grupos de fósforo en forma de C-O-PO, aunque pierden su actividad en 2-3 h, parecen ser regenerables mediante el proceso de oxidación con aire.

Con todo lo anterior se supone la presencia de dos grupos activos en el catalizador, los grupos de fósforo que se desactivan muy rápidamente pero pueden regenerarse, y los grupos de fosfato de circonio, que son los que dotan al catalizador de una actividad mantenida en el tiempo, pero una vez desactivados, no se pueden regenerar. Esto se corroboró mediante la realización de varios ciclos de reacción a 450 ºC-regeneración en aire a 350 ºC, puesto que tras cada regeneración aumentaba inicialmente la conversión, pero volvía al valor que tendría sin regenerar tras unas 2 h.

La caracterización mediante isotermas de las muestras tratadas con aire mostró una gasificación casi despreciable del coque. Esto está en consonancia con lo mostrado en los rendimientos de gasificación, puesto que la cantidad gasificada en la muestra desactivada (4 %) coincide con la cantidad gasificada cuando se somete el soporte a la

UNIVERSIDAD DE MÁLAGA

gasificación en las mismas condiciones. Esto indica la presencia de un coque muy estable térmicamente.

El análisis por TPD de las muestras parcialmente desactivadas a 450 ºC y 550 ºC muestra que no se encuentran interacciones asociadas a los grupos C-O-PO, mientras que tras su tratamiento en aire sí que se observa un hombro achacado a esos grupos C-O-PO, pero sin llegar al valor del catalizador fresco. Además, el análisis XPS muestra un aumento del fósforo en superficie, que puede deberse a cierta gasificación del coque, pero también a la del soporte, mostrando nuevos grupos de fósforo anteriormente cubiertos.

El análisis mediante ^{31}P MAS-NMR mostró un pico definido para el catalizador fresco y el soporte, asociado a fosfatos o fosfatos de circonio, así como otro de menor tamaño asociado con P-ésteres o fosfonatos. Tras mantener el catalizador en reacción, el pico asociado a P-ésteres/fosfonatos desaparece totalmente y el pico de fosfato/fosfato de circonio disminuye en gran medida. En contraposición, aumenta el grupo asociado con los grupos pirofosfato. Tras la oxidación, el grupo de fosfato/fosfato de circonio aumenta ligeramente, asociado a la oxidación de grupos C-PO en C-O-PO, como se observaba en el análisis TPD y XPS.

Con todo esto, se planteo un esquema de reacción en el que, partiendo del grupo Zr-O-P, se pueden presentar dos vías. La vía de producción de DME, en el que dos moléculas de metanol reaccionan en el sitio activo, produciendo DME, agua y la regeneración del sitio. O la otra vía, en la que a partir de las dos moléculas adsorbidas se forma un intermedio de formaldehido que, posteriormente, se descompone en coke y agua, inhabilitando el sitio activo, o en CO e H_2 (minoritariamente), regenerando también el sitio.

Por último, empleando la metodología propuesta por Froment, Bischoff and De Wilde, se planteó un modelo cinético para la cuantificación de la cantidad de coque depositado a diferentes temperaturas. Para ello, la velocidad de producción de coque (que varía con el tiempo de reacción) se igualó a una velocidad a tiempo cero de reacción multiplicado por un factor de desactivación en función de la cantidad de coque:

$$\frac{dC_c}{dt} = r_C^0 \cdot \Phi_C$$

$$\Phi_C = (1 - \alpha \cdot C_C)^2$$

UNIVERSIDAD DE MÁLAGA

En este modelo, la velocidad inicial se predijo con un pseudo primer orden:

$$r_C^0 = k_0' \cdot e^{-\frac{E_a}{R \cdot T}}$$

Empleando este modelo cinético, se obtuvieron energías de activación para la formación de coque en torno a 124 kJ/mol y una constante de desactivación α de 0.038.

El modelo planteado, cuantifica la cantidad de coque, pero no relaciona esta cantidad de coque con la disminución en la producción de DME o de los diferentes productos secundarios obtenidos. Por ellos, en la parte tercera parte de este capítulo se plantea un modelo cinético a los principales productos obtenidos que incluya la desactivación con el tiempo de reacción.

El planteamiento de estos estudios cinéticos puede ayudar a conocer la secuencia de reacción del catalizador, determinar las mejoras a realizar durante la síntesis de catalizador y definir las mejores condiciones de reacción para maximizar la producción alguno de los productos.

La caracterización del catalizador, un carbón activo con fósforo y circonio mostró una desarrollada porosidad (A_{BET} 1105 m^2/g), con gran cantidad de mesoporo. Por XPS se observó en torno a un 4 % atómico tanto de fósforo como de circonio, presentando especies C_3PO, $C{-}PO_3/C_2PO_2$, $C{-}O{-}PO_3$ y fosfato de circonio en el espectro del P y especies Zr-C, pirofosfato y fosfato de circonio para el espectro XPS del Zr.

Si se observa el comportamiento en reacción de este catalizador a 500 ºC, 0.04 atm de metanol y 75 $g_{cat}{\cdot}s/mmol_{metanol}$, inicialmente su conversión es total (superando el equilibro metanol-DME), pero decae con el tiempo. El producto principal es DME, llegando a un 50 % de rendimiento, pero que disminuye con el tiempo de reacción. Coque, metano, CO, hidrógeno y agua son también compuestos que aparecen en cantidades apreciables, pero siguiendo una tendencia similar. Por último, CO_2, etileno, etano, propileno y propano se encuentran en cantidades de trazas. Comportamientos similares se pueden observar con diferentes concentraciones (1.5-8% metanol), temperaturas (450-550ºC) y tiempos espaciales (50-100 $g_{cat}{\cdot}s/mmol_{metanol}$).

La secuencia de reacción, que también explicaría la distribución de productos mayoritarios ya se planteó anteriormente:

UNIVERSIDAD DE MÁLAGA

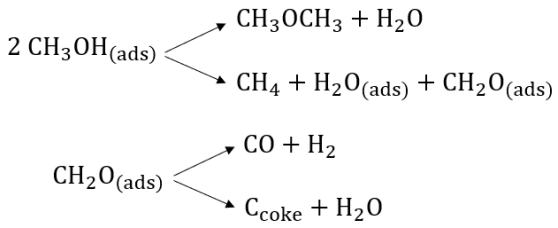

A modo de comprobación, y como el coque parecer provenir de un intermedio similar al formaldehido, este se añadió como reactivo, observándose una mayor cantidad de coque depositado.

Aunque el agua no es un reactivo en la formación de coque, se ha reportado en bibliografía su adsorción competitiva frente al metanol en los sitios activos. Por ello se estudió su influencia, observándose que al aumentar la cantidad de agua alimentada entre un 5-10 %, la conversión de metanol decaía en torno a un 30 %.

En términos de rendimiento, conforme se aumentaba la cantidad de agua, disminuía el rendimiento a DME, mientras que los rendimientos a coque, metano y CO permanecían constantes. Esto hace pensar que el principal precursor del coque en este catalizadore es el metanol, puesto que la cantidad de DME disminuye al aumentar la de agua. Todo esto parece plantear que el efecto de inhibición del agua para la producción de DME se debe a la hidrólisis del DME, reacción en equilibrio con la deshidratación de metanol hasta DME.

Antes de realizar el planteamiento del modelo cinético se realizó un estudio estequiométrico que corroborara las reacciones anteriormente planteadas. Para ello se comparó la cantidad de agua en el medio con la cantidad que debería haberse producido con la producción de DME y de coque, siendo estas muy similares en todas las temperaturas. A su vez, también se corroboró que eran similares la cantidad de metano en el medio y la cantidad que debería haberse producido de formaldehido, que rápidamente reacciona en coque y agua o CO e hidrógeno. Por último, también se observó concentraciones similares de CO e hidrógeno en el medio. Con estas comprobaciones realizadas, se planteó un modelo cinético a cero tiempo de reacción que cumpliera la secuencia de reacción propuesta.

El modelo planteado se basaba en un mecanismo Langmuir-Hinshelwood en el que se incluyen la formación a los productos carbonosos principales (DME, metano y CO) y abarcar temperaturas desde 450 a 550 ºC, concentraciones de metanol desde 0.015 a 0.08

UNIVERSIDAD DE MÁLAGA

atm y tiempos espaciales desde 50 a 100 g_{cat}·s/$mmol_{metanol}$. Para el ciclo de producción del DME, en un primer paso, una molécula se adsorbe en el centro activo. Seguidamente una segunda molécula se adsorbe en ese mismo centro, pasando al tercer paso en el que se desorbe DME y queda agua adsorbida en el centro activo. Finalmente, se desorbe agua y se regenera el centro activo. Para la formación del coque, se parte desde el punto en el que dos moléculas de metanol se encuentran adsorbidas y, en un siguiente paso se desorbe metano y se forma formaldehido, que tiene dos posibles reacciones. La primera, y principal, es su descomposición a coque y agua. La segunda, su descomposición a CO e hidrógeno.

Las asunciones tomadas fueron distribución uniforme del sitio activo y del catalizador en el lecho, flujo ideal sin gradientes, lecho isotermo y limitaciones de transferencia de masa y calor despreciables. En este supuesto la ecuación del reactor flujo pistón toma la forma:

$$-\frac{dX_i}{d\left(\frac{W}{F_{MeOH_0}}\right)} = r_i$$

Se han supuesto reacciones y adsorciones simples reversibles (salvo para la formación de metano y formaldehido), tomando la reacción superficial como velocidad determinante. Además, al ser el formaldehido un compuesto altamente reactivo, se ha considerado que su concentración en los sitios activos es despreciable. Con todo esto, la ecuación para la producción de DME es:

$$\mathrm{r_{DME}} = \mathrm{r_{13}} = \frac{\mathrm{k_{sr}} \cdot \left(\mathrm{K_{M,1}K_{M,2}P_M^2} - \frac{\mathrm{P_{DME}} \cdot \mathrm{K_W} \cdot \mathrm{P_W}}{\mathrm{K_{sr}}}\right)}{1 + \mathrm{K_{M,1}P_M} + \mathrm{K_{M,1}K_{M,2}P_M^2} + \mathrm{K_W} \cdot \mathrm{P_W}}$$

Ecuaciones similares se obtienen para la conversión de metanol y el rendimiento de metano y CO. Con estas ecuaciones se obtienen los parámetros cinéticos, determinándose energías de activación de 65 kJ/mol para la producción de DME y de 51 kJ/mol para la producción de metano. Además, la reacción de hidrólisis de DME parece tener bastante influencia, lo que corrobora el efecto de inhibición del agua previamente planteado.

La segunda parte del modelo cinético es la cuantificación del efecto en los diferentes rendimientos de la deposición de coque. Para ello, inicialmente se cuantificó el coque con la metodología propuesta por Froment, Brischops and De Wilde. Se probaron varios modelos, siendo el que mejor ajustaba los datos el siguiente:

UNIVERSIDAD DE MÁLAGA

$$C_{coke} = \frac{1}{\alpha}\left[1 - \frac{1}{1 + \alpha \cdot r_{coke}^{0} \cdot TOS}\right]$$

En esta ecuación, r_{coke}^{0} se corresponde con la ecuación de velocidad inicial de producción de coque de orden n y α con la constante de reacción. Realizando la obtención de parámetros, se obtuvo un orden de 0.79 y una energía de activación de 130 kJ/mol para la velocidad inicial, así como un factor de desactivación α de 0.038.

Finalmente, esas cantidades de coque se emplearon en una función de desactivación, que se añade al valor de velocidad a tiempo de reacción cero:

$$r_i = r_i^0 \cdot \Phi_i\,(C_{coke})$$

$$\Phi_i = \exp\,(-\alpha_i \cdot C_{coke})$$

Con estas ecuaciones aplicadas a los valores obtenidos anteriormente se obtuvo una buena correlación entre los datos experimentales y predichos por este modelo cinético.

Tras la recopilación y discusión de todos los datos mostrados en esta tesis, se puede obtener como conclusión general que la posibilidad de obtener DME es muy favorable mediante este tipo de catalizadores debido a su alta selectividad incluso en condiciones de conversión altas.

UNIVERSIDAD DE MÁLAGA

UNIVERSIDAD
DE MÁLAGA

GENERAL CONCLUSIONS AND PROSPECTS

As a general conclusion, the use of a waste biomass activated with phosphoric acid and loaded with Zr seems like a good alternative to conventional inorganic catalyst in the methanol to dimethyl ether reaction because of its high selectivity to dimethyl ether (DME) even at high-conversion operating conditions.

The catalyst support (P-containing activated carbon) has a high oxygen resistance, due to the presence of phosphorus groups, which needs for a high temperature to decompose from C-O-P to C-P and do not produce any carbon-oxygen surface groups when C-P groups are present in the carbon surface.

Moreover, the Zr/P-carbon catalyst has good characteristics as catalyst: high mesoporosity and high active phase dispersion. Those catalyst also have two different types of active groups: the phosphorus group and the zirconium-phosphate like group. Both groups were deactivated with time on stream (TOS) with the conditions tested in this thesis, but in a different way. The phosphorus one, is active only for a short time, but can be regenerated only by an air treatment. The zirconium-phosphate groups provide the catalyst with a long-term activity (as it maintains more than 50 % of methanol conversion after 24 h of TOS), but once they are deactivated, they cannot be recovered with an air treatment.

On the other hand, that coke deposition was caused by the formation of a formaldehyde type intermediate when two methanol molecules were adsorbed on the active site. That intermediate then decomposed into coke and water (mainly) o into CO and hydrogen. A kinetic model based on that reaction pathway successfully predicted the experimental data, including the competitive adsorption of water on the active site, as well as the deactivation effect with TOS of coke deposition.

UNIVERSIDAD DE MÁLAGA

Although this catalyst seems promising, some other points would need to be addressed in future works:

- The performance of those catalyst as acid counterpart of a bifunctional catalyst for syngas to DME reaction and, even a more interesting alternative, used in the reaction from CO_2 to DME or in CO_2-rich syngas.

- The reformulation of the catalyst using the kinetic model proposed to minimize the catalyst deactivation, but also use the operating condition that that kinetic model proposed.

- The complete gasification of the catalyst at the end of its catalytic life to recover the active phase and deposited on another biomass-derived support, enhancing the economy of the process.

UNIVERSIDAD DE MÁLAGA

Figure Caption

UNIVERSIDAD DE MÁLAGA

UNIVERSIDAD DE MÁLAGA

UNIVERSIDAD DE MÁLAGA

UNIVERSIDAD DE MÁLAGA

Table Caption

UNIVERSIDAD DE MÁLAGA

Scheme Caption

UNIVERSIDAD DE MÁLAGA

Curriculum Vitae

Research Articles

This work is a compendium of the following publications:

Javier Torres-Liñán, Miguel García-Rollán, Juana M. Rosas, José Rodríguez Mirasol, Tomás Cordero; Deactivation of a Biomass-Derived Zirconium-Doped Phosphorus-Containing Carbon Catalyst in the Production of Dimethyl Ether from Methanol Dehydration; Energy & Fuels 2021, 35, 21, 17225-17240. Doi: 10.1021/acs.energyfuels.1c01721

Javier Torres-Liñán, Ramiro Ruiz-Rosas, Juana María Rosas, José Rodríguez-Mirasol, Tomás Cordero; A Kinetic Model Considering Catalyst Deactivation for Methanol-to-Dimethyl Ether on a Biomass-Derived Zr/P-Carbon Catalyst; Materials 2022, 15(2), 596. Doi: 10.3390/ma15020596

Javier Torres Liñán, Alicia Villahermosa-López, Ramiro Ruiz-Rosas, Juana María Rosas, José Rodríguez-Mirasol, Tomás Cordero; On the kinetics of Oxidation and Decomposition of Phosphorus Surface groups on carbon materials; Carbon 2022. Submitted.

Other publications by the author:

Juan José Ternero-Hidalgo, Javier Torres-Liñán, María Olga Guerrero-Pérez, José Rodríguez-Mirasol, Tomás Cordero; Electrospun vanadium oxide based submicron diameter fiber catalysts. Part I: Preparation procedure and propane ODH application; Catalyst Today 2019, 325, 131-143

UNIVERSIDAD DE MÁLAGA

Congress contributions

This thesis has also generated the following congress contributions:

Javier Torres-Liñán, Juana María Rosas, Ramiro Ruiz-Rosas, José Rodríguez-Mirasol, Tomás Cordero. Catalytic performance of Zr-loaded P-containing activated carbon in the Methanol Dimethyl Ether process at high temperatures. RSEQ Symposium 2021, Online (2021)

Javier Torres-Liñán, Miguel García-Rollán, Juana María Rosas, José Rodríguez-Mirasol, Tomás Cordero. Catalyst deactivation and regeneration for MTD reaction on Zr carbon-based catalyst. 8th Invernational Conference on Carbon for Energy Storage and Environment Protection, Alicante, España (2019)

Javier Torres-Liñán, Miguel García-Rollán, Juana María Rosas, José Rodríguez-Mirasol, Tomás Cordero. On the deactivation of Zr-loading P-containing mesoporous carbon catalyst during methanol dehydration. 3rd ANQUE-ICCE 3 2019, Santander, España (2019)

Javier Torres-Liñán, Miguel García-Rollán, Juana María Rosas, José Rodríguez-Mirasol, Tomás Cordero. On the deactivation of ZrO2 supported-carbon-derived catalysts during methanol dehydration. XXIV Encontro Luso-Gallego de Química, Oporto, Portugal (2018)

Javier Torres-Liñán, Miguel García-Rollán, José Palomo-Jimenez, Juana María Rosas, José Rodríguez-Mirasol, Tomás Cordero. The world conference on Carbon, Madrid, España (2018)

UNIVERSIDAD DE MÁLAGA

Predoctoral research Internships

Department of Chemical Engineering, Norwegian University of Science and Technology (NTNU). Trondheim (Noruega)

Supervisor: Professor Hilde Johnsen Venvik

Period: From 1st September to 31st December 2020

Topic: Test catalítico de fibras de plata y zirconio en la reacción de metanol a formaldehído

UNIVERSIDAD DE MÁLAGA

UNIVERSIDAD
DE MÁLAGA

ACKNOWLEDGMENTS

Fin. Solo tres letras, pero de un profundo significado. Esas tres letras dejan atrás una etapa predoctoral cargada de buenos y malos momentos, y abren una gran puerta al futuro. Llegado este punto ya solo queda agradecer y tener unas palabras para todo aquel que de una u otra forma ha estado en esta odisea y han ayudado a que llegue hasta aquí.

En primer lugar, a mis padres María y Diego, la base y el sustento que me han permitido desarrollarme como trabajador y como persona. Ambos una inspiración y un reflejo en el que mirarse. También a mi hermano Carlos, compañero de habitación durante muchos años y con unas cualidades envidiables.

En segundo lugar, a Laura. Empecé esta tesis teniendo una buena amiga y la termino con la que espero sea la mujer de mi vida. Eres paciente, constante y amable, cualidades que me alegran el más oscuros de los días.

A mis smigos doctorandos. A Isa, de la que creo que, sinceramente, me conoce mejor que yo mismo. Un balón de oxígeno en todo este proceso. De seguro sin nuestras charlas quejándonos de todo, seguidas de las tonterías más grandes, no habría acabado todo esto. A Vir, mi compañera en la distancia con la que, aunque pasen los años que pasen, seguiremos igual.

A mis compañeros de laboratorio. A Miguel, luchador incansable y con un corazón tan grande que podría rellenar solo un campo de futbol. A Mari Carmen, la definición de buena persona y que seguro triunfará allá donde vaya, porque encandila a cualquiera que la conozca. A Miguel Ángel, el científico por excelencia, siempre dispuesto a ayudar en cualquier cosa, pero también a invitar a unas cervezas. A Juanjo y José, personas extraordinarias científicamente y compañeros de risas infinitas. A Paula, Nerea, Alicia, June, Behnam, Jose Luis y Sandra, por andar siempre por aquí para un rato de charla.

To Trondheim people. To Ainara, for your generosity and for including me in Trondheim life as one of your friends. Always in debt with you. To Oscar, Jose and Gonzalo, for sharing beers and travels. To Stine and Youri, my labmates, always a pleasure work with you. To Stelle and the whole IKP department, for all the support I received. To Prof. Hilde J.

UNIVERSIDAD DE MÁLAGA

Venvik, for open her lab for me and help me with everything I needed. I appreciated it so much.

A los doctores del grupo, Fran y María José, y a los que pasaron por aquí, Mari Carmen, por siempre estar dispuestos a echar una mano y resolver cualquier duda, así como para pasar un rato distendido de café/cerveza.

A los “jefecillos” del grupo. A Ramiro, por todo lo que me he aprendido de ti y tu optimismo incansable. A Nani, por absolutamente todo. Por tu dedicación conmigo, por tu ayuda, por tu conocimiento, por tus palabras, por tu confianza... Si he llegado hasta aquí es por ti.

A los jefes y mis directores. A Tomás, por acogerme como uno más dentro del grupo, por tus siempre buenas palabras y por tu gran conocimiento y visión de cualquier tema. A Pepe, por tu tiempo y todas las correcciones que necesitaba.

Al personal Técnico del SCAI, María, Valle, Goyo, Adolfo, Ana, Laura y demás. Sois todos unos grandes profesionales que me habéis ayudado muchísimo.

Al departamento de Ingeniería Química, por prestarme sus instalaciones e incluirme como uno más.

Al ministerio de Economía y competitividad, por concederme un contrato para formarme como doctor y a la Universidad de Málaga por ceder su infraestructura y concederme una beca post-doctoral.

UNIVERSIDAD DE MÁLAGA